



AUTHOR:

TITLE:

YEAR:

OpenAIR citation:

This work was submitted to- and approved by Robert Gordon University in partial fulfilment of the following degree:

OpenAIR takedown statement:

Section 6 of the “Repository policy for OpenAIR @ RGU” (available from <http://www.rgu.ac.uk/staff-and-current-students/library/library-policies/repository-policies>) provides guidance on the criteria under which RGU will consider withdrawing material from OpenAIR. If you believe that this item is subject to any of these criteria, or for any other reason should not be held on OpenAIR, then please contact openair-help@rgu.ac.uk with the details of the item and the nature of your complaint.

This is distributed under a CC _____ license.

STUDIES ON THE ROLE OF GPR55 IN CARDIOVASCULAR
PHYSIOLOGY AND PATHOPHYSIOLOGY

OLIVIA JANE ROBERTSON-GRAY

A thesis submitted in partial fulfilment of the requirements of
Robert Gordon University for the degree of
Doctor of Philosophy

Collaborating Establishment: AstraZeneca (Mölndal, Sweden)

December 2017

Declaration

This thesis in candidature for the degree of Doctor of Philosophy has been composed entirely by myself. The work which is documented was carried out by myself. All sources of information contained within which have not arisen from the results generated have been specifically acknowledged.

For my Mum

Whom I love so very much xx

“As you will find in multivariable calculus,
there is often a number of solutions for any given problem”

- John Forbes Nash

Contents

Acknowledgements	I
Publications	IV
Abstract	V
Abbreviations (alphabetical)	VI
Abbreviations (non-alphabetical)	XIV
Units of Measurements	XV

Chapter 1: General Introduction	1
1.1. GPR55/LPI system	2
1.1.1. G-protein-coupled receptors	2
1.1.2. GPR55	2
1.1.2.1. <i>Discovery</i>	2
1.1.2.2. <i>Tissue expression and distribution</i>	3
1.1.3. Pharmacology of GPR55	3
1.1.4. Signalling pathways	7
1.1.4.1. <i>Activation of GPR55 by synthetic and endocannabinoid ligands</i>	7
1.1.4.2. <i>GPR55 activation by LPI</i>	8
1.1.4.3. <i>Activation of GPR55 by LPI in the cardiovascular system</i>	8
1.1.5. The role of GPR55 in physiology and pathophysiology	12
1.1.5.1. <i>General overview</i>	12
1.1.5.2. <i>Metabolism and energy balance</i>	12
1.1.5.3. <i>GPR55 and cardiovascular physiology</i>	13
1.2. Atherosclerosis	14
1.2.1. Overview	14
1.2.2. Lipid homeostasis	14
1.2.3. Hyperlipidaemia	15
1.2.3.1. <i>Vascular impact of hyperlipidaemia</i>	15
1.2.3.2. <i>Cardiac impact of hyperlipidaemia</i>	16
1.2.4. The atherosclerotic plaque	16
1.2.4.1. <i>Vascular impact of atherosclerosis</i>	17
1.2.4.2. <i>Cardiac impact of atherosclerosis</i>	19
1.2.5. GPR55 and atherosclerosis	19

1.3.	Myocardial ischaemia	19
1.3.1.	Energy reduction-induced contractile dysfunction	20
1.3.2.	Metabolite accumulation	20
1.3.3.	Cell swelling and sarcolemmal disruption	21
1.3.4.	Cell necrosis	21
1.4.	Myocardial ischaemia/reperfusion Injury	24
1.4.1.	Mechanisms of immediate myocardial ischaemia/reperfusion injury	26
1.4.1.1.	<i>Oxidative stress</i>	26
1.4.1.2.	<i>Intracellular Ca²⁺ overload</i>	26
1.4.1.3.	<i>Restoration of the physiological pH</i>	26
1.4.1.4.	<i>Normalisation of tissue osmolality</i>	26
1.4.1.5.	<i>The opening of the mitochondrial permeability transition pore</i>	27
1.4.2.	Mechanisms of delayed myocardial ischaemia/reperfusion Injury	27
1.4.3.	LPI and myocardial ischaemia/reperfusion injury	28
1.5.	Cardiac function	29
1.5.1.	Excitation-contraction coupling	29
1.5.2.	Control of cardiac contractility	31
1.5.2.1.	<i>α₁-adrenoceptor activation</i>	31
1.5.2.2.	<i>β₁-adrenoceptor activation</i>	31
1.5.3.	The Frank-Starling principle	31
1.5.4.	Cardiac function in health and disease	32
1.5.4.1.	<i>Hypertension and cardiac function</i>	32
1.5.4.2.	<i>Dyslipidaemia and cardiac function</i>	32
1.5.4.3.	<i>Post-myocardial infarction and cardiac function</i>	33
1.5.5.	GPR55 and cardiac function	33
1.6.	Hypothesis	35
1.7.	Objectives	35

Chapter 2: General Methods 36

2.1.	<i>In vitro</i> studies	37
2.1.1.	Cell culture	37
2.1.1.1.	<i>Mouse and human induced pluripotent stem cell-derived cardiomyocytes</i>	37
2.1.2.	Corning® Epic® technology	37
2.2.	<i>In vivo</i> studies	38

2.2.1.	Animal ethics and husbandry	38
2.2.2.	Breeding program	40
2.2.2.1.	<i>Strains</i>	40
2.2.2.2.	<i>Genotyping protocol</i>	40
2.2.3.	High fat dietary intervention	40
2.2.4.	Measurement of cardiodynamics	42
2.2.4.1.	<i>Pressure-volume loop analysis</i>	42
2.2.4.2.	<i>Surgical procedure for pressure-volume loop analysis</i>	42
2.2.4.3.	<i>Parallel conductance</i>	44
2.2.4.4.	<i>Post-experimental volume calibration of the PVL catheter</i>	45
2.3.	<i>Ex vivo studies</i>	45
2.3.1.	Tissue harvest	45
2.3.2.	Plasma lipid analysis	46
2.3.3.	Small-vessel myography	46
2.3.4.	Histology	48
2.3.4.1.	<i>Oil Red O staining of the thoracic aorta</i>	48
2.3.4.2.	<i>Cryosectioning of ventricular tissue</i>	48
2.3.4.3.	<i>Haematoxylin and Eosin staining of ventricular tissue</i>	50
2.3.4.4.	<i>Picrosirius Red staining of ventricular tissue</i>	50
2.3.4.5.	<i>Oil Red O staining of ventricular tissue</i>	50
2.3.5.	Isolated Langerdorff-perfused heart studies	53
2.3.6.	Measurement of myocardial infarct size	53
2.4.	Statistical analysis	53
2.5.	Materials	55
2.5.1.	Composition of drugs and solutions	57

Chapter 3: Effect of a high fat diet in ApoE^{-/-} and ApoE^{-/-}/GPR55^{-/-}

	mouse models of atherosclerosis	60
3.1.	Introduction	61
3.1.1.	GPR55 and risk factors associated with atherosclerosis	61
3.1.2.	GPR55 and atherosclerosis	61
3.1.3.	Rodent models of atherosclerosis	62
3.1.3.1.	<i>ApoE^{-/-} mouse</i>	62
3.1.3.2.	<i>LDLR^{-/-} mouse</i>	63

3.1.4.	GPR55 knockout models	63
3.1.5.	Aims	64
3.2.	Methods	64
3.2.1.	Study design	64
3.2.2.	Body weight measurements	67
3.2.3.	Assessment of fat and lean mass composition	67
3.2.4.	Assessment of endothelial and smooth muscle function of the carotid artery ..	67
3.2.4.1.	<i>Contractile responses to U-46619</i>	67
3.2.4.2.	<i>Assessment of vasorelaxant responses to MCh and SNP</i>	68
3.2.5.	Assessment of plasma lipid profiles	68
3.2.6.	Histological assessment of the deposition of fatty streaks within the thoracic aorta	68
3.2.7.	Histological assessment of ventricular structure/composition	69
3.2.8.	Statistical analysis	69
3.3.	Results	70
3.3.1.	Impact of gene deletion and/or a high fat diet on body weight	70
3.3.2.	Impact of gene deletion and/or a high fat diet on body mass composition	74
3.3.2.1.	<i>Fat mass</i>	74
3.3.2.2.	<i>Lean mass</i>	74
3.3.3.	Impact of gene deletion and/or a high fat diet on tissue weights	79
3.3.4.	Impact of gene deletion and/or a high fat diet on endothelial and smooth muscle function of the carotid artery	83
3.3.5.	Impact of gene deletion and/or a high fat diet on plasma lipid profiles	91
3.3.6.	Impact of gene deletion and/or a high fat diet on the deposition of fatty streaks within the thoracic aorta	91
3.3.7.	Impact of gene deletion and/or a high fat diet on cardiac structure	96
3.3.8.	Impact of gene deletion and/or a high fat diet on ventricular collagen deposition	96
3.3.9.	Impact of gene deletion and/or a high fat diet on ventricular lipid deposition ..	96
3.4.	Discussion	101
3.4.1.	The impact of gene deletion on mouse phenotype	101
3.4.2.	The impact of a high fat diet on mouse phenotype	104
3.4.2.1.	<i>Body weight and composition</i>	104
3.4.3.	The impact of a high fat diet on lipid profiles	106

3.4.4.	The impact of a high fat diet on vascular function and fatty streak development.....	107
3.4.4.1.	<i>Vascular function</i>	107
3.4.4.2.	<i>Fatty streak development</i>	108
3.4.5.	The impact of a high fat diet on cardiac remodelling.....	109
3.4.5.1.	<i>Wall thickness of the LV, RV and IVS</i>	109
3.4.5.2.	<i>Ventricular lipid deposition</i>	110
3.4.6.	Conclusion.....	111

Chapter 4: Effect of a high fat diet on cardiac function in ApoE^{-/-} and ApoE^{-/-}/GPR55^{-/-} mouse models of atherosclerosis		112
4.1.	Introduction	113
4.1.1.	Assessment of cardiac function.....	113
4.1.1.1.	<i>Doppler echocardiography</i>	113
4.1.1.2.	<i>PVL analysis</i>	113
4.1.2.	GPR55 and cardiac function.....	115
4.1.3.	ApoE and cardiac function.....	115
4.1.4.	Aims.....	116
4.2.	Methods	116
4.2.1.	Study design.....	116
4.2.2.	Assessment of cardiac function via PVL analysis.....	116
4.2.3.	Statistical analysis.....	120
4.3.	Results	121
4.3.1.	Impact of gene deletion on load-dependent and -independent indices of baseline cardiac function.....	121
4.3.1.1.	<i>Systolic function</i>	121
4.3.1.2.	<i>Diastolic function</i>	121
4.3.2.	Impact of high fat feeding on load-dependent and -independent indices of baseline cardiac function.....	122
4.3.2.1.	<i>Systolic function</i>	122
4.3.2.2.	<i>Diastolic function</i>	122
4.3.3.	Impact of gene deletion on contractile reserve.....	125
4.3.3.1.	<i>Systolic function</i>	125
4.3.3.2.	<i>Diastolic function</i>	125

4.3.4.	Impact of high fat feeding on contractile reserve	125
4.3.4.1.	<i>Systolic function</i>	125
4.3.4.2.	<i>Diastolic function</i>	128
4.4.	Discussion	135
4.4.1.	The impact of gene deletion on baseline cardiac function	135
4.4.2.	The impact of high fat feeding on baseline cardiac function	137
4.4.3.	The impact of gene deletion on contractile reserve	139
4.4.4.	The impact of high fat feeding on contractile reserve	140
4.4.5.	Conclusion	141

Chapter 5: The impact of GPR55 activation in myocardial ischaemia/ reperfusion injury

	Introduction	144
5.1.1.	GPR55 signalling in the cardiomyocyte	144
5.1.2.	Aims	145
5.2.	Methods	145
5.2.1.	Effect of GPR55 activation on the DMR activity of cultured cardiomyocytes and investigation of the signalling pathway following GPR55 activation	145
5.2.2.	Isolated heart studies	146
5.2.3.	Statistics	147
5.3.	Results	147
5.3.1.	Effect of GPR55 activation on the DMR activity of cultured miPSC-derived cardiomyocytes and investigation of the signalling pathway following GPR55 activation	147
5.3.2.	Effect of GPR55 activation on the DMR activity of cultured hiPSC-derived cardiomyocytes and investigation of the signalling pathway following GPR55 activation	148
5.3.3.	Effect of GPR55 activation on myocardial I/R injury and investigation of the signalling pathway following GPR55 activation	153
5.4.	Discussion	153
5.4.1.	Investigation of the signalling pathway following GPR55 activation in miPSC and hiPSC-derived cardiomyocytes	156
5.4.2.	The impact of GPR55 activation on myocardial I/R injury	157
5.4.3.	Conclusion	162

Chapter 6: General Discussion	163
6.1. Key findings	164
6.1.1. GPR55 regulates fat deposition in atherosclerosis	164
6.1.2. The hyperlipidaemic plasma profile associated with atherosclerosis occurs via GPR55-independent mechanism	164
6.1.3. GPR55 promotes the development of fatty streaks within the vasculature	165
6.1.4. GPR55 maintains systolic function but impairs contractile reserve in atherosclerosis	165
6.1.5. LPI signals via a GPR55/ROCK-dependent mechanism in cardiomyocytes	166
6.1.6. LPI exacerbates myocardial I/R injury via a GPR55/ROCK-dependent mechanism	166
6.2. Clinical relevance	167
6.2.1. Obesity	167
6.2.2. Atherosclerosis development	167
6.2.3. Myocardial I/R injury	167
6.3. Future studies	168
6.3.1. Examination of the mechanism(s) via which the LPI/GPR55 system contributed to fatty streak development within the vasculature	168
6.3.2. Studies to confirm or deny the involvement of $[Ca^{2+}]_i$ overload in the myocardial I/R injury exacerbated by the LPI/GPR55 system	168
6.4. Limitations	168
6.5. Conclusions	169
 Chapter 7: References	 170

List of Figures

Chapter 1: General Introduction

Figure 1.1.	Molecular structure of L- α -LPI	5
Figure 1.2.	Molecular structure of 2-arachidonoyl LPI	5
Figure 1.3.	The endogenous synthesis of LPI	6
Figure 1.4.	Signalling pathways of GPR55	10
Figure 1.5.	The proposed site of endogenous LPI release within the cardiovascular system ..	11
Figure 1.6.	Atherosclerotic plaque development	18
Figure 1.7.	The response of the cardiomyocyte to ischaemia	22
Figure 1.8.	The wave front phenomenon of cardiomyocyte death in response to the duration of ischaemia	23
Figure 1.9.	The response of the cardiomyocyte to reperfusion	25
Figure 1.10.	The transport of Ca ²⁺ in a ventricular cardiomyocyte	30

Chapter 2: General Methods

Figure 2.1.	The methodology of Corning® Epic® Technology	39
Figure 2.2.	Diagram of a pressure-tipped conductance catheter	43
Figure 2.3.	Dual wire myograph system	47
Figure 2.4.	ORO staining of a thoracic aorta from a high fat fed ApoE ^{-/-} mouse	49
Figure 2.5.	Langendorff retrograde perfusion apparatus	54

Chapter 3: Effect of a high fat diet in ApoE^{-/-} and ApoE^{-/-}/GPR55^{-/-} mouse models of atherosclerosis

Figure 3.1.	Full nutritional details of the CRM (P) pellets (NC Diet)	65
Figure 3.2.	Full nutritional details of the R638 semi-synthetic pellets (HFC Diet)	66
Figure 3.3.	Weight gain over time in male mice	72
Figure 3.4.	Weight gain over time in female mice	73
Figure 3.5.	Fat mass (% of body weight; BW) of male and female mice at weeks 6 and 12, measured via EchoMRI™ body scanning	76
Figure 3.6.	Lean mass (g) of male and female mice at weeks 6 and 12, measured via EchoMRI™ body scanning	78

Figure 3.7.	Ratio of Liver weight (LW), ventricular weight (VW) and abdominal fat weight (AFW) to final body weight (BW).....	81
Figure 3.8.	The effect of high fat feeding on the contractile responses of the murine carotid artery to U-46619 (10^{-9} - 10^{-5} M).....	84
Figure 3.9.	Exemplar traces of vasodilator-induced relaxations of the murine carotid artery	86
Figure 3.10.	The effect of high fat feeding on the endothelium-dependent vasorelaxant responses of the murine carotid artery to MCh (10^{-9} - 10^{-4} M).....	87
Figure 3.11.	The effect of high fat feeding on the endothelium-independent vasorelaxant responses of the murine carotid artery to SNP (10^{-9} - 10^{-4} M).....	89
Figure 3.12.	Lipid profiling of mouse plasma.....	93
Figure 3.13.	Fatty streaks within the thoracic aortae of mice.....	95
Figure 3.14.	Left and right ventricular (LV and RV, respectively) wall thickness and that of the intraventricular septum (IVS) in mice.....	98
Figure 3.15.	Picrosirius Red staining of murine ventricular tissue.....	99
Figure 3.16.	Oil Red O staining of murine ventricular tissue.....	100

Chapter 4: Effect of a high fat diet on the cardiac function of ApoE^{-/-} and ApoE^{-/-}/GPR55^{-/-} mouse models of atherosclerosis

Figure 4.1.	The cardiac cycle illustrated in the form of pressure-volume loops.....	114
Figure 4.2.	Trace of baseline haemodynamic variables from an NC fed C57BL/6 mouse.....	118

Chapter 5: The impact of GPR55 activation in myocardial ischaemia/reperfusion injury

Figure 5.1.	DMR activity of miPSC-derived cardiomyocytes in response to LPI (1nM-30 μ M).....	149
Figure 5.2.	Investigation of the signalling pathway following receptor activation with LPI (10 μ M) in miPSC-derived cardiomyocytes.....	150
Figure 5.3.	DMR activity of hiPSC-derived cardiomyocytes in response to LPI (1nM-30 μ M)	151
Figure 5.4.	Investigation of the signalling pathway following receptor activation with LPI (10 μ M) in hiPSC-derived cardiomyocytes.....	152
Figure 5.5.	Effect of GPR55 gene deletion and GPR55 activation on myocardial I/R injury...	154
Figure 5.6.	Investigation of the signalling pathway following GPR55 activation in myocardial I/R injury.....	155

List of Tables

Chapter 1: General Introduction

Table 1.1.	The impact of dyslipidaemia on cardiac function	34
------------	---	----

Chapter 2: General Methods

Table 2.1.	ApoE and GPR55 primer sequences for the genotyping of mice	41
Table 2.2.	PCR thermocycler sequence for the genotyping of mice with gene mutations for ApoE and GPR55	41
Table 2.3.	Genotypes of mice according to band size(s) present in gels	41
Table 2.4.	ORO staining protocol for the identification of lipid deposition within the lumen of thoracic aortae	51
Table 2.5.	Haematoxylin and Eosin staining protocol used to visualise the cardiac structure of cardiac tissue sections	51
Table 2.6.	Picrosirius Red staining protocol for the detection of collagen in cardiac tissue sections	52
Table 2.7.	ORO staining protocol for the identification of lipid deposition in cardiac tissue sections	52
Table 2.8.	Source of drugs and solutions	55

Chapter 3: Effect of a high fat diet in ApoE^{-/-} and

ApoE^{-/-}/GPR55^{-/-} mouse models of atherosclerosis

Table 3.1.	Body weight of male and female mice at week 0	71
Table 3.2.	Body weight of male and female mice at week 12	71
Table 3.3.	Fat mass (% of body weight; BW) of male and female mice at week 0, measured via EchoMRI TM body scanning	75
Table 3.4.	Group sizes for fat mass (% of body weight; BW) of male and female mice at weeks 6 and 12, measured via EchoMRI TM body scanning	75
Table 3.5.	Lean mass (g) of male and female mice at week 0, measured via EchoMRI TM body scanning	77
Table 3.6.	Group sizes for lean mass (g) of male and female mice at weeks 6 and 12, measured via EchoMRI TM body scanning	77

Table 3.7.	Group sizes for tissue weights of mice.....	80
Table 3.8.	Ratio of spleen and kidney weight (SW and KW, respectively) to final body weight (BW).....	82
Table 3.9.	The effect of gene deletion and/or diet on the maximal (E_{max}) Δ in tension of the murine carotid artery to U-46619 (10^{-9} - 10^{-5} M) and the associated $\log EC_{50}$ values.....	85
Table 3.10.	The effect of gene deletion and/or diet on the maximal (E_{max}) Δ in % relaxation of the murine carotid artery to MCh (10^{-9} - 10^{-4} M) and the associated $\log EC_{50}$ values.....	88
Table 3.11.	The effect of gene deletion and/or diet on the maximal (E_{max}) Δ in % relaxation of the murine carotid artery to SNP (10^{-9} - 10^{-4} M) and the associated $\log EC_{50}$ values.....	90
Table 3.12.	Group sizes of the plasma lipids of mice.....	92
Table 3.13.	Groups sizes for Oil Red O staining of fatty streaks in the lumen of the thoracic aorta.....	94
Table 3.14.	Groups sizes for Haematoxylin and Eosin (H & E) staining of ventricular tissue.....	97
Table 3.15.	Groups sizes for Picrosirius Red staining of ventricular tissue.....	99
Table 3.16.	Groups sizes for Oil Red O staining of ventricular tissue.....	100

Chapter 4: Effect of a high fat diet on the cardiac function of ApoE^{-/-} and ApoE^{-/-}/GPR55^{-/-} mouse models of atherosclerosis

Table 4.1.	Load-dependent indices of cardiac function and their definitions.....	119
Table 4.2.	Load-independent indices of cardiac function and their definitions.....	119
Table 4.3.	Effect of gene deletion and/or high fat feeding on load-dependent indices of systolic function of mice.....	123
Table 4.4.	Effect of gene deletion and/or high fat feeding on load-dependent indices of diastolic function of mice.....	124
Table 4.5.	Effect of gene deletion and/or high fat feeding on load-independent indices of cardiac function of mice.....	124
Table 4.6.	Effect of gene deletion on the systolic indices of contractile reserve in mice.....	126
Table 4.7.	Effect of gene deletion on the diastolic indices of contractile reserve in mice.....	127
Table 4.8.	Effect of a high fat diet on the systolic indices of contractile reserve in C57BL/6 mice.....	129

Table 4.9.	Effect of a high fat diet on the systolic indices of contractile reserve in ApoE ^{-/-} mice	130
Table 4.10.	Effect of a high fat diet on the systolic indices of contractile reserve in GPR55 ^{-/-} mice	131
Table 4.11.	Effect of a high fat diet on the systolic indices of contractile reserve in ApoE ^{-/-} /GPR55 ^{-/-} mice	132
Table 4.12.	Effect of a high fat diet on the diastolic indices of contractile reserve in C57BL/6 mice	133
Table 4.13.	Effect of a high fat diet on the diastolic indices of contractile reserve in ApoE ^{-/-} mice	133
Table 4.14.	Effect of a high fat diet on the diastolic indices of contractile reserve in GPR55 ^{-/-} mice	134
Table 4.15.	Effect of a high fat diet on the diastolic indices of contractile reserve in ApoE ^{-/-} /GPR55 ^{-/-} mice	134

Acknowledgements

I would like express my sincere gratitude to the following organisations and people:

The Medical Research Council and AstraZeneca

- For providing the four-year CASE award which enabled me to conduct my studies.

Robert Gordon University

- First and foremost, I'd like to thank my principal supervisor, Professor Cherry Wainwright for her expertise, guidance and support throughout my PhD.
- My co-supervisor, Dr Sarah Walsh for the teaching of lab techniques, advice re data analysis and for the support provided throughout my time at RGU.
- Andrea MacMillan, for her administrative support throughout the four year period.
- To the staff at the MRF for providing expert advice and for looking after my animals whilst in their care. I'd also like to thank the MRF technicians who weighed and conducted the EchoMRI™ body scanning of my mice and for sending on the data generated for me to analyse and interpret.
- To the janitors of the Sir Ian Wood Building of RGU (Lukasz, Duncan, Stevie, Duke and Iain). All of you have helped me on many an occasion, whether it was letting me into the liquid nitrogen store, helping me move gas cylinders etc or just generally giving me abusive banter...on a daily basis!!

AstraZeneca

- Dr Ann-Cathrine Jönsson-Rylander, for affording me not only the opportunity to work in the labs of AstraZeneca and the experience of applying scientific techniques in an industrial environment but also for acquainting me with the beautiful sights and culture of Sweden. Each time I visited was a truly unforgettable experience. I'd also like to thank you for inviting me into your beautiful home and for introducing me to your family.
- Dr Erik Ryberg, for teaching me how to culture cardiomyocytes and for the detailed lessons on how to use the Corning® Epic® system. I'd also like to thank Dr Ryberg for conducting the

experiments involving the hiPSC-derived cardiomyocytes and for sending on the data generated from these studies for me to analyse and interpret.

- Anne-Christine Andréasson, for showing me the ropes regarding histology and immunohistochemistry.

The Research Hub

- Amy Arnold, my lab buddy and PhD bestie. We've witnessed some of each other's finest (and worst) lab moments!! We've laughed till we've cried on so many occasions!! We've featured in the British Pharmacological Society's magazine (after far too much wine), been stranded in an airport together, trekked around London on crutches and had ridiculous amounts of science chatter along the way. Believe it or not, I even have fond memories of when we took it in turns to hide out in the cell imaging lab to shed the odd tear. I cannot imagine having been on the PhD rollercoaster that has been the past four years without you...you're an incredible friend and true confidant.
- My wonderful friends, Sarah, Karen, Emma, Rachael (Twinnie) and Maria for ALL the amazing times we've shared in and out of Uni...you have made my time at RGU truly unforgettable. I'd also like to thank other members of the Research Hub (Saeed, Steve, Bazma, Fatma, Dean, Sanjoy and PJ) who have made my time here so memorable.

My Family

- First and foremost, my lovely Mum for her constant love, patience and never ending support - not just throughout the duration of my PhD but throughout the twenty-nine years of my life. Your strength to overcome the most challenging of times has given me the ability to overcome the problems in my personal life whilst studying at University. You are truly incredible and I will be eternally grateful for the unconditional love and unrelenting support you have shown me.
- My Dad, for the phone calls throughout my PhD, for the collection of original cardiology teaching charts from the University of Edinburgh and for persistently asking the all-important question 'are you any closer to making the heart beat that little bit longer?'. I think the heart is an interest we secretly share.
- My Grandparents, past and present. Gran and Papa, for always encouraging, loving and supporting me. Also Papa, for teaching me the importance of accuracy, attention to detail

and mathematical fractions (the latter was taught by dividing a cake into quarters!!). Your teaching of these skills has enabled me to do things I didn't know I was capable of. Grandma Anna and Papa Jim, for your love and encouragement in my early years. Papa Jim, the times we spent making random things together in your workshop (making little men by soldering pieces of copper wire together and making miniature Indian tepees out of garden sticks and ribbon) taught me that patience and perseverance pay off - two skills which have proven critical throughout my lab work and write-up. I never got to tell you but some of my fondest memories were spent with you.

- My aunts, Hilary and Patti, for their love and support throughout the years and for being there for me regardless of the problems I've had to face. I'd also like to thank Hilary for proof reading my thesis (no mean feat!!).

My Lifelong Friends

- To Ruth, Ali, Genna and Fiona. You have kept in touch throughout my PhD despite me moving 3-4 hours away. You've texted, phoned, visited and sent me amusing letters, postcards and presents. You are all amazing and I am truly honoured to call you my friends.

Morag Taylor

- Last but certainly not least, I'd like to say a special thanks to Morag Taylor for all the support and words of wisdom throughout the past year. You have had such a positive impact on my life.

Publications

Abstract for oral communication

Robertson-Gray, O.J., Walsh, S.K., Jönsson-Rylander, A.C. and Wainwright, C.L. (2014) Exogenous lysophosphatidylinositol exacerbates myocardial tissue injury via a GPR55/ROCK dependent mechanism. Proceedings of the British Pharmacological Society (*pA2* online). **12**, abst 160P

Abstracts for poster presentation

Robertson-Gray, O.J., Walsh, S.K., Jönsson-Rylander, A.C., Ryberg, E. and Wainwright, C.L. (2016) P7 The role of G-protein-coupled receptor 55 (GPR55) in atherosclerosis – induced cardiovascular remodelling and dysfunction. *Heart*. **102**, A4

Robertson-Gray, O.J., Walsh, S.K., Jönsson-Rylander, A.C. and Wainwright, C.L. (2014) Exogenous lysophosphatidylinositol exacerbates myocardial tissue Injury via a GPR55 dependent mechanism. *Heart*. **100**, A22

Robertson-Gray, O.J., Walsh, S.K., Gonca, E. Cruickshank, S.F., Jönsson-Rylander, A.C. and Wainwright, C.L. (2013) Exogenous lysophosphatidylinositol exacerbates myocardial tissue Injury via a GPR55 dependent mechanism. Proceedings of the British Pharmacological Society (*pA2* online). **11**, abst146P

Robertson-Gray, O.J., Walsh, S.K., Gonca, E. Cruickshank, S.F. and Wainwright, C.L. (2013) Exogenous lysophosphatidylinositol exacerbates myocardial tissue injury via a GPR55 dependent mechanism. *J Mol Cell Cardiol*. **65**, S123

Abstract

Atherosclerosis is a multifactorial, chronic inflammatory condition characterised by endothelial dysfunction, hyperlipidaemia and the accumulation of fatty deposits within the tunica intima of medium-to-large sized muscular arteries. This disease can prove fatal with patients suffering lethal myocardial infarction or stroke. Recently, two studies investigating the role of G-protein-coupled receptor 55 (GPR55) in atherosclerosis reported conflicting results; one reported a pro-atherogenic role for GPR55 and the other, an anti-atherogenic role for this receptor. Interestingly, another study demonstrated that the activation of GPR55 by lysophosphatidylinositol (LPI) in cultured rat neonatal ventricular cardiomyocytes provokes distinct cellular functions that are dependent on the location of GPR55, leading to suggestions that GPR55 may regulate cardiomyocyte function at two cellular sites and be a potential therapeutic target for cardiac disorders. While it has been demonstrated that GPR55 is important in the maintenance of cardiac function of healthy mice, what is currently unknown is if GPR55 has a role in the cardiovascular remodelling and cardiac function of atherosclerosis prone mice. To address this, the present studies were conducted to investigate 1) the role of GPR55 in atherogenesis, 2) if GPR55 has a role in the cardiac function of mice suffering from atherosclerosis, 3) the signalling pathway by which LPI activates cardiomyocytes, 4) the impact of GPR55 activation on the outcome of myocardial ischaemia/reperfusion (I/R) injury and, 5) the signalling mechanisms by which GPR55 elicits any observed effects on the myocardium in response to such injury. Using C57BL/6 (wildtype; WT), apolipoprotein E knockout (ApoE^{-/-}; mouse model of atherosclerosis), GPR55 knockout (GPR55^{-/-}) and novel ApoE^{-/-}/GPR55^{-/-} mice, this study has established that in the presence of high fat feeding (to accelerate atherosclerosis), GPR55 has a complex role whereby it both regulates risk factors associated with atherosclerosis (i.e. body weight and fat mass) yet promotes the development of fatty streaks within the vasculature, via a lipid independent mechanism. In terms of cardiac function, GPR55 exerted a protective role by maintaining the systolic function of high fat fed ApoE^{-/-} mice, yet negatively affected the contractile reserve of these mice. With regard to infarct size, the present study established that LPI-induced activation of GPR55 (pre-global ischaemia) exacerbates myocardial tissue injury via a Rho-associated protein kinase (ROCK) dependent mechanism. Finally, this study established that LPI signals through the same signalling pathway as it did in the isolated heart, in both mouse and human-induced pluripotent stem cell-derived cardiomyocytes thus suggesting a translational role for GPR55 in the human heart. In conclusion, despite further research being required, the data presented within this thesis provides evidence that GPR55 may have the potential to be targeted for therapeutic gains in atherosclerosis and myocardial I/R injury.

Keywords: Atherosclerosis, cardiac function, cardiovascular, GPR55, infarction, ischaemia, lysophosphatidylinositol, myocardial, obesity and reperfusion

Abbreviations (alphabetical)

A

Abn-CBD	Abnormal cannabidiol
ACh	Acetylcholine
ACS	Acute coronary syndrome
AEA	Anandamide
AFW	Abdominal fat weight
AHA	American Heart Association
Akt	Protein kinase B
AMP	Adenosine monophosphate
ANOVA	Analysis of variance
ApoE	Apolipoprotein E
ApoE ^{+/-}	Apolipoprotein E heterozygous knockout
ApoE ^{-/-}	Apolipoprotein E homozygous knockout
ApoE ^{-/-} /GPR55 ^{-/-}	Apolipoprotein E / G-protein-coupled receptor 55 homozygous double knockout
ARRIVE	Animal Research: Reporting of <i>In Vivo</i> Experiments
ATF-2	Activating transcription factor 2
ATP	Adenosine triphosphate

B

BHF	British Heart Foundation
BK _{Ca}	Large conductance, Ca ²⁺ -activated, K ⁺ channel
BMI	Body mass index
bpm	Beats per minute
BSA	Bovine serum albumin
BW	Body weight

C

CaCl ₂	Calcium chloride
Ca ²⁺	Calcium ion
CBD	Cannabidiol
CB ₁	Cannabinoid receptor 1
CB ₂	Cannabinoid receptor 2
CB ₃	Cannabinoid receptor 3
cdc42	Cell division control protein 42 homolog
cDNA	Complimentary deoxyribonucleic acid
CHD	Coronary heart disease
CHO	Chinese hamster ovary
CICR	Calcium-induced calcium release
CO	Cardiac output
CoA	Coenzyme A
CO ₂	Carbon dioxide
CRC	Concentration response curve
CVF	Collagen volume fraction
C ₆ H ₆ O ₆	Glucose

D

DAG	Diacylglycerol
dH ₂ O	Deionised water
DMEM	Dulbecco's Modified Eagle's Medium
DMR	Dynamic mass redistribution
DMSO	Dimethyl Sulfoxide
DNA	Deoxyribonucleic acid
dP/dt_{\max}	Maximum first derivative of left ventricular pressure
dP/dt_{\min}	Minimum first derivative of left ventricular pressure

E

E_a	Arterial elastance
EA.hy296	Human umbilical vein derived endothelial cell line
ECM	Extracellular matrix
ECS	Endocannabinoid system

EC ₅₀	The concentration of a drug that gives the half-maximal response
EC ₈₀	The concentration of a drug that gives 80% of the maximal response
E-C coupling	Excitation-contraction coupling
EDP	End-diastolic pressure
EDPVR	End-diastolic pressure-volume relationship
EDTA	Ethylenediaminetetraacetic acid
EDV	End-diastolic volume
EF	Ejection fraction
E _{max}	Maximal
E _{max}	Intrinsic ventricular contractility
eNOS	Endothelial nitric oxide synthase
ERK	Extracellular signal-regulated kinase
ESP	End-systolic pressure
ESPVR	End-systolic pressure-volume relationship
EST	Expressed sequence tags
ESV	End-systolic volume
ET-1	Endothelin-1

F

FA(s)	Fatty acid(s)
-------	---------------

G

G	Gauge
GDP	Guanosine diphosphate
GEN	Genetic Engineering & Biotechnology News
GI	Global ischaemia
GPCR	G-protein-coupled receptor
GPR18	G-protein-coupled receptor 18
GPR55	G-protein-coupled receptor 55
GPR55-HEK293	Human embryonic kidney cells expressing G-protein-coupled receptor 55
GPR55+CB ₁ -HEK293	Human embryonic kidney cells expressing G-protein-coupled receptor 55 and cannabinoid receptor 1
GPR55 ^{+/-}	G-protein-coupled receptor 55 heterozygous knockout
GPR55 ^{-/-}	G-protein-coupled receptor 55 homozygous knockout

GTP	Guanosine triphosphate
GTP γ S	Guanosine 5'-[γ - ³⁵ S]-triphosphate
G $_{\alpha}$	G-protein homologous to the alpha subunit

H

HBSS	Hanks' Balanced Salt Solution
HClO	Hypochlorous acid
hCMEC/D3	Human brain microvascular endothelial cell line
HEK293	Human embryonic kidney derived cell line
HEPES	4-(2-Hydroxyethyl)piperazine-1-ethanesulfonic acid, N-(2-Hydroxyethyl)piperazine-N'-(2-ethanesulfonic acid)
HDL	High density lipoprotein
HFC	High fat chow
HHD	Hypertensive heart disease
hiPSC	Human induced pluripotent stem cell
HLA	Human leukocyte antigen
HL60	Human promyelocytic leukaemia cell line
HR	Heart rate
H & E	Haematoxylin & Eosin
H ₂ O	Water
H ₂ O ₂	Hydrogen peroxide
H ⁺	Proton or hydrogen ion

I

ICAM-1	Intercellular adhesion molecule 1
IK _{Ca}	Intermediate conductance, Ca ²⁺ -activated, K ⁺ channel
IL-1	Interleukin 1
IL-6	Interleukin 6
I.M.A.G.E.	Integrated Molecular Analysis of Genomes and their Expression
INO	Inosine
i.p.	Intraperitoneal
IP ₃	Inositol 1,4,5-trisphosphate
IP ₃ R	Inositol 1,4,5-trisphosphate receptor
I/R	Ischaemia/reperfusion

IVS Intraventricular septum

J

JAX Jackson

K

kb kilobase

KCl Potassium chloride

KHS Krebs's Henseleit solution

KH_2PO_4 Potassium phosphate

K^+ Potassium ion

L

LDL Low density lipoprotein

LDLR Low density lipoprotein receptor

$\text{LDLR}^{-/-}$ Low density lipoprotein receptor knockout

LDL:HDL Ratio of low density lipoprotein to high density lipoprotein

Log Logarithm

LogEC_{50} The logarithm of the concentration of a drug that gives the half-maximal response

LPC Lysophosphatidycholine

L- α -LPI L- α -Lysophosphatidylinositol

LPI Lysophosphatidylinositol

LTCC L-Type calcium channel

LV Left ventricle or left ventricular

LW Liver weight

M

MCh Methacholine

MCP-1 Monocyte chemoattractant protein 1

MgSO_4 Magnesium sulphate

miPSC Mouse induced pluripotent stem cell

MMP(s) Matrix metalloproteinase(s)

X

MPTP	Membrane permeability transition pore
MRF	Medical Research Facility
mRNA	Messenger ribonucleic acid
MT	Masson Trichrome
Myh6	Gene which codes for alpha-myosin heavy chain
MI	Myocardial infarction

N

NAADP	Nicotinic acid adenine dinucleotide phosphate
NADPH	Nicotinamide adenine dinucleotide phosphate
NaCl	Sodium chloride
NaHCO ₃	Sodium bicarbonate
Na ₂ HPO ₄	Sodium phosphate
Na ⁺	Sodium
Na ⁺ -K ⁺ -ATPase	Sodium-potassium-adenosine triphosphatase
NC	Normal chow
NCX	Na ⁺ -Ca ²⁺ exchanger
NCX2	Na ⁺ -Ca ²⁺ exchanger protein 2
NCX3	Na ⁺ -Ca ²⁺ exchanger protein 3
NFAT	Nuclear factor of activated T-cells
NHX	Na ⁺ -H ⁺ exchanger
NO	Nitric oxide
N/A	Not applicable

O

O.C.T.	Optimal cutting temperature
OEA	oleylethanolamide
OH [·]	Hydroxyl radical
ORO	Oil Red O
ox-LDL	Oxidised-LDL
O ₂	Oxygen
O ₂ ⁻	Superoxide anion

P

PBS	Phosphate buffered saline
PCR	Polymerase chain reaction
PEA	Palmitoylethanolamide
pH	Potential of hydrogen
pH _i	Intracellular potential of hydrogen
PI	Phosphatidylinositol
PIL	Personal license
PIP ₂	Phosphatidyl inositol biphosphate
PI3K-Bmx/Etk-PLCγ	Phosphoinositide 3 kinase-bone marrow kinase X-linked/epithelial and endothelial tyrosine kinase-phospholipase C gamma
PI3K	Phosphoinositide 3 kinase
PLA1	Phospholipase A1
PLA2	Phospholipase A2
PLB	Phospholamban
PLC	Phospholipase C
PPL	Project license
Prostacyclin	Prostaglandin I ₂
PVAT	Perivascular adipose tissue
PVL	Pressure-volume loop
p38 MAPK	p38 mitogen-activated protein kinase

Q

qPCR	Quantitative polymerase chain reaction
------	--

R

rac1	Ras-related C3 botulinum toxin substrate 1
rac2	Ras-related C3 botulinum toxin substrate 2
Ref	Reference
RESSA	Research ethics: student and supervisor appraisal
RGU	Robert Gordon University
RhoA	Ras homolog gene family member A
ROCK	Rho-associated protein kinase
ROS	Reactive oxygen species

rpm	Revolutions per minute
RV	Right ventricle or right ventricular
RyR or RyR2	Ryanodine receptor or ryanodine receptor 2

S

SA	Sinoatrial
S.E.M.	Standard error of the mean
SERCA2a	Sarcoplasmic/endoplasmic reticulum calcium-adenosine triphosphatase 2a
SMC	Smooth muscle cell
SNP	Sodium nitroprusside
SR	Sarcoplasmic reticulum
SV	Stroke volume
SW	Stroke work
Syk	spleen tyrosine kinase

T

TBE	Tris-Borate-EDTA buffer
TC	Total cholesterol
TCA	Tricarboxylic acid
TEM	Transmission electron microscopy
TGs	Triglycerides
TNF- α	Tumour necrosis factor alpha
TTC	2,3,5-Triphenyl-tetrazolium chloride

U

UK	United Kingdom
USA	Unites States of America

V

VCAM-1	Vascular cell adhesion molecule 1
VLDL	Very low density lipoprotein
V_p	Parallel conductance
vs.	Versus

VW	Ventricular weight
VW:BW	Ratio of ventricular weight to body weight

W

WT	Wildtype
----	----------

X

Xest C	Xestospongine C
--------	-----------------

Y

Y-27632	Y-27632 dihydrochloride
---------	-------------------------

Abbreviations (non-aphabetical)

α	Alpha
α GP	Alpha glycerol phosphate
α -GTP	GTP bound alpha subunit
α MHC	Alpha-myosin heavy chain
α_1	Alpha one
β	Beta
$\beta\gamma$	Beta-gamma complex
β_1	Beta one
γ	Gamma
Δ	Change
Δ^9 -THC	Δ^9 -tetrahydrocannabinol
$[Ca^{2+}]_i$	Intracellular calcium
$[H^+]_i$	Intracellular hydrogen
$[Na^+]_i$	Intracellular sodium
2-APB	2-aminoethoxydiphenil borate
?	Symbolises that involvement of G_q in the study was neither confirmed nor excluded
(-)	Signifies an inhibitory effect

Units of Measurements

bp	base pair(s)
g	gram(s)
g/g	gram per gram
g ⁻¹	per gram
kb	kilobase
kDa	kilodalton
kg	kilogram(s)
kg ⁻¹	per kilogram
kPa	kilopascal(s)
M	Molar
mg	milligram(s)
mg/dL	milligram(s) per decilitre
mg/g	milligram(s) per gram
mg kg ⁻¹	milligram(s) per kilogram
mg ml ⁻¹	milligram(s) per millilitre
min	minute(s)
ml	millilitre(s)
ml min ⁻¹	millilitre(s) per minute
ml ⁻¹	per millilitre
mm	millimetre(s)
mM	millimolar
mN	millinewton(s)
mmHg	millimetre(s) of mercury
mmol/l	millimole(s) per litre
ng	nanogram(s)
nmol/g	nanomole(s) per gram
nM	nanomolar
RVU	Relative Volume Units
sec	second(s)
U ml ⁻¹	Unit(s) per millilitre
V	volt(s)
v/v	volume per volume

w/v	weight per volume
µg	microgram(s)
µg kg ⁻¹	microgram(s) per kilogram
µl	microlitre(s)
µm	micrometre(s)
µM	micromolar
°C	degrees Celsius

Chapter 1:

General Introduction

1.1. GPR55/LPI system

1.1.1. G-protein-coupled receptors

G-protein-coupled receptors (GPCRs) form the largest subgroup of the receptor family. They are 7-transmembrane-spanning receptors. G-proteins are heterotrimeric protein complexes each consisting of an alpha (α), beta (β) and gamma (γ) subunit. The G-protein is situated on the intracellular surface of the plasma membrane and its subunits are secured through a fatty acid chain coupled to them via prenylation. The G-protein remains unattached and guanosine diphosphate (GDP) remains bound to the α subunit's binding site until a substrate binds to the GPCR. When a substrate does associate with the GPCR, the GPCR undergoes a conformational change causing the cytoplasmic domain to have a high affinity for the G-protein and consequently the α , β and γ subunits collectively couple to the GPCR. This results in GDP dissociation from the α subunit and the subsequent binding of guanosine triphosphate (GTP); a process known as GDP-GTP exchange. GDP-GTP exchange causes the α , β and γ trimer to dissociate releasing the GTP bound α subunit (α -GTP) and the β and γ subunits together as a complex ($\beta\gamma$). These dissociated forms of the G-protein are now 'active' and can freely bind to plasma membrane effector proteins such as enzymes or ion channels, in turn instigating the cell's next intracellular response(s). It should be noted that various forms of the G-protein's α subunit exist therefore the effector protein targeted is dependent on the form of α subunit involved (i.e. $G_{\alpha s}$, $G_{\alpha i}$, $G_{\alpha o}$, $G_{\alpha q}$; Rang *et al.*, 2007 and Widmaier *et al.*, 2006).

The human genome contains genes that encode for approximately 800 GPCRs, of which approximately 350 exhibit non-sensory functions. A number of GPCRs were classified as "orphan" receptors due to the lack of a known endogenous ligand. Among the orphan receptors is G-protein-coupled receptor 55 (GPR55). Although there are multiple reports that GPR55 can be activated *in vitro* by lysophosphatidylinositol (LPI), there is limited evidence of LPI-induced activation of GPR55 *in vivo*. Consequently, GPR55 has retained its orphan status (Alexander *et al.*, 2015).

1.1.2. GPR55

1.1.2.1. Discovery

The gene for GPR55 was first identified '*in silico*' through the expressed sequence tags (EST) database. A partial complementary deoxyribonucleic acid (cDNA) clone (clone identification: 248165)

of GPR55 (acquired from the I.M.A.G.E. Consortium) was utilised to screen a human genomic library to obtain the full length gene which was subsequently cloned (Sawzdargo *et al.*, 1999). GPR55 is comprised of 319 amino acids and has been located on chromosome 2q37 through fluorescence *in situ* hybridization (Sawzdargo *et al.*, 1999).

1.1.2.2. *Tissue expression and distribution*

In 1999, GPR55 messenger ribonucleic acid (mRNA) transcripts (4.3, 7.0 and 10-kb) were first identified in human caudate and putamen through Northern blot analysis (Sawzdargo *et al.*, 1999) and subsequent studies in rat brain revealed that GPR55 mRNA is also present in the hippocampus, various thalamic nuclei and parts of the midbrain (Sawzdargo *et al.*, 1999). More recently, it has been established that GPR55 is widely expressed (mRNA and/or protein) in the periphery, including human adipose tissue (visceral and subcutaneous) and the liver (Moreno-Navarrete *et al.*, 2012). Such expression has also been detected in the murine spleen, adrenal glands, jejunum and ileum (Ryberg *et al.*, 2007). In terms of the cardiovascular system, GPR55 expression has been reported in human endothelial cells (Waldeck-Weiermair *et al.*, 2008, Kargl *et al.*, 2013, Wilhelmssen *et al.*, 2014, Kremshofer *et al.*, 2015 and Al Suleimani and Hiley, 2016), human heart tissue (Henstridge *et al.*, 2011), rat neonatal ventricular cardiomyocytes (Yu *et al.*, 2013) and, through the use of immunostaining, Walsh and colleagues (2014) recently demonstrated the presence of GPR55 in the ventricular tissue of C57BL/6 (wildtype; WT) mice and its absence in that of GPR55 knockout (GPR55^{-/-}) mice. Interestingly, earlier studies involving quantitative polymerase chain reaction (qPCR) failed to detect GPR55 in the murine (Ryberg *et al.*, 2007) and human heart (Oka *et al.*, 2010), however, despite the reported differences in expression, it has been proposed that GPR55 may be involved in the regulation of a number of physiological processes as a consequence of its extensive expression throughout the body (Henstridge *et al.*, 2011). On the other hand, an alternative proposal is that GPR55 may lie dormant under normal physiological conditions and become activated in pathological situations; for example, GPR55 expression is relatively low in the visceral and subcutaneous adipose tissue of humans who are within the normal weight range but is markedly increased in those exhibiting an obese phenotype (Moreno-Navarrete *et al.*, 2012).

1.1.3. **Pharmacology of GPR55**

Originally, it was thought that cannabinoid receptors (CB₁ and CB₂) were responsible for the majority of actions elicited by the endocannabinoid system (ECS). However, animal models deficient in the

genes encoding these two receptors responded to cannabinoids even in their absence (reviewed by Mackie and Stella, 2006) suggesting the existence of another or other unidentified cannabinoid receptor(s). Due to the fact that GPR55 is activated by some endocannabinoid ligands such as anandamide and virodhamine (Ryberg *et al.*, 2007), it was proposed as a CB₃ receptor. However, the lack of homology with CB₁ and CB₂ receptors and the finding that non-cannabinoid ligands activate GPR55 has led to a decline in this concept.

Over recent years, L- α -lysophosphatidylinositol (L- α -LPI), derived from soybean (for chemical structure see Figure 1.1.) has been used as a tool to investigate if this lysophospholipid subspecies could be the endogenous ligand of GPR55. Oka and colleagues (2007) first demonstrated that L- α -LPI activated GPR55 in human embryonic kidney (HEK293) cells expressing GPR55 (GPR55-HEK293 cells) which consequently resulted in the rapid phosphorylation of extracellular signal-regulated kinase (ERK), Ca²⁺ transients and the stimulation of [³⁵S]guanosine-5'-O-(3-thio)triphosphate ([³⁵S]GTP γ S) binding. It has since been demonstrated that L- α -LPI activates GPR55 in other cell types such as cardiomyocytes (Yu *et al.*, 2013), endothelial cells (Al Suleimani and Hiley, 2015) and breast cancer cells (Andradas *et al.*, 2016).

LPI is generated from phosphatidylinositol hydrolysis by the action of the Ca²⁺-independent phospholipase A1 (PLA1) and Ca²⁺-dependent phospholipase A2 (PLA2) (Piñeiro and Falasca, 2012). For an extensive and comprehensive review of LPI's synthesis and metabolism see Yamashita and colleagues (2013). Several endogenous species of LPI exist including 1-stearoyl LPI and 2-arachidonoyl LPI. However, 2-arachidonoyl LPI (for chemical structure see Figure 1.2.) has been proposed as the natural ligand of GPR55 as it was the second most prominent LPI species in rat brain (8.3nmol/g tissue; 22.1% of total LPI present) and provoked the highest level of biological activity (EC₅₀=30nM) in GPR55-expressing HEK293 cells, which was 8-15 times greater than the other endogenous LPI species present in this tissue (Oka *et al.*, 2009). Nevertheless, this particular species is challenging to synthesise due to its complex synthesis pathway (for diagram of pathway see Figure 1.3.), therefore in relation to GPR55 activation in studies, L- α -LPI has been most widely utilised.

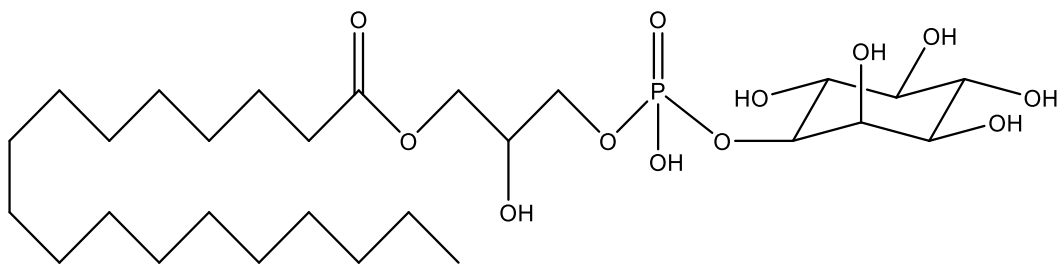


Figure 1.1. Molecular structure of L- α -LPI.

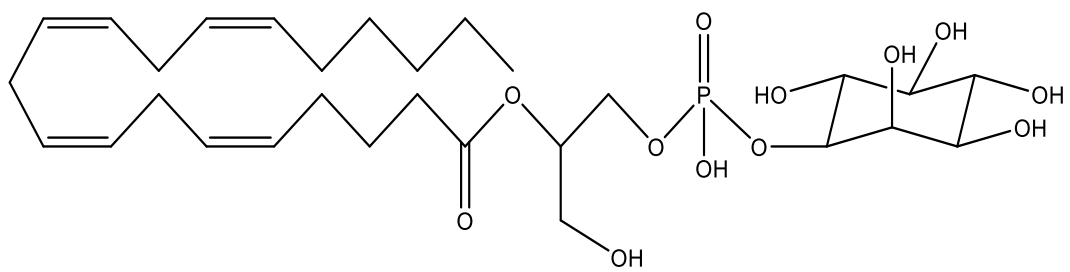


Figure 1.2. Molecular structure of 2-arachidonoyl LPI.

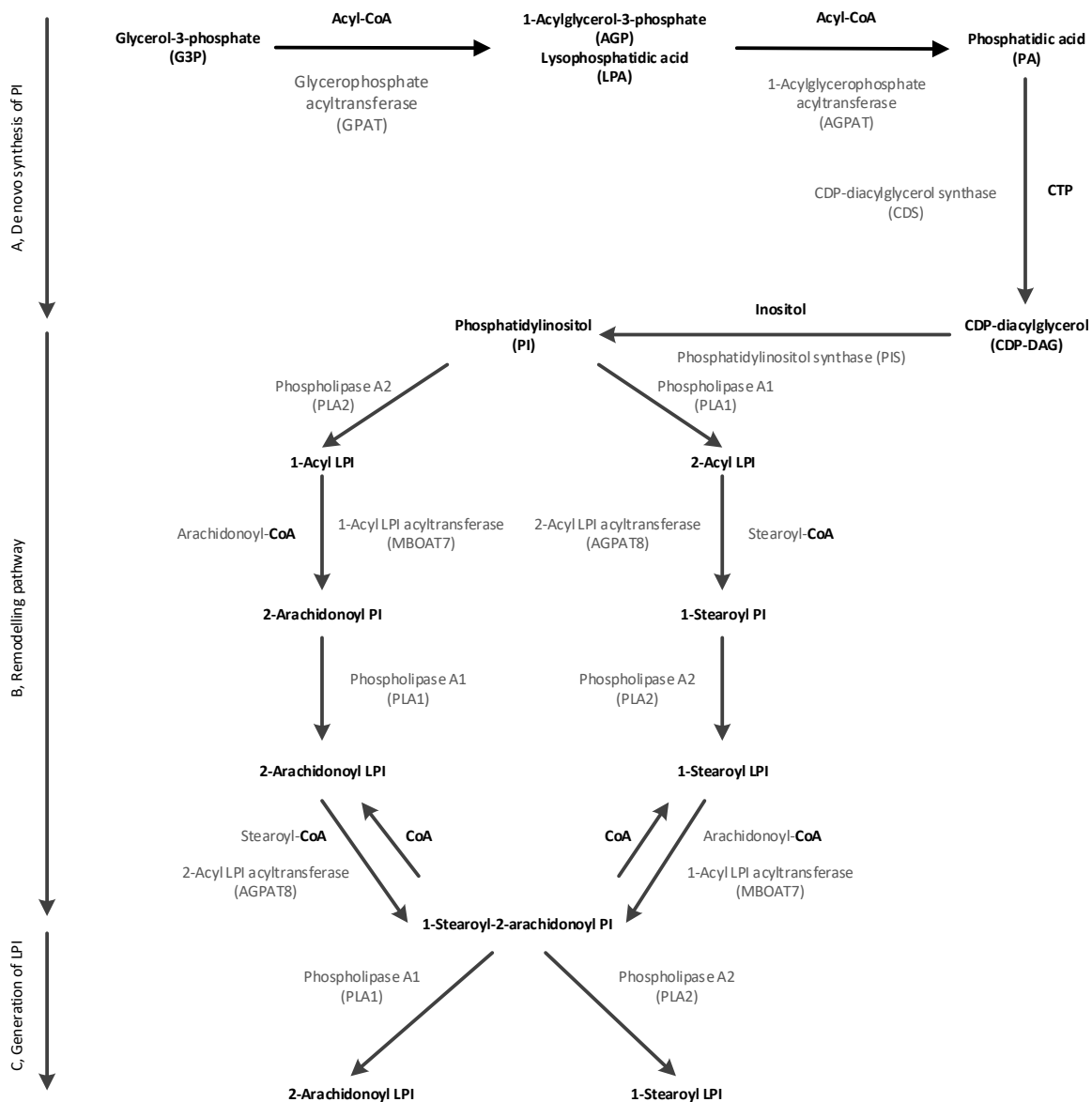


Figure 1.3. The endogenous synthesis of LPI. Diagram modified from Yamashita and colleagues (2013). CDP; cytidine diphosphate, CTP; cytidine triphosphate, CoA; coenzyme A, LPI; lysophosphatidylinositol and PI, phosphatidylinositol.

1.1.4. Signalling pathways

Despite the complex pharmacology and lack of selective ligands for GPR55, a number of downstream signalling pathways have been reported upon its activation (Figure 1.4.).

1.1.4.1. Activation of GPR55 by synthetic and endocannabinoid ligands

Studies with synthetic (i.e. O-1602) and endocannabinoid (i.e. anandamide) ligands have demonstrated that GPR55 signals through $G\alpha_{13}$ with the subsequent activation of the Rho subfamily of small GTPases; Ras homolog gene family member A (RhoA), cell division control protein 42 homolog (cdc42) and Ras-related C3 botulinum toxin substrate 1 (rac1) (Ryberg *et al.*, 2007), as demonstrated by a GTP γ S binding assay using GPR55-HEK293 cells and Western blotting. Moreover, in HEK293 cells transiently expressing human GPR55, several cannabinoids (JWH015, Δ^9 -tetrahydrocannabinol (Δ^9 -THC) and methanandamide) have been shown to increase intracellular Ca^{2+} ($[Ca^{2+}]_i$) via a pathway involving $G\alpha_q$, $G\alpha_{12}$ and RhoA activation, resulting in the downstream activation of the actin cytoskeleton and phospholipase C (PLC), consequently increasing $[Ca^{2+}]_i$ via inositol 1,4,5-trisphosphate (IP_3) receptor-gated stores (Lauckner *et al.*, 2008). In addition, activation of GPR55 by anandamide has been shown to require integrin clustering in a human umbilical vein derived endothelial cell line (EA.hy926; Waldeck-Weiermair *et al.*, 2008). When the $\alpha v\beta 3$ and $\alpha 5\beta 1$ integrins are clustered, anandamide activates the phosphoinositide 3 kinase-bone marrow kinase X-linked/epithelial and endothelial tyrosine kinase-PLC (PI3K-Bmx/Etk-PLC γ) pathway through GPR55, which consequently triggers the production of IP_3 resulting in the release of Ca^{2+} from the endoplasmic reticulum and the subsequent activation of ERK1/2 and nuclear factor of activated T-cells (NFAT). However, when $\alpha v\beta 3$ and $\alpha 5\beta 1$ are inactive (unclustered), anandamide initiates signalling via CB_1 to activate spleen tyrosine kinase (Syk), which in turn inhibits PI3K and therefore blocks anandamide-induced GPR55 signalling in these cells. Therefore, in this setting, GPR55 signalling is negatively regulated by CB_1 when the latter is activated.

Limited reports of crosstalk between GPR55 and other receptors have been documented. However, using human neutrophils, human promyelocytic leukaemia (HL60) cells and GPR55-HEK293 cells, Balenga and colleagues (2011) observed crosstalk between GPR55 and CB_2 at the level of the small GTPases, cdc42 and Ras-related C3 botulinum toxin substrate 2 (rac2). Such crosstalk between receptors reduced CB_2 mediated inflammatory responses associated with tissue injury while recruiting neutrophils to inflammatory regions more efficiently. Furthermore, crosstalk between CB_1

and GPR55 has been reported in HEK293 cells co-expressing both receptors (GPR55+CB₁-HEK293 cells). These receptors formed heteromers which influenced the signalling processes of each; the signalling of GPR55 was inhibited in the presence of CB₁ (only when CB₁ was in the inactive state), whereas, in the presence of GPR55, CB₁ signalling was enhanced (Kargl *et al.*, 2012).

1.1.4.2. *GPR55 activation by LPI*

The downstream signalling pathways of LPI-induced GPR55 activation have also been investigated. Oka and colleagues (2007) first reported that GPR55 activation by LPI in GPR55-HEK293 cells elicited a dose dependent Ca²⁺ transient in addition to the rapid phosphorylation of ERK. Similar findings in the same cell type were later reported by Oka and colleagues (2009) who documented that multiple species of LPI (1-Palmitoyl LPI, 1-Stearoyl LPI, 1-Oleoyl LPI, 2-Oleoyl LPI, 2-Linleoyl LPI and 2-Arachidonoyl LPI), other than the previously reported L- α -LPI species, could elicit dose-dependent Ca²⁺ transients as well as the rapid phosphorylation of ERK. It has also been reported in GPR55-HEK293 cells, that the LPI/GPR55 system signals via G α_{13} with the subsequent activation of RhoA and Rho-associated protein kinase (ROCK). Such activation stimulates the activity of PLC resulting in an oscillatory and prolonged IP₃-mediated Ca²⁺ release from intracellular stores, which consequently leads to the activation of NFAT and its subsequent nuclear translocation (Henstridge *et al.*, 2009). Further investigation regarding the signalling of the LPI/GPR55 system in GPR55-HEK293 cells was conducted by Oka and colleagues (2010) who reported that LPI-induced GPR55 activation resulted in the activation of RhoA and ROCK and that downstream of this, the rapid phosphorylation of p38 mitogen-activated protein kinase (MAPK) and activating transcription factor 2 (ATF-2) took place.

1.1.4.3. *Activation of GPR55 by LPI in the cardiovascular system*

Al Suleimani and Hiley (2015) observed that the LPI/GPR55 system mediated endothelium-dependent relaxation of the rat mesenteric artery, an effect which involved the activation of the PLC-IP₃ pathway, RhoA-ROCK and intermediate conductance, Ca²⁺-activated, K⁺ channels (IK_{Ca}). In another study, it was reported that LPI induced a biphasic increase in [Ca²⁺]_i in EA.hy926 endothelial cells. The initial phase was GPR55-dependent, mediated by the activation of large conductance, Ca²⁺-activated, K⁺ channels (BK_{Ca}) and resulted in temporary membrane hyperpolarization. However, the second phase occurred independently of GPR55 and involved the activation of non-selective cation channels and inhibition of the sodium-potassium adenosine triphosphatase (Na⁺-K⁺-ATPase), culminating in sustained membrane depolarization (Bondarenko *et al.*, 2010). Additionally, Al Suleimani and Hiley

(2016) reported that LPI mediated a biphasic increase in $[Ca^{2+}]_i$ in human brain microvascular endothelial cells (hCMEC/D3), the first phase of which involved the activation of the PLC-IP₃ pathway and the latter, the activation of RhoA-ROCK. Taken together, the vascular data pertaining to the LPI/GPR55 system suggest that GPR55 may have a role in the control of vascular tone. In terms of GPR55 signalling in the heart, Yu and colleagues (2013) reported that LPI-induced GPR55 activation in cultured rat neonatal ventricular cardiomyocytes provokes distinct signalling pathways and cellular functions that are dependent on the cellular location of GPR55 i.e. at the sarcolemma or the membrane of intracellular organelles (discussed in detail in section 1.1.5.3.). Furthermore, studies investigating the role of LPI-induced GPR55 activation in the cardiovascular system have utilised exogenous LPI, however, it has been suggested that the endogenous source of LPI within the cardiovascular system is activated platelets at the site of atherosclerotic plaque rupture (Kurano *et al.*, 2015). For a diagram illustrating the proposed source of endogenous LPI release see Figure 1.5.

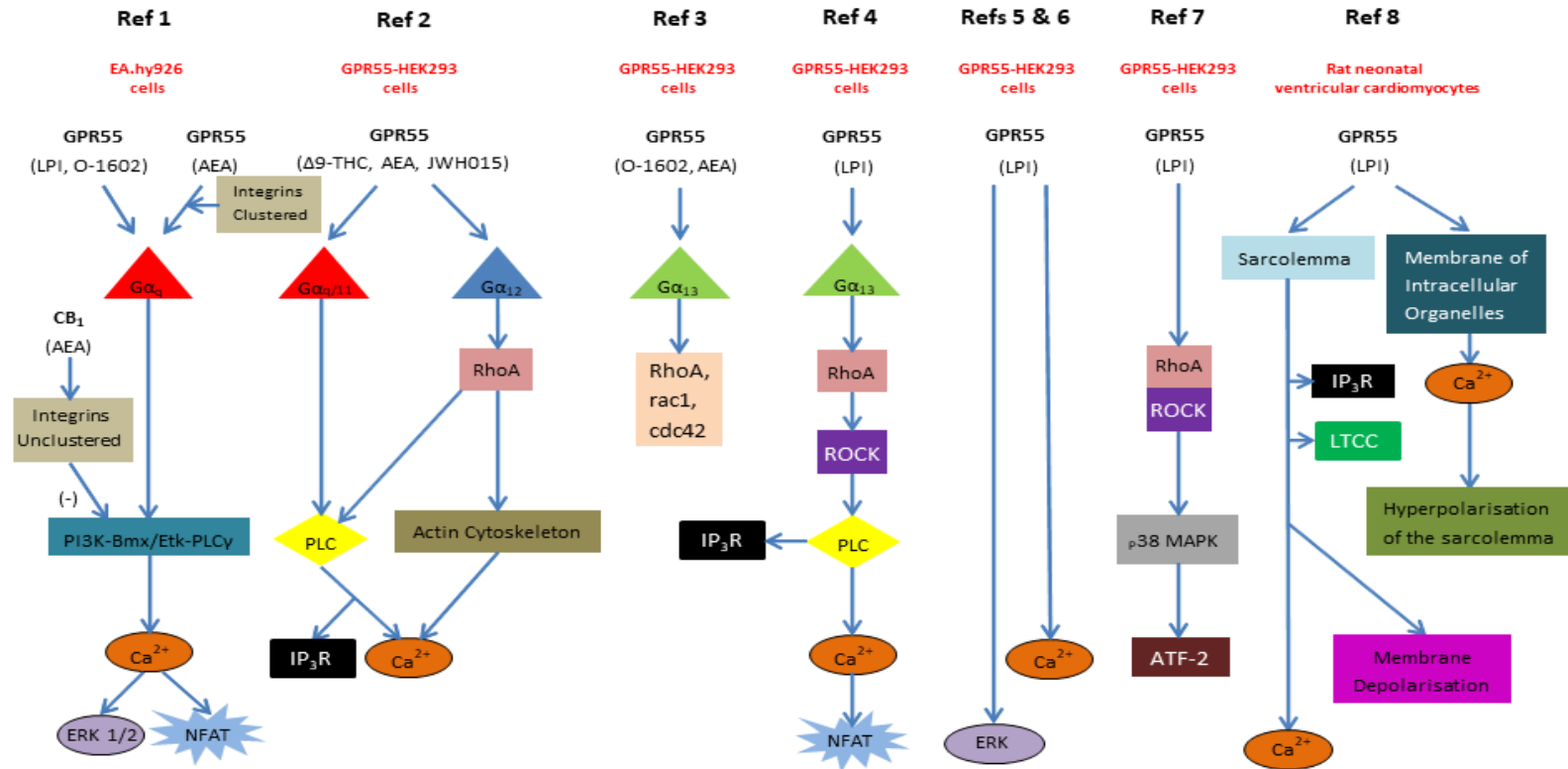


Figure 1.4. Signaling pathways of GPR55. AEA; anandamide, ATF-2; activating transcription factor 2, Ca^{2+} ; calcium, CB₁; cannabinoid receptor 1, cdc42; cell division control protein 42 homolog, EA.hy926; human umbilical vein derived endothelial cell line, ERK; extracellular signal-regulated kinase, GPR55-HEK293; human embryonic kidney cells expressing G-protein-coupled receptor 55, IP_3 R; inositol 1,4,5-trisphosphate receptor, NFAT; nuclear factor of activated T-cells, LPI; lysophosphatidylinositol, LTCC; L-Type calcium channel, p38 MAPK; p38 mitogen-activated protein kinase, PI3K-Bmx/Etk-PLC γ ; phosphoinositide 3 kinase-bone marrow kinase X-linked/epithelial and endothelial tyrosine kinase-phospholipase C gamma, PLC; phospholipase C, Rac1; Ras-related C3 botulinum toxin substrate 1, RhoA; Ras homolog gene family member A, ROCK; Rho-associated protein kinase and Δ^9 -THC; Δ^9 -tetrahydrocannabinol. The '?' symbolises that involvement of G_q in the study was neither confirmed nor excluded and '-' signifies an inhibitory effect. References (Refs) 1-8 refer to Waldeck-Weiermair *et al.*, 2008, Lauckner *et al.*, 2008, Ryberg *et al.*, 2007, Henstridge *et al.*, 2009, Oka *et al.*, 2007, Oka *et al.*, 2009, Oka *et al.*, 2010 and Yu *et al.*, 2013, respectively. Diagram modified from Ross, 2009.

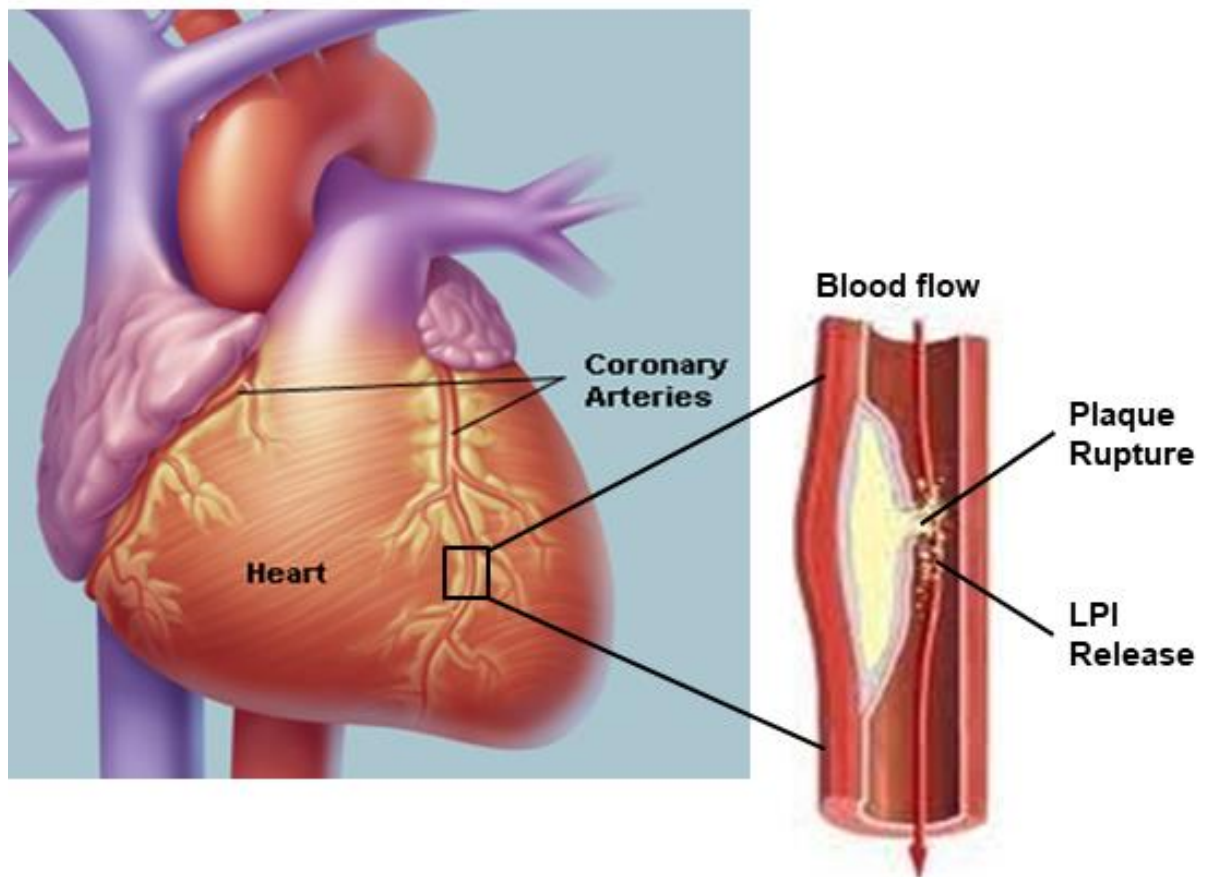


Figure 1.5. The proposed site of endogenous LPI release within the cardiovascular system. Endogenous LPI release from activated platelets at the site of atherosclerotic plaque rupture within a coronary artery. Heart diagram modified from WebMD®, 2017 and coronary artery diagram modified from Heart Diseases, 2017.

1.1.5. The role of GPR55 in physiology and pathophysiology

1.1.5.1. General overview

Many of the studies conducted on GPR55 have focussed on elucidating its pharmacological properties whilst searching for its endogenous ligand. However, a number of studies have provided insight into the physiological role of GPR55. For example, it has been demonstrated that GPR55 is involved in the regulation of colonic motility (Li *et al.*, 2013), has a role in regulating osteoclast number and function in bone physiology (Whyte *et al.*, 2009) and has a pro-inflammatory role in innate immunity (Chiurchiù *et al.*, 2015).

1.1.5.2. Metabolism and energy balance

Over recent years, an increasing number of studies have reported a function for GPR55 in energy metabolism. Romero-Zerbo and colleagues (2011) were first to publish on the role of GPR55 in the homeostatic control of glucose and documented that it could be a potential target for the management of type 2 diabetes and associated conditions as it was demonstrated that a GPR55 agonist (O-1602) mediated insulin release, in part through activation of GPR55 in isolated islets of Langerhans. Since this report, several studies have investigated the role of GPR55 in glucose homeostasis, the results of which have unanimously indicated that the activation of GPR55 by agonists (abnormal cannabidiol (Abn-CBD), AM-251, oleoylethanolamide (OEA), O-1602 and palmitoylethanolamide (PEA)) in islets of Langerhans stimulates insulin secretion (McKillop *et al.*, 2013; Liu *et al.*, 2016 and McKillop *et al.*, 2016).

An orexigenic action of GPR55 has also been suggested since O-1602 increases food consumption and adiposity in rats (Diaz-Arteaga *et al.*, 2012), although the augmented food intake was also evident in GPR55^{-/-} mice, suggesting that the orexigenic effects of O-1602 are likely to occur via actions independent of GPR55; indeed O-1602 is also a well described agonist of G-protein-coupled receptor 18 (GPR18; McHugh *et al.*, 2012 and Console-Bram *et al.*, 2014). However, it has been demonstrated that GPR55 and LPI are associated with human obesity as GPR55 mRNA expression is increased in both the visceral and subcutaneous adipose tissue of obese subjects when compared to lean subjects and even more so in obese subjects suffering from type 2 diabetes (Moreno-Navarrete *et al.*, 2012). Moreover, the concentration of circulating plasma LPI of obese subjects is increased and correlates with the body weight, fat percentage and the body mass index (BMI) of females.

Furthermore, this study revealed that LPI increases the expression of genes associated with lipogenesis in visceral adipose tissue and also increases $[Ca^{2+}]_i$ in differentiated visceral adipocytes.

GPR55 expression in gonadal fat and serum LPI levels are also affected by factors such as nutritional status, pregnancy and gender in rats (Imbernon *et al.*, 2014). In male mice fed a normal diet, GPR55 deletion leads to an increased fat mass (epididymal fat, inguinal fat and brown adipose tissue), insulin resistance and liver steatosis (Meadows *et al.*, 2016). Moreover, while a lack of GPR55 did not modify food consumption or feeding patterns of the mice, there was a reduction in their spontaneous and voluntary physical activity, implying that the reduced physical activity of GPR55^{-/-} mice results in diminished energy expenditure, which in turn, increases the ir adiposity. In contrast, a study in male GPR55^{-/-} mice fed a café diet (a normal chow diet with high fat diet options) reported no differences between the body weights or fat masses of WT and GPR55^{-/-} mice after short (2 months) or long term (7 months) feeding of this diet (Bjursell *et al.*, 2016). Moreover, GPR55^{-/-} mice fed normal chow exhibited only subtle reductions in both diurnal and nocturnal energy expenditure which led the authors to conclude that GPR55 does not appear to be a critical requirement for overall metabolism. With the exception of the latter study, reports suggest an important role for GPR55 in metabolism and energy balance, although further studies are required to gain a more comprehensive understanding of the role of GPR55 in these settings.

1.1.5.3. *GPR55 and cardiovascular physiology*

As previously mentioned, low levels of GPR55 mRNA expression in the human heart have been detected (Henstridge *et al.*, 2011) and immunostaining has demonstrated the presence of GPR55 in the murine heart (Walsh *et al.*, 2014). Despite this, little research has been carried out to investigate the role of GPR55 in cardiac physiology. As previously mentioned in section 1.1.4.3., Yu and colleagues (2013) reported that LPI-mediated GPR55 activation in cultured rat neonatal ventricular cardiomyocytes provokes distinct signalling pathways and cellular functions that are dependent on the cellular location of GPR55. Activation of GPR55 located on the sarcolemma increases $[Ca^{2+}]_i$ via Ca^{2+} influx through L-Type Ca^{2+} channels (LTCCs) and IP₃-dependent Ca^{2+} release. $[Ca^{2+}]_i$ is further enhanced by Ca^{2+} -induced Ca^{2+} release (CICR) via ryanodine receptors (RyRs) located on the membrane of the sarcoplasmic reticulum (SR). Despite the activation of GPR55 at the sarcolemma increasing $[Ca^{2+}]_i$, activation at this site mediates Ca^{2+} -independent membrane depolarisation. On the other hand, activation of GPR55 at the membrane of intracellular organelles promotes Ca^{2+} release via endolysosomal nicotinic acid adenine dinucleotide phosphate (NAADP)-sensitive two-pore

channels with $[Ca^{2+}]_i$ being further augmented by CICR via RyRs. The pathways triggered by the activation of GPR55 on the membrane of intracellular organelles converge consequently causing membrane hyperpolarisation. Together, these findings suggest that GPR55 may regulate cardiac function at two distinct cellular sites. To gain insight into the physiological role of GPR55 in cardiac function, Walsh and colleagues (2014) utilised pressure-volume loop (PVL) analysis to determine the cardiac function of GPR55^{-/-} mice at differing ages (see section 1.5.5. for further details).

1.2. Atherosclerosis

1.2.1. Overview

Coronary heart disease (CHD) is the umbrella term for diseases that arise when the walls of the coronary arteries become constricted by fatty deposits, otherwise known as atheroma. It is one of the principal causes of death in the United Kingdom with the most recent statistics published by the British Heart Foundation (BHF) revealing that CHD was responsible for 69,163 deaths in 2014; that is 15% and 10%, of all male and female deaths, respectively (Townsend *et al.*, 2015). Atherosclerosis, one of the main risk factors for CHD, is a multifactorial, chronic inflammatory condition characterised by endothelial dysfunction, hyperlipidaemia and the accumulation of fatty deposits (lesions or plaques) within the tunica intima of medium-to-large sized muscular arteries. Without intervention, this disease can prove fatal with patients suffering lethal myocardial infarction or stroke, depending on the artery affected.

1.2.2. Lipid homeostasis

The liver plays a key role in lipid homeostasis by stabilising the concentration of plasma cholesterol through two major pathways: 1) stimulation of the hepatic synthesis and release of cholesterol when the plasma concentration falls below the optimal physiological concentration, and 2) removal of cholesterol when it is present in excess in the plasma. Plasma cholesterol circulates as various lipoprotein complexes; chylomicrons i.e. triglycerides (TGs), very low density lipoprotein (VLDL), low density lipoprotein (LDL) and high density lipoprotein (HDL). In humans, LDL is the main carrier of cholesterol within the circulation and delivers it to the appropriate cell types throughout the body. HDL has an opposing function to LDL as it is responsible for the removal of surplus cholesterol by transporting its excess to the liver for conversion into bile salts. In a healthy individual, LDL and HDL

work in conjunction to maintain a homeostatic level of circulating cholesterol; thus if the concentration of one increases or decreases, the other adjusts accordingly (Widmaier *et al.*, 2006).

1.2.3. Hyperlipidaemia

Several lifestyle factors such as smoking (reviewed by Messner and Bernhard, 2014) and physical inactivity (Laufs *et al.*, 2005) increase the likelihood of developing atherosclerosis. Other risk factors for this condition include obesity, diabetes and hyperlipidaemia (reviewed by Rafieian-Kopaei *et al.*, 2014). Hyperlipidaemia is defined as an elevated concentration of one or more plasma lipids/lipoproteins (HDL excluded). Clinically, four plasma lipid/lipoprotein concentrations are typically reported when investigating the cholesterol status of a human; total cholesterol (TC), TGs, LDL and HDL, with normolipidaemic concentrations deemed as being less than 4, 1.7, 2 and more than 1 mmol/l, respectively (BHF, 2017). Consequently, maintenance of cholesterol homeostasis within the circulation is fundamental with regard to preventing or reducing the severity of atherosclerosis.

1.2.3.1. Vascular impact of hyperlipidaemia

Endothelial cells of the tunica intima serve to regulate its vascular tone in response to physiological and pathophysiological stimuli and do so by releasing agents capable of signalling to the smooth muscle cells of the tunica media, which in turn, trigger their contraction or relaxation accordingly. For example, an increase in blood flow within the tunica intima of an artery prompts endothelial cells to release vasodilators such as prostaglandin I₂ (PGI₂) and nitric oxide (NO) while reducing the secretion of the vasoconstrictor, endothelin-1 (ET-1), resulting in the relaxation of the arterial smooth muscle and consequently, dilatation of the artery (Widmaier *et al.*, 2006). In instances of hyperlipidaemia, there is an increased generation of reactive oxygen species (ROS) which consequently react with NO and reduce its bioavailability. Moreover, in this pathophysiological setting, ROS also interferes with the activity of endothelial nitric oxide synthase (eNOS), the enzyme primarily responsible for the generation of NO within the vascular endothelium, and impairs NO production (reviewed by Kim *et al.*, 2012). Consequently, endothelial dysfunction ensues and a pro-atherogenic environment is formed i.e. leukocyte adherence (Kubes *et al.*, 1991) and platelet activation (Schäfer *et al.*, 2004).

1.2.3.2. *Cardiac impact of hyperlipidaemia*

Prolonged hyperlipidaemia causes cellular lipotoxicity, which is characterised by an excessive accumulation of intracellular lipids and the over activation of lipid signalling pathways. Insulin resistance (Sheu *et al.*, 1993) and/or endoplasmic reticulum stress (Borradaile *et al.*, 2006) are just two examples of the cellular dysfunction that occur in response to lipotoxicity. With regard to cardiac lipotoxicity, myocardial lipid deposition occurs in instances where the uptake of fatty acids (FAs) exceeds oxidation (Chiu *et al.*, 2001). Consequently, there are excess FAs for non-oxidative metabolic pathways and the accumulation of FA metabolites such as ceramides (Park *et al.*, 2008), diacylglycerols (Basu *et al.*, 2009) and long-chain acyl-CoAs (Chiu *et al.*, 2001) which are toxic to cardiac cells as they cause inflammation, mitochondrial dysfunction, defective intracellular signalling and/or apoptosis (Drosatos and Schulze, 2013). TGs are also increased in instances of cardiac lipotoxicity (Zhou *et al.*, 2000), although it remains unresolved as to whether they are cytotoxic or simply a marker of cardiac lipotoxicity.

Myocardial fibrosis, defined as a significant increase in the collagen volume fraction (CVF) of myocardial tissue (Mewton *et al.*, 2011) also occurs in response to hypercholesterolaemia (Zhu *et al.*, 2007), resulting in electrical (McLenachan and Dargie, 1990; Kawara *et al.*, 2001), mechanical (López *et al.*, 2012) and vasomotor dysfunction (Schwartzkopff *et al.*, 2000), all of which provide the environment for progression to heart failure (reviewed in detail in Gyöngyösi *et al.*, 2017).

1.2.4. **The atherosclerotic plaque**

Endothelial dysfunction is generally regarded as the initiating factor in terms of atherosclerotic plaque development. In instances of such dysfunction, monocytes are encouraged to bind to the endothelial cells via adhesion molecules such as vascular cell adhesion molecule 1 (VCAM-1) and intercellular adhesion molecule 1 (ICAM-1). Monocyte chemoattractant protein 1 (MCP-1) then recruits these monocytes into the sub-endothelial space, where they subsequently develop into macrophages. Furthermore, LDL is transported via transcytosis across the endothelium into the sub-endothelial space where it binds to proteoglycans of the extracellular matrix and undergoes oxidation (ox-LDL). Macrophages of the vessel wall phagocytose the ox-LDL via endocytosis and consequently become lipid laden foam cells. The subsequent failure of macrophages to remove ox-LDL from the sub-endothelial space instigates their apoptotic death consequently releasing ox-LDL back into the vessel wall and releasing pro-inflammatory substances which degrade the extracellular

matrix (reviewed by Toth, 2008). For a diagram detailing atherosclerotic plaque development see Figure 1.6.

The progression and severity of an atherosclerotic plaque is influenced by a wide range of factors including gender (Lansky *et al.*, 2012), age (Van Oostrom *et al.*, 2005), activity level (Shimada *et al.*, 2007), smoking (Kangavari *et al.*, 2004), plaque composition (Kwon *et al.*, 2010) and the presence of systemic risk factors such as hypertension (Beaussier *et al.*, 2008). The American Heart Association (AHA) compiled two reviews which separated morphologically distinct lesions into different groups. These groups were categorised as follows: type I; the initial lesion, type II; the fatty streak, type III; the intermediate lesion, type IV; atheroma and, type V; fibroatheroma (Stary *et al.*, 1994 and Stary *et al.*, 1995). The latter review, which predominantly focussed on lesion types IV and V, further segregated type V lesions into subtypes; Va, Vb and Vc; the fibroatheroma, the calcified lesion and the fibrotic lesion, respectively. The same review also detailed that complications associated with lesion types IV and V can occur and may manifest as disruptions to the surface of the lesion, haematoma, haemorrhage and/or the deposition of a thrombus. The authors consequently defined a type VI lesion as a type IV or V lesion exhibiting at least one of the aforementioned complications.

1.2.4.1. *Vascular impact of atherosclerosis*

Sabaté and colleagues (1999) demonstrated that atherosclerosis affecting the coronary arteries varies according to the composition and location of the plaque and the latter two variables influence both the pattern and severity of vascular remodelling that is to follow. Moreover, it has been demonstrated in animal models such as the cynomolgus monkey (Armstrong *et al.*, 1985) and humans (Glasgow *et al.*, 1987) that during the early stages of plaque development, the diameter of the lumen remains unaffected due to positive remodelling of the artery wall. In such instances, the artery wall compensates for the plaque volume by bulging outwards, rendering blood flow through the artery unchanged. However, this positive remodelling cannot be sustained indefinitely but delays luminal compromise until a plaque inhabits approximately 40% of the internal elastic lamina (Glasgow *et al.*, 1987). From this point onwards, negative remodelling of the artery wall ensues and the plaque progressively encroaches on the area that the lumen would normally occupy. Consequently, this negative remodelling increases the shear stress at the proximal end of the stenosis and instigates a host of undesirable events such as angiogenesis, intraplaque haemorrhage(s) and an increase in the likelihood of plaque rupture (reviewed by Wang *et al.*, 2016).

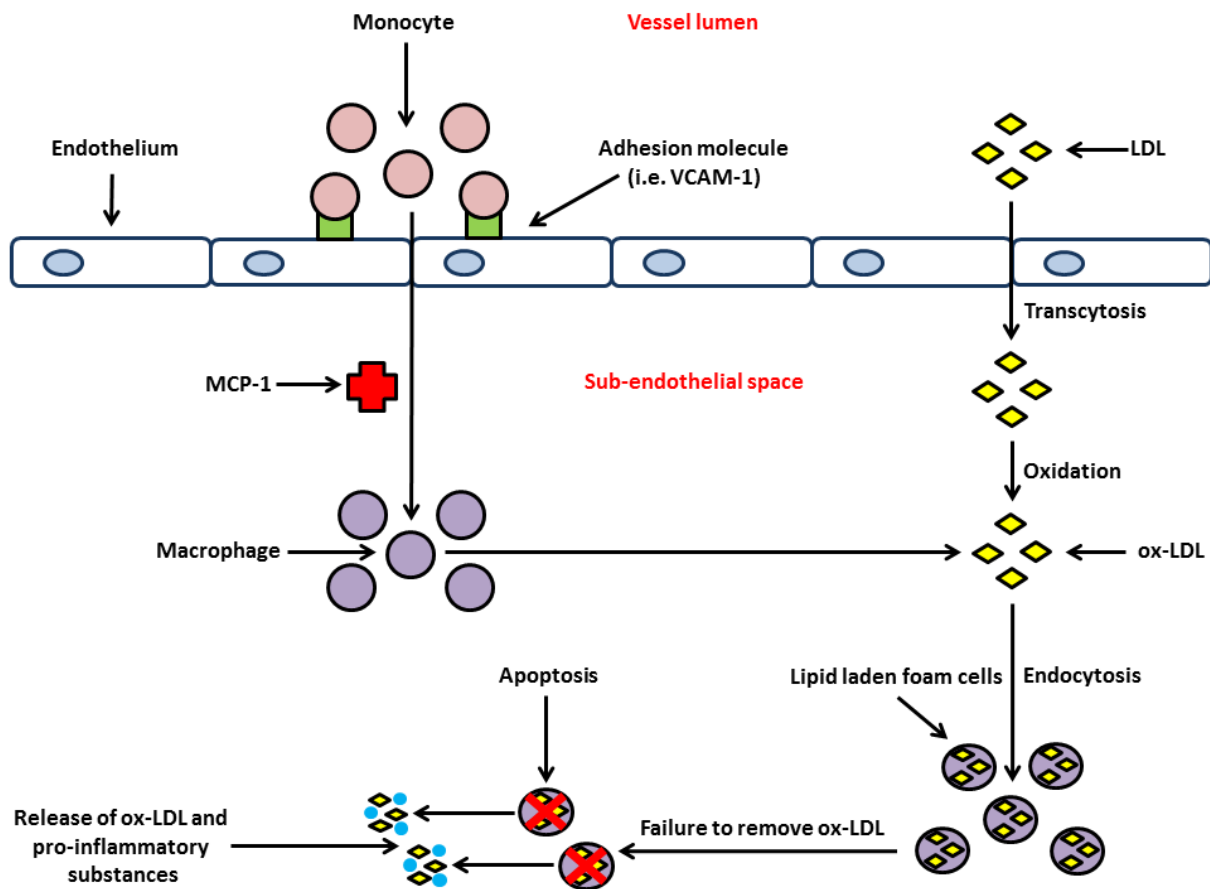


Figure 1.6. Atherosclerotic plaque development. In instances of endothelial dysfunction, monocytes are encouraged to bind to endothelial cells via adhesion molecules i.e. VCAM-1. MCP-1 consequently recruits these monocytes into the sub-endothelial space, where they develop into macrophages. LDL is transported via transcytosis across the endothelium into the sub-endothelial space where it binds to proteoglycans of the extracellular matrix and undergoes oxidation (ox-LDL). Macrophages of the vessel wall phagocytose the ox-LDL via endocytosis and consequently, become lipid laden foam cells. The subsequent failure of macrophages to remove ox-LDL from the sub-endothelial space instigates their apoptotic death consequently releasing ox-LDL back into the vessel wall and releasing pro-inflammatory substances which degrade the extracellular matrix. LDL; low density lipoprotein, MCP-1; monocyte chemoattractant protein 1, ox; oxidised and VCAM-1; vascular cell adhesion molecule 1.

1.2.4.2. *Cardiac impact of atherosclerosis*

In instances of atherosclerotic plaque formation where positive remodelling of a coronary artery wall can no longer be sustained and negative remodelling ensues, the flow of oxygen rich blood to the corresponding area of the myocardium becomes reduced. As a result, the myocardial oxygen demand exceeds supply. This condition is termed 'angina pectoris', three forms of which exist; stable, unstable and variant angina. Symptoms of angina include chest pain, breathlessness, sweating and nausea and is clinically detectable via an electrocardiogram (ECG) i.e. ST segment depression, if conducted during an angina attack (Levick, 2010).

1.2.5. **GPR55 and atherosclerosis**

To date, only two studies have been published on the role of GPR55 in atherosclerosis. The first study reported that the activation of GPR55 with O-1602, augmented ox-LDL-induced lipid accumulation and inflammatory responses, while reducing the efflux of cholesterol from human foam cells (Lanuti *et al.*, 2015), suggesting a pro-atherogenic role for this receptor. In contrast, in an *in vivo* model of atherogenesis, the GPR55 antagonist, CID16020046, mediated an increase in neutrophil activation and recruitment in the early stages of atherogenesis and degranulation in the later stages of atherosclerosis (Montecucco *et al.*, 2016), suggesting an anti-atherogenic role for GPR55. Considering that atherosclerosis is a multifactorial disease, these studies suggest a complex role for GPR55 in this condition and highlight the need for further investigation.

1.3. **Myocardial ischaemia**

The word ischaemia is derived from the Greek words 'isch' and 'haema' meaning 'restriction' and 'blood', respectively. Myocardial ischaemia occurs when there is an imbalance between myocardial oxygen demand and supply (Hoffman and Buckberg, 1978) and typically arises when the flow of oxygen rich blood through a coronary artery becomes restricted due to the development of an atherosclerotic plaque or the formation of a thrombus at the site of plaque rupture. Myocardial ischaemia manifests itself in a number of different ways, the critical events being a switch from aerobic to anaerobic metabolism resulting in adenosine triphosphate (ATP) depletion and a consequent reduction in contractile function, the build-up of metabolic end products, sarcolemmal disruption and cell swelling, myocardial necrosis, ion disturbances and arrhythmias.

1.3.1. Energy reduction-induced contractile dysfunction

In the normal myocardium, aerobic respiration takes place allowing for all three metabolic pathways (glycolysis, the tricarboxylic acid (TCA) cycle and oxidative phosphorylation) to function and generate ATP from the breakdown of fuel molecules. Briefly, fatty acids are transported in the form of acyl-Coenzyme A (CoA) to mitochondria which leads to the β -oxidation and release of acetyl-CoA, the latter then enters the TCA cycle, generating ATP, CO_2 and H_2O . In addition, glucose molecules undergo glycolysis, a metabolic pathway that breaks down each glucose molecule into two molecules of pyruvate. Upon entering mitochondria, pyruvate is converted to acetyl-CoA and CO_2 . The newly generated acetyl-CoA enters the TCA cycle producing ATP, CO_2 and H_2O (Sambandam and Lopaschuk, 2003).

As the TCA cycle and oxidative phosphorylation are only able to function under aerobic conditions, both pathways are inhibited during myocardial ischaemia. Fortunately, glycolysis can function anaerobically therefore making it the only pathway capable of producing ATP during ischaemic periods. However, this pathway on its own is inefficient with regard to ATP production as it only produces two ATP molecules per glucose molecule in comparison to the 38 molecules of ATP which are generated per glucose molecule during aerobic respiration (Widmaier *et al.*, 2006). This lack of energy consequently reduces the contractile function of the heart and depresses cardiac function. Additionally, under anaerobic conditions, pyruvate generated from glycolysis does not enter the TCA cycle and is converted to lactate which has deleterious cellular effects (discussed in section 1.3.2.).

1.3.2. Metabolite accumulation

The anaerobic respiration of cardiomyocytes triggers a cascade of biochemical and metabolic reactions which ultimately manifest in the intracellular accumulation of toxic metabolic end products. Under such conditions, the intracellular production of lactate increases, augmenting intracellular H^+ ($[\text{H}^+]_i$) (Khandoudi *et al.*, 1990), both of which occur proportionally to the restriction of blood flow (Neely *et al.*, 1975). Elevated $[\text{H}^+]_i$ reduces the intracellular pH (pH_i) of affected cardiomyocytes causing acidosis which inhibits cardiomyocyte myofibril contracture and protects the membrane permeability transition pore (MPTP) from opening and mediating damage (Halestrap, 1991). In an attempt to counteract the intracellular acidosis and maintain ion homeostasis, the sarcolemmal Na^+ - H^+ exchangers (NHX) each begin extruding a H^+ ion in return for the importation of a Na^+ ion. However, intracellular Na^+ ($[\text{Na}^+]_i$) consequently becomes elevated, causing each of the

sarcolemmal Na^+ - Ca^{2+} exchangers (NCX) to work in reverse mode to extrude 3Na^+ ions from the cell, in return for a Ca^{2+} ion. The NCXs working in reverse mode successfully reduce $[\text{Na}^+]_i$, however, the resultant importation of Ca^{2+} increases $[\text{Ca}^{2+}]_i$ and causes $[\text{Ca}^{2+}]_i$ overload (Piper *et al.*, 2004). See Figure 1.7. depicting the response of the cardiomyocyte to ischaemia.

1.3.3. Cell swelling and sarcolemmal disruption

The duration and severity of myocardial ischaemia are the two key factors which determine whether injury to a cardiomyocyte is 'reversible' or 'irreversible'. Either way, injury occurs as a transmural wavefront which begins in the subendocardium and extends towards the epicardium (Reimer *et al.*, 1977). For timescales regarding reversible and irreversible injury see Figure 1.8. Irreversible injury is characterised by many features including: 1) a reduced ATP concentration (<10% of control), 2) increased concentrations of H^+ , adenosine monophosphate (AMP), inosine (INO), lactate and alpha glycerol phosphate (αGP), 3) an increased osmolar load, 4) the termination of anaerobic glycolysis, 5) the swelling of mitochondria, and 6) sarcolemmal disruption (Jennings and Reimer, 1991). Sarcolemmal disruption occurs during myocardial ischaemia as a consequence of cell swelling caused by fluid uptake and an increase in the tissue's water volume (Tranum-Jensen *et al.*, 1981). There are two major consequences of this disruption; excessive Ca^{2+} entry which disturbs cellular metabolism and the leaking of cellular components into the extracellular space (Jennings and Reimer, 1981). Such consequences generally result in lethal injury manifesting as cell rupture and necrosis.

1.3.4. Cell necrosis

The homeostatic imbalance caused by ischaemia in cardiomyocytes ultimately causes cell death (necrosis) and prompts a local inflammatory response, the activation of endothelial cells, monocyte chemoattraction and infiltration (Anselmi *et al.*, 2004) and differs to apoptosis in that the latter is highly regulated, requires caspase activation and is a process that requires energy (Anselmi *et al.*, 2004). Furthermore, cell necrosis is generally associated with myocardial ischaemia and apoptosis with that of delayed myocardial ischaemia/reperfusion injury (discussed in section 1.4.2.). Interestingly, cell necrosis was originally reported as an unregulated process (Sun and Wang, 2014), however, studies over recent years have reported a programmed form of cell necrosis and coined it 'necroptosis' (reviewed by Oberst, 2016). Nevertheless, the extent to which necroptosis is involved during myocardial ischaemia still remains to be elucidated.

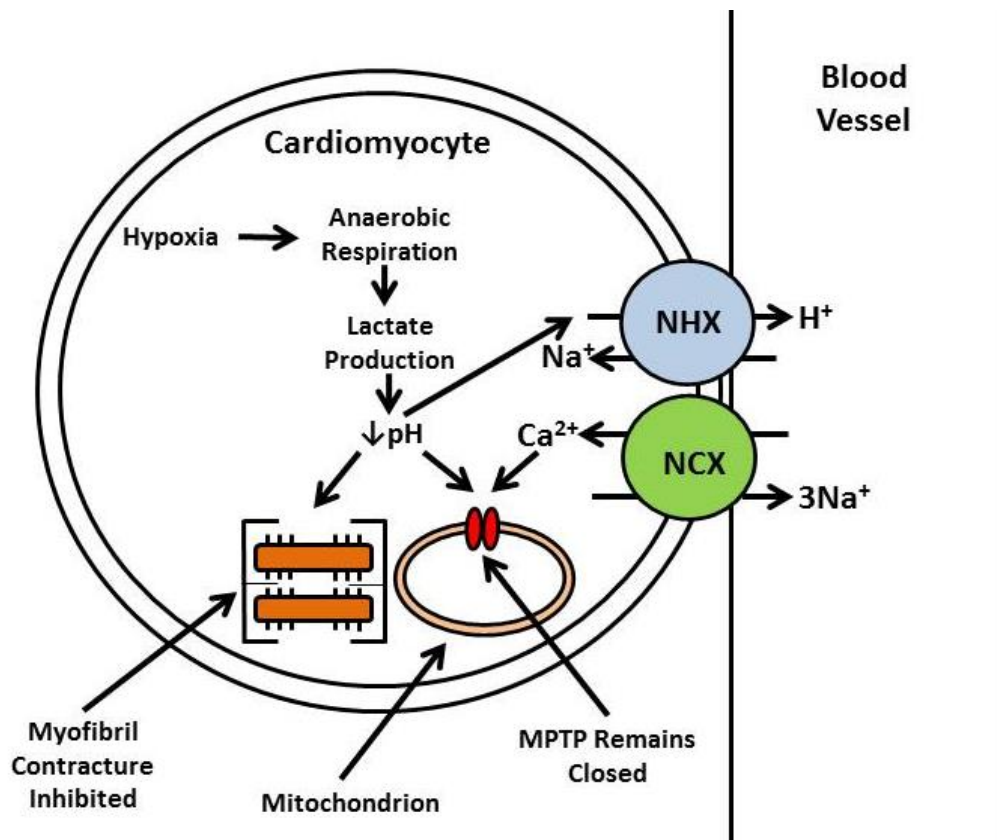


Figure 1.7. The response of the cardiomyocyte to ischaemia. During acute myocardial ischaemia, the lack of oxygen shifts cellular metabolism from aerobic to anaerobic respiration. This induces an increase in the intracellular production of lactate and a resultant reduction in the pH_i , the latter inhibiting myofibril contracture and preventing the MPTP pore from opening. To reduce the $[\text{H}^+]_i$, the NHX extrudes a H^+ ion in exchange for a Na^+ ion, however, this results in $[\text{Na}^+]_i$ overload. The $[\text{Na}^+]_i$ overload triggers the NCX to work in reverse mode to extrude 3Na^+ ions in exchange for a Ca^{2+} ion, however, $[\text{Ca}^{2+}]_i$ overload consequently ensues. Ca^{2+} ; calcium, H^+ ; hydrogen, MPTP; mitochondrial permeability transition pore, Na^+ ; sodium, NCX; Na^+ - Ca^{2+} exchanger, NHX; Na^+ - H^+ exchanger, pH ; potential of hydrogen and SR; sarcoplasmic reticulum. Diagram modified from Hausenloy and Yellon (2013).

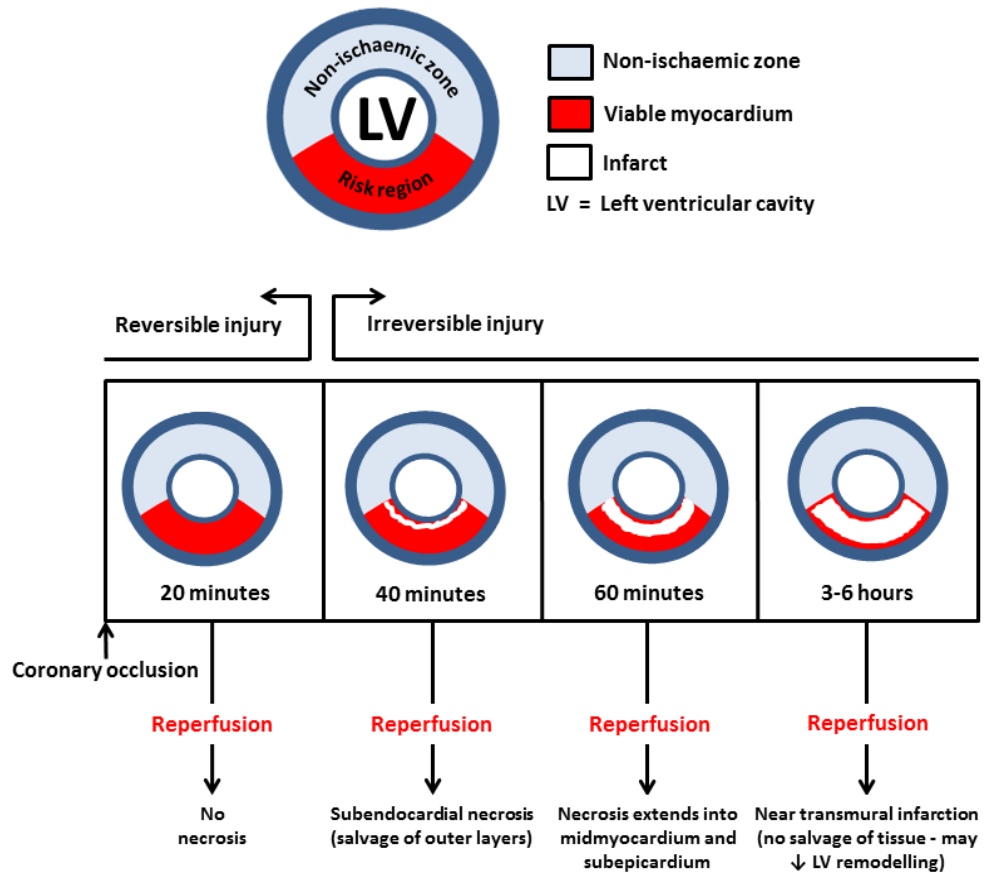


Figure 1.8. The wave front phenomenon of cardiomyocyte death in response to the duration of ischaemia. Cardiomyocyte death occurs as a transmural wave front which begins in the subendocardium and extends towards the epicardium. Reversible injury occurs in instances where the ischaemic period is less than 20 minutes (followed by reperfusion), whereas injury is irreversible with reperfusion at time points thereafter. Diagram modified from Kloner and Jennings (2001) and Kloner (2013).

1.4. Myocardial ischaemia/reperfusion Injury

While the reperfusion of an occluded artery is vital to salvage the myocardium affected by ischaemia, the re-introduction of blood and oxygen paradoxically causes further injury and cardiomyocyte death (Ferrari *et al.*, 2017). This phenomenon is termed myocardial ischaemia/reperfusion (I/R) injury and occurs in stages. Immediate “lethal” reperfusion injury occurs within the first few minutes of reperfusion and delayed reperfusion injury occurs over a period of several hours to days (Hausenloy and Yellon, 2013). Immediate I/R injury manifests itself in a number of different ways, the critical early events being an increase in oxidative stress, $[Ca^{2+}]_i$ overload, the restoration of the physiological pH, the normalisation of tissue osmolality, and the opening of the MPTP (summarised in Figure 1.9.), while delayed injury involves the activation of the complement system, resulting in neutrophil migration, adherence and activation. Moreover, apoptotic cell death also contributes to the loss of cardiomyocytes during delayed injury.

Reperfusion promptly reactivates aerobic respiration, the consequence being a ‘respiratory burst’ involving the rapid production of ROS (Zweier *et al.*, 1987). Such oxidants include superoxide anions ($O_2^{\cdot-}$), hydrogen peroxide (H_2O_2), hydroxyl radicals (OH^{\cdot}), and hypochlorous acid (HClO) (Kurian *et al.*, 2016), which are generated by xanthine oxidase, nicotinamide adenine dinucleotide phosphate (NADPH) oxidase and the mitochondrial electron transport chain (Mozaffari *et al.*, 2013). Suppression of the endogenous antioxidant defences (i.e. catalase and superoxide dismutase) during ischaemia (Mozaffari *et al.*, 2013) results in excessive amounts of ROS, inducing cellular damage via mechanisms such as protein denaturation (Zhou *et al.*, 2015), the activation of matrix metalloproteinases (MMPs) (Kurian *et al.*, 2016), and DNA damage (Zhou *et al.*, 2015). ROS production also triggers the opening of the MPTP which further contributes to cellular damage by instigating ROS-induced ROS release from the mitochondria (Zorov *et al.*, 2006).

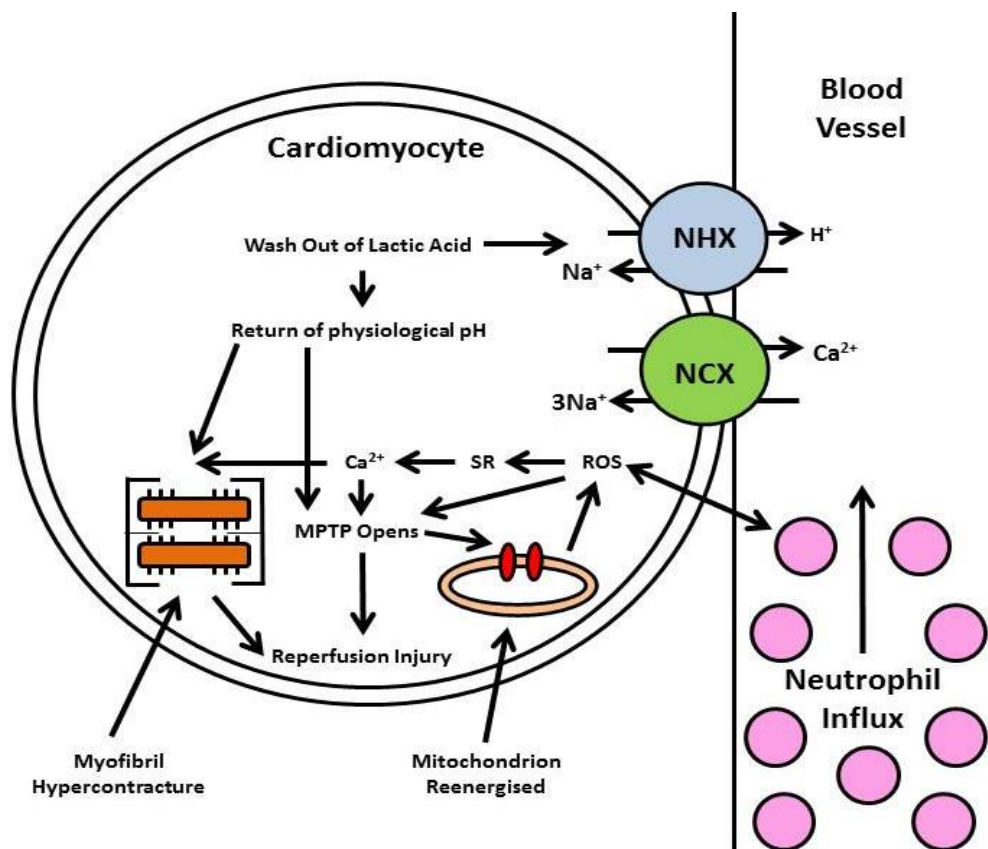


Figure 1.9. The response of the cardiomyocyte to reperfusion. During reperfusion, the pH_i of affected cardiomyocytes is rapidly restored by the washout of lactate and the activation of the NHX. Consequently, the acidosis-mediated inhibition on myofibril contracture and MPTP opening is lifted. Reperfusion also causes a ‘respiratory burst’ involving the rapid production of ROS. ROS act as a neutrophil chemoattractant and further promote the opening of the MPTP which in turn instigates ROS-induced ROS release from mitochondria. ROS also mediates dysfunction of the SR which contributes to $[Ca^{2+}]_i$ overload, promoting myofibril hypercontracture and MPTP opening, both of which lead to reperfusion injury. Ca^{2+} ; calcium, H^+ ; hydrogen, MPTP; mitochondrial permeability transition pore, Na^+ ; sodium, NCX; Na^+ - Ca^{2+} exchanger, NHX; Na^+ - H^+ exchanger, pH; potential of hydrogen, ROS; reactive oxygen species and SR; sarcoplasmic reticulum. Diagram modified from Hausenloy and Yellon (2013).

1.4.1. Mechanisms of immediate myocardial ischaemia/reperfusion injury

1.4.1.1. Oxidative stress

1.4.1.2. Intracellular Ca^{2+} overload

Myocardial ischaemia results in $[Ca^{2+}]_i$ overload which is partly due to ATP depletion-induced suppression of the sarcoplasmic/endoplasmic reticulum calcium-adenosine triphosphatase 2a (SERCA2a) and Na^+-K^+ -ATPase pumps, both of which are important for cellular ion homeostasis. However, upon reperfusion, reoxygenation leads to the reactivation of both SERCA2a and Na^+-K^+ -ATPase pumps (Murphy and Steenbergen, 2008). Consequently, cytosolic Ca^{2+} is driven into the SR by SERCA2a, reducing the $[Ca^{2+}]_i$. Despite this, cardiomyocytes may still suffer from $[Ca^{2+}]_i$ overload and in such instances, further Ca^{2+} extrusion from the cell is reliant upon the NCX working in forward mode. However, the NCX working in forward mode is dependent on $[Na^+]_i$, the homeostasis of which is maintained by the sarcolemmal Na^+-K^+ -ATPase pumps. In situations where the Na^+-K^+ -ATPase pumps have not been irreversibly damaged and $[Ca^{2+}]_i$ is restored to within the physiological range, cardiomyocyte myofibril hypercontracture may occur, consequently deforming the cytoskeleton and altering cell shape, causing irreversible cell shortening and cardiomyocyte death (Ladilov *et al.*, 1997).

1.4.1.3. Restoration of the physiological pH

The pH_i of affected cardiomyocytes is rapidly restored by the washout of lactate and the activation of the NHX upon reperfusion of the occluded coronary artery, thus lifting the acidosis-mediated inhibition of myofibril contracture. However, myofibril hypercontracture consequently ensues and severely distorts cell architecture, resulting in cell death (Hausenloy and Yellon, 2013).

1.4.1.4. Normalisation of tissue osmolality

As mentioned in section 1.3.2., anaerobic respiration of cardiomyocytes triggers a multitude of biochemical and metabolic reactions which ultimately manifest in the intracellular accumulation of toxic metabolic end products. The accumulation of such end products increases the osmotic load in both the intracellular and interstitial space (Grinstein *et al.*, 1992). Reperfusion consequently causes the rapid washout of the extracellular surplus of osmotically active molecules causing an osmotic gradient to form between the intra- and extracellular space (Garcia-Dorado and Oliveras, 1993). This,

in combination with $[\text{Na}^+]_i$ overload (mediated by the NHX) causes the influx of water into affected cells. Consequently, the intracellular pressure increases and stretches the sarcolemma of cells which have previously become fragile as a consequence of ATP depletion during ischaemia (Piper *et al.*, 1998). Cell rupture may occur as a consequence, however, this is dependent on the severity of cell swelling and cellular fragility. Also, hypercontracture can spread to adjacent cardiomyocytes via the passage of Na^+ through gap junctions from cardiomyocytes exhibiting hypercontracture and ruptured sarcolemma. The NCX also contributes to this propagation of hypercontracture by working in reverse mode and increasing $[\text{Ca}^{2+}]_i$ (Ruiz-Meana *et al.*, 1999).

1.4.1.5. *The opening of the mitochondrial permeability transition pore*

Under physiological conditions, the mitochondrial permeability transition pore (MPTP), a non-selective pore of the inner mitochondrial membrane is either not present or closed (Heusch *et al.*, 2010). However, under pathological conditions the MPTP opens and is permeable to any molecule with a molecular weight less than 1.5kDa (Halestrap *et al.*, 2004). Despite ischaemia being a pathological state, the MPTP remains closed (Griffiths and Halestrap, 1995) due to acidosis inhibiting its opening (Halestrap, 1991). Reperfusion restores the pH_i (Bond *et al.*, 1991) and increases the mitochondrial calcium concentration (Allen *et al.*, 1993 and Varadarajan *et al.*, 2001), both of which mediate the opening of the MPTP (reviewed by Halestrap *et al.*, 2004). Consequently, there is a sudden influx of water through the MPTP into the mitochondria resulting in mitochondrial swelling and rupture (Kalogeris *et al.*, 2012). Moreover, the opening of the MPTP mediates mitochondrial membrane depolarization and the uncoupling of oxidative phosphorylation, leading to a reduction in ATP and cell necrosis (Hausenloy and Yellon, 2013).

1.4.2. **Mechanisms of delayed myocardial ischaemia/reperfusion Injury**

Inflammatory responses are mediated by both the complement system and activation of the endothelium in response to the reperfusion of an occluded artery. Complement is "a system of serum and cell surface proteins that interact with one another and other molecules of the immune system to generate important effectors of innate and adaptive immune responses" (Abbas *et al.*, 2007 p. 494) that can be activated by three pathways; the classical pathway, the alternative pathway and the lectin pathway. Walsh and colleagues (2005) established that mice deficient in mannose-binding lectin, which are devoid of lectin pathway activation but have fully functional classical and alternative pathways, are protected from myocardial I/R injury and have preserved cardiac function.

It has also been established in mice, that complement component 5 (C5) which is involved in both the classical and alternative pathways of the complement system, is involved in the pathogenesis of myocardial I/R injury (Busche and Stahl, 2010). Together, these findings suggest the involvement of all three pathways in the development of such injury.

Under normal physiological conditions, endothelial cells form a protectant barrier against inflammation by preventing the activation of both neutrophils and platelets. However, during myocardial I/R injury, endothelial cells become activated. According to Hunt and Jurd (1998), there are five key changes associated with endothelial cell activation: 1) loss of vascular integrity, 2) the expression of leukocyte adhesion molecules, 3) a shift from an anti-thrombotic to pro-thrombotic phenotype, 4) an upregulation of human leukocyte antigen (HLA) molecules and, 5) the production of cytokines. Cytokines stimulate the expression of adhesion molecules (i.e. ICAM-1) on cardiomyocytes, consequently causing neutrophils to adhere to these cells (Smith *et al.*, 1991) and mediate injury. For an extensive review on the role of neutrophils in this type of injury see Hansen, 1995.

Programmed cell death, more commonly referred to as 'apoptosis', contributes to the loss of cardiomyocytes in the pathophysiological setting of myocardial I/R injury. Unlike necrosis, apoptosis is ATP-dependent (Leist *et al.*, 1997), highly regulated (Krijnen *et al.*, 2002) and does not mediate an inflammatory response in response to stimuli (Saraste and Pulkki, 2000). Additionally, due to apoptosis being energy dependent, it seems likely that the upsurge of apoptotic activity during reperfusion is due to the restoration of energy. Studies have established specific mediators of apoptosis associated with myocardial I/R injury such as caspase -3 and/or -9 (McCully *et al.*, 2004) and components of the complement system including C5a and C5b-9 (Vakeva *et al.*, 1998). Despite this, the exact role of apoptosis in myocardial I/R injury remains to be elucidated.

1.4.3. LPI and myocardial ischaemia/reperfusion injury

While the role of GPR55 in myocardial I/R injury has not been directly investigated, it has been demonstrated that the plasma concentration of total LPI increases two-fold (from 1.5µM to 3µM) in patients undergoing coronary angiography at the time of an acute coronary event (Kurano *et al.*, 2015). Moreover, in an experimental setting, a direct correlation between myocardial ischaemia and LPI release was observed in a rat model of asphyxia-induced cardiac arrest (Kim *et al.*, 2015a). In this study, the relative abundance of cardiac lysophospholipids was normalised to the content of the

corresponding phospholipids in the heart, revealing that the 18:0 species of LPI increased approximately six-fold. Moreover, resuscitation (reperfusion) significantly reduced the relative abundance of this LPI species. A later study by the same group using the same model (Kim *et al.*, 2016) demonstrated a 5.5 fold increase in the ratio of LPI (18:0 species) to phosphatidylinositol (PI; 18:0, 22:4 species) and that the LPI/PI ratio was proportional to the duration of the ischaemic period (up to 60 minutes). Together, this data raises the notion that measurement of LPI (18:0 species) in patients presenting with symptoms of myocardial infarction, may be an indicator of the duration of ischaemia that has preceded the point of intervention. However, further research is now required to investigate if LPI activates GPR55 in this pathophysiological setting and if so, what the consequence(s) of this may be.

1.5. Cardiac function

1.5.1. Excitation-contraction coupling

Excitation-contraction (E-C) coupling (reviewed by Bers, 2002) instigates the contraction of cardiac muscle through a number of intracellular events which are provoked by the electrical excitation of the cardiomyocyte. An action potential prompts Ca^{2+} movement over the cardiomyocyte membrane via LTCCs, which in turn activates the many RyRs located on the membrane of the SR, prompting CICR. Consequently, there is an increased concentration of cytosolic Ca^{2+} which binds to troponin C and instigates contraction by causing cross bridging of actin and myosin filaments.

With regard to cardiomyocyte relaxation (also reviewed by Bers, 2002), SERCA2a transports Ca^{2+} into the SR from the cytosol of the cell. To further reduce the cytosolic Ca^{2+} concentration, the NCX works in forward mode to expel a Ca^{2+} ion in exchange for 3 Na^{+} ions. Consequently, troponin C and Ca^{2+} unbind resulting in cell relaxation. See Figure 1.10. depicting the transport of Ca^{2+} in a ventricular cardiomyocyte.

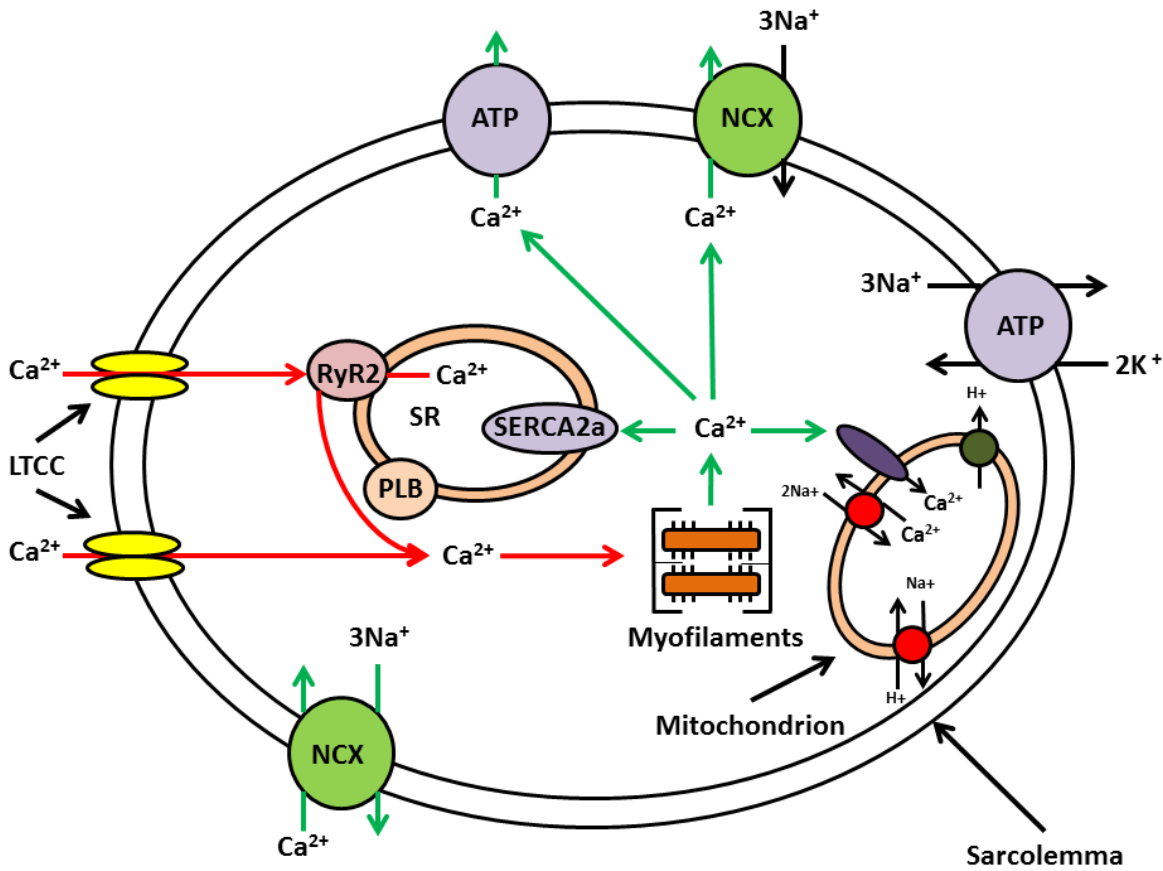


Figure 1.10. The transport of Ca^{2+} in a ventricular cardiomyocyte. With regard to cardiomyocyte contraction, an action potential triggers Ca^{2+} movement over the cell membrane via LTCCs, which in turn activates RyR2s located on the SR and prompts Ca^{2+} -induced Ca^{2+} release. This newly released Ca^{2+} , which is now in the cytosol of the cell, instigates contraction by binding to the myofilament protein troponin C, in turn causing cross bridging of actin and myosin filaments. In terms of cell relaxation, SERCA2a drives Ca^{2+} from the cytosol of the cell into the SR. To further reduce the cytosolic Ca^{2+} concentration, the NCX works in forward mode to extrude a Ca^{2+} ion in exchange for 3Na^+ ions. Ca^{2+} consequently becomes unbound from troponin C resulting in relaxation of the cell. ATP; adenosine triphosphate, Ca^{2+} ; calcium, H^+ ; hydrogen K^+ ; potassium, LTCC; L-Type Ca^{2+} channel, Na^+ ; sodium, NCX; Na^+ - Ca^{2+} exchanger, PLB; phospholamban, RyR2; ryanodine receptor 2, SERCA2a; sarcoplasmic/endoplasmic reticulum calcium-adenosine triphosphatase 2a and SR; sarcoplasmic reticulum. Diagram modified from Bers (2002).

1.5.2. Control of cardiac contractility

1.5.2.1. α_1 -adrenoceptor activation

The activation of α_1 -adrenoceptors in the vasculature indirectly contributes to the ventricles contracting with increased force (positive inotropy). Activation of α_1 -adrenoceptors causes this adrenoceptor subtype to couple to G_q , which activates PLC. PLC then splits phosphatidyl inositol bisphosphate (PIP_2) into IP_3 and diacylglycerol (DAG). IP_3 subsequently binds to IP_3 Rs causing Ca^{2+} release from the SR, increasing $[Ca^{2+}]_i$ and causing vasoconstriction. Vasoconstriction consequently increases afterload, therefore the ventricles have to contract with a greater force to maintain cardiac output (Levick, 2010). To do so, the sympathetic nervous system releases noradrenaline and/or adrenaline to activate β_1 -adrenoceptors on cardiomyocytes. An increased inotropic response consequently ensues, as detailed below.

1.5.2.2. β_1 -adrenoceptor activation

β_1 -adrenoceptors are the adrenoceptor subtype principally involved in cardiac contractility. Upon activation, their cytoplasmic domain has a high affinity for the G-protein, G_s . The subsequent release of this G-protein's α subunit activates adenylyl cyclase, catalysing the conversion of ATP to cyclic adenosine monophosphate (cAMP). cAMP has a number of actions including activating protein kinase A (PKA) in atrial and ventricular cardiomyocytes, which catalyses the phosphorylation of LTCCs, increasing their open state probability and duration, in turn augmenting the Ca^{2+} current and contributing to the inotropic response. In cardiomyocytes of the sinoatrial (SA) node, LTCCs are also phosphorylated by cAMP-induced PKA activation. The augmented Ca^{2+} current consequently accelerates the pacemaker potential decay and contributes to the chronotropic response. In terms of lusitropy, PKA (activated by cAMP) phosphorylates phospholamban (PLB), a protein which in the unphosphorylated state inhibits the uptake of Ca^{2+} into the SR by SERCA2a. The phosphorylation of PLB therefore reduces the inhibitory effect on SERCA2a thus increasing the uptake of Ca^{2+} into the SR and enhancing the rate of relaxation (positive lusitropy) (Levick, 2010).

1.5.3. The Frank-Starling principle

In instances of increased metabolic demand i.e. during exercise, the end-diastolic volume (EDV) of a ventricle increases causing the ventricle to expand, augmenting the ventricle's length-tension

relationship. Assuming all other factors remain constant, the ventricle consequently recoils with increased inotropy upon systole, resulting in a greater stroke volume (SV) – a relationship known as the Frank-Starling principle, which is imperative for maintaining cardiac output (CO). SV is also influenced by the degree of afterload (aortic pressure) which opposes the ejection of blood from the ventricle. In the absence of compensatory changes to enhance the inotropic response i.e. increased sympathetic activity, a greater afterload will reduce the SV and attenuate the CO (Levick, 2010).

1.5.4. Cardiac function in health and disease

In health, the heart functions at its optimal capacity, however, in pathophysiological settings such as hypertension, dyslipidaemia and post-myocardial infarction, cardiac function becomes altered.

1.5.4.1. Hypertension and cardiac function

Hypertension can progress to hypertensive heart disease (HHD) which encompasses a spectrum of abnormalities such as left ventricular (LV) hypertrophy, systolic and diastolic dysfunction, as well as their clinical manifestations i.e. arrhythmias (Drazner, 2011). In this disease state, LV hypertrophy typically occurs as a compensatory response in an effort to reduce LV wall stress. However, over time, LV dilatation occurs with a gradual decline in ejection fraction, leading to dilated heart failure. However, as with every disease, there is a considerable amount of inter-individual variability. HHD may therefore manifest itself differently in some patients but not others i.e. patients with this condition can develop ‘diastolic dysfunction’ or ‘heart failure with preserved ejection fraction’ as a consequence of extracellular matrix (ECM) remodelling and augmented LV filling pressures (Hoey *et al.*, 2014).

1.5.4.2. Dyslipidaemia and cardiac function

It is well established that hypercholesterolaemia is a risk factor for the development of endothelial dysfunction (Stokes *et al.*, 2002) and coronary heart disease (Castelli *et al.*, 1992), however, studies have demonstrated that hypercholesterolaemia can also impair cardiac function both *in vivo* (Huang *et al.*, 2004 and Varga *et al.*, 2013) and clinically (Dalen *et al.*, 2011), independently of coronary heart disease (CAD). Huang and colleagues (2004) conducted an in depth study and reported that in the absence of CAD, a diet high in cholesterol causes both systolic and diastolic function. This study also reported findings suggesting that such dysfunction is linked to an increase in the membrane

cholesterol content, a reduction in SERCA2a mRNA/protein expression and a reduction in the uptake of Ca^{2+} into the SR. Furthermore, hypercholesterolaemia reportedly mediates an increase in myocardial oxidative and nitrative stress, contributing to cardiac dysfunction (Csont *et al.*, 2007). The effects of dyslipidaemia on cardiac function vary from species to species - for a brief summary see Table 1.1.

1.5.4.3. *Post-myocardial infarction and cardiac function*

Cardiac dysfunction and heart failure are often observed post-myocardial infarction, although the extent of such dysfunction is dependent upon a number of variables including the degree of ischaemia, the duration of the ischaemic period, the degree of reperfusion injury and the extent of scar formation (reviewed by Minicucci *et al.*, 2011). Post-myocardial infarction, cardiac dysfunction may manifest itself as an increased susceptibility to ventricular arrhythmias due to disturbances in electrical conduction and ventricular stiffness due to scar formation. What's more, those who suffer from another health condition i.e. diabetes, and concurrently suffer a myocardial infarction, often have a worse prognosis (Mak *et al.*, 1997 and Donnan *et al.*, 2002). In contrast, an 'obesity paradox' exists whereby obese patients are often associated with improved short (Bucholz *et al.*, 2012) and long term (Bucholz *et al.*, 2016) survival post-acute myocardial infarction, however, the mechanisms by which this paradox occurs are not yet clear and remain to be elucidated.

1.5.5. **GPR55 and cardiac function**

To gain insight into the role of GPR55 in the control of cardiac function, previous work from this laboratory utilised both pressure volume loop (PVL) and histological analysis to examine cardiac function and cardiac morphology/composition in GPR55^{-/-} mice at 10 weeks (young) and 8 months (mature) (Walsh *et al.*, 2014). This study revealed that GPR55^{-/-} mice exhibit age-related systolic dysfunction and adverse ventricular remodelling, and assessment of cardiac reserve by the α_1/β_1 -adrenoceptor agonist, dobutamine, demonstrated that both young and mature GPR55^{-/-} mice exhibit maladaptive adrenergic signalling. Beyond this, no other studies have explored the role of GPR55 in cardiac function.

Lipid/ lipoprotein	Species	Gender	Diet	Impact	Method of measurement	Reference
↑TC, ↑LDL & ↓HDL	Human	Unreported	N/A	Systolic & diastolic dysfunction	Echocardiography & pulsed wave tissue Doppler imaging	Talini <i>et al.</i> , 2008
↑ TC, ↑LDL & ↓HDL	ApoE ^{-/-} mouse	Unreported	High fat (8 or 16 weeks)	Normal systolic function	Echocardiography	Hans <i>et al.</i> , 2011
↑TC	LDLR ^{-/-} ApoE ^{100/100} Mouse	Male & Female	High fat (3 months)	Severe systolic dysfunction	Echocardiography	Heinonen <i>et al.</i> , 2011
↑TC & ↑LDL	New Zealand Rabbit	Male	High fat (2 or 3 months)	Systolic dysfunction	Speckle-tracking echocardiography	Liu <i>et al.</i> , 2014

Table 1.1. The impact of dyslipidaemia on cardiac function. ApoE^{-/-}; Apolipoprotein E knockout, HDL; high density lipoprotein, LDL; low density lipoprotein and TC; total cholesterol.

1.6. Hypothesis

Over recent decades, it has been widely documented that obesity and diabetes are risk factors for the development of atherosclerosis. Given that the causative mechanisms by which atherosclerosis occur remain to be fully elucidated and that previous studies have demonstrated that GPR55 plays a role in obesity (Moreno-Navarette *et al.*, 2012), diabetes (Romero-Zerbo *et al.*, 2011) and the control of cardiac function (Walsh *et al.*, 2014), it is plausible that this receptor may play a role in atherogenesis. The present study was therefore carried out to firstly, elucidate any role of GPR55 in the cardiovascular remodelling and the cardiac function of mice suffering from atherosclerosis. Secondly, due to the plasma (Kurano *et al.*, 2015) and cardiac (Kim *et al.*, 2015a and Kim *et al.*, 2016) concentrations of LPI (the most widely reported agonist of GPR55) being increased in cases of myocardial ischaemia, an event often associated with atherosclerosis, the latter part of this study aimed to determine the role of GPR55 in myocardial I/R injury.

1.7. Objectives

The objectives of the present study were to test the following hypotheses:

1. GPR55 promotes atherogenesis by negatively affecting one or more of the following in the ApoE^{-/-} mouse model of atherosclerosis: endothelium-dependent relaxation of the carotid artery, plasma lipid profiles, lipid deposition within the thoracic aorta and/or the heart (Chapter 3). The involvement of GPR55 will be confirmed using the novel ApoE^{-/-}/GPR55^{-/-} mouse model of atherosclerosis.
2. GPR55 is detrimental to the cardiac function of ApoE^{-/-} mice (Chapter 4). This will be tested by conducting PVL analysis on ApoE^{-/-} and ApoE^{-/-}/GPR55^{-/-} mice which have been fed a normal or high fat chow diet for 12 weeks.
3. LPI activates mouse and human induced pluripotent stem cell-derived cardiomyocytes via a GPR55/ROCK/IP₃R-dependent signalling pathway (Chapter 5).
4. The exogenous administration of LPI to the isolated heart increases myocardial I/R injury via a GPR55/ROCK-dependent mechanism (Chapter 5).

Chapter 2:

General Methods

2.1. In vitro studies

2.1.1. Cell culture

2.1.1.1. Mouse and human induced pluripotent stem cell-derived cardiomyocytes

Mouse induced pluripotent stem cell (miPSC)-derived cardiomyocytes (Cor.At[®] CL-i cardiomyocytes; source tissue: mouse tail tip) and human induced pluripotent stem cell (hiPSC)-derived cardiomyocytes (iCell[®] cardiomyocytes; batch number: 1099441) were seeded (7,500 and 12,000 per well, respectively) in an Epic[®] 384 well, fibronectin coated, cell assay microplate (Corning Life Sciences, UK) using a Multi-drop Combi cell dispenser (Thermo Electron Corporation, UK). miPSC and hiPSC-derived cardiomyocytes were cultured in Dulbecco's Modified Eagle's Medium (DMEM) and incubated at 37°C in a 5% CO₂ atmosphere for 7 days and 12 hours, respectively until a cell monolayer had formed and the cells had reached a confluent state of 80-100% per well. As miPSC-derived cardiomyocytes had been genetically modified (prior to purchase) to be resistant to the antibiotic puromycin (resistance gene driven by the Myh6 (alpha-myosin heavy chain, α MHC/Myh6) promoter), the latter (10mg ml⁻¹) was included in DMEM to prevent the growth of any cell type other than miPSC-derived cardiomyocytes. With regard to the hiPSC-derived cardiomyocytes, the company from which they were purchased provided assurance that such cardiomyocytes were a 95% pure population of ventricular, atrial and nodal cells.

2.1.2. Corning[®] Epic[®] technology

Corning Epic[®] technology is a label-free and non-invasive, high throughput screening method for the identification of compound hits on different cell types. Using this technology, receptor activation can be identified by the optical detection of dynamic changes in cellular density (dynamic mass redistribution; DMR), a variable measured in real time following the application of a compound. Changes in the DMR activity of cells is indicated by a change in wavelength (Figure 2.1.).

The microplate containing the cultured miPSC or hiPSC-derived cardiomyocytes and the microplate containing the relevant compounds (compound source plate) to be added to the cardiomyocytes were incubated in the Epic[®] System (Corning[®], UK) at 26°C for 1 hour. This allowed the compounds on the source plate and the cells on the microplate to reach thermal equilibrium prior to the compounds being added to the appropriate wells of the microplate; a step intended to minimise the effect of temperature on assay variability. The wells of the compound source plate contained increasing

concentrations of GPR55-related ligand(s) and compounds that may inhibit GPR55's signalling pathways. Baseline readings were recorded every minute for a 3-minute period, the microplate removed and the relevant compounds from the source plate added to the appropriate wells of the microplate using a Biomek[®] NM^P laboratory automated workstation (Beckman Coulter, Sweden). The microplate was then reinserted into the Epic[®] System and the DMR activity of the cells within each well recorded at 1-minute intervals over a 90-minute period. These studies were performed in the laboratories of AstraZeneca (Mölndal, Sweden). Due to time constraints, Dr Erik Ryberg performed the study with the hiPSC-derived cardiomyocytes, but I was responsible for analysing and interpreting the data generated from these experiments.

2.2. *In vivo* studies

2.2.1. Animal ethics and husbandry

Studies undertaken were in accordance with the Animals (Scientific Procedures) Act 1986 under the Home Office project license number (PPL) 60/4231 and the personal license number (PIL) 60/13552. Prior to the commencement of experiments, a research ethics: student and supervisor appraisal (RESSA) form was submitted to and approved by the animal ethics committee of Robert Gordon University (RGU). Mice were bred and/or housed at the Medical Research Facility (MRF), University of Aberdeen, UK where they were grouped according to their gender and genotype and housed in temperature and humidity (19-23°C and 45-65%, respectively) controlled rooms on a 12-hour light/dark cycle (7am-7pm). The mice were housed according to the husbandry guidelines set by the UK Home Office in groups not exceeding eight with unlimited access to water and food in pellet form. In addition to mice being housed at the MRF, all dietary intervention studies and EchoMRI[™] body scanning studies were conducted there also. Mice were transported from the MRF to RGU at the start of the week where all *in vivo/ex vivo* experimentation took place. Mice were housed at RGU for a maximum of 5 days and allotted a minimum period of 30 minutes to acclimatise to their new surroundings prior to the commencement of any experiments. All *in vivo* work in this document is reported in accordance with the ARRIVE guidelines (Kilkenny *et al.*, 2010).

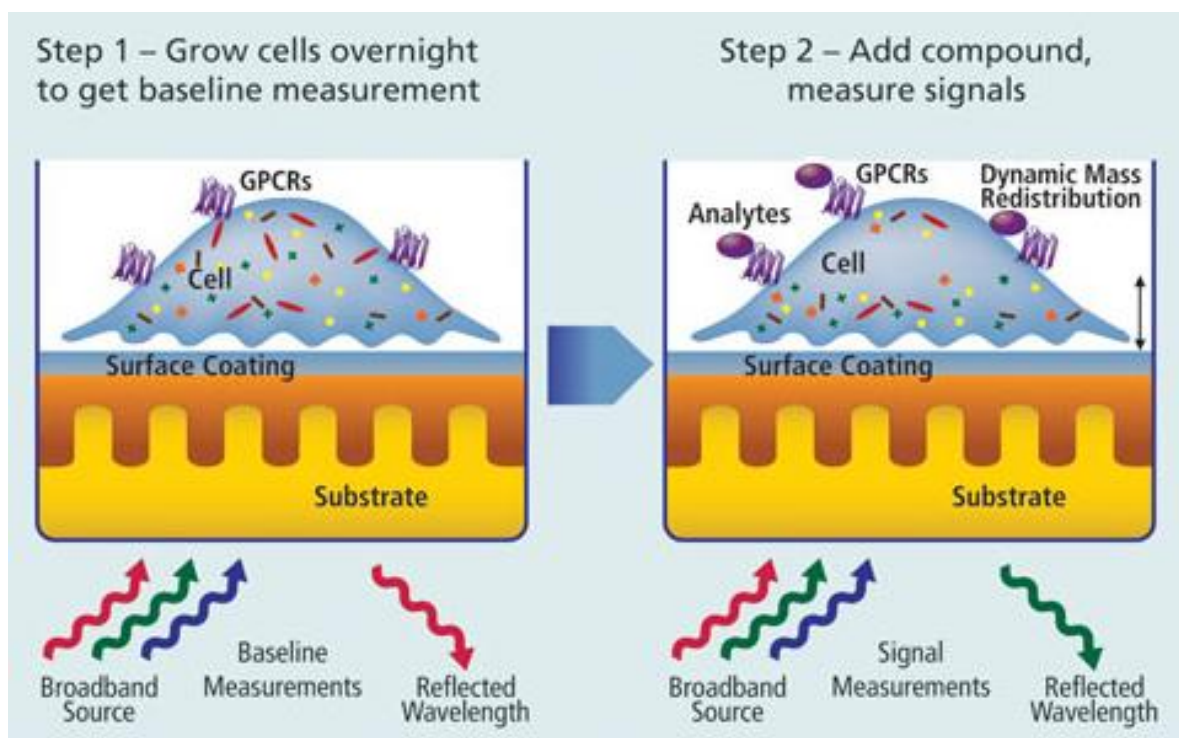


Figure 2.1. The methodology of Corning® Epic® Technology. Diagram from Genetic Engineering & Biotechnology News (GEN, 2017).

2.2.2. Breeding program

2.2.2.1. Strains

All strains of mice utilised were on the JAX background. C57BL/6 and apolipoprotein E knockout (ApoE^{-/-}) mice were purchased from Charles River Laboratories International Inc. (Margate, UK) and housed at the MRF, where a breeding colony of ApoE^{-/-} mice was established. Homozygous GPR55 knockout (GPR55^{-/-}) mice were obtained from an existing colony maintained at the MRF under PPL 60/4231. Furthermore, heterozygous double knockout (ApoE^{-/-}/GPR55^{+/-}) breeding pairs were kindly gifted (under a material transfer agreement) to RGU by AstraZeneca (Mölndal, Sweden) and inter-bred at the MRF to generate a colony of homozygous ApoE^{-/-}/GPR55^{-/-} mice. Mice from the different colonies were bred in advance of when they were scheduled for use.

2.2.2.2. Genotyping protocol

Genotyping of mice was conducted according to a protocol developed by AstraZeneca. In brief, DNA was isolated from mouse ear clips using a QIAmp[®] DNA Mini Kit as per manufacturer's instructions. Polymerase chain reaction (PCR) was subsequently carried out using a mix of the isolated DNA (50-100ng/μl) from each mouse, REDtaq[®] ReadyMix[™] PCR Reaction Mix, sterile H₂O and primers (at a final concentration of 2μM) directed at the gene mutations for ApoE or GPR55 (Table 2.1.). The ApoE and GPR55 PCR samples were then subjected to various cycles (Table 2.2.) in the thermocycler (Biometra, Germany) and run at 123V for 60 minutes on 1.6% agarose gels (all contained GelRed[™] nucleic acid gel stain and were made up with UltraPure[™] TBE buffer) against a PCR marker in electrophoresis tanks containing TBE buffer. Gels were photographed using fluorescent imaging (Peqlab Ltd, UK) and genotypes determined according to the band size(s) present (Table 2.3.).

2.2.3. High fat dietary intervention

Control groups of male and female C57BL/6 (wildtype; WT), ApoE^{-/-} (model of atherosclerosis), GPR55^{-/-} and ApoE^{-/-}/GPR55^{-/-} mice, aged 4-7 weeks were fed pellets of CRM (P) chow (normal chow; NC) for 12 weeks. In the high fat feeding groups, age-matched mice of both genders were fed pellets of Western diet R638 semi-synthetic feed containing 0.15% cholesterol and 21% fat (high fat chow; HFC) for the 12 week period (for the full nutritional details of the NC and HFC diets see Chapter 3, Figures 3.1. and 3.2., respectively).

Primer Sequences	
ApoE	GPR55
5'- CAGAAAGCGAAGGAGCAAAG - 3'	5'- ATGCGGAATTCCTGTTACCCA - 3'
5'- AAAAAGCTCGGGATGAGCCTT - 3'	5'- CACCCTAGGGCCTCAGTTGTA - 3'
5'- CAGCTCCCTCTCCTAGGGTT - 3'	5'- GGAAAGCTGAGATACAGACTT - 3'

Table 2.1. ApoE and GPR55 primer sequences for the genotyping of mice.

Name of Cycle	ApoE Protocol			GPR55 Protocol		
	No. of Cycles	Temp (°C)	Time (sec)	No. of Cycles	Temp (°C)	Time (sec)
Initialisation	1	95	120	1	94	120
Denaturation	28	95	30	30	94	30
Annealing	28	60	30	30	60	30
Extension/elongation	28	68	120	30	72	60
Final elongation	1	68	600	1	72	420

Table 2.2. PCR thermocycler sequence for the genotyping of mice with gene mutations for ApoE and GPR55. °C; degrees Celsius and sec; seconds.

Genotype	Band size (bp)
WT	288
ApoE ^{-/-}	462
ApoE ^{+/-}	288 & 462
WT	330
GPR55 ^{-/-}	550
GPR55 ^{+/-}	330 & 550

Table 2.3. Genotypes of mice according to band size(s) present in gels. bp; base pairs.

2.2.4. Measurement of cardiodynamics

2.2.4.1. Pressure-volume loop analysis

Pressure-volume loop (PVL) analysis is based on the principle that blood volume is directly proportional to its electrical conductance, or inversely proportional to its resistance. A pressure-tipped conductance catheter (Figure 2.2.) is composed of four platinum electrodes which are arranged in two pairs and a pressure sensor which is situated between each. Upon insertion of a conductance catheter into the left ventricle (LV), the proximal and distal electrode pairs should be located under the aortic valve and at the apex of the LV, respectively. The proximal electrode pair emit a constant current signal which flows to the distal electrode pair, consequently generating an electric field within this chamber. The cardiac cycle induces changes in the resistance of the blood pool within the LV accordingly and the electrodes of the catheter detect the resultant voltage potentials which are inversely proportional to the volume of the LV. During the cardiac cycle, the catheter simultaneously measures pressure changes within the LV. Data are collected and processed in real time by a computer software program (LabChart; ADInstruments, UK) which generates PVLs for cardiac function to be accurately assessed.

2.2.4.2. Surgical procedure for pressure-volume loop analysis

Mice were anaesthetised with a mixture of 120mg kg⁻¹ ketamine & 16mg kg⁻¹ xylazine via intraperitoneal (i.p.) injection. Monitoring of anaesthesia was achieved by conducting the pedal withdrawal reflex test every 15 minutes and, if necessary, maintained by the i.p. administration of 50µl 25g⁻¹ (body weight) of the anaesthetic mixture. All surgical procedures were performed using aseptic techniques, which included swabbing the skin with 70% ethanol prior to incision. In advance of any surgery, the tidal volume (ml) and respiratory rate (bpm) of the mouse was calculated according to the equations below and the ventilator (Harvard small animal respiration pump; Edenbridge, Kent, UK) adjusted accordingly.

$$\text{Tidal Volume} = 6.02 \times \text{Mass}^{1.01} \text{ (kg)}$$

$$\text{Respiratory Rate} = 53.5 \times \text{Mass}^{-0.26} \text{ (kg)}$$

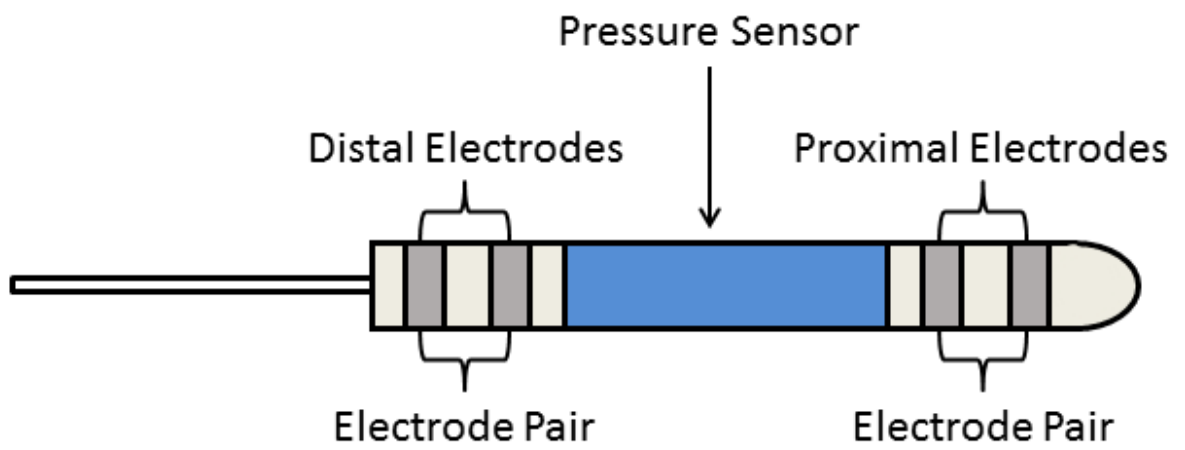


Figure 2.2. Diagram of a pressure-tipped conductance catheter.

All mice were artificially ventilated via tracheostomy. Furthermore, throughout each experiment, core body temperature was maintained at 37-38°C using a Vetcare heat pad (Harvard Apparatus Ltd, UK) in conjunction with a rectal probe (Fisher Scientific Ltd, UK). Following an incision in the neck, the right jugular vein was cannulated with a saline-filled heat-stretched cannula (Portex polythene tubing (internal and outer diameter; 0.58mm and 0.96mm, respectively); Smiths Medical International Ltd., Hyde, Kent, UK) and secured in place using size 5/0 silk suturing thread (InterFocus LTD, UK) for future saline/drug administration. The chest wall was subsequently cut either side of the xiphoid process to expose the underside of the diaphragm. During this procedure, blood loss was minimised by the use of a cauteriser (Interfocus LTD, UK). The pericardium was then removed and a piece of size 5/0 silk suturing thread (InterFocus LTD, UK) placed loosely around the inferior vena cava (IVC) for its later partial occlusion. To measure indices of cardiac function, the apex of the LV was punctured using a 27 gauge (G) needle to allow for smooth insertion of the 1.4-Fr pressure-tipped conductance catheter (SPR-839; Millar Instruments, USA) into this ventricle (pressure and volume calibrations of the catheter were conducted prior to commencing each experiment via the MPVS-Ultra Single Segment Foundation System (Millar Instruments, USA)). The placement of the catheter was adjusted until the largest stroke volume on the PVL recording software (LabChart) was observed. PVL data was recorded for the duration of each experiment and analysis later conducted using PVAN *Ultra*[™] software (Millar Instruments, USA).

2.2.4.3. *Parallel conductance*

Parallel conductance refers to the conductance of the cardiac muscle enveloping the blood pool of the LV. Ideally, the current applied through a catheter's electrodes should only flow through the blood, however, some of this current radiates into the surrounding cardiac muscle, which is also a conductor. Consequently, this often leads to an overestimation of the LV blood volume. To acquire the absolute LV volume measurements in the present study, the blood conductance within the LV was measured (calibrated conductance) and the contribution of the ventricular wall (parallel conductance; V_p) subtracted from the calibrated conductance. The V_p for each mouse was calculated by conducting a saline calibration during each experiment. This involved administering a bolus of saline (0.9% NaCl; 10 μ l) to each mouse at the start of an experiment via the pre-inserted cannula in the right jugular vein. The PVLs generated during this calibration were subsequently exported into PVAN *Ultra*[™] software and the V_p value for each mouse automatically generated.

2.2.4.4. *Post-experimental volume calibration of the PVL catheter*

During the PVL experiments, blood volume was measured in relative volume units (RVU) therefore blood volume had to be converted from RVU to μl at the time of data analysis. For accuracy, volume calibration of the PVL catheter was conducted once per mouse group. To do this, a calibration cuvette containing wells of known diameters (Millar instruments, USA) was warmed on a Vetcare heat mat (Harvard Apparatus Ltd, UK) for 20 minutes (37°C). On completion of the *in vivo* protocol, blood was collected via cardiac puncture and the wells of the cuvette immediately filled with this blood. The catheter was then placed in each well for 5-10 seconds during which time the MPVS-Ultra Single Segment Foundation System recorded changes in conductance. Subsequently, the conductance output (RVU) of each well was correlated with the known volume of the associated well using the MPVS-Ultra Single Segment Foundation System and converted to μl .

2.3. ***Ex vivo* studies**

2.3.1. **Tissue harvest**

Upon completion of the *in vivo* PVL procedure, blood was withdrawn from each mouse via cardiac puncture of the ventricles using a 29G needle, collected in an Eppendorf containing heparinised saline (0.9% NaCl; final heparin concentration of 20U ml^{-1}), inverted twice to mix the blood and heparin and the mixture centrifuged at 13,000 revolutions per minute (rpm) for 3 minutes (room temperature). The plasma fraction was then removed, transferred to an Eppendorf which was snap frozen in liquid nitrogen and stored at -80°C for future plasma lipid profiling. The heart was excised, the atria removed, the ventricular tissue weighed, snap frozen in liquid nitrogen and stored at -80°C for future cryosectioning and histological staining. Post blood extraction, the carotid arteries were removed and stored in Krebs' Henseleit solution (KHS; 119mM NaCl, 4.7mM KCl, 1.18mM KH_2PO_4 , 2.41mM MgSO_4 , 25mM NaHCO_3 , 2.52mM CaCl_2 and 10.88mM $\text{C}_6\text{H}_{12}\text{O}_6$) overnight (4°C) for small-vessel myography experiments the following day. Following the harvesting of the carotid arteries, the abdomen was cut longitudinally for the liver, spleen, kidneys and abdominal fat to be removed and weighed. These tissues were then snap frozen in liquid nitrogen and stored at -80°C for future analysis. To determine fatty streak deposition, the thoracic aorta was dissected, cleaned thoroughly and stored in 10% neutral buffered formalin (Formal FixxTM; Thermo Scientific, UK) prior to staining.

2.3.2. Plasma lipid analysis

Analysis of the plasma lipid fraction of blood was carried out using a Konelab 30 discrete clinical analyser (Thermo Scientific, UK). The analyser was calibrated with standards for HDL, LDL, TGs and TC prior to plasma samples (60µl) being placed inside the analyser. Pre-programmed lipid profiling assays were then conducted to detect the aforementioned lipid concentrations (mmol/l) within each sample.

2.3.3. Small-vessel myography

The purpose of conducting small-vessel myography on the murine carotid artery was to assess the endothelial and smooth muscle function of these vessels. Prior to experimentation, the force transducers of the dual wire myograph system; Model 410 A (Danish Myo Technology, Denmark) were calibrated using a 2g weight. One carotid artery ring (mean diameter; $296.6 \pm 6.1 \mu\text{m}$) was subsequently mounted between each jaw of the myograph chamber (containing KHS) by inserting two intra-luminal wires (Tungsten; $40 \mu\text{m}$) and manoeuvring either end of these wires underneath the corresponding screw and tightening it (Figure 2.3.). Moreover, isometric tension was recorded throughout each experiment using a PowerLab in conjunction with LabChart software (both ADInstruments, UK). Carotid arteries were first normalised to the target transmural pressure of 100mmHg (13.3kPa) by gradually increasing the distance between the intra-luminal wires. Vessels were then left to stabilise for 45 minutes prior to sensitisation with potassium chloride (KCl) solution (80mM) which was subsequently washed out of the myograph chamber using KHS (process repeated 3 times). Following sensitisation to KCl, the rings were left for 15 minutes to allow time for vessels to recover prior to experimentation.

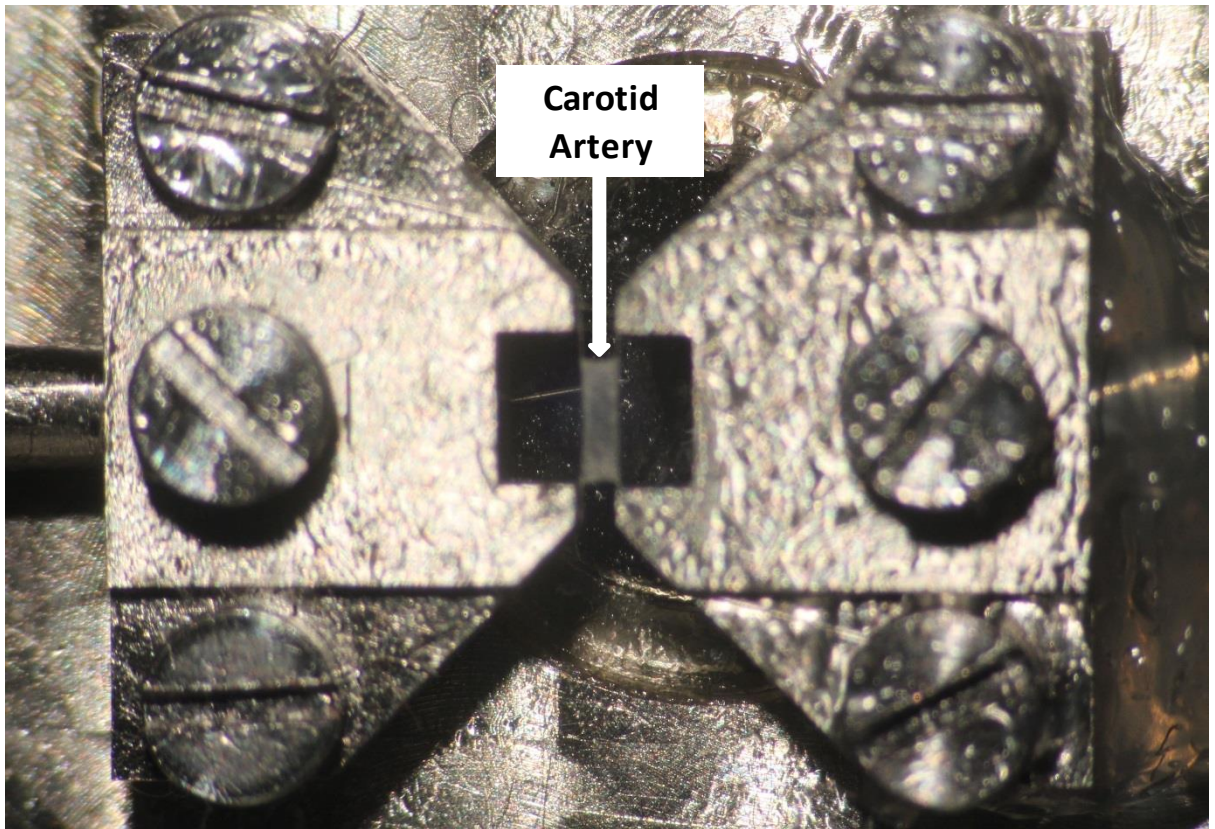


Figure 2.3. Dual wire myograph system. Carotid artery ring mounted to the system via intra-luminal wires.

2.3.4. Histology

2.3.4.1. Oil Red O staining of the thoracic aorta

Oil Red O (ORO), a lysochrome diazo dye, was used to stain for lipid deposition within the lumen of thoracic aortae (Figure 2.4.). 1% ORO stock solution was prepared in 100% isopropanol and stirred for 3 hours at room temperature. Subsequently, the stock solution was filtered using 110mm diameter, grade 1 filter paper (Whatman®, UK) and diluted 3:2 with deionised H₂O (dH₂O) to produce the working solution (0.6%). The working solution was only used on the day it was made and prior to use, it was filtered using grade 1 filter paper (Whatman®, UK) and refiltered using 33mm diameter, 0.22µm syringe driven filter units (Millipore, Ireland). Each individual thoracic aorta was placed in a well of a 96-well plate (Sigma Aldrich, UK) and taken through the ORO staining protocol (Table 2.4.), after which they were cut longitudinally and pinned out on a gel mounting board. Images of stained thoracic aortae were then captured using an EOS 1100D camera (Canon, UK) attached to a Leica S4E microscope (Leica Microsystems Ltd, UK), coded for blinded analysis and the percentage area of fatty streaks within the lumen measured via computerised planimetry (ImageJ software, National Institute of Health, Rockville Pike Bethesda, Maryland) where red staining identified lipid deposition (fatty streaks) within the vessel wall.

2.3.4.2. Cryosectioning of ventricular tissue

Frozen ventricular tissue (for removal and storage see section 2.3.1.) was transferred to the Shandon Cryotome FSE (Thermo Electron Corporation, USA) where chamber, specimen and cryobar temperatures were set to -23°C, -17°C and -35°C, respectively. Tissue acclimatised to chamber temperature for 30 minutes prior to being mounted onto individual cryocassettes (Thermo Electron Corporation, USA) using Tissue-Tek® Optimal Cutting Temperature (O.C.T.) compound (setting time approximately 1 minute). Longitudinal sections (10µm) were cut and mounted onto 0.8-1.0mm superfrost slides (Fisher Scientific, USA) which were subsequently air dried for 30 minutes and stored at -80°C. Prior to staining, the slides were removed from storage and left at room temperature for approximately 5 minutes. Slides were then submerged in buffered zinc formalin for 15 minutes to fix, after which they were rinsed in running tap H₂O for 5 minutes, air dried and stored at 4°C until stained.

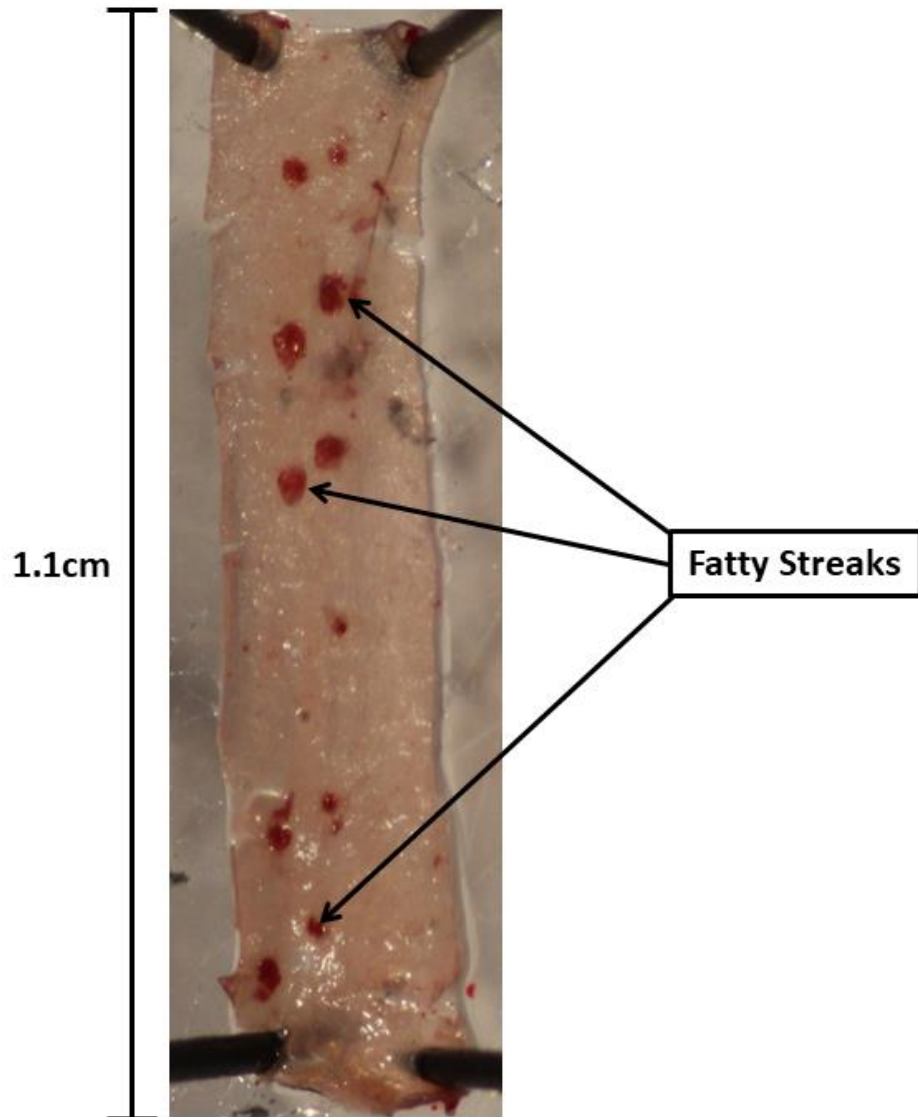


Figure 2.4. ORO staining of a thoracic aorta from a high fat fed ApoE^{-/-} mouse. Red staining is indicative of lipid deposition (fatty streaks).

2.3.4.3. *Haematoxylin and Eosin staining of ventricular tissue*

Cardiac tissue sections were manually stained with Haematoxylin and Eosin dyes (for staining protocol see Table 2.5.) which stain the nuclei blue/black and the cytoplasm and/or connective tissue pink/orange/red for the visualisation of cardiac structure. Following staining, tissue sections were left to air dry prior to a Menzel-Gläser coverslip (Thermo Scientific, Germany) being mounted onto each stained slide using Pertex Mounting Solution. Photomicrographs of cardiac tissue were captured using a high resolution Mirax Scan automated imaging system (Carl Zeiss MicroImaging GmbH, Germany) at a magnification of 20x and then coded for blinded analysis. For gross morphology, multiple measurements of the right ventricular (RV) wall, the left ventricular (LV) wall and that of the intraventricular septum (IVS) were calculated via computerised planimetry (ImageJ software) and subsequently averaged.

2.3.4.4. *Picrosirius Red staining of ventricular tissue*

Picrosirius Red, a linear anionic dye was used to detect collagen. Cardiac tissue sections were stained (for staining protocol see Table 2.6.) using an IntelliPATH™ autostainer (BioCare, USA), left to air dry prior to a coverslip being mounted onto each slide using Pertex Mounting Solution. Under light microscopy, collagen was stained red and muscle fibres and cytoplasm both stained yellow. Photomicrographs of cardiac tissue were captured using the Mirax Scan automated imaging system at a magnification of 20x and coded for blinded analysis. The total collagen present in each cardiac tissue section was subsequently quantified using computerised planimetry (BioPix, Sweden) and calculated as a percentage of the total ventricular area.

2.3.4.5. *Oil Red O staining of ventricular tissue*

Cardiac tissue sections were manually stained for lipid deposition using ORO (staining as described in Table 2.7.) and left to air dry. A coverslip was then mounted onto each slide using Mount-Quick “Aqueous” solution (a H₂O soluble mounting medium) and photomicrographs of slides captured using the Mirax Scan automated imaging system at a magnification of 20x. Images were coded for blinded analysis prior to using computerised planimetry (BioPix software) to quantify lipid deposition. The total lipid deposition was subsequently calculated as a percentage of the total ventricular area.

Step	Constituent	Time
1	dH ₂ O	1 min
2	60% isopropanol	10 sec
3	ORO working solution (made from ORO powder)	30 min
4	60% isopropanol	10 sec
5	dH ₂ O	30 sec

Table 2.4. ORO staining protocol for the identification of lipid deposition within the lumen of thoracic aortae.

Step	Constituent	Time
1	Distilled H ₂ O	5 sec
2	Mayer's haematoxylin	1 min
3	Distilled H ₂ O	5 sec
4	Bluing in warm tap H ₂ O	5 min
5	0.1% Eosin Y disodium salt (in 95% ethanol)	10 sec
6	95% Ethanol	5 sec
7	95% Ethanol	5 sec
8	Xylene	5 sec
9	Xylene	5 sec

Table 2.5. Haematoxylin and Eosin staining protocol used to visualise the cardiac structure of cardiac tissue sections.

Step	Constituent	Time
1	Distilled H ₂ O	5 sec
2	Tap H ₂ O	5 min
3	Tap H ₂ O	5 min
4	Picrosirius Red	1 hour
5	1% acetic acid	3 min
6	1% acetic acid	3 min
7	1% acetic acid	3 min
8	100% ethanol	3 min
9	100% ethanol	3 min
10	100% ethanol	3 min
11	Xylene	3 min
12	Xylene	3 min

Table 2.6. Picrosirius Red staining protocol for the detection of collagen in cardiac tissue sections.

Step	Constituent	Time
1	Distilled H ₂ O	5 sec
2	ORO working solution (made from purchased pre-made ORO solution)	10 min
3	Distilled H ₂ O	5 sec
4	60% isopropanol	5 sec
5	Mayer's haematoxylin	30 sec
6	Running tap H ₂ O	10 min

Table 2.7. ORO staining protocol for the identification of lipid deposition in cardiac tissue sections.

2.3.5. Isolated Langendorff-perfused heart studies

Mice were anaesthetised with a mixture of ketamine & xylazine (120mg kg⁻¹ & 16mg kg⁻¹, respectively, i.p.) and anaesthesia confirmed via the absence of the pedal withdrawal reflex. Each heart was rapidly excised and arrested in ice cold KHS. The aorta was cannulated with a 23G needle and the needle attached to the mounting head (Figure 2.5.) of Langendorff retrograde perfusion apparatus (ADInstruments LTD, UK). KHS was immediately perfused (37°C; 2-2.5ml min⁻¹) through the cannula into the heart and a 15-minute stabilisation period allotted for the adoption of sinus rhythm. Post stabilisation, each heart was subjected to 30 minutes global ischaemia (GI) followed by 30 minutes reperfusion, induced by ceasing and resuming the flow of KHS to the heart, respectively. The heart was then stored at -20°C (for a minimum of 24 hours) prior to the measurement of infarct size.

2.3.6. Measurement of myocardial infarct size

Frozen hearts were sectioned into 4 slices (2-3mm thickness), the 3rd slice (from the apex) incubated in 1% 2,3,5-Triphenyl-tetrazolium chloride (TTC) solution for 30 minutes at 37°C and the remaining slices stored at -20°C for future analysis. The 3rd slice from the apex was chosen for infarct analysis as it was deemed to be the slice where viable and infarcted tissue could be most clearly observed. The TTC stained slices were subsequently fixed in 10% neutral buffered formalin (Formal Fixx™; Thermo Scientific, UK) for 2 hours prior to being imaged with an EOS 1100D camera (Canon, UK) attached to a Leica S4E microscope (Leica Microsystems Ltd, UK). Images were subsequently coded for blinded analysis and infarct size determined via computerised planimetry (ImageJ software) where red and peach staining was indicative of viable and infarcted tissue, respectively.

2.4. Statistical analysis

Power calculations for group sizes and statistical analysis for each study are discussed within the relevant chapter. However, in general, data are expressed as mean±S.E.M. Differences between paired and unpaired data were established by conducting a paired or unpaired *t*-test, respectively. Multiple comparisons were performed using a one-way analysis of variance (ANOVA) test followed by a 'Bonferroni' post-hoc test. Where appropriate, multiple comparisons were performed using a two-way ANOVA followed by a 'Bonferroni' post-hoc test. All statistical tests were carried out using GraphPad Prism® 4 software (GraphPad Software, Inc., USA) and differences between data deemed as significant where *P*<0.05.

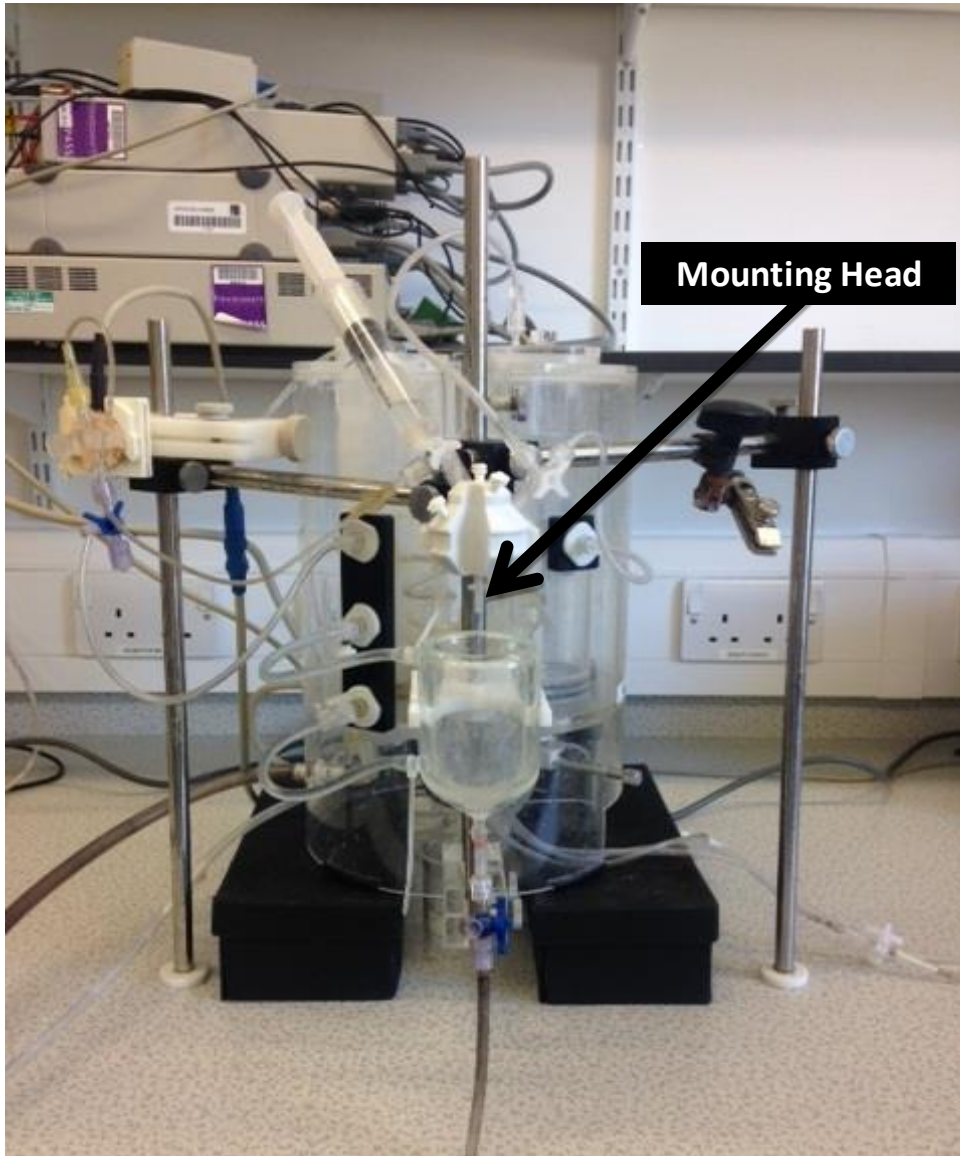


Figure 2.5. Langendorff retrograde perfusion apparatus.

2.5. Materials

Drugs, solutions and diets were purchased from various sources (see Table 2.8.).

Drug/Solution	Source
Acetic Acid	Merck Millipore, USA
Agarose	Sigma-Aldrich [®] , UK
ATP	Sigma-Aldrich [®] , UK
BSA (essentially fatty acid free; ≥96%)	Sigma-Aldrich [®] , UK
CaCl ₂	Sigma-Aldrich [®] , UK
Cor.At [®] CL-i cardiomyocytes (miPSC-derived) 1M kit with Puromycin and medium	Sigma-Aldrich [®] , UK
CRM (P) chow pellets	Special Diets Services, UK
(-)-Cannabidiol	Tocris Bioscience, UK
DMEM	Invitrogen, UK
DMSO	Fisher Scientific, Ireland
Dobutamine Hydrochloride	Sigma-Aldrich [®] , UK
Eosin Y disodium salt	Sigma-Aldrich [®] , UK
Formal Fixx [™] (Shandon [™] 10% Neutral buffered formalin)	Thermo Scientific, UK
GelRed [™] Nucleic Acid Gel Stain	Biotium, UK
Glacial Acetic Acid	Fisher Scientific, UK
Glucose (D-(+)-Glucose)	Sigma-Aldrich [®] , UK
HBSS	Sigma-Aldrich [®] , UK
HDL/LDL calibrator	Thermo Scientific, UK
Heparin sodium	Roche, UK
HEPES	Invitrogen, UK
iCell [®] Cardiomyocytes	Cellular Dynamics, USA
Isopropanol	Fisher Scientific, UK
KCl	Sigma-Aldrich [®] , UK
Ketamine (Vetalar [™])	Pfizer, UK
KH ₂ PO ₄	Sigma-Aldrich [®] , UK
LPI sodium salt from <i>Glycine max</i> (soybean)	Sigma-Aldrich [®] , UK
Mayer's Haematoxylin	HistoLab [®] , Sweden
Methacholine (Acetyl-β-methylcholine chloride)	Sigma-Aldrich [®] , UK

MgSO₄	Sigma-Aldrich [®] , UK
Mount-Quick “Aqueous” mounting medium	Daido Sanyo Co., Ltd, Japan
NaCl	Fisher Scientific, Ireland
NaHCO₃	Fisher Scientific, Ireland
ORO powder	Sigma-Aldrich [®] , UK
95% O₂ and 5% CO₂	Boc, UK
PBS (Dulbecco A) Tablets	Oxoid Limited, UK
PCR Marker, 250µl (50 lanes)	Promega, UK
PERTEX[®] mounting medium	HistoLab [®] , Sweden
Picrosirius Red	HistoLab [®] , Sweden
Primers (ApoE and GPR55)	Sigma-Aldrich [®] , UK
QIAmp[®] DNA Mini Kit	Qiagen, UK
REDTaq[®] ReadyMix[™] PCR Reaction Mix	Sigma-Aldrich [®] , UK
sCal (lipid calibrator)	Thermo Scientific, UK
Sodium Nitroprusside Dihydrate	Sigma-Aldrich [®] , UK
Tissue-Tek[®] O.C.T. Compound	Sakura Finetek UK Ltd, UK
TTC powder	Sigma-Aldrich [®] , UK
TTC solution (pre-made; 1%)	Sigma-Aldrich [®] , UK
UltraPure[™] TBE Buffer	Life Technologies, UK
U-46619	Enzo Life Sciences, UK
Western diet R638 semi-synthetic feed	Lantmannen, Sweden
(-)-Xestospongine C	Tocris Bioscience, UK
Xylazine (Rompun[®])	Bayer Healthcare, UK
Xylene	VWR Chemicals, Sweden
Y-27632 Dihydrochloride	Tocris Bioscience, UK
Zinc Formalin (buffered; Thermo Scientific[™] Richard-Allan Scientific[™])	Fisher Scientific, UK

Table 2.8. Source of drugs, solutions and diets.

2.5.1. Composition of drugs and solutions

- 1% Acetic acid (1% v/v): 1ml of acetic acid and 99ml of dH₂O
- Agarose gels: 1.6% w/v agarose in 100ml dH₂O
- Anaesthesia: 600µl Vetalar™ (100mg/ml ketamine hydrochloride with 0.01% w/v benzethonium chloride as a preservative) and 400µl Rompun® (23.32mg/ml xylazine hydrochloride and 1.5mg methyl 4-hydroxy-benzoate) were mixed with 4ml dH₂O
- CBD stock solution (1mM): 10mg CBD in 31.8ml 100% DMSO
 - For 1µM CBD (0.1% DMSO): A 1 in 1000 dilution of CBD stock solution (1mM) in KHS was carried out. 0.1% DMSO was used as the vehicle
- Dobutamine hydrochloride (10µg kg⁻¹): 10µg/1ml saline; injection volume: 10µl per 10g body weight
- Eosin (0.1% v/v): 1ml Eosin Y in 999ml 95% ethanol
- 70% ethanol (70% v/v): 70ml absolute ethanol and 30ml dH₂O
- 95% ethanol (95% v/v): 95ml absolute ethanol and 5ml dH₂O
- 100% ethanol (100% v/v): 100ml absolute ethanol
- Heparinised saline: 1000U ml⁻¹ heparin sodium diluted with 0.9% saline
- 60% isopropanol (60% v/v): 60ml absolute isopropanol (molecular biology grade) and 40ml dH₂O
- 98% isopropanol (98% v/v): 98ml absolute isopropanol and 2ml dH₂O
- KCl (80mM): 2.982g KCl in 500ml dH₂O

- KHS: 119mM NaCl, 4.7mM KCl, 1.18mM KH₂PO₄, 2.41mM MgSO₄, 25mM NaHCO₃, 2.52mM CaCl₂ and 10.88mM C₆H₁₂O₆; pH7.4 via bubbling with 95% O₂ and 5% CO₂
- LPI stock solution (100μM): 1mg LPI in 27.2ml 1% DMSO
 - For 10μM LPI (0.1% DMSO): A 1 in 10 dilution of LPI stock solution (100μM) in KHS was carried out. 0.1% DMSO was used as the vehicle
- MCh stock solution (100mM): 100mg MCh in 5.1ml dH₂O
 - For 10⁻⁹-10⁻⁴M: 1 in 10 serial dilutions (starting with MCh stock solution; 100mM) in KHS were carried out
- ORO stock solution: (1% w/v): 5g Oil Red O in 500ml 98% isopropanol (stored at 4°C)
 - ORO working solution: Dilute ORO stock solution 3:2 with dH₂O
- Phosphate buffered saline (PBS): 1 PBS tablet dissolved in 100ml of dH₂O. Final PBS concentration; 136.9mM NaCl, 8.1mM Na₂HPO₄, 1.5mM KH₂PO₄ and 2.7mM KCl (pH7.3±0.2 at 25°C)
- Primers (ApoE stock solution; 100μM):
 - 5'- CAGAAAGCGAAGGAGCAAAG - 3': 411.6μg in 659μl dH₂O
 - 5'- AAAAAGCTCGGGATGAGCCTT - 3': 472.6μg in 768μl dH₂O
 - 5'- CAGCTCCCTCTCCTAGGGTT - 3': 490μg in 813.5μl dH₂O
- Primers (GPR55 stock solution; 100μM):
 - 5'- ATGCGGAATTCCTGTTACCCA - 3': 615.3μg in 963.8μl dH₂O
 - 5'- CACCCTAGGGCCTCAGTTGTA - 3': 515.2μg in 806.9μl dH₂O
 - 5'- GGAAAGCTGAGATACAGACTT - 3': 465.2μg in 714.9μl dH₂O
- Saline: 0.9% w/v NaCl in 100ml dH₂O (stored at room temperature)
- SNP stock solution (100mM): 200mg SNP in 6.7ml dH₂O
 - For 10⁻⁹-10⁻⁴M: 1 in 10 serial dilutions (starting with SNP stock solution; 100mM) in KHS were carried out

- TBE buffer: 0.1M Tris, 0.09M Boric Acid and 1mM EDTA (pH 8.4±0.1 at 25°C)
- 1% TTC (1% w/v): 1g TTC in 100ml of PBS
- U-46619 stock solution (1mM): 1mg U-46619 in 2.9ml PBS
 - For 10^{-9} - 10^{-5} M: 1 in 10 serial dilutions (starting with U-46619 stock solution; 1mM) in KHS were carried out
- Y-27632 dihydrochloride stock solution (1mM): 10mg Y-27632 dihydrochloride in 31.2ml KHS
 - For 10µM Y-27632 dihydrochloride: A 1 in 100 dilution of Y-27632 dihydrochloride stock solution (1mM) in KHS was carried out
 - For 50µM Y-27632 dihydrochloride: A 1 in 20 dilution of Y-27632 dihydrochloride stock solution (1mM) in KHS was carried out

Chapter 3:

**Effect of a high fat diet in ApoE^{-/-} and
ApoE^{-/-}/GPR55^{-/-} mouse models of
atherosclerosis**

3.1. Introduction

3.1.1. GPR55 and risk factors associated with atherosclerosis

Increasing evidence is emerging that GPR55 is associated with risk factors that are linked with the development of atherosclerosis (e.g. obesity and diabetes). For example, Moreno-Navarrete and colleagues (2012) reported that GPR55 mRNA expression was increased in the visceral and subcutaneous adipose tissue of obese human subjects when compared to those with a lean phenotype. Additionally, the plasma LPI (16:0, 18:0 and 20:4 species) concentration was also increased in the obese subjects. With regard to diabetes, several studies have investigated the role of GPR55 in glucose homeostasis, the results of which have unanimously indicated that GPR55 activation in the islets of Langerhans stimulates insulin secretion (Romero-Zerbo *et al.*, 2011, McKillop *et al.*, 2013, Liu *et al.*, 2016 and McKillop *et al.*, 2016). In light of these findings, GPR55 may represent a potential therapeutic target for obesity and diabetes, which may indirectly reduce the prevalence of atherosclerosis. What is not known is whether GPR55 has a role in the development of risk factors for vascular disease such as hyperlipidaemia and/or inflammation, which ultimately influence the development of atherosclerosis.

3.1.2. GPR55 and atherosclerosis

To date, few studies have investigated the direct role of GPR55 in atherosclerosis *per se*, and two recent studies have shown conflicting results. Lanuti and colleagues (2015) demonstrated that GPR55 activation with O-1602 augmented ox-LDL-induced lipid accumulation and inflammatory responses, while reducing the efflux of cholesterol from human foam cells, suggesting a pro-atherogenic role for GPR55. In contrast, GPR55 antagonism with CID16020046, increased neutrophil activation and recruitment in the early stages of atherogenesis and neutrophil degranulation in the later stages of atherosclerosis (Montecucco *et al.*, 2016), suggesting an anti-atherogenic role for this receptor. The opposing findings may be due to the conclusions of the first study being based upon data that was generated using O-1602, which has previously been reported to mediate effects beyond GPR55 (Schicho *et al.*, 2011). On this basis, a more targeted approach to assessing the importance of GPR55 in atherogenesis would be beneficial, for example, through the genetic deletion of GPR55.

3.1.3. Rodent models of atherosclerosis

C57BL/6 mice fed an atherogenic diet (1.25% cholesterol, 15% fat and 0.5% cholic acid) develop atherosclerotic lesions (Paigen *et al.*, 1987a and Paigen *et al.*, 1987b), however, their lesions differ from those of humans, both histologically and in terms of their location within the vasculature (Jawień *et al.*, 2004). On this basis, the C57BL/6 mouse is not used to study the development of atherosclerosis. As other strains of wildtype mice are highly resistant to the development of atherosclerotic lesions (Meyrelles *et al.*, 2011) the manipulation of the murine genome has proven necessary to generate more clinically relevant models of atherosclerosis. Consequently, a number of mouse models are now available, however, the apolipoprotein E (ApoE) knockout (ApoE^{-/-}) and the LDL receptor knock out (LDLR^{-/-}) are the two most frequently used in the research of atherosclerosis (Getz and Reardon, 2012).

3.1.3.1. ApoE^{-/-} mouse

ApoE is a glycoprotein which is predominantly synthesised in the liver and brain of mice and humans and is a component of all lipoproteins with the exception of LDL (Jawień *et al.*, 2004). It functions as a ligand for lipoprotein receptors (e.g. LDLR), triggering the hepatic uptake of lipoproteins from the circulation. Thus, mice lacking the gene for ApoE fail to remove circulatory lipoproteins. When fed a normal chow diet, ApoE^{-/-} mice exhibit an elevated plasma cholesterol concentration of 606mg/dL (34mmol/l) compared to control mice with 109mg/dL (6mmol/l) (Nakashima *et al.*, 1994) and develop fatty streaks (type II lesions; lesion classification is defined in Chapter 1, section 1.2.4.) at approximately 4-5 months of age, which subsequently progress to type V lesions at 10 months of age onwards (Whitman, 2004). Plaque development in ApoE^{-/-} mice is histopathologically similar to that of humans (Coleman *et al.*, 2006) making this model particularly attractive for the research of atherosclerosis. Atherogenesis can also be accelerated in the ApoE^{-/-} mouse by the feeding of a high fat diet which consequently elevates the plasma cholesterol concentration of these mice to 1085-4402mg/dL (60-244mmol/l) depending on the duration (6-40 weeks) of the dietary period (Nakashima *et al.*, 1994). Unsurprisingly, ApoE^{-/-} mice develop fatty streaks throughout the arterial tree at an earlier time point, approximately 8-10 weeks, in response to high fat feeding and progression to the type V lesion is usually reported within 18-20 weeks of starting this diet (Whitman, 2004). However, ApoE^{-/-} mice do present with limitations; for example, their plasma cholesterol is mostly carried on lipoprotein remnants rather than LDL, as it is in humans (Getz and Reardon, 2012). Additionally, plaque development within the coronary vasculature occurs in human

sufferers of atherosclerosis and not in ApoE^{-/-} mice, regardless of the diet with which they are fed (Coleman *et al.*, 2006), therefore this model is not suitable for studies investigating the association of coronary plaque rupture and myocardial infarction.

3.1.3.2. LDLR^{-/-} mouse

The LDLR is responsible for lipoprotein uptake from the circulation to the liver, therefore genetic ablation of the LDLR increases the plasma lipoprotein concentration. However, the response of LDLR^{-/-} mice to a normal chow diet is not as severe as that of ApoE^{-/-} mice, with the total plasma cholesterol concentration only reaching approximately 240mg/dL (13mmol/l) at approximately 7 weeks of age (Ishibashi *et al.*, 1993). Consequently, lesion development within the vasculature of these mice is limited, even in 6 month old LDLR^{-/-} mice (Hasty *et al.*, 2001). However, Ma and colleagues (2012) demonstrated that the LDLR^{-/-} mouse is diet responsive, as high fat feeding of this strain for 12 months increased their total plasma cholesterol concentration from 180mg/dL (10mmol/l) to 400mg/dL (22mmol/l) and caused lesion development which worsened with the duration of high fat feeding. Akin to ApoE^{-/-} mice, LDLR^{-/-} mice do not develop coronary atherosclerosis, however, the simultaneous deletion of the genes for both ApoE and LDLR in the same mice results in lesion development within the coronary arteries and myocardial infarction (Caligiuri *et al.*, 1999).

The present study required a model of progressive atherosclerosis to investigate the role of GPR55 in the development of this condition. As ApoE^{-/-} mice develop atherosclerosis even on normal chow and exhibit similarities to humans with regard to the way in which they develop lesions, the ApoE^{-/-} mouse was deemed the more appropriate model for use in the present study.

3.1.4. GPR55 knockout models

GPR55 knockout (GPR55^{-/-}) mouse models have aided in the investigation of the role of GPR55 in physiology for a number of years (Johns *et al.*, 2007, Whyte *et al.*, 2009, Romero-Zerbo *et al.*, 2011, Walsh *et al.*, 2014, Bjursell *et al.*, 2016, Meadows *et al.*, 2016, and Carey *et al.*, 2017). However, advances in genetics have introduced double knockout mouse models allowing for more complex studies to take place to further characterise the role of a gene in the absence of another. In recent years, a novel mouse model of atherosclerosis has been generated by AstraZeneca (Mölnådal, Sweden) where both the ApoE and GPR55 genes have been deleted (ApoE^{-/-}/GPR55^{-/-}). Rather than

administering GPR55 antagonists to mice deficient only in the gene for ApoE, research involving the ApoE^{-/-}/GPR55^{-/-} mouse model will rule out the possibility of such antagonists mediating any off target effects and will provide a more accurate insight into the role of GPR55 in atherosclerosis.

3.1.5. Aims

The principle aims of this study were to characterise the phenotype of the novel ApoE^{-/-}/GPR55^{-/-} mouse in response to high fat feeding and to investigate the role of GPR55 in the development of atherosclerosis. In order to do this, C57BL/6 (wildtype; WT), ApoE^{-/-} (model of atherosclerosis), GPR55^{-/-} and ApoE^{-/-}/GPR55^{-/-} mice were fed a normal chow (NC) or high fat chow (HFC) diet for 12 weeks to determine the effect(s) of gene deletion and/or high fat feeding on the following parameters 1) body weight, 2) fat and lean mass composition, 3) tissue weights, 4) endothelial and smooth muscle function of the carotid artery, 5) plasma lipid profiles, 6) fatty streaks within the thoracic aorta, and 7) cardiac remodelling.

3.2. Methods

3.2.1. Study design

Male and female WT, ApoE^{-/-}, GPR55^{-/-} and ApoE^{-/-}/GPR55^{-/-} mice, aged 4-7 weeks (approximately 5 of each gender per strain) were purchased or bred according to Chapter 2, section 2.2.2.1. The mice within each strain were randomly assigned to NC or HFC groups and received either CRM (P) chow pellets (Special Diets Services, UK) or Western diet R638 semi-synthetic pellets (0.15% cholesterol and 21% fat; Lantmannen, Sweden), respectively for a 12 week period (full nutritional details of each diet are detailed in Figure 3.1. and 3.2., respectively). Groups starting each diet were staggered over a 6 month period, during which time the mice were housed at the MRF in accordance with the animal ethics and husbandry guidelines set by the Home Office (Chapter 2, section 2.2.1). Following completion of the 12 week dietary period, animals were transported to RGU where all *in vivo/ex vivo* studies were conducted. On arrival at RGU, mice were allotted a minimum period of 30 minutes to acclimatise to their new surroundings prior to the commencement of any experiments.

INGREDIENTS

Wheat, Wheatfeed, Barley, De-hulled Extracted Toasted Soya, Maize, Macro Minerals, Soya Oil, Potato Protein, Hydrolysed Wheat Gluten, Full Fat Soya, Maize Gluten Meal, Vitamins, Micro Minerals, Amino Acids.

Calculated Analysis

Rat and Mouse Breeder and Grower (P)

NUTRIENTS		Total	Supp (9)	NUTRIENTS		Total	Supp (9)
Proximate Analysis				Glutamic Acid			
Moisture (1)	%	10.00		Glutamic Acid	%	3.72	
Crude Oil	%	3.36		Proline	%	1.34	
Crude Protein	%	18.35		Serine	%	0.78	
Crude Fibre	%	4.23		Hydroxyproline	%		
Ash	%	6.27		Hydroxylysine	%		
Nitrogen Free Extract	%	57.39		Alanine	%	0.21	
Digestibility Co-Efficients (7)				Macro Minerals			
Digestible Crude Oil	%	3.05		Calcium	%	0.83	0.72
Digestible Crude Protein	%	16.44		Total Phosphorus	%	0.64	0.19
Carbohydrates, Fibre and Non Starch Polysaccharides (NSP)				Phytate Phosphorus	%	0.23	
Total Dietary Fibre	%	15.06		Available Phosphorus	%	0.41	0.19
Pectin	%	1.40		Sodium	%	0.27	0.22
Hemicellulose	%	8.85		Chloride	%	0.40	0.35
Cellulose	%	3.89		Potassium	%	0.69	
Lignin	%	1.40		Magnesium	%	0.22	0.01
Starch	%	42.37		Micro Minerals			
Sugar	%	3.90		Iron	mg/kg	130.65	60.21
Energy (5)				Copper	mg/kg	16.42	6.90
Gross Energy	MJ/kg	15.01		Manganese	mg/kg	91.05	44.90
Digestible Energy (15)	MJ/kg	12.27		Zinc	mg/kg	86.59	52.86
Metabolisable Energy (15)	MJ/kg	11.19		Cobalt	µg/kg	494.92	420.30
Atwater Fuel Energy (AFE) (8)	MJ/kg	13.93		Iodine	µg/kg	390.43	310.17
AFE from Oil	%	9.08		Selenium	µg/kg	265.49	100.34
AFE from Protein	%	22.03		Fluorine	mg/kg	9.63	
AFE from Carbohydrate	%	68.90		Vitamins			
Fatty Acids				β-Carotene (2)	mg/kg	1.28	
Saturated Fatty Acids				Retinol (2)	µg/kg	5218.35	4500.38
C12:0 Lauric	%	0.03		Vitamin A (2)	iu/kg	17376.38	15001.26
C14:0 Myristic	%	0.14		Cholecalciferol (3)	µg/kg	76.94	75.00
C16:0 Palmitic	%	0.33		Vitamin D (3)	iu/kg	3077.42	3000.00
C18:0 Stearic	%	0.06		α-Tocopherol (4)	mg/kg	93.03	72.81
Monounsaturated Fatty Acids				Vitamin E (4)	iu/kg	102.81	80.09
C14:1 Myristoleic	%	0.02		Vitamin B ₁ (Thiamine)	mg/kg	15.84	9.83
C16:1 Palmitoleic	%	0.10		Vitamin B ₂ (Riboflavin)	mg/kg	13.28	11.76
C18:1 Oleic	%	0.87		Vitamin B ₆ (Pyridoxine)	mg/kg	17.65	13.74
Polyunsaturated Fatty Acids				Vitamin B ₁₂ (Cyanocobalamin)	µg/kg	78.17	75.00
C18:2(ω6) Linoleic	%	0.96		Vitamin C (Ascorbic Acid)	mg/kg	1.80	
C18:3(ω3) Linolenic	%	0.11		Vitamin K (Menadione)	mg/kg	185.05	180.00
C20:4(ω6) Arachidonic	%	0.11		Folic Acid (Vitamin B ₉)	mg/kg	4.30	2.94
C22:5(ω3) Clupanodonic	%			Nicotinic Acid (Vitamin PP) (6)	mg/kg	78.92	27.65
Amino Acids				Pantothenic Acid (Vitamin B ₅)	mg/kg	25.24	11.56
Arginine	%	1.19		Choline (Vitamin B ₄)	mg/kg	899.51	75.63
Lysine (6)	%	1.04	0.17	Inositol	mg/kg	2253.88	12.78
Methionine	%	0.28	0.02	Biotin (Vitamin H) (6)	µg/kg	488.74	230.85
Cystine	%	0.29		Notes			
Tryptophan	%	0.22		1. All values are calculated using a moisture basis of 100%. Typical moisture levels will range between 9.5 - 11.5%.			
Histidine	%	0.46		2. a. Vitamin A includes Retinol and the Retinol equivalents of β-carotene.			
Threonine	%	0.69		b. Retinol includes the Retinol equivalents of β-carotene.			
Isoleucine	%	0.77		c. 0.48 µg Retinol = 1 µg β-carotene = 1.6 iu Vitamin A activity			
Leucine	%	1.46		d. 1 µg Retinol = 3.33 iu Vitamin A activity			
Phenylalanine	%	0.96		e. 1 iu Vitamin A = 0.3 µg Retinol = 0.6 µg β-carotene			
Valine	%	0.91		f. The standard analysis for Vitamin A does not detect β-carotene			
Tyrosine	%	0.69		3. 1 µg Cholecalciferol (D ₃) = 400 iu Vitamin D			
Taurine	%			4. 1 mg all-rac-α-tocopherol = 1.1 iu Vitamin E activity			
Glycine	%	1.55		5. 1 mg all-rac-α-tocopherol acetate = 1.0 iu Vitamin E activity			
Aspartic Acid	%	1.00		6. These nutrients coming from natural raw materials such as cereals may have low availabilities due to the interactions with other compounds.			
				7. Based on in-vitro digestibility analysis.			
				8. AF Energy = Atwater Fuel Energy = ((CP% / 100) * 9000) + ((CP% / 100) * 4000) + ((NFE% / 100) * 4000) / 2.39.23			
				9. Supplemented nutrients from manufactured and mined sources.			
				15. Calculated.			

Figure 3.1. Full nutritional details of the CRM (P) pellets (NC Diet).

Western Diet R638 Semi-synthetic feed

Ingredients:

Cornstarch, cocoa butter, casein, glucose, icing sugar, cellulose flour, minerals, vitamins, cholesterol

Energy calculation semi-synthetic feed

Feed: Semi-synthetic feed, R638

	Content (%)	Factor	kJ/100 g	Energy (%)
Raw protein	17.2	15.466	265.40	17.0
Fat	21.0	29.687	623.43	40
Crude fibre	3.9	2.926	11.26	0.7
Ash	4.1	-	-	-
Water	10.0	-	-	-
NFE	43.9	15.048	660.46	42.3
Total	100.0		1560.55	100.0

Energy value 15.6 Mj/kg

Analysis

		Unit	Content
Protein N*6.25	%	17.2	
Fat as per EC	%	21	
Crude fibre		%	3.9
Ash		%	4.1
Water		%	10
NFE		%	43.9
Phosphorus		%	0.4
Iron		mg/kg	350
Calcium		%	0.5
Copper		mg/kg	8
Magnesium	%	0.05	
Manganese	mg/kg	70	
Sodium		%	0.3
Selenium		mg/kg	0.23
Zinc		mg/kg	30
Cholesterol		%	0.15
Vitamin A		IE/kg	12000
D		IE/kg	1500
E		mg/kg	42
K3		mg/kg	0.7
B1		mg/kg	4
B2		mg/kg	12
B6		mg/kg	6
B12		mg/kg	0.02
Pantothenic acid	mg/kg	12	
Folic acid		mg/kg	0.5
Niacin		mg/kg	40
Biotin		mg/kg	0.3
Vitamin C		mg/kg	500
Choline		mg/kg	1000



Vill du veta mer är du välkommen att kontakta oss på
special@lantmannen.com, tfn 0510-885 99 eller www.labfor.se.



Figure 3.2. Full nutritional details of the Western diet R638 semi-synthetic pellets (HFC Diet).

3.2.2. Body weight measurements

All mice were weighed the day on which they commenced either the NC or HFC diet (Week 0) and fortnightly thereafter for the duration of the dietary period by technicians at the MRF.

3.2.3. Assessment of fat and lean mass composition

To determine the fat and lean mass composition of mice throughout the dietary period, conscious mice were coaxed into a translucent tube where they were body scanned at 0, 6 and 12 weeks by trained technicians at the MRF using an EchoMRI™ Body Composition Analyser (EchoMRI™ LLC, USA). For accuracy, each mouse was scanned in triplicate at each time point and the values for each variable subsequently averaged.

3.2.4. Assessment of endothelial and smooth muscle function of the carotid artery

Small vessel myography was conducted with murine carotid arteries to assess their endothelial and smooth muscle function. For removal and storage of these vessels see Chapter 2, section 2.3.1. Primarily, the force transducers of the dual wire myograph system were calibrated, the carotid arteries mounted between each jaw of the myograph chamber and normalised to the target transmural pressure of 100mmHg (13.3kPa) as described in Chapter 2, section 2.3.3. All vasoconstrictors /vasodilators used throughout the study were serially diluted on experimental days from stocks previously prepared and stored at -20°C.

3.2.4.1. Contractile responses to U-46619

Post mounting and normalisation of the vessels, sensitisation to KCl was carried out as described in Chapter 2, section 2.3.3. and each vessel left to stabilise for 15 minutes. A concentration response curve (CRC) was then carried out with the vasoconstrictor U-46619 (10^{-9} - 10^{-5} M), which was administered in cumulative concentrations allowing for the tension to plateau prior to the addition of the next concentration. The data regarding vessel contraction was calculated as the mean \pm S.E.M. of the response (mN) produced by each concentration. Moreover, the maximal (E_{max}) change (Δ) in tension (mN) to U-46619 was calculated from the CRC for each strain. The logEC₅₀ values were also calculated from the CRC for each strain by applying a nonlinear curve fit using a variable Hill slope. Any vessels which failed to contract by 3mN were excluded from the associated data analysis.

Subsequently, the EC_{80} of U-46619 was calculated for each individual vessel and that concentration used for the following vasorelaxant studies. Carotid arteries were washed 6 times using KHS and left to equilibrate for a 45-minute period prior to any vasorelaxant studies being conducted.

3.2.4.2. Assessment of vasorelaxant responses to MCh and SNP

In order to assess endothelial function, carotid arteries were pre-constricted with U-46619 (EC_{80} value) and vessel tension left to plateau. A CRC was then carried out with the endothelium dependent vasodilator, methacholine (MCh; 10^{-9} - 10^{-4} M), which was administered in cumulative doses allowing for the tension to plateau prior to the addition of the next concentration. The carotid arteries were subsequently washed 6 times using KHS and allowed to equilibrate for a 45 minute period. Vessels were then pre-constricted with U-46619 (EC_{80} value) and a CRC carried out with the endothelium independent vasodilator, sodium nitroprusside (SNP; 10^{-9} - 10^{-4} M) to assess smooth muscle function. Furthermore, the order in which the vasodilators were applied to the bath was alternated from one experiment to the next to remove any influence of order of delivery on the responsiveness of the vessels to each agent. Finally, vessel relaxation was calculated as the mean \pm S.E.M. of the percentage relaxation of the U-46619-induced contraction. Moreover, the E_{max} Δ in % relaxation to either MCh or SNP was calculated from the respective CRC for each strain. The $\log EC_{50}$ values for either MCh or SNP were also calculated from the respective CRC for each strain by applying a nonlinear curve fit using a variable Hill slope. Any vessels which failed to contract by 3mN in response to the EC_{80} value of U-46619 were excluded from the associated data analysis.

3.2.5. Assessment of plasma lipid profiles

Blood samples were extracted from anaesthetised mice via cardiac puncture of the ventricles and the plasma fraction harvested according to the protocol described in Chapter 2, section 2.3.1. Subsequently, lipid profiling assays referred to in Chapter 2, section 2.3.2. were conducted to determine the concentration (mmol/l) of TC, LDL, HDL and TGs within the plasma.

3.2.6. Histological assessment of the deposition of fatty streaks within the thoracic aorta

The thoracic aorta of each mouse was removed, cleaned and stored according to the protocol detailed in Chapter 2, section 2.3.1. Each thoracic aorta was placed in a well of a 96 well plate and

subsequently stained with Oil Red O, imaged and analysed for the deposition of fatty streaks according to the protocol described in Chapter 2, section 2.3.4.1.

3.2.7. Histological assessment of ventricular structure/composition

Frozen ventricular tissue from mice (for removal and storage see Chapter 2, section 2.3.1.) was cryosectioned longitudinally (10 μ m), mounted onto slides and subsequently fixed for histological staining according to the protocol detailed in Chapter 2, section 2.3.4.2. Haematoxylin & Eosin (H & E) staining of the tissue was carried out to enable measurement of the LV and RV wall thickness and that of the IVS. Additionally, Picrosirius Red and Oil Red O staining of the ventricular tissue were conducted to determine collagen and lipid deposition, respectively (subsequently calculated as a percentage of the total ventricular area). For details regarding the staining, imaging and analysis of the ventricular tissue using H & E, Picrosirius Red and Oil Red O see Chapter 2, sections 2.3.4.3., 2.3.4.4. and 2.3.4.5., respectively.

3.2.8. Statistical analysis

To ensure that the studies planned within this chapter had sufficient statistical power, power calculations were conducted prior to experiments taking place and were based on data from previous experiments performed in the lab. With the exception of the isolated vessel studies where power calculations recommended an n=9, an n=5 was recommended for all other variables measured in this chapter. Examples of power calculations performed for studies conducted within this chapter:

Cardiac morphology studies: Pooled standard deviations from data for both LV wall thickness and HW:BW were 0.11 and 0.14, respectively. With a sample size for each experimental group of n=5, a one-way ANOVA would detect differences of 0.26mm (LV wall thickness; 80% power) and 0.39mg/g (HW:BW; 92% power) between the group means.

Isolated vessel studies: Pooled standard deviations from pilot data for vasoconstriction (U-46619) and vasorelaxation (MCh and SNP) responses were 1, 14 and 9, respectively. With a sample size for each experimental group of n=9, a one-way ANOVA would have 80% power to detect differences of 1.65mN/mm (active wall tension), 86% power to detect a 25% change in relaxation to MCh and a 13% change in relaxation to SNP between the intervention means.

In addition to any experiment specific exclusion criteria already detailed, data was excluded if it was outwith the mean \pm 2x(standard deviations). Data are expressed as mean \pm S.E.M throughout. Multiple comparisons were performed using a two-way ANOVA followed by a 'Bonferroni' post hoc test to examine: 1) the influence of gene deletion, and 2) the impact of high fat feeding on all indices measured. All statistical tests were carried out using GraphPad Prism[®] 4 software (GraphPad Software, Inc., USA) and differences between data deemed significant where $P < 0.05$.

3.3. Results

3.3.1. Impact of gene deletion and/or a high fat diet on body weight

Mice within each strain were randomly allocated to an NC or HFC diet group (approximately 5 of each gender per strain) and were weighed the day on which they commenced their allotted diet (Week 0). In terms of the male mice, all experimental groups were of similar starting weights with the exception of the ApoE^{-/-} mice allocated to the NC diet which were lighter compared to NC fed C57BL/6 mice ($P < 0.05$; Table 3.1). Similarly in the female mice, all experimental groups were of similar starting weights with the exception of the ApoE^{-/-}/GPR55^{-/-} mice allocated to the HFC diet, which were heavier compared to their NC fed counterparts ($P < 0.001$; Table 3.1). Mice were weighed on the day in which they ended the dietary period (week 12). For both male and female mice, the HFC fed GPR55^{-/-} and ApoE^{-/-}/GPR55^{-/-} groups were heavier than their NC fed counterparts ($P < 0.05$; Table 3.2).

Weight gain in response to both the NC and HFC diets was calculated every two weeks as the change (Δ) in body weight of each animal from week 0. All male mice gained weight throughout the study as expected, and weight gain was enhanced in each strain of mice fed a HFC diet with the exception of the ApoE^{-/-} mice (Figure 3.3. A-D). When compared to their NC fed counterparts, HFC fed C57BL/6 male mice significantly gained weight at weeks 10 and 12 ($P < 0.05$, Figure 3.3. A), whereas HFC fed male GPR55^{-/-} and ApoE^{-/-}/GPR55^{-/-} mice exhibited significantly greater and earlier increases in weight gain (from week 4; $P < 0.05$; Figure 3.3. C and D, respectively) compared to C57BL/6 HFC fed mice. In female mice, weight gain over the duration of the dietary intervention study was of a smaller magnitude than observed in male mice, regardless of diet. Furthermore, only high fat feeding in female GPR55^{-/-} mice resulted in a significant weight gain (compared to NC fed counterparts) at weeks 10 and 12 of the dietary period ($P < 0.001$; Figure 3.4. C).

Weight (g)				
Week 0				
	Male		Female	
	NC	HFC	NC	HFC
C57BL/6	22.7±0.5 (4)	21.4±0.7 (6)	17.9±0.2 (6)	18.9±0.4 (4)
ApoE^{-/-}	18.1±1.8* (5)	22.4±0.9 (5)	17.9±0.7 (5)	19.2±0.7 (5)
GPR55^{-/-}	22.8±0.6 (5)	23.4±0.6 (5)	19.4±0.6 (5)	19.2±0.9 (5)
ApoE^{-/-}/GPR55^{-/-}	20.1±1.4 (3)	21.2±1.7 (7)	16.2±0.6 (7)	19.1±0.3# (10)

Table 3.1. Body weight of male and female mice at week 0. Data are expressed as mean±S.E.M; n-numbers are in brackets. * $P<0.05$ vs. male C57BL/6 NC and # $P<0.001$ vs. female ApoE^{-/-}/GPR55^{-/-} NC; 2-way ANOVA and a ‘Bonferroni’ post hoc test.

Weight (g)				
Week 12				
	Male		Female	
	NC	HFC	NC	HFC
C57BL/6	32.7±0.7 (4)	34.4±1.6 (6)	23.4±0.4 (6)	26.0±1.2 (4)
ApoE^{-/-}	29.9±0.9 (5)	33.6±1.0 (4)	23.8±0.2 (5)	23.3±0.3 (5)
GPR55^{-/-}	31.4±1.2 (5)	40.8±1.7# (5)	24.8±0.5 (5)	27.9±1.1# (5)
ApoE^{-/-}/GPR55^{-/-}	30.3±1.3 (3)	40.6±1.4# (6)	24.3±0.4 (7)	28.6±0.8# (11)

Table 3.2. Body weight of male and female mice at week 12. Data are expressed as mean±S.E.M; n-numbers are in brackets. # indicates a significant effect ($P<0.05$) of diet within the same strain and gender; 2-way ANOVA and a ‘Bonferroni’ post hoc test.

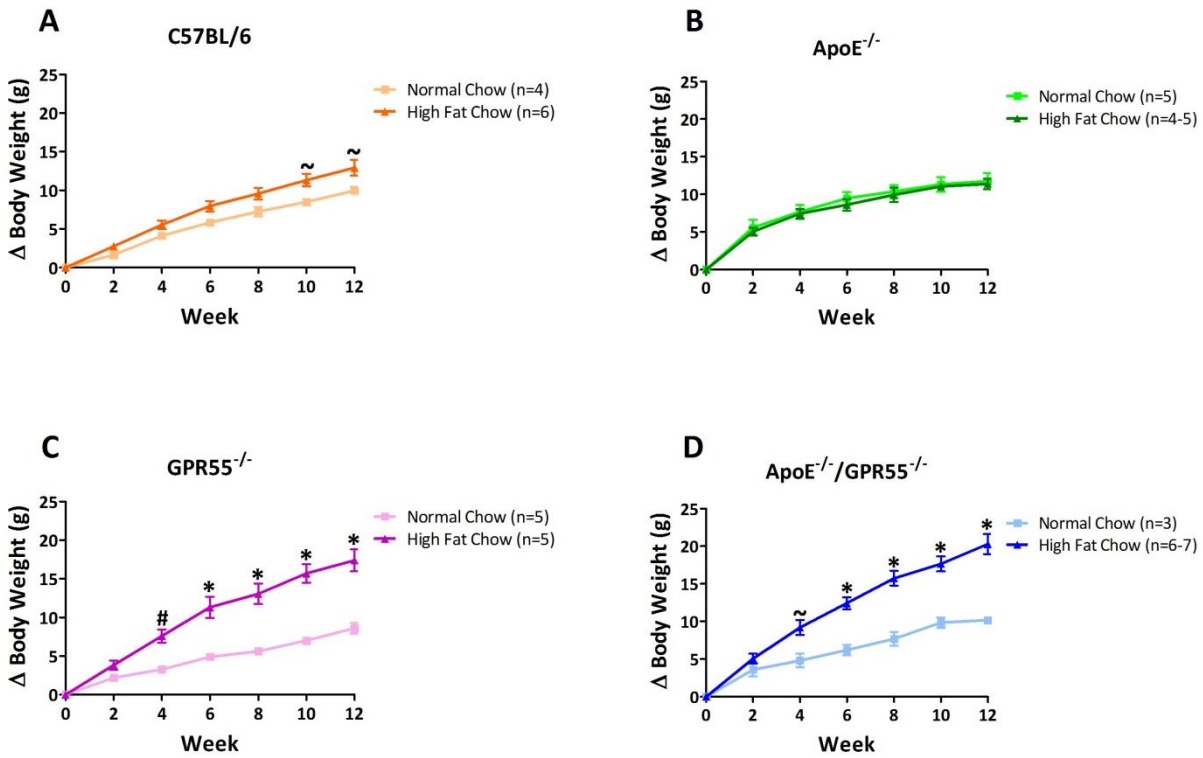


Figure 3.3. Weight gain over time in male mice. Data are expressed as mean±S.E.M. * $P < 0.001$ vs. normal chow, # $P < 0.01$ vs. normal chow and ~ $P < 0.05$ vs. normal chow; 2-way ANOVA and a 'Bonferroni' post hoc test.

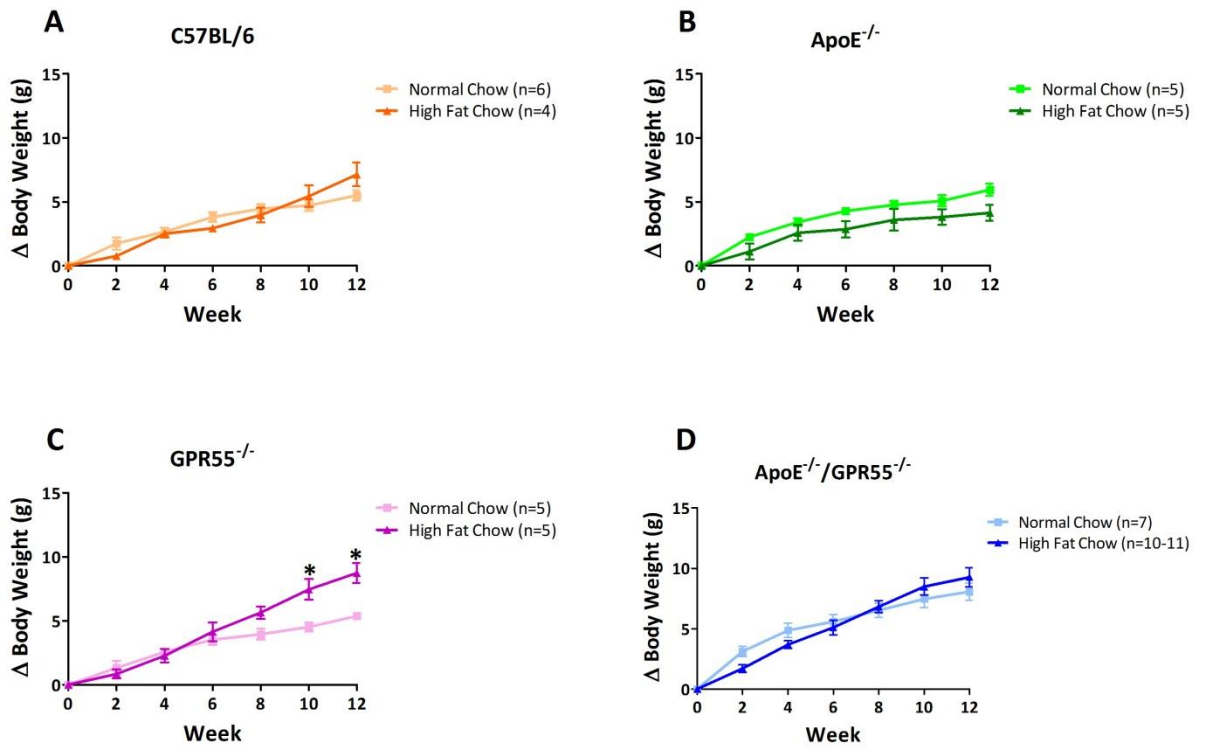


Figure 3.4. Weight gain over time in female mice. Data are expressed as mean±S.E.M. * $P < 0.001$ vs. normal chow; 2-way ANOVA and a 'Bonferroni' post hoc test.

3.3.2. Impact of gene deletion and/or a high fat diet on body mass composition

3.3.2.1. Fat mass

EchoMRI™ body scanning was conducted at weeks 0, 6 and 12 of the dietary period to identify changes in fat and lean mass composition. With the exception of female GPR55^{-/-} mice, which exhibited a lower starting fat mass ($P<0.001$; Table 3.3), all strains assigned to an NC diet had similar fat masses (% body weight; BW) at week 0 compared to NC fed C57BL/6 mice. After 6 and 12 weeks of NC consumption, strain had no effect on fat mass, regardless of gender (Figure 3.5. A-D). In contrast, HFC significantly increased the fat mass of male C57BL/6, GPR55^{-/-} and ApoE^{-/-}/GPR55^{-/-}, but not ApoE^{-/-} mice, at both 6 and 12 weeks of dietary intervention when compared to their NC fed equivalents ($P<0.05$, Figure 3.5. A and C, respectively). The high fat feeding of female mice only increased fat mass by the 6 week time point in the ApoE^{-/-}/GPR55^{-/-} mice ($P<0.05$; Figure 3.5. B). However, consumption of this diet for an additional 6 weeks significantly increased the fat masses of C57BL/6, GPR55^{-/-} and ApoE^{-/-}/GPR55^{-/-} mice ($P<0.05$; Figure 3.5. D). Group sizes at week 0 are indicated in brackets in Table 3.3., while group sizes for weeks 6 and 12 are detailed in Table 3.4.

3.3.2.2. Lean mass

At week 0, female ApoE^{-/-} and GPR55^{-/-} mice allocated to eat NC exhibited greater lean masses than their WT counterparts ($P<0.05$; Table 3.4.). At this time point, male ApoE^{-/-} mice and female C57BL/6 and ApoE^{-/-}/GPR55^{-/-} mice assigned to eat HFC also had greater lean masses than their counterparts allotted to the NC diet ($P<0.05$; Table 3.4.). By week 6, the lean mass of NC fed male ApoE^{-/-}/GPR55^{-/-} mice was reduced when compared to male C57BL/6 mice on NC ($P<0.01$; Figure 3.6. A). In addition, high fat feeding of male C57BL/6 and ApoE^{-/-} mice reduced and increased their lean masses (compared to their NC fed counterparts), respectively at the 6 week time point ($P<0.05$; Figure 3.6. A). At week 12, lean mass was significantly reduced in both male GPR55^{-/-} and ApoE^{-/-}/GPR55^{-/-} mice fed NC compared with C57BL/6 mice on the same diet ($P<0.01$; Figure 3.6. C). Additionally, high fat feeding of male C57BL/6 mice significantly reduced their lean mass by week 12 compared to their NC fed counterparts ($P<0.05$; Figure 3.6. C) and the HFC induced increase in lean mass observed in male ApoE^{-/-} mice at 6 weeks was no longer present by week 12 of this study (Figure 3.6. C). Finally, the lean mass of female mice was not altered by strain and/or diet at either the 6 or 12 week time points (Figure 3.6. B and D, respectively). Group sizes at week 0 are indicated in brackets in Table 3.5., while group sizes for weeks 6 and 12 are detailed in Table 3.6.

Fat Mass (% BW)				
Week 0				
	Male		Female	
	NC	HFC	NC	HFC
C57BL/6	7.7±0.3 (4)	9.1±0.3 (6)	10.2±0.6 (6)	9.3±0.7 (4)
ApoE^{-/-}	8.5±0.6 (5)	8.5±0.5 (4)	10.2±0.7 (5)	8.9±0.2 (5)
GPR55^{-/-}	7.1±0.2 (5)	8.2±0.5 (5)	7.2±0.2* (5)	7.8±0.5 (5)
ApoE^{-/-}/GPR55^{-/-}	8.0±0.2 (3)	7.9±0.5 (4)	9.9±0.4 (7)	8.4±0.4 (6)

Table 3.3. Fat mass (% of body weight; BW) of male and female mice at week 0, measured via EchoMRI™ body scanning. Data are expressed as mean±S.E.M; n-numbers are in brackets. **P*<0.001 vs. female C57BL/6 NC; 2-way ANOVA and a ‘Bonferroni’ post hoc test.

Group Sizes for Fat Mass (% BW)					
		Male		Female	
		Week 6	Week 12	Week 6	Week 12
C57BL/6	NC	4	4	6	5
	HFC	6	6	4	4
ApoE^{-/-}	NC	5	5	5	5
	HFC	4	4	5	5
GPR55^{-/-}	NC	3	5	3	5
	HFC	5	5	5	5
ApoE^{-/-}/GPR55^{-/-}	NC	3	3	7	7
	HFC	4	4	6	6

Table 3.4. Group sizes for fat mass (% of body weight; BW) of male and female mice at weeks 6 and 12, measured via EchoMRI™ body scanning. See Figure 3.5. for the corresponding graphs.

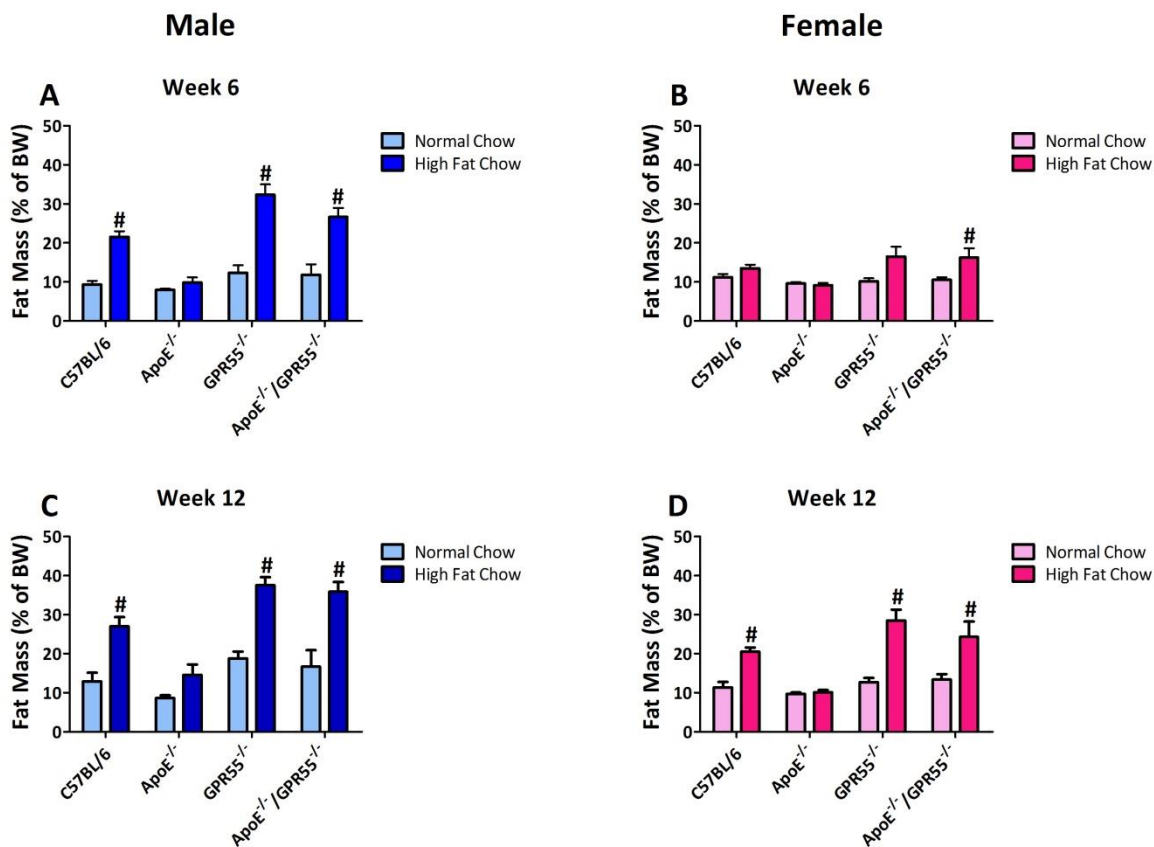


Figure 3.5. Fat mass (% of body weight; BW) of male and female mice at weeks 6 and 12, measured via EchoMRI™ body scanning. Male and female mice at week 6; A and B, respectively. Male and female mice at week 12; C and D, respectively. Data are expressed as mean±S.E.M. # indicates a significant effect ($P < 0.05$) of diet within the same strain; 2-way ANOVA and a ‘Bonferroni’ post hoc test.

Lean Mass (g)				
Week 0				
	Male		Female	
	NC	HFC	NC	HFC
C57BL/6	15.9±2.0 (4)	17.5±0.9 (6)	13.3±0.5 (6)	15.6±0.2# (4)
ApoE^{-/-}	14.8±0.8 (5)	19.4±0.8# (5)	15.1±0.4* (5)	15.2±0.4 (5)
GPR55^{-/-}	19.0±0.6 (5)	19.6±0.4 (5)	15.3±0.5* (5)	15.7±0.6 (5)
ApoE^{-/-}/GPR55^{-/-}	15.4±1.7 (3)	14.6±1.8 (4)	12.7±0.6 (7)	14.8±0.3# (6)

Table 3.5. Lean mass (g) of male and female mice at week 0, measured via EchoMRI™ body scanning. Data are expressed as mean±S.E.M; n-numbers are in brackets. **P*<0.05 vs. female C57BL/6 NC and #*P*<0.05 vs. same strain (NC) and gender; 2-way ANOVA and a ‘Bonferroni’ post hoc test.

Group Sizes for Lean Mass (g)					
		Male		Female	
		Week 6	Week 12	Week 6	Week 12
C57BL/6	NC	4	4	6	5
	HFC	6	6	4	4
ApoE^{-/-}	NC	5	5	5	5
	HFC	5	4	5	5
GPR55^{-/-}	NC	3	5	3	5
	HFC	5	5	5	5
ApoE^{-/-}/GPR55^{-/-}	NC	3	3	7	7
	HFC	4	4	6	6

Table 3.6. Group sizes for lean mass (g) of male and female mice at weeks 6 and 12, measured via EchoMRI™ body scanning. See Figure 3.6. for the corresponding graphs.

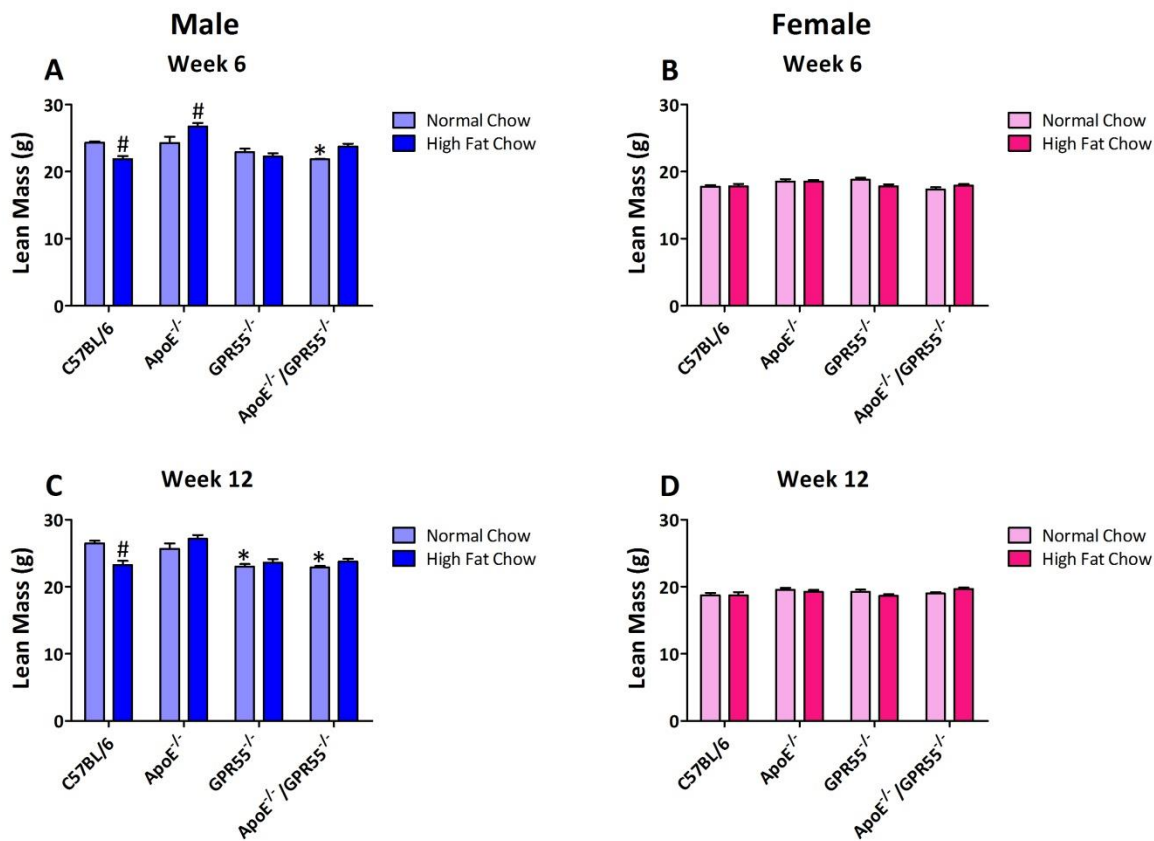


Figure 3.6. Lean mass (g) of male and female mice at weeks 6 and 12, measured via EchoMRI™ body scanning. Male and female mice at week 6; A and B, respectively. Male and female mice at week 12; C and D, respectively. Data are expressed as mean±S.E.M. * indicates a significant effect (vs. C57BL/6 normal chow; $P < 0.01$) of strain and # indicates a significant effect ($P < 0.05$) of diet within the same strain; 2-way ANOVA and a ‘Bonferroni’ post hoc test.

3.3.3. Impact of gene deletion and/or a high fat diet on tissue weights

Following completion of *in vivo* protocols, tissues were harvested, weighed and calculated as the ratio of tissue weight to final body weight (BW). The liver weights (LW) of both male and female mice were not altered by either strain or diet (Figure 3.7. A and B, respectively). Conversely, ventricular weight (VW) was significantly reduced in male ApoE^{-/-} mice on the NC diet compared to their WT counterparts ($P<0.05$; Figure 3.7. C). Interestingly, high fat feeding significantly reduced the VW:BW ratio in male C57BL/6, GPR55^{-/-} and ApoE^{-/-}/GPR55^{-/-} and female ApoE^{-/-}/GPR55^{-/-} mice compared to the NC fed strain equivalent ($P<0.05$; Figure 3.7. C and D, respectively). Additionally, abdominal fat weight (AFW) of mice was similar across the strains, regardless of gender, when compared to their WT counterparts (Figure 3.7. E and F). However, high fat feeding caused an increase in AFW in all strains of male mice and an increase in female GPR55^{-/-} and ApoE^{-/-}/GPR55^{-/-} mice compared to their NC fed strain equivalent ($P<0.05$, Figure 3.7. E and F, respectively). The ratio of spleen weight (SW) and kidney weight (KW) to the final BW of male and female mice was also calculated. With regard to these two tissues, the only difference between NC fed strains was exhibited in female ApoE^{-/-} mice whose spleens were heavier than those of WT mice fed this diet ($P<0.01$; Table 3.8.). Furthermore, high fat feeding of female ApoE^{-/-} mice induced a further increase in spleen weight when compared to those of the same strain who were fed NC ($P<0.05$; Table 3.8.). Finally, high fat feeding resulted in a significant reduction in kidney weight of male ApoE^{-/-}/GPR55^{-/-} and female GPR55^{-/-} and ApoE^{-/-}/GPR55^{-/-} mice compared to their NC fed counterparts ($P<0.05$; Table 3.8.). Group sizes for LW:BW, VW:BW and AFW:BW are detailed in Table 3.7., while group sizes for SW:BW and KW:BW are indicated in brackets in Table 3.8.

Group Sizes for tissue weights							
		LW:BW		VW:BW		AFW:BW	
		Male	Female	Male	Female	Male	Female
C57BL/6	NC	7	6	6	7	7	6
	HFC	5	3	5	3	5	3
ApoE ^{-/-}	NC	7	5	7	5	6	5
	HFC	5	5	5	5	5	5
GPR55 ^{-/-}	NC	5	5	5	5	5	3
	HFC	5	3	3	3	4	3
ApoE ^{-/-} /GPR55 ^{-/-}	NC	5	7	5	6	5	6
	HFC	4	6	4	5	4	6

Table 3.7. Group sizes for tissue weights of mice. AFW; abdominal fat weight, BW; final body weight, LW; liver weight and VW; ventricular weight. See Figure 3.7. for the corresponding graphs.

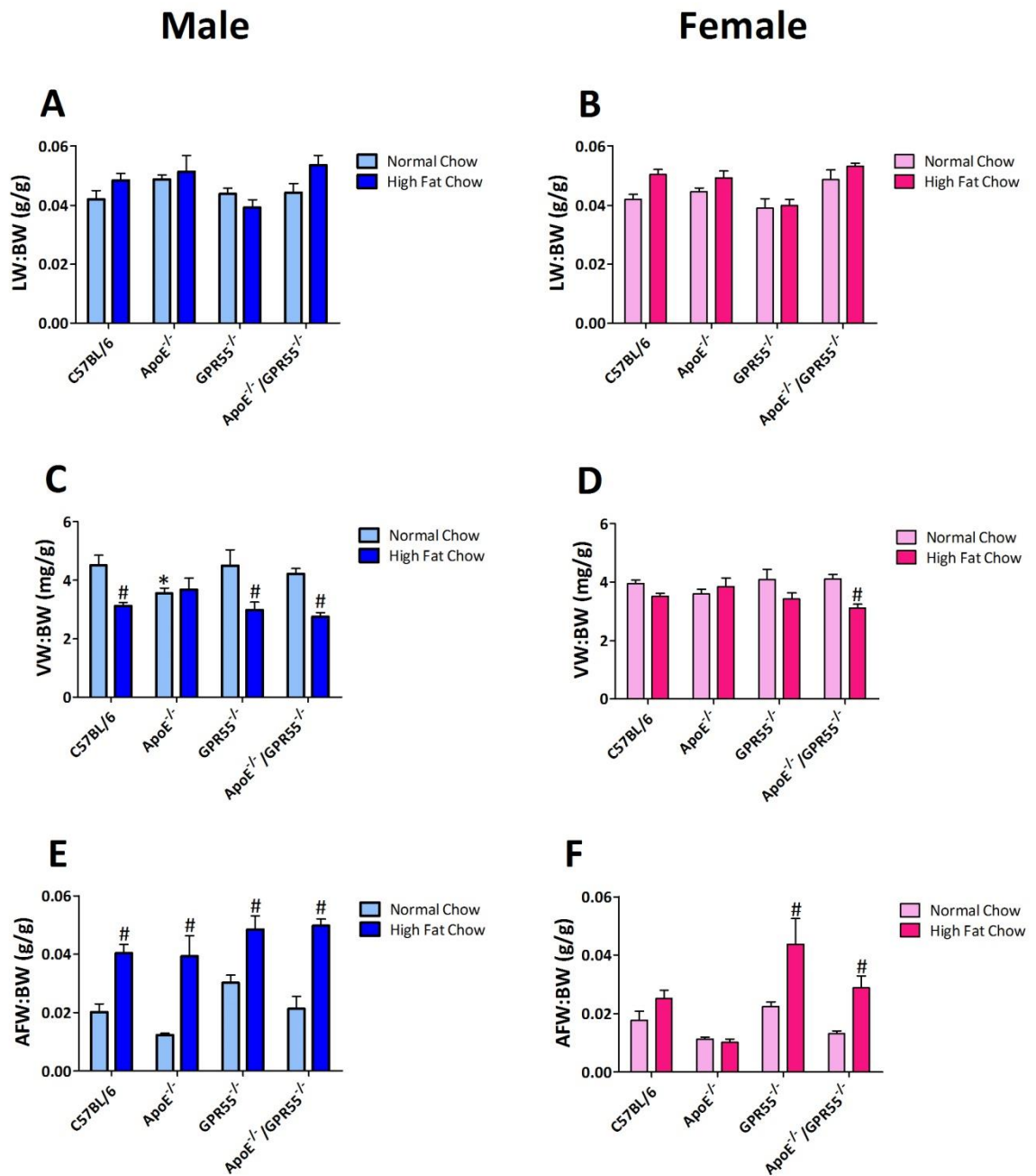


Figure 3.7. Ratio of Liver weight (LW), ventricular weight (VW) and abdominal fat weight (AFW) to final body weight (BW). Tissues from male and female mice; A, C, E and B, D, F, respectively. Data are expressed as mean±S.E.M. * indicates a significant effect (vs. C57BL/6 normal chow; $P < 0.05$) of strain and # indicates a significant effect ($P < 0.05$) of diet within the same strain; 2-way ANOVA and a ‘Bonferroni’ post hoc test.

		Normal Chow		High Fat Chow	
		SW:BW	KW:BW	SW:BW	KW:BW
		(mg/g)	(mg/g)	(mg/g)	(mg/g)
Male	C57BL/6	2.8±0.2 (6)	12.2±0.6 (7)	2.3±0.4 (5)	10.7±0.7 (5)
	ApoE ^{-/-}	3.8±0.4 (6)	12.8±0.4 (6)	3.9±0.5 (5)	10.8±0.7 (5)
	GPR55 ^{-/-}	2.4±0.2 (5)	13.0±0.3 (5)	2.8±0.5 (5)	10.5±1.6 (5)
	ApoE ^{-/-} /GPR55 ^{-/-}	2.7±0.2 (5)	12.8±0.6 (5)	2.5±0.2 (4)	8.6±0.3# (4)
Female	C57BL/6	3.2±0.1 (6)	11.2±0.3 (6)	3.2±0.4 (3)	10.0±0.3 (3)
	ApoE ^{-/-}	4.6±0.3* (5)	11.1±0.3 (5)	5.9±0.7# (5)	10.5±0.3 (5)
	GPR55 ^{-/-}	3.7±0.1 (3)	11.4±0.4 (3)	3.3±0.2 (3)	8.7±0.6# (3)
	ApoE ^{-/-} /GPR55 ^{-/-}	3.6±0.3 (7)	10.9±0.2 (6)	3.9±0.2 (6)	8.8±0.6# (6)

Table 3.8. Ratio of spleen and kidney weight (SW and KW, respectively) to final body weight (BW).

Data are expressed as mean±S.E.M; n-numbers are in brackets. * indicates a significant effect (vs. female C57BL/6 normal chow; $P<0.01$) of strain and # indicates a significant effect ($P<0.05$) of diet within the same strain and gender; 2-way ANOVA and a 'Bonferroni' post hoc test.

3.3.4. Impact of gene deletion and/or a high fat diet on endothelial and smooth muscle function of the carotid artery

Vascular function was assessed in carotid arteries from all experimental groups to determine the impact of strain and/or diet on the contractile, endothelial and smooth muscle function of these vessels. To perform meaningful statistical analysis, data from both male and female mice of each strain were combined. To assess contractile activity, increasing concentrations of U-46619 (10^{-9} - 10^{-5} M) were added to the myograph bath. High fat feeding in control (C57BL/6) mice resulted in a rightward shift of the CRC and a significant attenuation of the contractile response at 10^{-7} , 3×10^{-7} , and 10^{-6} M U-46619 compared with vessels from NC fed C57BL/6 mice ($P < 0.05$; Figure 3.8. A), while the high fat feeding of GPR55^{-/-} mice resulted in a significant augmentation of the contractile response at 10^{-7} M compared to vessels from GPR55^{-/-} mice fed an NC diet ($P < 0.01$; Figure 3.8. C). In contrast, high fat feeding did not significantly alter U-46619-induced vasoconstriction in vessels from ApoE^{-/-} or ApoE^{-/-}/GPR55^{-/-} mice (Figure 3.8. B and D). With regard to E_{\max} Δ in tension, the only difference was seen in NC fed GPR55^{-/-} mice, where the E_{\max} value was lower than that of WT mice fed an NC diet ($P < 0.05$; Table 3.9). LogEC₅₀ values revealed that U-46619 was less potent in vessels from HFC fed C57BL/6 mice compared to NC fed C57BL/6 mice ($P < 0.05$; Table 3.9) and that U-46619 was more potent in the carotid arteries of HFC fed GPR55^{-/-} mice than GPR55^{-/-} mice fed an NC diet ($P < 0.05$; Table 3.9). Group sizes for the contractile responses to U-46619 are indicated in brackets in Figure 3.8., while the group sizes for the E_{\max} Δ in tension and logEC₅₀ values to this agent are indicated in brackets in Table 3.9.

To examine the impact of strain and/or diet on both endothelium-dependent and -independent vasorelaxation, vessels were pre-constricted with U-46619 (EC₈₀ concentration) and CRCs to both MCh (10^{-9} - 10^{-4} M) and SNP (10^{-9} - 10^{-4} M) carried out (for exemplar traces of MCh and SNP-induced relaxations see Figure 3.9. A and B, respectively). High fat feeding did not alter the MCh (Figure 3.10.) or SNP-induced (Figure 3.11.) relaxation of vessels from any strain of mice. Additionally, neither strain nor diet altered the E_{\max} Δ in relaxation or the logEC₅₀ values to either MCh or SNP (Tables 3.10. and 3.11., respectively). Group sizes for the vasorelaxant responses to MCh and SNP are indicated in brackets in Figures 3.10. and 3.11., respectively, while the group sizes for the E_{\max} Δ in relaxation and logEC₅₀ values to MCh and SNP are indicated in brackets in Tables 3.10 and 3.11., respectively.

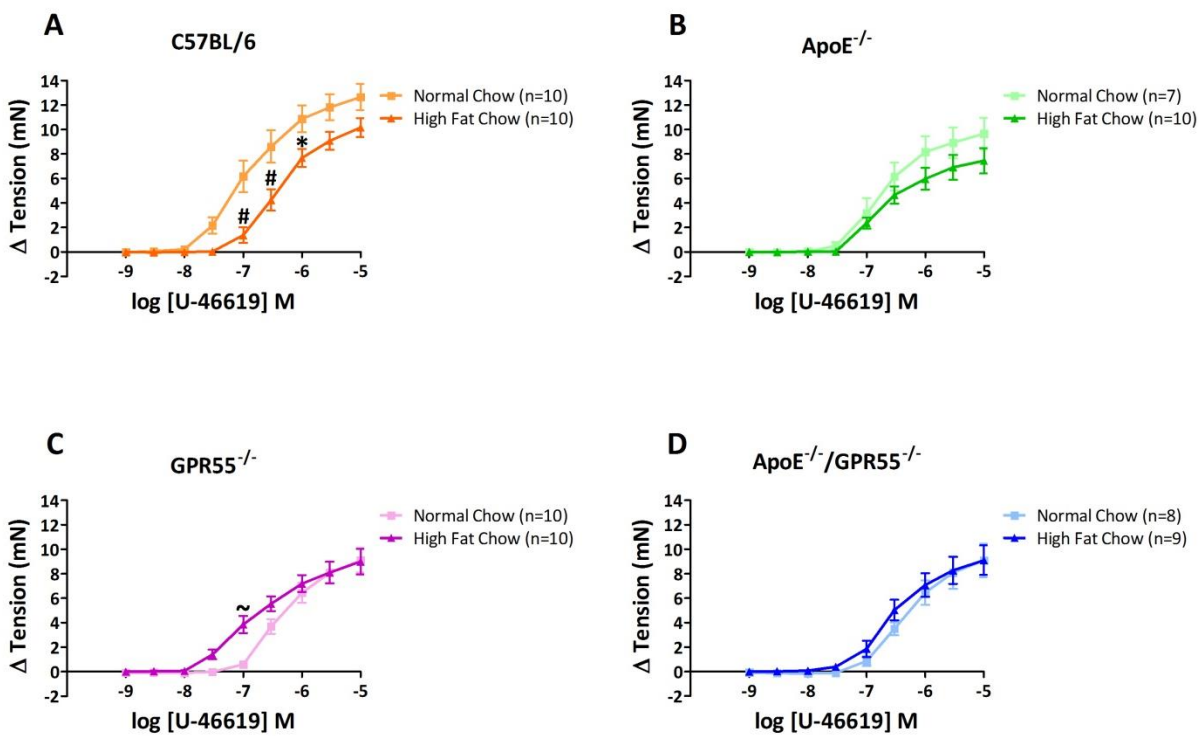


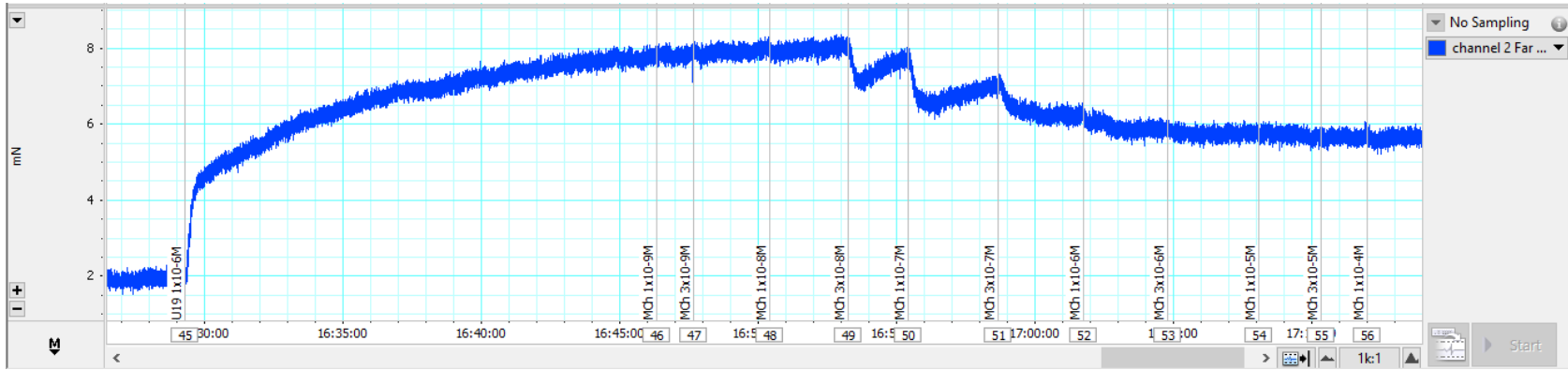
Figure 3.8. The effect of high fat feeding on the contractile responses of the murine carotid artery to U-46619 (10^{-9} - 10^{-5} M). Data are expressed as mean \pm S.E.M. # P <0.001 vs. normal chow, $\sim P$ <0.01 vs. normal chow and $*P$ <0.05 vs. normal chow; 2-way ANOVA and a 'Bonferroni' post-hoc test. Data from both male and female mice were combined in the analysis of responses to U-46619.

U-46619

		E_{max} Δ in Tension (mN)	logEC₅₀ Value (M)
C57BL/6	NC	12.7±1.1 (10)	-7.0±0.1 (10)
	HFC	10.2±0.8 (10)	-6.4±0.1# (10)
ApoE^{-/-}	NC	9.7±1.3 (7)	-6.7±0.1 (7)
	HFC	7.5±1.1 (10)	-6.7±0.1 (10)
GPR55^{-/-}	NC	9.1±1.0* (10)	-6.4±0.1 (10)
	HFC	9.0±1.0 (10)	-6.8±0.1# (10)
ApoE^{-/-}/GPR55^{-/-}	NC	9.1±1.4 (8)	-6.3±0.1 (8)
	HFC	9.1±1.2 (9)	-6.6±0.1 (9)

Table 3.9. The effect of gene deletion and/or diet on the maximal (E_{max}) Δ in tension of the murine carotid artery to U-46619 (10⁻⁹-10⁻⁵M) and the associated logEC₅₀ values. Data are expressed as mean±S.E.M; n-numbers are in brackets. * indicates a significant effect (vs. C57BL/6 normal chow; *P*<0.05) of strain and # indicates a significant effect (*P*<0.05) of diet within the same strain; 2-way ANOVA and a ‘Bonferroni’ post hoc test. Data from both male and female mice were combined in the analysis of the E_{max} responses of the murine carotid artery to U-46619 and the associated logEC₅₀ values.

A



B

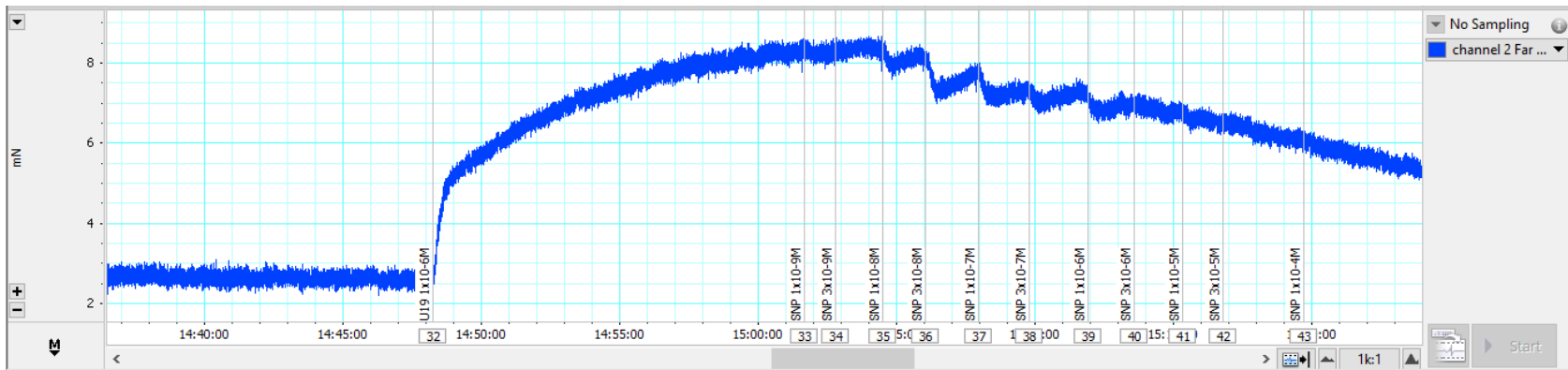


Figure 3.9. Exemplar traces of vasodilator-induced relaxations of the murine carotid artery. Relaxations induced by MCh; A and SNP; B.

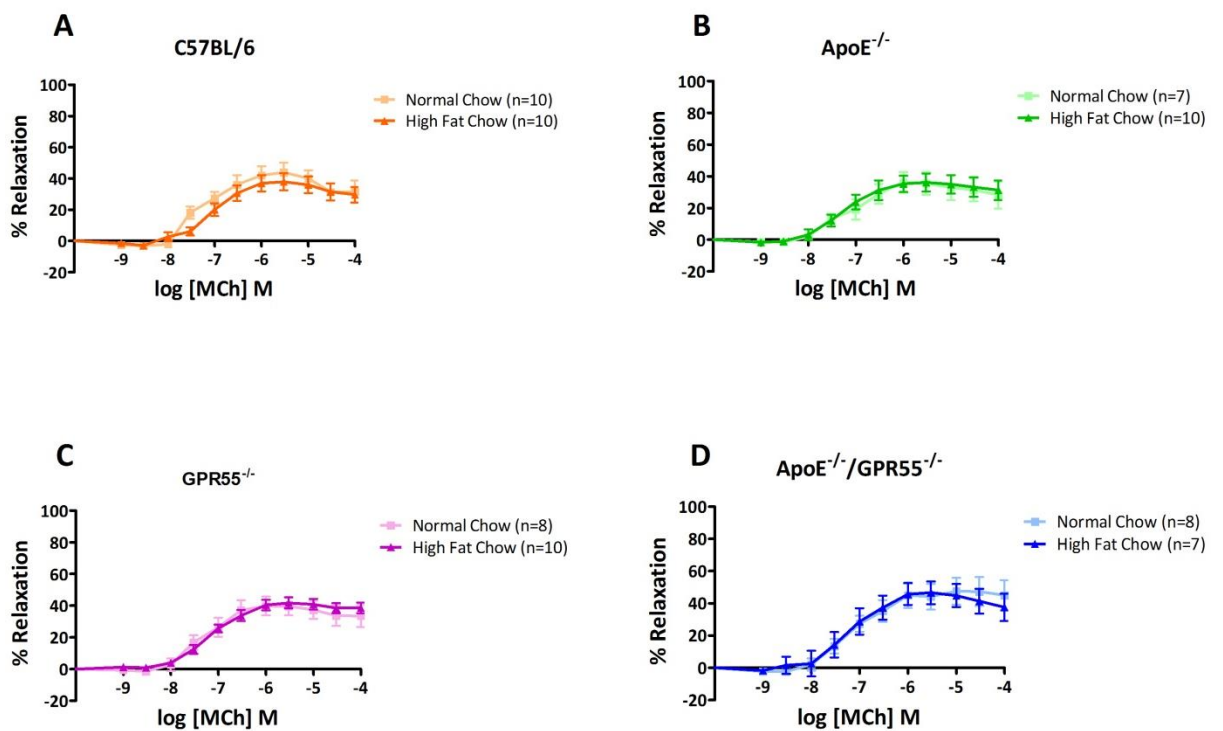


Figure 3.10. The effect of high fat feeding on the endothelium-dependent vasorelaxant responses of the murine carotid artery to MCh (10^{-9} - 10^{-4} M). Data are expressed as mean \pm S.E.M. 2-way ANOVA and a 'Bonferroni' post-hoc test. Data from both male and female mice were combined in the analysis of vasorelaxant responses to MCh.

		MCh	
		E_{\max} Δ in relaxation (%)	logEC ₅₀ (M)
C57BL/6	NC	45.4±6.2 (10)	-7.5±0.1 (10)
	HFC	38.9±5.5 (10)	-7.1±0.1 (10)
ApoE^{-/-}	NC	37.3±6.8 (7)	-7.3±0.3 (7)
	HFC	37.8±5.7 (10)	-7.4±0.2 (10)
GPR55^{-/-}	NC	40.9±6.1 (8)	-7.4±0.2 (8)
	HFC	44.5±3.1 (10)	-7.2±0.1 (10)
ApoE^{-/-}/GPR55^{-/-}	NC	48.9±8.5 (8)	-7.2±0.2 (8)
	HFC	48.5±7.0 (7)	-7.3±0.2 (7)

Table 3.10. The effect of gene deletion and/or diet on the maximal (E_{\max}) Δ in % relaxation of the murine carotid artery to MCh (10^{-9} - 10^{-4} M) and the associated logEC₅₀ values. Carotid arteries were pre-constricted with U-46619 (EC₈₀ concentration) prior to being relaxed with MCh. Data are expressed as mean±S.E.M; n-numbers are in brackets. 2-way ANOVA and a 'Bonferroni' post-hoc test. Data from both male and female mice were combined in the analysis of E_{\max} responses to MCh and the associated logEC₅₀ values.

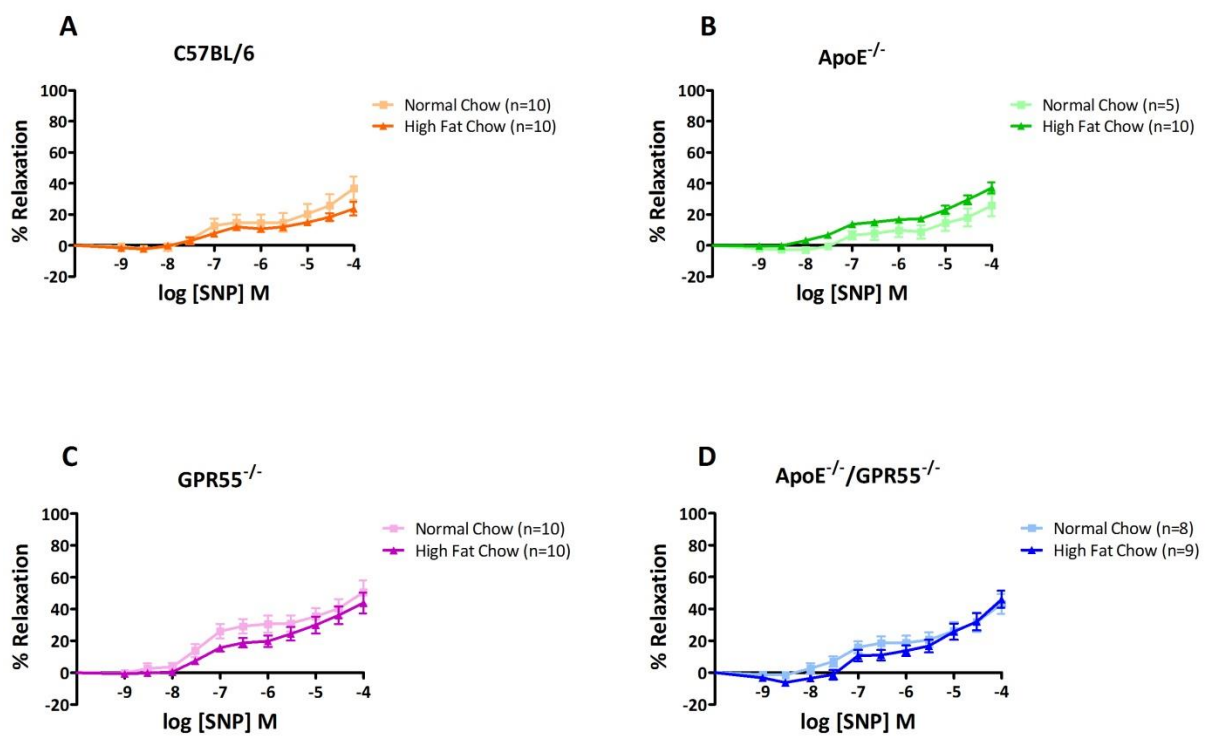


Figure 3.11. The effect of high fat feeding on the endothelium-independent vasorelaxant responses of the murine carotid artery to SNP (10^{-9} - 10^{-4} M). Data are expressed as mean \pm S.E.M. 2-way ANOVA and a 'Bonferroni' post-hoc test. Data from both male and female mice were combined in the analysis of vasorelaxant responses to SNP.

		SNP		
		1 st E _{max} Δ in Relaxation (%)	1 st logEC ₅₀ (M)	2 nd E _{max} Δ in Relaxation (%)
C57BL/6	NC	20.9±4.6 (10)	-7.4±0.2 (10)	36.8±7.6 (10)
	HFC	13.8±1.9 (10)	-7.3±0.2 (10)	24.7±3.1 (10)
ApoE ^{-/-}	NC	10.4±4.5 (5)	-7.2±0.3 (5)	25.9±6.9 (5)
	HFC	18.7±2.0 (10)	-7.5±0.1 (10)	35.4±3.1 (10)
GPR55 ^{-/-}	NC	33.2±5.4 (10)	-7.5±0.2 (10)	50.6±7.3 (10)
	HFC	25.2±4.2 (10)	-7.3±0.2 (10)	44.6±6.4 (10)
ApoE ^{-/-} /GPR55 ^{-/-}	NC	21.9±4.3 (8)	-7.4±0.2 (8)	43.1±6.3 (8)
	HFC	17.6±3.7 (9)	-7.3±0.2 (9)	46.0±5.4 (9)

Table 3.11. The effect of gene deletion and/or diet on the maximal (E_{max}) Δ in % relaxation of the murine carotid artery to SNP (10⁻⁹-10⁻⁴M) and the associated logEC₅₀ values. Carotid arteries were pre-constricted with U-46619 (EC₈₀ concentration) prior to being relaxed with SNP. Data are expressed as mean±S.E.M; n-numbers are in brackets. 2-way ANOVA and a 'Bonferroni' post-hoc test. As the CRCs to SNP were biphasic, the statistics were inconclusive. However, the E_{max} Δ in % relaxation and the logEC₅₀ value of the first phase of each CRC could be calculated as this phase was sigmoidal and are reported as '1st E_{max} Δ in relaxation (%)' and '1st logEC₅₀', respectively. The E_{max} Δ in % relaxation of the second phase for each CRC was also calculated and is reported as '2nd E_{max} Δ in relaxation (%)', however, the associated logEC₅₀ values could not be determined. Data from both male and female mice were combined in the analysis of E_{max} responses to SNP and the associated logEC₅₀ values.

3.3.5. Impact of gene deletion and/or a high fat diet on plasma lipid profiles

Lipid profiling assays were conducted to determine the plasma concentration (mmol/l) of TC, TGs, LDL and HDL and the LDL:HDL ratio. As male mice exhibited the most profound phenotypic changes (i.e. increased body weight and fat mass), plasma lipid profiles were only assessed in mice of this gender. TC, TGs, LDL, HDL and the LDL:HDL ratio were increased in NC fed ApoE^{-/-} and ApoE^{-/-}/GPR55^{-/-} mice compared to C57BL/6 mice fed the same diet ($P<0.05$; Figure 3.12. A-E). In contrast, the plasma lipid profile of NC fed GPR55^{-/-} mice was similar to that of NC fed C57BL/6 mice (Figure 3.12. A-E). Unfortunately, despite having assayed 6 plasma samples from NC fed ApoE^{-/-} mice using the Konelab 30 discrete clinical analyser (Thermo Scientific, UK), LDL readings were only generated for two of these samples. However, Stapleton and colleagues (2007) reported an increase in the concentration of plasma LDL from NC fed ApoE^{-/-} mice compared to NC fed C57BL/6 mice (15.8 vs. 2.9 mmol/l), which is in line with the results of the two readings obtained in the present study. High fat feeding for 12 weeks did not alter lipid profiles in either C57BL/6 or GPR55^{-/-} mice (Figure 3.12. A-E), however, the concentrations of TC, LDL and HDL were further elevated in both HFC fed ApoE^{-/-} and ApoE^{-/-}/GPR55^{-/-} mice compared to their NC fed equivalents ($P<0.05$; Figure 3.12. A, C and D). Consumption of a high fat diet did not alter the LDL:HDL ratios in any mouse strain (Figure 3.12. E) but did reduce the concentration of TGs in the plasma of ApoE^{-/-} and ApoE^{-/-}/GPR55^{-/-} mice ($P<0.05$; Figure 3.12. B). Group sizes for the plasma lipid profiles of each strain are detailed in Table 3.12.

3.3.6. Impact of gene deletion and/or a high fat diet on the deposition of fatty streaks within the thoracic aorta

Oil Red O staining of the murine thoracic aorta was conducted to identify fatty streaks within this vessel (for representative images of Oil Red O stained thoracic aortae from HFC fed ApoE^{-/-} and ApoE^{-/-}/GPR55^{-/-} mice see Figure 3.13. A and B, respectively). As there were no apparent gender-related differences in fatty streak deposition, data from both male and female mice of each strain were combined. When compared to NC fed C57BL/6 mice, only NC fed ApoE^{-/-} mice exhibited an increased deposition of fatty streaks ($P<0.05$; Figure 3.13. C). In response to high fat feeding, fatty streak deposition was significantly enhanced in ApoE^{-/-} mice ($P<0.05$; Figure 3.13. C) whereas ApoE^{-/-}/GPR55^{-/-} mice developed fewer fatty streaks in response to this diet ($P<0.05$; Figure 3.13. C). Neither C57BL/6 nor GPR55^{-/-} mice developed significant fatty streaks in their thoracic aortae in response to HFC (Figure 3.13. C). Group sizes for the deposition of fatty streaks within the thoracic aortae of mice from each strain are detailed in Table 3.13.

		Group Sizes of plasma Lipids				
		TC	TGs	LDL	HDL	LDL:HDL
C57BL/6	NC	5	5	4	5	4
	HFC	5	5	5	5	5
ApoE ^{-/-}	NC	6	6	2	6	2
	HFC	7	7	4	7	4
GPR55 ^{-/-}	NC	5	5	5	5	5
	HFC	5	5	5	5	5
ApoE ^{-/-} /GPR55 ^{-/-}	NC	5	5	5	5	5
	HFC	4	4	4	4	4

Table 3.12. Group sizes of the plasma lipids of mice. HDL; high density lipoprotein, LDL; low density lipoprotein, LDL:HDL; ratio of LDL to HDL, TC; total cholesterol and TGs; triglycerides. Data are from male mice only. See Figure 3.12. for the corresponding graphs.

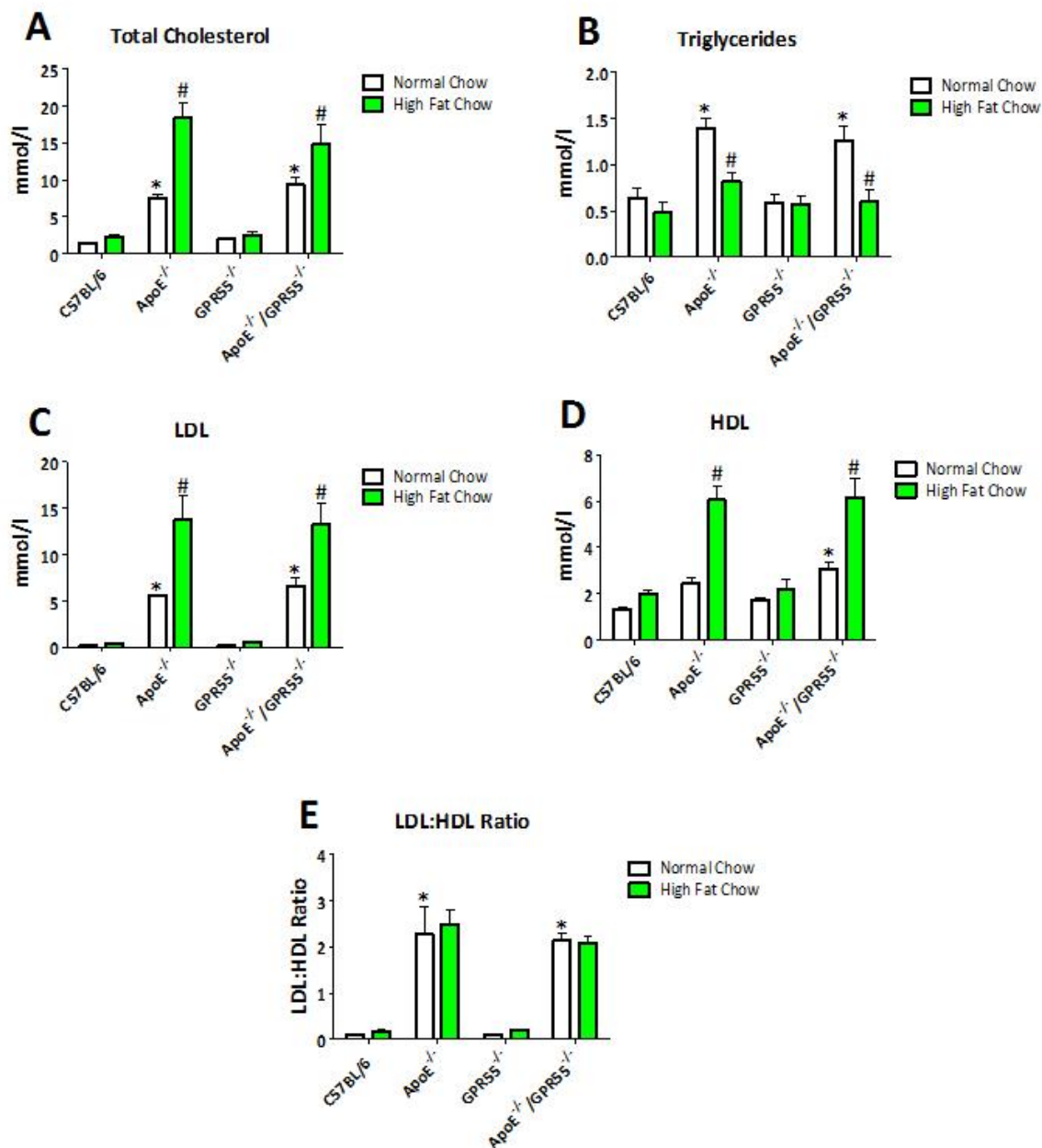


Figure 3.12. Lipid profiling of mouse plasma. Data are expressed as mean±S.E.M. * indicates a significant effect (vs. C57BL/6 normal chow; $P<0.05$) of strain and # indicates a significant effect ($P<0.05$) of diet within the same strain; 2-way ANOVA and a 'Bonferroni' post-hoc test. Data are from male mice only.

Group Sizes for Oil Red O Staining of Fatty Streaks in the Thoracic Aorta

C57BL/6	NC	11
	HFC	8
ApoE^{-/-}	NC	10
	HFC	9
GPR55^{-/-}	NC	10
	HFC	10
ApoE^{-/-}/GPR55^{-/-}	NC	12
	HFC	8

Table 3.13. Groups sizes for Oil Red O staining of fatty streaks in the lumen of the thoracic aorta.

Data from both male and female mice were combined. See Figure 3.13. for the corresponding graphs.

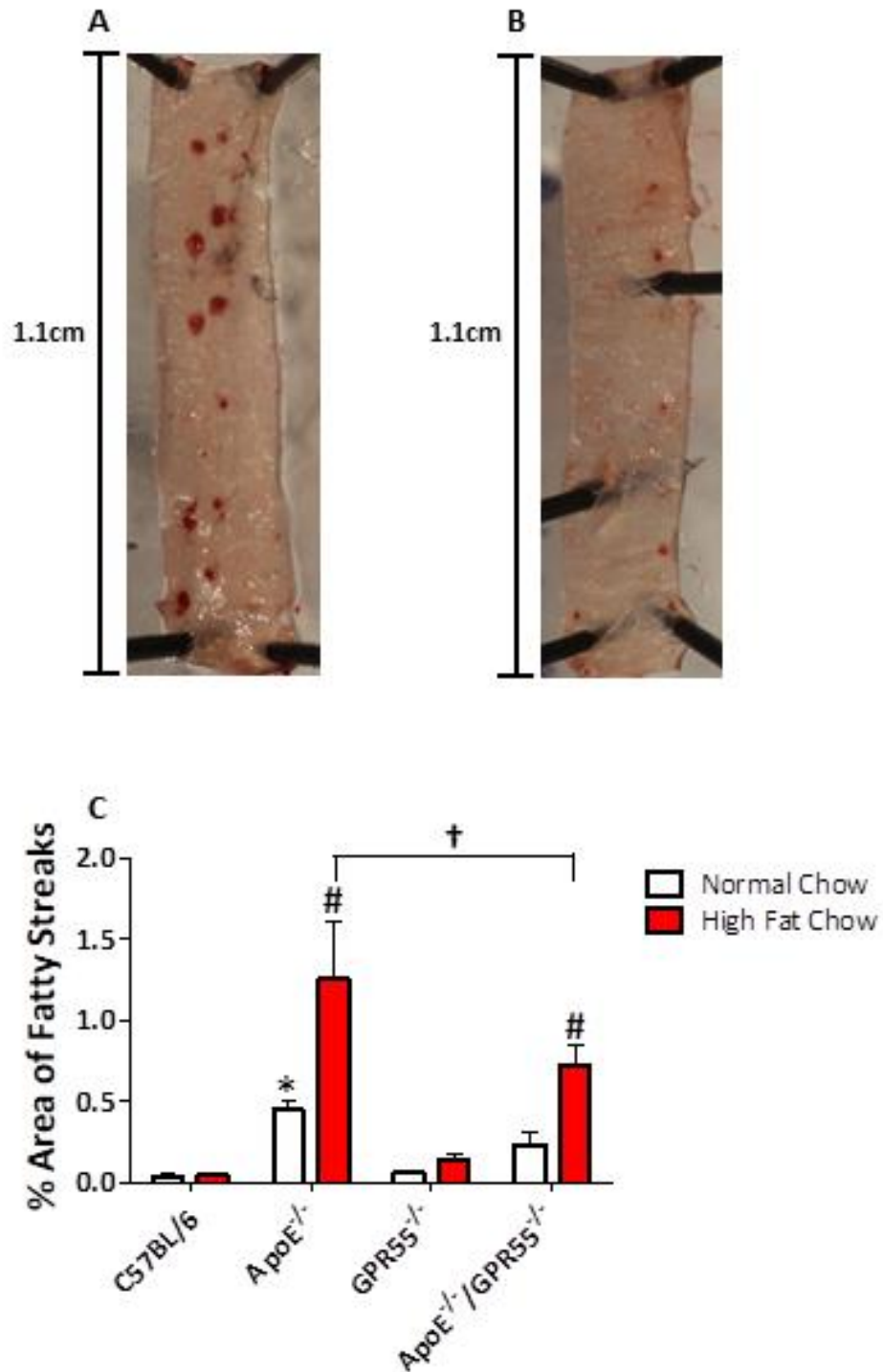


Figure 3.13. Fatty streaks within the thoracic aortae of mice. Exemplar images of Oil Red O stained thoracic aortae from (A) a HFC fed ApoE^{-/-} mouse and, (B) a HFC fed ApoE^{-/-}/GPR55^{-/-} mouse. Percentage area of fatty streaks within the lumen of thoracic aortae; C. Data are expressed as mean±S.E.M. * indicates a significant effect (vs. C57BL/6 normal chow; $P<0.05$) of strain, # indicates a significant effect ($P<0.05$) of diet within the same strain and † indicates a significant effect (vs. ApoE^{-/-} high fat chow; $P<0.05$); 2-way ANOVA and a ‘Bonferroni’ post-hoc test. Data from both male and female mice were combined in the analysis of the % area of fatty streaks.

3.3.7. Impact of gene deletion and/or a high fat diet on cardiac structure

As male mice exhibited the most profound phenotypic changes (i.e. increased body weight and fat mass), cardiac structure, collagen content and lipid deposition were only assessed in mice of this gender. Ventricular tissue sections were stained with H & E for the assessment of cardiac structure (for a representative image of an H & E stained ventricular tissue section illustrating the regions of cardiac structure measured see Figure 3.14. A). The wall thickness of the IVS did not differ with strain and/or diet (Figure 3.14. B). RV wall thickness was unaffected by strain (Figure 3.14. C), however, high fat feeding of ApoE^{-/-} mice increased the RV wall thickness ($P<0.05$; Figure 3.14. C). With regard to LV wall thickness, hearts from NC fed ApoE^{-/-}/GPR55^{-/-} mice exhibited a reduced LV wall thickness compared to NC fed WT mice ($P<0.05$; Figure 3.14. D). High fat feeding did not alter the LV wall thickness of any mouse strain with the exception of C57BL/6 mice, where their LV wall thickness was reduced in response to HFC ($P<0.05$; Figure 3.14. D). Group sizes for the H & E staining of cardiac structure in the ventricular tissue of each strain are detailed in Table 3.14.

3.3.8. Impact of gene deletion and/or a high fat diet on ventricular collagen deposition

Ventricular tissue sections were stained with Picrosirius Red for the detection and quantification of collagen within this tissue. In NC fed mice, collagen deposition was less than 1% of the total ventricular area, an amount which was further reduced in the ventricles of GPR55^{-/-} mice ($P<0.05$; Figure 3.15.). Moreover, high fat feeding did not significantly alter collagen deposition in any strain of mice involved in this study (Figure 3.15.). Group sizes for the Picrosirius Red staining of collagen in the ventricular tissue of each strain are detailed in Table 3.15.

3.3.9. Impact of gene deletion and/or a high fat diet on ventricular lipid deposition

Ventricular tissue sections were stained with Oil Red O to identify and quantify lipid deposition within this tissue. However, significant lipid deposition was not detectable in ventricular tissue from any of the mice examined in this study. To confirm the effectiveness of the staining protocol, a section of human abdominal fat was also stained and used as a positive control. For representative images of an Oil Red O stained murine ventricular tissue section and a section of human abdominal fat see Figure 3.16. A and B, respectively. Group sizes for the Oil Red O staining of lipid deposition in the ventricular tissue of each strain are detailed in Table 3.16.

Group Sizes for H & E Staining of Ventricular Tissue		
C57BL/6	NC	4
	HFC	5
ApoE ^{-/-}	NC	5
	HFC	5
GPR55 ^{-/-}	NC	5
	HFC	3
ApoE ^{-/-} /GPR55 ^{-/-}	NC	5
	HFC	4

Table 3.14. Groups sizes for Haematoxylin and Eosin (H & E) staining of ventricular tissue. See Figure 3.14. for the corresponding graphs. Data are from male mice only.

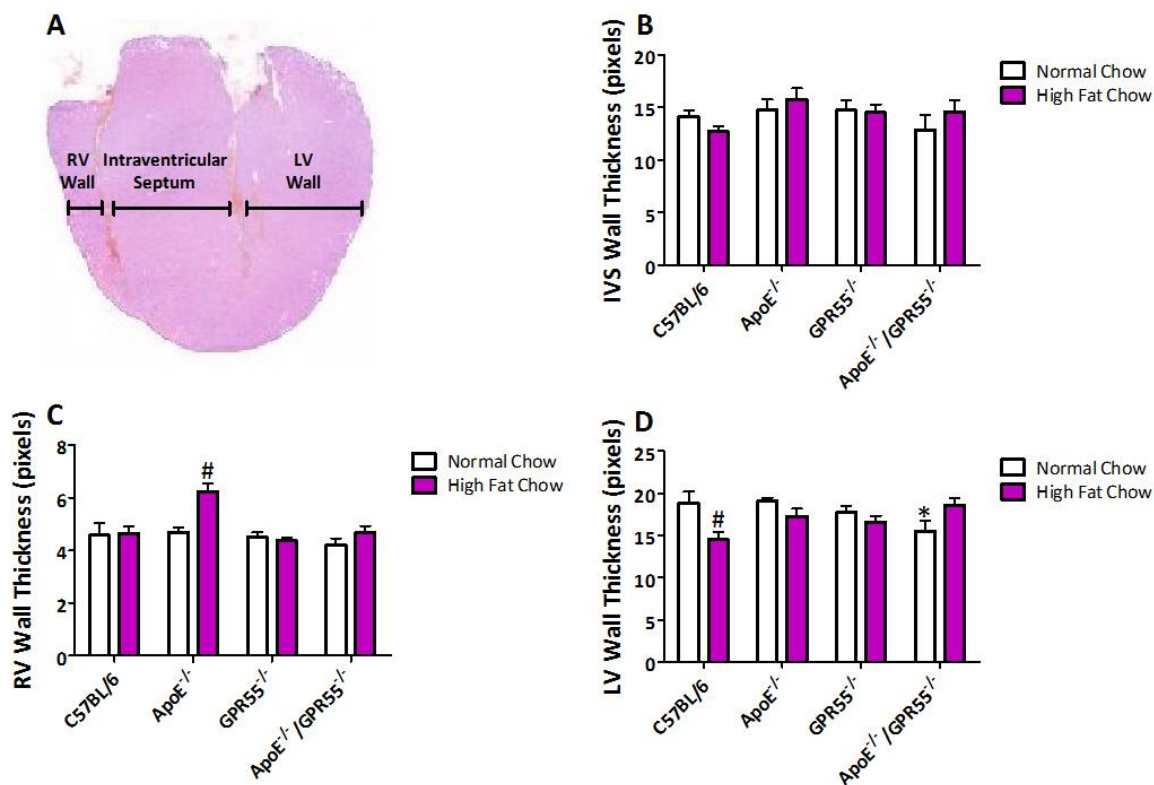


Figure 3.14. H & E staining in murine ventricular tissue for the detection of cardiac structure . An exemplar H&E stained section of ventricular tissue detailing the location of the LV and RV walls and that of the IVS; A. Measurements of IVS thickness, RV wall thickness and LV wall thickness; B, C and D, respectively. Data are expressed as mean±S.E.M. * indicates a significant effect (vs. C57BL/6 normal chow; $P<0.05$) of strain and # indicates a significant effect of ($P<0.05$) of diet within the same strain; 2-way ANOVA and a ‘Bonferroni’ post-hoc test. Data are from male mice only. H & E; haematoxylin and eosin, IVS; intraventricular septum, LV; left ventricle and RV; right ventricle.

Group Sizes for Picrosirius Red Staining of Ventricular Tissue		
C57BL/6	NC	4
	HFC	5
ApoE ^{-/-}	NC	5
	HFC	5
GPR55 ^{-/-}	NC	5
	HFC	3
ApoE ^{-/-} /GPR55 ^{-/-}	NC	5
	HFC	4

Table 3.15. Groups sizes for Picrosirius Red staining of ventricular tissue. See Figure 3.15. for the corresponding graphs. Data are from male mice only.

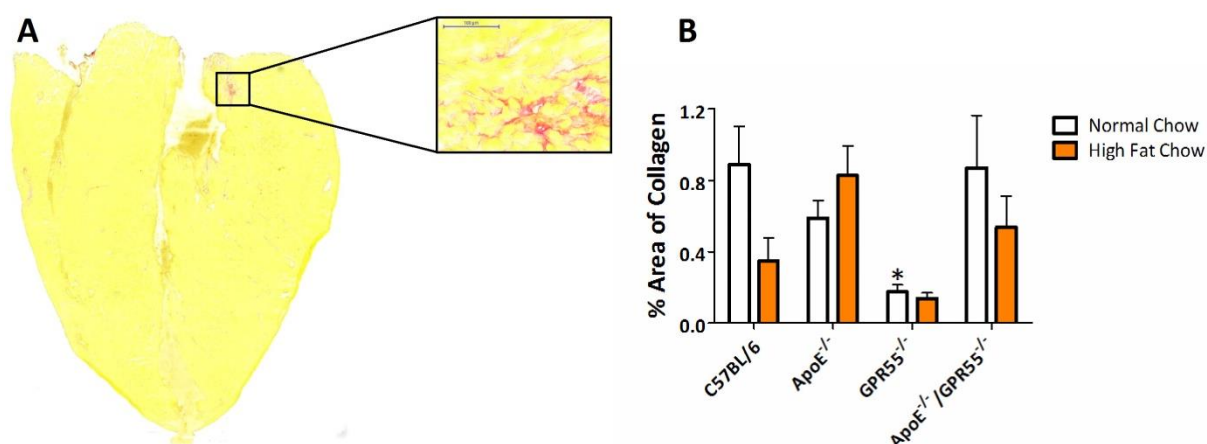


Figure 3.15. Picrosirius Red staining of murine ventricular tissue for the detection of collagen. An exemplar Picrosirius Red stained section of ventricular tissue where red staining is indicative of collagen deposition; A (calibration bar = 100 μ m). Percentage area of collagen within ventricular tissue; B. Data are expressed as mean \pm S.E.M. * indicates a significant effect (vs. C57BL/6 normal chow; $P < 0.05$) of strain; 2-way ANOVA and a 'Bonferroni' post-hoc test. Data are from male mice only.

Group Sizes for Oil Red O Staining of Ventricular Tissue

C57BL/6	NC	4
	HFC	5
ApoE ^{-/-}	NC	5
	HFC	5
GPR55 ^{-/-}	NC	5
	HFC	3
ApoE ^{-/-} /GPR55 ^{-/-}	NC	5
	HFC	4

Table 3.16. Groups sizes for Oil Red O staining of ventricular tissue. See Figure 3.16. for the corresponding graphs. Data are from male mice only.

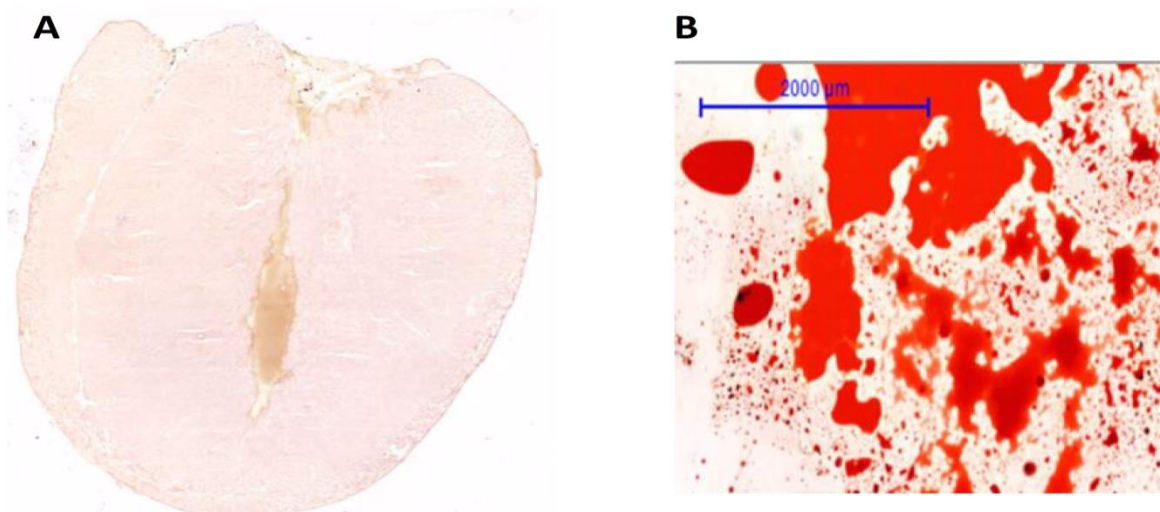


Figure 3.16. Oil Red O staining of murine ventricular tissue for the detection of lipid deposition. A representative image of an Oil Red O stained murine ventricular tissue section from a male mouse; A, and a human abdominal fat section; B (calibration bar = 2000 μ m).

3.4. Discussion

The principle aims of this study were to characterise the phenotype of the novel ApoE^{-/-}/GPR55^{-/-} mouse in response to high fat feeding and to investigate the role of GPR55 in the development of atherosclerosis. Analysis of the data revealed that GPR55 has a complex role whereby it both regulates risk factors associated with atherosclerosis (i.e. body weight and fat mass) while promoting the development of fatty streaks within the vasculature, via a lipid independent mechanism.

3.4.1. The impact of gene deletion on mouse phenotype

When fed NC, few phenotypic differences existed between the strains. Male and female ApoE^{-/-}, GPR55^{-/-} and ApoE^{-/-}/GPR55^{-/-} mice exhibited similar weight gain as their WT counterparts and fat mass remained similar across the groups, regardless of gender. Despite this, a trend of increased fat mass in male GPR55^{-/-} and ApoE^{-/-}/GPR55^{-/-} mice was observed, while the lean mass of these mice was significantly reduced, indicating that male mice deficient in the gene for GPR55 alter their body composition in order to maintain overall body weight. The findings of Meadows and colleagues (2016) differ in that their male, NC fed GPR55^{-/-} mice exhibited a trend of increased body weight and a significant increase in fat mass. The increase in the fat mass of their GPR55^{-/-} mice was only detected from 18-19 weeks of age and although the GPR55^{-/-} mice of the present study were 16-19 weeks of age at the time of analysis, it may be that this group contained a greater number of younger mice which could explain why the increased fat mass of these mice did not reach statistical significance. Meadows and colleagues (2016) also reported that GPR55^{-/-} mice had a similar food intake and eating pattern to that of C57BL/6 mice fed the same diet, therefore the trend of increased fat mass in GPR55^{-/-} mice observed in the present study is unlikely to have occurred as a consequence of increased food intake. Although the present study suggests a role for GPR55 in the regulation of obesity, this effect was more profound in HFC fed animals and so will be discussed in detail in section 3.4.2.1.

Plasma lipids (TC, TGs, LDL and the LDL:HDL ratio) were augmented in both ApoE^{-/-} and ApoE^{-/-}/GPR55^{-/-} mice whereas the concentrations of these lipids in the plasma of GPR55^{-/-} mice were similar to those of C57BL/6 mice. ApoE^{-/-} mice exhibiting elevated plasma lipid profiles has previously been reported (Stapleton *et al.*, 2007) and occurs due to the inability of ApoE to act as a ligand for lipoprotein receptors, thus the hepatic uptake of lipoproteins from the circulation cannot be instigated. Hyperlipidaemic plasma profiles negatively impact the vasculature by causing endothelial

dysfunction, which occurs in response to a reduced availability of vasodilators i.e. NO (Bonetti *et al.*, 2003). As previously mentioned in Chapter 1, section 1.2.3.1, in instances of hyperlipidaemia, there is an increased generation of ROS which consequently react with NO and reduce its bioavailability. In this pathophysiological setting, ROS also interferes with the activity of eNOS, the enzyme primarily responsible for the generation of NO within the vascular endothelium, and impairs NO production (reviewed by Kim *et al.*, 2012). Consequently, endothelial dysfunction ensues and a pro-atherogenic environment is formed i.e. leukocyte adherence (Kubes *et al.*, 1991) and platelet activation (Schäfer *et al.*, 2004). In terms of cardiac function, hyperlipidaemia leads to cellular toxicity, in turn causing secondary conditions i.e. insulin resistance. Myocardial fibrosis also occurs in response to hyperlipidaemia causing electrical (McLenachan and Dargie, 1990; Kawara *et al.*, 2001), mechanical (López *et al.*, 2012) and vasomotor dysfunction (Schwartzkopff *et al.*, 2000), all of which provide the environment for the progression to heart failure (reviewed in detail in Gyöngyösi *et al.*, 2017). Importantly, as ApoE^{-/-} but not GPR55^{-/-} mice of the present study exhibited dyslipidaemic plasma profiles, this would indicate that the dyslipidaemia exhibited by the ApoE^{-/-}/GPR55^{-/-} mice was a characteristic of the ApoE gene deletion and that GPR55 does not regulate lipid levels in the early stages of atherosclerosis. Consequently, any influence GPR55 has on atherogenesis in NC fed mice is independent of circulating lipids.

Additionally, fatty streaks were almost undetectable in the thoracic aortae of both GPR55^{-/-} and C57BL/6 mice. However, there was a significant increase in the deposition of fatty streaks in the thoracic aortae of ApoE^{-/-} mice, which was not evident in ApoE^{-/-}/GPR55^{-/-} mice, therefore this is the first piece of evidence to demonstrate a pro-atherogenic role for GPR55 in the present study. Although there was a pro-atherogenic effect of GPR55 in NC fed ApoE^{-/-} mice, this effect was more profound in HFC fed animals and so will be discussed in section 3.4.4.2.

NC fed ApoE^{-/-}/GPR55^{-/-} mice exhibited a reduced LV wall thickness compared to their WT counterparts. A reduction in the thickness of a ventricular wall is often associated with the death of cardiomyocytes due to myocardial infarction (Kehat and Molkentin, 2010). However, the ApoE^{-/-} mouse model of atherosclerosis is resistant to the development of coronary artery lesions, even when fed a high fat diet, thus making cell death from myocardial infarction improbable (Coleman *et al.*, 2006). Nevertheless, other possibilities include matrix metalloproteinase (MMP)-induced extracellular matrix degradation (Spinale *et al.*, 1998, McElmurray *et al.*, 1999 and Chancey *et al.*, 2002) or volume overload resulting in eccentric hypertrophy (reviewed by Dorn, 2007). However, as this is the first study to document any experimental data pertaining to the novel ApoE^{-/-}/GPR55^{-/-}

mouse model, further research is therefore required to accurately determine the cause of such remodelling.

The ventricular tissue of GPR55^{-/-} mice exhibited a reduced deposition of the structural protein, collagen, whereas the ventricular tissue of ApoE^{-/-} and ApoE^{-/-}/GPR55^{-/-} mice exhibited a similar deposition of this protein to that of C57BL/6 mice. Collagen can influence the compliance of a ventricle to contract, as evidenced by Yamamoto and colleagues (2002) who demonstrated that myocardial stiffening in hypertensive rat hearts is linked to collagen accumulation, in addition to a shift in collagen phenotype and augmented collagen cross-linking (for an extensive review on myocardial collagen deposition see Fan *et al.*, 2012). The finding that ventricular tissue of GPR55^{-/-} mice was characterised by a reduced collagen deposition in the present study is not entirely in line with that reported by Walsh and colleagues (2014), in which GPR55^{-/-} mice exhibited an increase in LV collagen deposition. However, the authors of this study reported that there was an increased loss/death of cells from the hearts of GPR55^{-/-} mice compared to their WT counterparts. On this basis, it was suggested that the increased collagen deposition within the LV of the GPR55^{-/-} hearts may only appear to be increased in light of the cell loss/death. Additionally, the present study stained for collagen using Picrosirius Red, a stain which specifically targets collagen I and III fibers whereas Walsh and colleagues (2014) stained for collagen using Masson Trichrome (MT) stain, which can also detect muscle fibers and amongst other proteins, keratin. It therefore seems likely that the results of the present study more accurately represent the collagen deposition within the hearts of GPR55^{-/-} mice, although another possibility for consideration is the age of the mice at the time in which ventricular collagen deposition was measured. In the present study, collagen deposition was assessed when mice were 16-19 weeks of age whereas those of the study conducted by Walsh and colleagues (2014) were 8 months old. Therefore, it may also be possible that in the absence of GPR55, interstitial collagen deposition increases with age, however, this remains to be investigated. Another possibility is that the genetic ablation of GPR55 increases MMP expression/activity, consequently reducing the ventricular collagen deposition in GPR55^{-/-} mice. In support of this, Montecucco and colleagues (2016) reported that the GPR55 antagonist, CID1602004, increased the intraplaque content of MMP-9 in NC and HFC ApoE^{-/-} mice. However, as MMP-9 degrades type IV collagen fibers (reviewed by Yabluchanskiy *et al.*, 2013) and the present study demonstrated that the ventricular tissue of GPR55^{-/-} mice is characterised by a reduction in type I and III collagen fibers, MMP-9 involvement seems unlikely. Investigation is now required to confirm or deny if another or other MMPs are responsible for the reduced collagen deposition within the ventricular tissue of these mice.

To summarise, the present study suggests a regulatory role for GPR55 in energy metabolism yet a pro-atherogenic role for GPR55 in terms of the deposition of fatty streaks within the thoracic aorta, via a lipid independent mechanism. The structural changes in the hearts of ApoE^{-/-}/GPR55^{-/-} mice were fairly minor, but may suggest that GPR55 plays an important role in maintaining tissue structure in the hyperlipidaemic heart, possibly through extracellular matrix regulation. However, with the exception of Montecucco and colleagues (2016) reporting an increase in the intraplaque content of MMP-9 in NC and HFC fed ApoE^{-/-} mice, there is no data regarding GPR55 and MMP activity and so opens up possible new avenues of enquiry.

3.4.2. The impact of a high fat diet on mouse phenotype

3.4.2.1. Body weight and composition

Male C57BL/6 mice fed HFC exhibited an obesogenic response, as shown by a modest (but significant) increase in weight gain which correlated with an increase in fat mass. In contrast, the body weight and adiposity of ApoE^{-/-} mice was unaffected by high fat feeding. Some studies have previously reported that weight gain in ApoE^{-/-} mice is exacerbated in response to a HFC diet (Sinha-Hikim *et al.*, 2011, Han *et al.*, 2015 and Kim *et al.*, 2015b), while Fukao and colleagues (2010) have reported that it is unchanged. Interestingly, some studies have documented a reduction in the body weight of ApoE^{-/-} mice in response to a diabetogenic high fat diet (Gao *et al.*, 2007 and Hofmann *et al.*, 2008), although the mechanisms underlying this apparent 'anti-obesity' effect in ApoE^{-/-} mice are not entirely clear. However, a number of mechanisms have been proposed including decreased food intake and increased energy expenditure (Gao *et al.*, 2007), impaired delivery of liver-derived VLDL to adipocytes (Pendse *et al.*, 2009) and the modulation of adipocyte triglyceride storage (Huang *et al.*, 2006). ApoE^{-/-}/GPR55^{-/-} mice also developed an obese phenotype and exhibited increased weight gain when fed a HFC diet, similar to that seen in the HFC fed GPR55^{-/-} mice. Taken together, the data suggests that the diet-induced obesity observed in both strains is due to the deletion of GPR55 and that GPR55 has a regulatory role in energy metabolism. In the present study food intake was not measured therefore it cannot be definitively concluded if the GPR55^{-/-} mice were consuming more food. However, a parallel study from this laboratory (Hair, 2016; unpublished data) measured food intake in male C57BL/6 and GPR55^{-/-} mice that were fed the same HFC diet for 12 weeks and established that food intake did not differ between the strains, therefore it is unlikely that the GPR55^{-/-} and ApoE^{-/-}/GPR55^{-/-} mice of the present study consumed a greater quantity of HFC than their C57BL/6 and ApoE^{-/-} counterparts. A plausible hypothesis for the increase in fat mass and the

associated weight gain of the HFC fed GPR55^{-/-} and ApoE^{-/-}/GPR55^{-/-} mice is that these mice exhibited a reduced energy expenditure. Indeed, indirect calorimetry and wheel running tests in male GPR55^{-/-} mice have revealed that these mice exhibit decreased spontaneous and voluntary physical activity, consequently leading to diminished energy expenditure and increased fat accumulation (Meadows *et al.*, 2016). However, while it has been suggested that the increased adiposity in these mice occurred due to the lack of movement, increased adiposity may well be the reason for the reduced physical activity. While the precise cause for the reduced movement in GPR55^{-/-} mice is not yet known, it has previously been reported that these mice are characterised by impaired motor coordination (Wu *et al.*, 2013) which may account for this finding. Alternatively, as wheel running is associated with the brain reward system i.e. incentive salience whereby there is motivation in return for a rewarding stimulus (e.g. neurochemicals), it may be that the brain reward system of GPR55^{-/-} mice is impaired.

Other roles for GPR55 in energy metabolism have been suggested with studies unanimously reporting that the activation of GPR55 by agonists in the islets of Langerhans stimulates insulin release (McKillop *et al.*, 2013; Liu *et al.*, 2016, McKillop *et al.*, 2016 and Romero-Zerbo *et al.*, 2011). On the other hand, it has been reported that GPR55^{-/-} mice have higher basal insulin levels, however, upon stimulation with glucose, these mice release less insulin (Meadows *et al.*, 2016). Furthermore, the Meadows study conducted insulin tolerance tests and established that GPR55^{-/-} mice suffer from insulin resistance which is likely caused by an increased fat mass and liver steatosis in these animals.

Interestingly, in terms of energy regulation it would appear that GPR55 exhibits differential effects on adiposity in humans compared to mice. GPR55 mRNA expression is increased in both the visceral and subcutaneous adipose tissue of obese subjects compared to lean subjects and even more so in obese subjects suffering from type 2 diabetes (Moreno-Navarrete *et al.*, 2012). Moreover, the concentration of circulating plasma LPI of obese subjects is increased and correlates with body weight, fat percentage and the BMI of females. Furthermore, this study revealed that LPI increases the expression of genes associated with lipogenesis in visceral adipose tissue and also increases [Ca²⁺]_i in differentiated visceral adipocytes.

Female mice, on the other hand, exhibited a much smaller increase in fat mass and body weight than male mice. One explanation for this could be the role of oestrogen, which has been previously reported to protect against obesity in female C57BL/6 mice, potentially through modulation of the expression of genes regulating adipogenesis, lipogenesis and lipolysis (Stubbins *et al.*, 2012).

3.4.3. The impact of a high fat diet on lipid profiles

Both ApoE^{-/-} and ApoE^{-/-}/GPR55^{-/-} mice exhibited marked dyslipidaemia in response to HFC feeding, whereas GPR55^{-/-} mice exhibited plasma profiles similar to those of C57BL/6 mice. This data therefore indicates that the severe hyperlipidaemic profiles exhibited by the HFC fed ApoE^{-/-}/GPR55^{-/-} mice were due to the lack of ApoE and that GPR55 does not regulate lipid levels, which is in agreement with the data from the NC fed animals. Elevated total plasma cholesterol (Fukao *et al.*, 2010, Raman *et al.*, 2011, Sinha-Hikim *et al.*, 2011, Han *et al.*, 2015, Lin *et al.*, 2015 and Kim *et al.*, 2015b) and LDL (Fukao *et al.*, 2010, Han *et al.*, 2015 and Kim *et al.*, 2015b) in response to high fat feeding in ApoE^{-/-} mice is well documented, although it is an elevated plasma LDL concentration which is most commonly associated with the development of atherosclerosis (Bentzon *et al.*, 2014). Moreover, in line with the findings of the present study, Kim and colleagues (2015b) reported that ApoE^{-/-} mice are characterised by an elevated plasma HDL concentration in response to high fat feeding. However, other studies have reported that plasma HDL is unaltered in high fat fed ApoE^{-/-} mice (Fukao *et al.*, 2010 and Han *et al.*, 2015), although it is suspected that differences in the composition of the high fat diet and/or the duration of the dietary period are to account for the inconsistency between studies. Furthermore, as LDL and HDL work in conjunction to maintain a homeostatic level of circulating cholesterol (Widmaier *et al.*, 2006), it is therefore likely that the increased plasma HDL concentration observed in the present study occurred as a means to combat the increasing concentration of LDL. Interestingly, the plasma concentration of TGs was reduced in response to high fat feeding in both ApoE^{-/-} and ApoE^{-/-}/GPR55^{-/-} mice. While other studies have reported no change (Fukao *et al.*, 2010 and Raman *et al.*, 2011) or an increase in plasma TGs (Sinha-Hikin *et al.*, 2011, Han *et al.*, 2015, Kim *et al.*, 2015b and Lin *et al.*, 2015), it can be speculated as to why this may have occurred. It may be that the HFC fed ApoE^{-/-} mice in this study were suffering from a condition known as hepatic steatosis, a condition where there is an abnormal retention of hepatic TGs due to an imbalance between lipid acquisition and removal. Interestingly, Schierwagen and colleagues (2015) reported that high fat feeding ApoE^{-/-} mice for 7 weeks induced this condition. In terms of the present study demonstrating that ApoE^{-/-} and ApoE^{-/-}/GPR55^{-/-} mice exhibit a reduced concentration of plasma TGs, it may be that 12 weeks of high fat feeding exacerbates hepatic steatosis to a degree where the plasma concentration of TGs is significantly reduced.

3.4.4. The impact of a high fat diet on vascular function and fatty streak development

3.4.4.1. Vascular function

Endothelial dysfunction is a key event in the development of atherosclerosis (Freiman *et al.*, 1986, Verbeuren *et al.*, 1990, Zeiher *et al.*, 1991, d'Uscio *et al.*, 2001, Crauwels *et al.*, 2003 and Cola *et al.*, 2010) and refers to the impairment of endothelium-dependent vasodilation, which occurs in response to a reduced availability of vasodilators i.e. NO (Bonetti *et al.*, 2003). On this basis, the present study set out to investigate the involvement of GPR55 in endothelial dysfunction associated with atherosclerosis development, as well as any involvement that GPR55 may have in terms of contractile function. The contractile function of the carotid artery was attenuated in C57BL/6 mice fed a HFC diet, but modestly increased in HFC fed GPR55^{-/-} mice. In contrast, the contractile function of the carotid artery of ApoE^{-/-} and ApoE^{-/-}/GPR55^{-/-} mice was unaffected by diet. With regard to the ApoE^{-/-} mice, this is in line with published findings where the contractile function of the thoracic aortae from ApoE^{-/-} mice is unaffected after 21 weeks of being fed an NC or HFC diet (Yaghoubi *et al.*, 2000). Moreover, endothelial function was unaffected by gene deletion and/or diet in the present study. The lack of endothelial dysfunction in NC fed mice lacking ApoE is also in line with the findings of Yaghoubi and colleagues (2000). Their study demonstrated that endothelium dependent relaxation of the thoracic aortae of ApoE^{-/-} mice remains unaffected after 35 weeks of being fed an NC diet. However, the lack of effect of HFC on endothelial function in the present study is somewhat in contrast to the findings of the Yaghoubi study where thoracic aortae of ApoE^{-/-} mice fed HFC for 21 weeks exhibit a reduced sensitivity to NO, despite a normal response to acetylcholine (ACh) and that with 35 weeks of high fat feeding, these vessels exhibited a reduced sensitivity to both agents. Together, the findings of the present study and those reported by Yaghoubi and colleagues (2000) suggest that short-term high fat feeding does not affect endothelial function, yet long-term feeding does. In support of this, endothelial dysfunction in the carotids of ApoE^{-/-} mice has been reported following 26 weeks of high fat feeding (d'Uscio *et al.*, 2001). Additionally, an important point for consideration here is that while endothelium dependent relaxation was not affected in the carotid artery of the present study, vasorelaxation may be affected in another vessel type. Furthermore, for all that muscarinic receptor mediated relaxation does not appear to be affected in the current study, other vasorelaxant receptors may be involved. However, further investigation is required to confirm or refute this suggestion.

Endothelial dysfunction is normally exacerbated by obesity due to the generation of pro-inflammatory cytokines (e.g. interleukin 6 (IL-6) and tumour necrosis factor alpha (TNF- α)) by endothelial cells and pre-adipocytes (Iantorno *et al.*, 2014). It may therefore have been expected that HFC fed GPR55^{-/-} and ApoE^{-/-}/GPR55^{-/-} mice, which both developed an obese phenotype, would exhibit endothelial dysfunction, however, this was not the case. Perivascular adipose tissue (PVAT) promotes endothelial dysfunction via mechanisms that are linked to increased NADPH oxidase-derived oxidative stress and an increased generation of pro-inflammatory cytokines (Ketonen *et al.*, 2010). Interestingly, studies have demonstrated that the vasodilator response to ACh is reduced in aortic ring preparations with PVAT isolated from diet-induced obese mice, while aortic ring preparations isolated from diet-induced obese mice which were free of PVAT exhibited a normal vasodilator response to this agent (Ketonen *et al.*, 2010 and Xia *et al.*, 2016a) thus indicating a role for PVAT in obesity-induced endothelial dysfunction. On this basis, it may be that endothelial dysfunction was not evident in the present study due to the carotid arteries being devoid of PVAT, which was removed during their isolation. For an extensive review on the role of PVAT in obesity-induced vascular dysfunction see Xia and Li., 2016b.

3.4.4.2. *Fatty streak development*

In agreement with the literature (Zhao *et al.*, 2015 and Kumar *et al.*, 2016), C57BL/6 mice fed HFC did not develop fatty streaks within their thoracic aortae. Furthermore, HFC fed GPR55^{-/-} mice similarly did not develop fatty streaks, which in both instances may be in part due to their normolipidaemic plasma profiles. On the other hand, HFC fed ApoE^{-/-} mice developed fatty streaks within their thoracic aortae, particularly at branch points, which are sites characterised by disturbed blood flow and low shear stress. Genes and proteins of endothelial cells (i.e. MCP-1) are generally upregulated at these branch points promoting atherogenesis (reviewed by Chiu and Chien, 2011). This finding is consistent with other studies that have shown atheroma development within the vasculature of ApoE^{-/-} mice (Beattie *et al.*, 2009 and Lin *et al.*, 2015). However, in HFC fed ApoE^{-/-}/GPR55^{-/-} mice, the extent of fatty streak formation was significantly less than in the ApoE^{-/-} mice fed this diet, suggesting that the presence of a functioning GPR55, while not initiating atherogenesis *per se*, may contribute in some way to atheroma development. This data supports that of Lanuti and colleagues (2015) who reported that the activation of GPR55 with O-1602 in foam cells exacerbates ox-LDL-induced lipid accumulation and inflammatory responses, while reducing cholesterol efflux from human macrophages - processes which suggest a pro-atherogenic role for GPR55. However, the finding that GPR55 may be pro-atherogenic in terms of the development of fatty streaks is somewhat in conflict

to reports that the GPR55 antagonist, CID16020046, does not reduce lesion size in the thoraco-abdominal aortas of HFC fed ApoE^{-/-} mice (Montecucco *et al.*, 2016). However, Montecucco and colleagues (2016) did not demonstrate that the dose of CID16020046 administered to their ApoE^{-/-} mice was sufficient to antagonise GPR55. On this basis, it cannot be definitively concluded that CID16010046 was blocking GPR55 and having no effect on plaque size. In support of this, the authors advise that the limited exposure to CID16020046 (one dose per day, five days per week for a maximum of three weeks) may not have been sufficient to produce long-term and complete blockade of GPR55.

The precise mechanism(s) by which GPR55 contributes to atheroma development was not addressed in the present study, although it is likely to be via a lipid independent mechanism, since a lack of GPR55 did not influence the lipid profiles in response to HFC, but did suppress the development of fatty streaks. Atherogenesis is initiated by endothelial dysfunction and a high circulating concentration of plasma LDL. Monocytes are subsequently encouraged to bind to dysfunctional endothelial cells via adhesion molecules such as VCAM-1 and ICAM-1 (Toth, 2008). LPI has been shown to upregulate VCAM-1 and ICAM-1 in rabbit aortic endothelial cells and human umbilical vein endothelial cells, respectively (Kume *et al.*, 1992), although whether or not this is via an action at GPR55 was not investigated. Following monocyte binding, MCP-1 encourages the recruitment of monocytes to the subendothelial space where they subsequently develop into macrophages (Toth, 2008). The GPR55 antagonist, CID16020046, protects against intestinal inflammation by reducing the migration of macrophages (Stančić *et al.*, 2015). Although this observation was not in the vasculature, as atherosclerosis is also an inflammatory condition, GPR55 may play a role in monocyte/macrophage migration associated with the early development of fatty streaks.

3.4.5. The impact of a high fat diet on cardiac remodelling

3.4.5.1. Wall thickness of the LV, RV and IVS

Ventricular tissue sections were stained with H & E and Oil Red O to determine the effects of diet on cardiac structure and lipid accumulation, respectively. IVS wall thickness was not affected by diet. However, an increase in the RV wall thickness (RV hypertrophy) of HFC fed ApoE^{-/-} mice was detected and would suggest that these mice may have been suffering from the early stages of pulmonary hypertension, a condition which has previously been reported in ApoE^{-/-} mice fed a high fat diet

(Hansmann *et al.*, 2007). However, as yet, no other reports have provided evidence to support a role for GPR55 in this condition.

The LV wall thickness remained similar within each strain of mouse in response to HFC, with the exception of C57BL/6 mice which exhibited a reduced LV wall thickness compared to their NC fed equivalents. This finding is in contrast to that of Naresh and colleagues (2016) who demonstrated that high fat feeding in C57BL/6 mice for 18 and 24 weeks augmented LV wall thickness. As previously mentioned in section 3.4.1., a reduced ventricular wall thickness is often associated with the death of cardiomyocytes due to myocardial infarction (Kehat and Molkentin, 2010). However, this seems an unlikely cause in the case of the HFC fed C57BL/6 mice as these mice exhibited plasma profiles within the normal range and showed no evidence of fatty streak development within their thoracic aortae. Interestingly, Wang and colleagues (2012a) investigated the mRNA expression of MMP-9 in the LV of C57BL/6 mice and reported that its expression was increased in response to a high fat diet. Whether this expression translates to protein within the LV of these mice remains to be determined, however, increased MMP-9 activity poses a plausible mechanism by which the LV wall thickness became reduced in the HFC fed C57BL/6 mice of the present study.

3.4.5.2. *Ventricular lipid deposition*

Lipid deposition was not detected within the ventricular tissue of any HFC fed mouse strain involved in the present study. To test the staining protocol, a section of human abdominal fat was used as a positive control and demonstrated a high level of lipid deposition therefore it seems unlikely that the lack of ventricular lipid deposition was due to a problem with the protocol. Interestingly, a small number of individual lipid droplets in the cardiac tissue of C57BL/6 mice were previously reported in response to high fat feeding (Ge *et al.*, 2012). A likely reason for the contrast in findings is the differing amounts of fat contained within the high fat diet of each study. The diet utilised by Ge and colleagues (2012) contained 35% fat whereas the high fat diet used in the present study contained less fat (21%). A further explanation is the difference in the detection method as Ge and colleagues (2012) utilised both light microscopy and transmission electron microscopy (TEM) and reported that lipid droplets were more visible using TEM as this method captures images at a higher resolution. The present study utilised light microscopy, which may therefore account for the contrast in findings. Despite a thorough literature search, it appears that previous studies have (perhaps surprisingly) not investigated lipid accumulation in ventricular tissue of ApoE^{-/-} mice and therefore the results of the present study are a novel finding.

3.4.6. Conclusion

In conclusion, the results of Chapter 3 indicate that in the ApoE^{-/-} mouse model of high fat diet-induced atherosclerosis, GPR55 plays a complex role, whereby it regulates risk factors associated with this condition (i.e. body weight and fat mass). GPR55 is expressed in the mouse hypothalamus (Ryberg *et al.*, 2007), however, it has not yet been investigated if GPR55 is involved in the satiety centre; an area of the hypothalamus associated with the regulation of food intake. If GPR55 were to positively affect this centre in mice, this may explain GPR55's ability to regulate the body weight and fat mass of the atherosclerosis prone mice of the present study. If future studies find this to be the case, GPR55 may be a potential target for the central regulation of food intake.

Intriguingly, GPR55 promoted the development of fatty streaks within the vasculature, via a lipid-independent mechanism. In humans, elevated plasma lipids contribute to the development of fatty streaks within the vasculature (Newman *et al.*, 1986), as does maternal hypercholesterolaemia (Napoli *et al.*, 1997). On this basis, it may be that this finding is one which is species dependent.

Finally, having established a detrimental role for GPR55 in atherogenesis, and a protective role in fat accumulation, it was of interest to see what role (if any) GPR55 may play on the cardiac function of HFC fed ApoE^{-/-} and ApoE^{-/-}/GPR55^{-/-} mice.

Chapter 4:

**Effect of a high fat diet on cardiac
function in ApoE^{-/-} and ApoE^{-/-}/GPR55^{-/-}
mouse models of atherosclerosis**

4.1. Introduction

4.1.1. Assessment of cardiac function

Several technologies are employed clinically and within research to assess cardiac function, however, two of the most widely utilised technologies include Doppler echocardiography and pressure-volume loop (PVL) analysis.

4.1.1.1. Doppler echocardiography

Doppler echocardiography is often used as a diagnostic test in cardiology as it is a non-invasive method which can image the heart. In brief, a transceiver placed on the chest area above the heart, emits ultrasound waves which are reflected back to the transceiver on coming into contact with cardiac tissue. These returning waves are then passed to and processed by a computer software program to generate real-time images of the heart. Using this technology, the velocity, the direction in which blood is flowing and the dimensions of the heart can be determined.

4.1.1.2. PVL analysis

Cardiac function can be effectively illustrated by the pressure-volume loop; a plot of LV blood pressure against LV blood volume. Each corner of a loop represents the mitral or aortic valve opening or closing and each side of a loop represents a phase of the cardiac cycle (see Figure 4.1. illustrating exemplar PVL loops and the various stages of the cardiac cycle). From these loops, a wide range of indices of cardiac function can be accurately determined to develop a comprehensive understanding of LV performance and how such performance can be affected by certain variables, for example, gene deletion and/or high fat feeding.

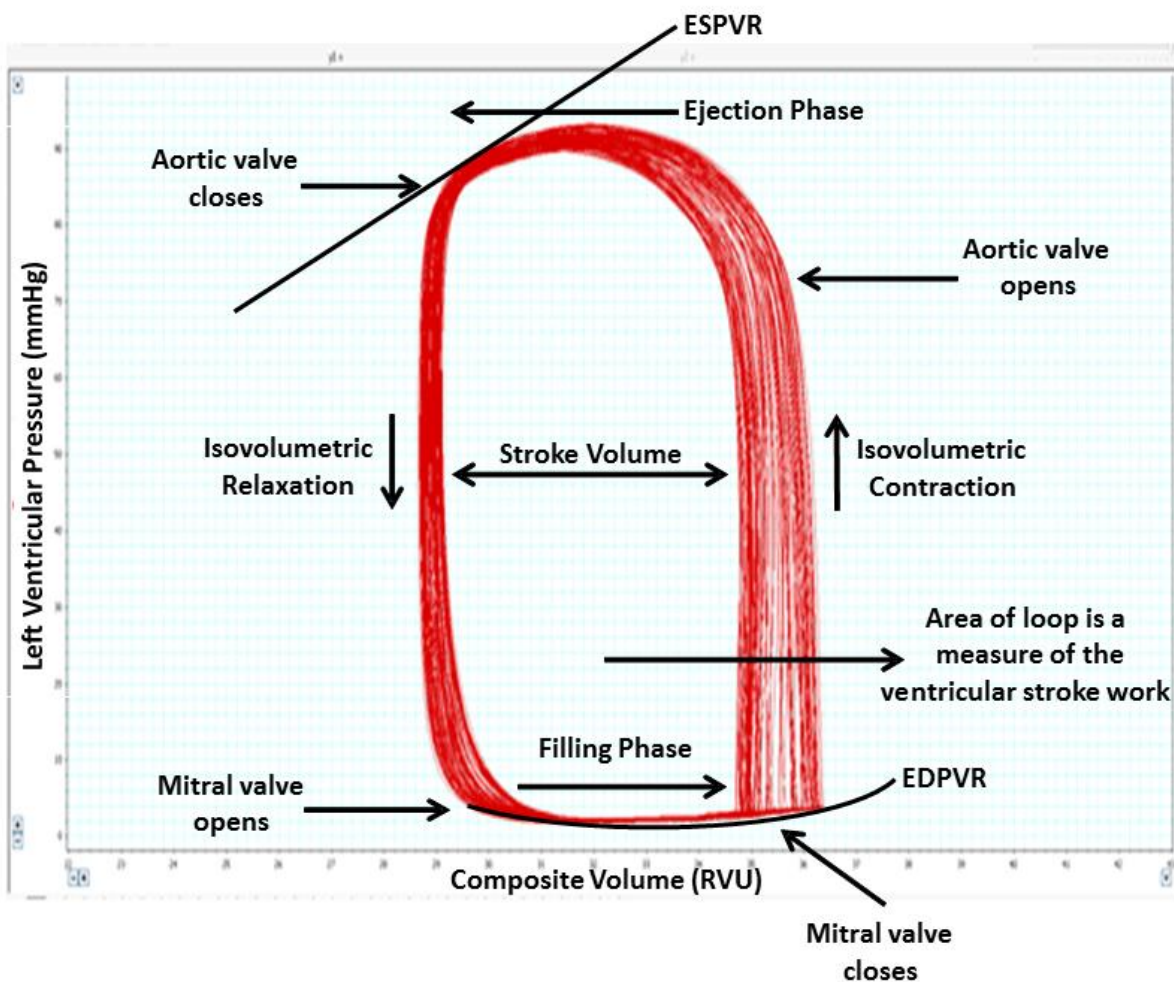


Figure 4.1. The cardiac cycle illustrated in the form of pressure-volume loops. The loops illustrate the points at which the relevant valves open or close during the cycle and the different phases of the cycle. EDPVR; end-diastolic pressure-volume relationship, ESPVR; end-systolic pressure-volume relationship, mmHg; millimetres of mercury and RVU; relative volume units – normally converted to blood volume post experiment.

PVL analysis of LV function is generally regarded as the 'gold standard' in the assessment of load-dependent and load-independent indices of cardiac function in both humans and animals. It is an invasive technique requiring the careful insertion of a conductance catheter into the LV. In patients, the conductance catheter is introduced through either of the femoral arteries and gently advanced up the thoraco-abdominal aorta and aortic arch and down through the aortic valve into the LV. In experimental animals, there are two ways in which a catheter can be inserted into the LV, one of which is via the right carotid artery and gently pushed down through the aortic valve and into the LV. However, this method of insertion can disrupt atherosclerotic plaques, therefore the second method of insertion is often utilised in atherosclerosis prone mice. The second method involves opening the chest, removing the pericardium and inserting the catheter into the LV via its apex. Regardless of the route of entry, a conductance catheter will measure the pressure and the electrical conductance of blood within the LV and generate pressure-volume loops to accurately assess LV function.

4.1.2. GPR55 and cardiac function

LPI-mediated GPR55 activation in cultured rat neonatal ventricular cardiomyocytes provokes distinct cellular functions that are dependent on the cellular location of GPR55 i.e. at the sarcolemma or the membrane of intracellular organelles (Yu *et al.*, 2013), suggesting that GPR55 may regulate cardiomyocyte activity at these two sites. To gain insight into the role of GPR55 in the control of cardiac function, Walsh and colleagues (2014) utilised PVL analysis to examine cardiac function in GPR55^{-/-} mice at 10 weeks (young) and 8 months (mature) of age. While young GPR55^{-/-} mice demonstrated a similar baseline cardiac function to that of age-matched WT mice, mature GPR55^{-/-} mice demonstrated signs of systolic dysfunction in both load-dependent and -independent indices of cardiac function, alongside a reduced free LV wall thickness, reduced myocardial nuclei number and an approximate 3-fold increase in collagen deposition. This study also demonstrated a reduced contractile reserve (response to the α_1/β_1 -adrenoceptor agonist, dobutamine) in young and mature GPR55^{-/-} mice, suggesting that GPR55^{-/-} mice exhibit maladaptive adrenergic signalling. Collectively, the data suggests that GPR55 plays an important role in cardiac function.

4.1.3. ApoE and cardiac function

Several studies have investigated the cardiac function of ApoE^{-/-} mice. In the resting state, aged NC fed ApoE^{-/-} mice (16 month old) exhibit an augmented peak aortic flow velocity acceleration rate (an index of LV contractility), elevated aortic flow velocity and stroke volume (indices of cardiac output),

suggesting enhanced systolic function in these mice (Vincelette *et al.*, 2006). Despite this, dobutamine stress testing revealed an impaired contractile reserve compared to WT mice, which was proposed to be due to coronary insufficiency arising from atherosclerosis and endothelial dysfunction. In contrast, young (9 week old) ApoE^{-/-} mice fed a high cholesterol diet over a short term period (4 weeks) do not appear to have altered cardiac function (Johansson *et al.*, 2005), while more prolonged high fat feeding (8 and 16 weeks) similarly had no effect on ejection fraction and fractional shortening (indices representative of LV systolic function; Hans *et al.*, 2011). Overall, it would appear that genetic ablation of ApoE in NC fed mice improves baseline systolic function but impairs contractile reserve, while high fat feeding has no effect on the systolic function of these mice.

4.1.4. Aims

In light of the fact that GPR55 plays an important role in maintaining cardiac performance but a detrimental role in the development of atherosclerosis, it was of interest to investigate if GPR55 plays a role in the cardiac function of ApoE^{-/-} mice. To address this aim, C57BL/6 (wildtype; WT), ApoE^{-/-}, GPR55^{-/-} and ApoE^{-/-}/GPR55^{-/-} mice were fed an NC or HFC diet for 12 weeks. Post the dietary period, PVL analysis was conducted on all groups to assess the impact of gene deletion and/or diet on 1) baseline cardiac function, and 2) contractile reserve.

4.2. Methods

4.2.1. Study design

Male and female WT, ApoE^{-/-}, GPR55^{-/-} and ApoE^{-/-}/GPR55^{-/-} mice, aged 4-7 weeks (approximately 5 of each gender per strain) were purchased or bred as previously described (Chapter 2, section 2.2.2.1.). Mice within each strain were randomly assigned to NC or HFC groups as described in Chapter 3, section 3.2.1. For the final body weights of each mouse strain see Chapter 3, Table 3.2.

4.2.2. Assessment of cardiac function via PVL analysis

Each mouse was anaesthetised and ventilated as described in Chapter 2, section 2.2.4.2. Following this, a cannula was inserted into the right jugular vein for drug administration and a pressure-tipped conductance catheter (SPR-839; Millar Instruments, USA) inserted via the apex of the LV for the measurement of a range of indices of cardiac function (for full details of the surgical procedure see

Chapter 2, section 2.2.4.2.). Following a stabilisation period of approximately 15 minutes, a bolus injection of saline (10 μ l) was administered via the right jugular vein to obtain a parallel conductance (V_p) value (detailed in Chapter 2, section 2.2.4.3.). This process was repeated 3 times and the V_p value for each mouse calculated as an average of the 3 saline boluses. Hemodynamic variables (pressure, composite volume, the rate of pressure change in the ventricle (dP/dt) and heart rate) were then left to stabilise for approximately 5 minutes prior to baseline variables being recorded for 10 minutes (for an exemplar trace of baseline haemodynamic variables from an NC fed C57BL/6 mouse see Figure 4.2.). To assess contractile reserve, dobutamine (α_1/β_1 -adrenoceptor agonist; 10 μ g/kg) was administered intravenously as a bolus dose and its effects compared with a bolus administration of vehicle (0.9% NaCl). Following the recovery of haemodynamic parameters, venous return (left ventricular pre-load) was altered via the transient occlusion of the inferior vena cava (IVC) to acquire the slopes of both the end-systolic pressure-volume relationship (ESPVR) and end-diastolic pressure-volume relationship (EDPVR). Post completion of the *in vivo* protocol, blood was collected via cardiac puncture to conduct a catheter volume calibration. In brief, this involved the blood being immediately distributed into wells of a known volume in a calibration cuvette and the catheter being placed in each well for 5-10 seconds while the MPVS-Ultra Single Segment Foundation System (ADInstruments, UK) recorded the changes in conductance output (RVU). Subsequently, the conductance output of each well was correlated with the known volume of the associated well and converted to μ l (for a full description of the volume calibration of the catheter see Chapter 2, section 2.2.4.4.). For definitions of the load-dependent and -independent indices of cardiac function that were recorded throughout each experiment, see Tables 4.1. and 4.2., respectively.



Figure 4.2. Trace of baseline haemodynamic variables from an NC fed C57BL/6 mouse. bpm; beats per minute, composite vol; composite volume, dP/dt; the rate of pressure change in the ventricle, mmHg; millimetres of mercury, RVU; relative volume units and s; seconds.

Indices of Systolic Function	Abbreviation	Units	Definition
Heart Rate	HR	bpm	Number of beats per minute
End-systolic volume	ESV	μL	Volume of blood present in the ventricle at the end of systole
End-diastolic volume	EDV	μL	Volume of blood present in the ventricle at the end of diastole
End-systolic pressure	ESP	mmHg	The pressure in the ventricle at the end of systole
End-diastolic pressure	EDP	mmHg	The pressure in the ventricle at the end of diastole
Stroke Volume	SV	μL	Volume of blood ejected per contraction (EDV – ESV)
Ejection Fraction	EF	%	Fraction of blood ejected from a ventricle per contraction $((\text{SV}/\text{EDV}) \times 100)$
Cardiac Output	CO	$\mu\text{L}/\text{min}$	Volume of blood ejected by one ventricle in one minute (SV x HR)
Stroke Work	SW	mmHg* μL	The work done by the ventricle to eject a volume of blood (SV x mean arterial pressure)
Arterial elastance	E_a	mmHg/ μL	Elastance of artery (ESP/SV)
dP/dt_{min}	-	mmHg/s	Minimum first derivative of left ventricular pressure
dP/dt_{max}	-	mmHg/s	Maximum first derivative of left ventricular pressure

Table 4.1. Load-dependent indices of cardiac function and their definitions.

Indices of Systolic Function	Abbreviation	Units	Definition
End-systolic pressure-volume relationship	ESPVR	mmHg/ μL	The maximal pressure developed by the ventricle at any given LV volume
End-diastolic pressure-volume relationship	EDPVR	mmHg/ μL	A measure of ventricular chamber stiffness (indicative of the relaxation rate)

Table 4.2. Load-independent indices of cardiac function and their definitions.

4.2.3. Statistical analysis

To ensure that the studies planned within this chapter had sufficient statistical power, power calculations were conducted prior to experiments taking place and were based on data from previous experiments performed in the lab. Power calculations recommended an $n=10$ for PVL studies. Examples of power calculations performed for the PVL studies conducted within this chapter:

Using existing systolic function data, pooled standard deviations for both ejection fraction (EF) and the end-systolic pressure-volume relationship (ESPVR) were 7.1 and 2, respectively. With a sample size for each experimental group of $n=10$, a one-way ANOVA would have 82% power to detect a difference of 11.4% (EF) and 99% power to detect a difference of 4.8mmHg/ μ L (ESPVR) between the means for each group.

PVL analysis was conducted using PVAN *Ultra*TM software (Millar Instruments, USA). Data from both male and female mice of each strain were combined in order to perform meaningful statistical analysis. Throughout the chapter, data from a mouse was excluded if said mouse had a baseline EF < 30% (C57BL/6 and GPR55^{-/-} mice) or < 25% (ApoE^{-/-} and ApoE^{-/-}/GPR55^{-/-} mice). Data was also excluded if it was outwith the mean ± 2 x (standard deviations). Data are expressed as mean \pm S.E.M throughout. Comparisons were performed using either a paired *t*-test (two-tailed) or an unpaired *t*-test (two-tailed) and multiple comparisons were performed using a one- or two-way ANOVA followed by a 'Bonferroni' post-hoc test. All statistical tests were carried out using GraphPad Prism[®] 4 software (GraphPad Software, Inc., USA) and differences between data deemed significant where $P < 0.05$. Of note, E_{\max} , a measure of intrinsic ventricular contractility was not reported in the present study. E_{\max} values were excluded for two reasons: 1) such values are influenced by body size and there was significant variation in the fat mass between the groups of mice involved, 2) such values are also influenced by heart size and the present study did not perfuse fix the hearts to preserve them in their end-diastolic state, therefore, their maximum dimensions in the diastolic phase could not be determined or compared with those of WT mice.

4.3. Results

4.3.1. Impact of gene deletion on load-dependent and -independent indices of baseline cardiac function

4.3.1.1. *Systolic function*

From the measurements of load-dependent indices of cardiac function, in particular, HR, CO and dP/dt_{\max} , systolic function was found to be enhanced in both NC fed ApoE^{-/-} and GPR55^{-/-} mice compared to their NC fed WT counterparts ($P < 0.05$; Table 4.3.). ApoE^{-/-} mice also exhibited an augmented ESV, while GPR55^{-/-} mice were further characterised by an elevated ESP and SW ($P < 0.05$; Table 4.3.). In contrast, none of the load-dependent indices of systolic function recorded in NC fed ApoE^{-/-}/GPR55^{-/-} mice differed significantly from their WT counterparts (Table 4.3.). Load-independent measurements were obtained by transiently occluding the inferior vena cava (to alter pre-load) and, with the exception of NC fed GPR55^{-/-} mice which exhibited a significantly increased ESPVR ($P < 0.01$; Table 4.5.), indicative of increased contractility/inotropy, the ESPVR of both NC fed ApoE^{-/-} and ApoE^{-/-}/GPR55^{-/-} mice remained similar to that of NC fed WT mice (Table 4.5.). For exemplar PVL loops with the ESPVR slope indicated, see Figure 4.1. In summary, load-dependent systolic function was enhanced in ApoE^{-/-} and GPR55^{-/-} mice but not in ApoE^{-/-}/GPR55^{-/-} mice, while load-independent indices of systolic function were only increased in GPR55^{-/-} mice.

4.3.1.2. *Diastolic function*

Both NC fed ApoE^{-/-} and GPR55^{-/-} mice were characterised by a positive lusitropic response when compared to NC fed WT mice, as evidenced by an augmented dP/dt_{\min} ($P < 0.05$; Table 4.4.). In contrast, indices of load-dependent diastolic function were not different in NC fed ApoE^{-/-}/GPR55^{-/-} mice compared to WT controls fed NC (Table 4.4.). In terms of load-independent diastolic function, NC fed ApoE^{-/-} mice exhibited a significantly increased EDPVR compared to NC fed WT mice ($P < 0.01$), however, the EDPVR was unaffected in NC fed GPR55^{-/-} and ApoE^{-/-}/GPR55^{-/-} mice (Table 4.5.). For exemplar PVL loops with the EDPVR slope indicated, see Figure 4.1. To summarise, load-dependent diastolic function was enhanced in both ApoE^{-/-} and GPR55^{-/-} mice and unaffected in ApoE^{-/-}/GPR55^{-/-} mice. Moreover, load-independent diastolic function was enhanced in ApoE^{-/-} mice and unaffected in GPR55^{-/-} and ApoE^{-/-}/GPR55^{-/-} mice.

4.3.2. Impact of high fat feeding on load-dependent and -independent indices of baseline cardiac function

4.3.2.1. Systolic function

High fat feeding of C57BL/6 mice improved load-dependent systolic function as evidenced by an increased HR, ESV and CO ($P < 0.05$), while that of high fat fed ApoE^{-/-} mice was not different from ApoE^{-/-} mice fed NC (Table 4.3.). High fat feeding of GPR55^{-/-} mice slightly reduced systolic function, as evidenced by a reduced ESP and dP/dt_{\max} ($P < 0.05$; Table 4.3.). Moreover, ApoE^{-/-}/GPR55^{-/-} mice fed a HFC diet were characterised by an elevated ESV and a significantly reduced EF, indicative of marginal systolic dysfunction ($P < 0.05$; Table 4.3.). In terms of load-independent systolic function, the ESPVR of high fat fed WT, ApoE^{-/-}, GPR55^{-/-} and ApoE^{-/-}/GPR55^{-/-} mice remained similar to that of their respective NC fed counterparts (Table 4.5.). In summary, HFC fed C57BL/6 mice exhibited enhanced load-dependent systolic function. In contrast, GPR55^{-/-} and ApoE^{-/-}/GPR55^{-/-} were characterised by slightly reduced systolic function in response to the HFC diet, while HFC fed ApoE^{-/-} mice exhibited similar load-dependent systolic function to that of NC fed ApoE^{-/-} mice. Furthermore, high fat feeding did not affect the load-independent systolic function of any group of mice.

4.3.2.2. Diastolic function

High fat feeding of WT, ApoE^{-/-} and GPR55^{-/-} mice had no effect on load-dependent indices of diastolic function (Table 4.4.), however, ApoE^{-/-}/GPR55^{-/-} mice fed the HFC diet exhibited a significantly increased EDV ($P < 0.01$; Table 4.4.) which is most likely responsible for the reduced EF of these mice reported above ($EF = (SV/EDV) \times 100$). Since the increased EDV was not accompanied by an increase in EDP or dP/dt_{\min} , it is unlikely that the overall load-dependent diastolic function of HFC fed ApoE^{-/-}/GPR55^{-/-} mice was significantly impaired. Load-independent measurements of diastolic function were similarly unaffected by high fat feeding in WT, ApoE^{-/-} and GPR55^{-/-} mice (Table 4.5.). In contrast, HFC fed ApoE^{-/-}/GPR55^{-/-} mice exhibited a reduction in EDPVR indicating that these mice are characterised by load-independent diastolic dysfunction ($P < 0.05$; Table 4.5.). To summarise, load-dependent and -independent diastolic function was unaffected by high fat feeding in WT, ApoE^{-/-} and GPR55^{-/-} mice. In contrast, high fat feeding resulted in a load-independent decrease in diastolic function in ApoE^{-/-}/GPR55^{-/-} mice.

	C57BL/6		ApoE ^{-/-}		GPR55 ^{-/-}		ApoE ^{-/-} /GPR55 ^{-/-}	
	NC (9-10)	HFC (7-8)	NC (9-10)	HFC (7)	NC (8-9)	HFC (7-8)	NC (13-14)	HFC (7)
HR (bpm)	324±19	413±17#	375±15*	429±18	423±14*	406±14	351±15	378±12
ESV (μL)	14.5±1.2	19.2±1.1#	19.0±1.3*	20.2±2.5	17.3±0.8	17.8±1.0	16.7±0.8	25.0±0.9#
ESP (mmHg)	80±4.3	89±5.2	86.5±1.6	81±4.4	101.8±2.4*	77.7±4.6#	77.7±2.8	74.5±3.1
SV (μL)	11.6±0.6	13.9±1.7	14.1±1.0	10.8±1.3	13.3±0.6	12.4±1.6	13.2±0.7	14.7±1.7
EF (%)	49±2.0	44.6±1.6	45.6±2.1	37.4±3.1	47.3±1.1	44.0±3.4	47.1±2.1	37.9±2.3#
CO (μL/min)	3733±304	6175±410#	5261±419*	4589±555	5601±234*	5221±674	4750±286	5467±536
SW (mmHg*μL)	726±61	980±150	939±66	704±133	1072±73*	792±128	788±58	845±106
E _a (mmHg/μL)	6.7±0.5	6.3±0.6	6.2±0.3	8.3±1.2	7.6±0.4	7.0±1.0	6.1±0.4	5.6±0.7
dP/dt _{max} (mmHg/s)	4572±297	5999±670	6289±353*	5706±577	7795±710*	5592±676#	5254±317	4787±425

Table 4.3. Effect of gene deletion and/or high fat feeding on load-dependent indices of systolic function of mice. Data are expressed as mean±S.E.M; n-numbers are in brackets. * indicates a significant effect (vs. C57BL/6 NC; $P<0.05$) of strain and # indicates a significant effect ($P<0.05$) of diet within the same strain; 2-way ANOVA and a 'Bonferroni' post-hoc test. The red framed boxes highlight the values most relevant.

	C57BL/6		ApoE ^{-/-}		GPR55 ^{-/-}		ApoE ^{-/-} /GPR55 ^{-/-}	
	NC (10)	HFC (8)	NC (10)	HFC (7)	NC (8-9)	HFC (7-8)	NC (13-14)	HFC (7)
EDV (μL)	24.6±1.9	30.8±2.6	29.6±1.9	28.6±3.5	27.4±1.5	26.3±2.0	26.2±1.2	36.5±2.5#
EDP (mmHg)	5.9±0.7	7.6±0.9	5.9±0.3	6.7±0.8	5.5±0.5	6.5±0.2	4.6±0.3	4.6±0.5
dP/dt _{min} (mmHg/s)	-4770±390	-6169±711	-6349±413*	-6021±625	-7839±315*	-6086±673	-3037±329	-4941±397

Table 4.4. Effect of gene deletion and/or high fat feeding on load-dependent indices of diastolic function of mice. Data are expressed as mean±S.E.M; n-numbers are in brackets. * indicates a significant effect (vs. C57BL/6 NC; $P<0.05$) of strain and # indicates a significant effect ($P<0.01$) of diet within the same strain; 2-way ANOVA and a 'Bonferroni' post-hoc test.

	C57BL/6		ApoE ^{-/-}		GPR55 ^{-/-}		ApoE ^{-/-} /GPR55 ^{-/-}	
	NC (7-8)	HFC (5)	NC (8)	HFC (7)	NC (8)	HFC (8)	NC (8-9)	HFC (7)
ESPVR (mmHg/μL)	4.3±0.6	4.7±1.0	6.0±0.9	5.8±0.5	6.8±0.5*	7.0±0.5	4.0±0.3	4.8±1.3
EDPVR (mmHg/μL)	0.2±0.0	0.1±0.0	0.2±0.0*	0.2±0.0	0.2±0.0	0.2±0.0	0.2±0.0	0.1±0.0#

Table 4.5. Effect of gene deletion and/or high fat feeding on load-independent indices of cardiac function of mice. Data are expressed as mean±S.E.M; n-numbers are in brackets. * indicates a significant effect (vs. C57BL/6 normal chow; $P<0.01$) of strain and # indicates a significant effect ($P<0.05$) of diet within the same strain; 2-way ANOVA and a 'Bonferroni' post-hoc test. The red framed box highlights the value most relevant.

4.3.3. Impact of gene deletion on contractile reserve

4.3.3.1. Systolic function

In NC fed C57BL/6 mice, dobutamine induced the classical changes in systolic function seen upon adrenoceptor activation, these included an increase in EF, CO (as a consequence of increased SV and HR, respectively), SW and dP/dt_{max} with a concomitant decrease in ESV ($P<0.05$; Table 4.6.). Changes of a similar magnitude were seen in response to dobutamine in NC fed ApoE^{-/-}, GPR55^{-/-} and ApoE^{-/-}/GPR55^{-/-} mice ($P<0.05$; Table 4.6), indicating no influence of genetic status on contractile reserve.

4.3.3.2. Diastolic function

Dobutamine induced a lusitropic response in NC fed GPR55^{-/-} and ApoE^{-/-}/GPR55^{-/-} mice as evidenced by an augmented dP/dt_{min} ($P<0.05$) but had no effect on the dP/dt_{min} of C57BL/6 or ApoE^{-/-} mice fed the same diet (Table 4.7). In terms of EDV and EDP, adrenoceptor activation had no effect on these indices in NC fed WT mice but did however, reduce both indices in NC fed ApoE^{-/-}, GPR55^{-/-} and ApoE^{-/-}/GPR55^{-/-} mice ($P<0.05$; Table 4.7).

4.3.4. Impact of high fat feeding on contractile reserve

4.3.4.1. Systolic function

Dobutamine induced positive chronotropic (\uparrow HR) and inotropic responses (\uparrow EF and dP/dt_{max}) in all HFC fed mice ($P<0.05$; Tables 4.8.-4.11.). Additionally, ESV was reduced while CO, SV and SW were all increased by dobutamine in all mice fed the HFC diet ($P<0.05$; Tables 4.8.-4.11.). Dobutamine also increased ESP in both HFC fed ApoE^{-/-} and GPR55^{-/-} mice ($P<0.05$; Tables 4.9. and 4.10., respectively) but had no effect on that of HFC fed C57BL/6 and ApoE^{-/-}/GPR55^{-/-} mice (Tables 4.8. and 4.11., respectively). Finally, E_a was unchanged in response to dobutamine in all groups (Tables 4.8.-4.11.).

Systolic indices of contractile reserve in HFC fed C57BL/6 mice did not significantly differ from those in NC fed WT mice (Table 4.8.). In contrast, HFC fed ApoE^{-/-} mice were characterised by a reduced contractile reserve, as evidenced by attenuated increases in SV, CO and EF, when compared to their NC fed counterparts ($P<0.05$; Table 4.9.). HFC fed GPR55^{-/-} mice were characterised by an increased inotropic response (augmented increase in dP/dt_{max}) compared to NC fed GPR55^{-/-} mice ($P<0.05$;

		C57BL/6 NC (6-7)	ApoE ^{-/-} NC (8-9)	GPR55 ^{-/-} NC (8-9)	ApoE ^{-/-} /GPR55 ^{-/-} NC (10-11)
Δ HR (bpm)	veh	3±3	-4±2	-5±8	-10±5
	dob	57±11•	76±13•	93±17•	55±9•
Δ ESV (μL)	veh	4.9±1.2	8.8±1.0	8.1±1.0	9.1±0.8
	dob	-1.9±1.3•	-1.1±1.3•	-2.7±1.3•	-1.5±1.6•
Δ ESP (mmHg)	veh	12.9±3.2	10.8±2.0	16.3±5.3	11.7±1.4
	dob	25.6±8.6	15±3.5	11.7±5.6	21.6±2.2•
Δ SV (μL)	veh	3.3±0.4	6.1±1.0	3.6±0.6	5.8±0.4
	dob	8.2±1.2•	10±0.8•	8.7±1.2•	9.7±0.7•
Δ EF (%)	veh	-2.3±0.5	1.1±1.0	-4.1±1.0	-1.2±1.2
	dob	16.2±3.3•	14.1±1.8•	15.7±2.1•	19.7±3.5•
Δ CO (μL/min)	veh	1031±152	2053±341	1165±205	1792±236
	dob	3906±648•	5001±771•	5541±834•	4926±459•
Δ SW (mmHg*μL)	veh	270.7±45.5	437±60.8	364.3±64.8	364.0±33.5
	dob	1019.7±260.6•	882.9±112.4•	910.8±136.2•	1006.6±57.0•
Δ E_a (mmHg/μL)	veh	-1.3±0.3	-1.7±0.3	-0.8±0.2	-1.8±0.3
	dob	-1.5±0.5	-1.5±0.4	-1.5±0.4•	-1.7±0.3
Δ dP/dt_{max} (mmHg/s)	veh	925±235	1008±120	737±381	795±152
	dob	5611±1256•	3851±382•	4246±511•	5181±320•

Table 4.6. Effect of gene deletion on the systolic indices of contractile reserve in mice. Contractile reserve was assessed by the change from baseline cardiac function in response to the α_1/β_1 -adrenoceptor agonist, dobutamine (vehicle; saline). Data are expressed as mean±S.E.M; n-numbers are in brackets. • indicates a significant effect ($P<0.05$) of dobutamine (dob) vs. vehicle (veh) within the same strain (paired t -test; two tailed). A one-way ANOVA followed by a ‘Bonferroni’ post-hoc test was also conducted to assess the impact of strain (vs. C57BL/6 NC) on each index in response to dobutamine, however, all indices were unaffected by strain.

		C57BL/6 NC (6-7)	ApoE ^{-/-} NC (9)	GPR55 ^{-/-} NC (8-9)	ApoE ^{-/-} /GPR55 ^{-/-} NC (10-11)
Δ EDV (μL)	Veh	9.0±1.1	14±1.7	11.1±1.5	14.1±0.9
	Dob	6.6±1.8	8.2±1.3•	5.2±0.9•	7.5±1.1•
Δ EDP (mmHg)	Veh	2.0±0.2	2.7±0.2	2.0±0.2	2.1±0.2
	Dob	1.7±0.5	1.2±0.4•	0.4±0.2•	0.5±0.3•
Δ dP/dt_{min} (mmHg/s)	Veh	-1122±366	-663±191	-1063±470	-764±198
	Dob	-3385±1229	-1486±474	-2933±926•	-3334±258•

Table 4.7. Effect of gene deletion on the diastolic indices of contractile reserve in mice. Data are expressed as mean±S.E.M; n-numbers are in brackets. • indicates a significant effect ($P<0.05$) of dobutamine (dob) vs. vehicle (veh) within the same strain (paired t -test; two-tailed).

Table 4.10.). There was also an increase in the ESP of HFC fed GPR55^{-/-} mice ($P < 0.05$) which did not occur in NC fed GPR55^{-/-} mice in response to adrenoceptor activation (Table 4.10.). Furthermore, HFC fed ApoE^{-/-}/GPR55^{-/-} mice exhibited an increased inotropic response to dobutamine (augmented increase in CO) compared to their NC fed counterparts ($P < 0.05$; Table 4.11.). To summarise, the systolic indices of contractile reserve in HFC fed C57BL/6 mice were similar to those of NC fed WT mice. HFC fed ApoE^{-/-} mice were characterised by a reduced contractile reserve, while HFC fed GPR55^{-/-} and ApoE^{-/-}/GPR55^{-/-} mice exhibited augmented contractility in response to dobutamine.

4.3.4.2. Diastolic function

Dobutamine induced positive lusitropic responses in all groups of HFC fed mice, as evidence by an augmented dP/dt_{\min} ($P < 0.05$; Tables 4.12.-4.15.). Additionally, all groups of HFC fed mice were characterised by a significantly reduced EDV and EDP ($P < 0.05$; Tables 4.12.-4.15.).

HFC fed C57BL/6 mice exhibited a reduced EDV and EDP and an increased dP/dt_{\min} in response to dobutamine, while adrenoceptor activation did not affect these indices in C57BL/6 mice fed NC (Table 4.12.). While HFC fed ApoE^{-/-} mice exhibited an enhanced lusitropic response, as evidenced by an increase in dP/dt_{\min} ($P < 0.01$), this was not apparent in NC fed ApoE^{-/-} mice in response to dobutamine (Table 4.13.). Adrenoceptor activation in HFC fed GPR55^{-/-} mice induced an increased lusitropic response (augmented increase in dP/dt_{\min}) when compared to NC fed GPR55^{-/-} mice administered dobutamine ($P < 0.05$; Table 4.14.). Furthermore, diastolic indices of contractile reserve in HFC fed ApoE^{-/-}/GPR55^{-/-} mice did not significantly differ from those of ApoE^{-/-}/GPR55^{-/-} mice fed an NC diet (Table 4.15). To summarise, adrenoceptor activation induced a lusitropic response in HFC fed C57BL/6, ApoE^{-/-} and GPR55^{-/-} mice compared to their NC fed counterparts, while high fat feeding did not alter the rate of relaxation in ApoE^{-/-}/GPR55^{-/-} mice.

C57BL/6			
		NC (6-7)	HFC (6-7)
Δ HR (bpm)	veh	3 \pm 3	-3 \pm 3
	dob	57 \pm 11•	76 \pm 12•
Δ ESV (μ L)	veh	4.9 \pm 1.2	11.2 \pm 1.3
	dob	-1.9 \pm 1.3•	-1.6 \pm 1.2•
Δ ESP (mmHg)	veh	12.9 \pm 3.2	12.6 \pm 3.1
	dob	25.6 \pm 8.6	19.1 \pm 5.0
Δ SV (μ L)	veh	3.3 \pm 0.4	4.6 \pm 0.8
	dob	8.2 \pm 1.2•	9.6 \pm 1.3•
Δ EF (%)	veh	-2.3 \pm 0.5	-3.3 \pm 2.3
	dob	16.2 \pm 3.3•	15.5 \pm 2.2•
Δ CO (μ L/min)	veh	1031 \pm 152	1423 \pm 153
	dob	3906 \pm 648•	5741 \pm 779•
Δ SW (mmHg* μ L)	veh	270.7 \pm 45.5	338.8 \pm 23.5
	dob	1019.7 \pm 260.6•	928.0 \pm 152.2•
Δ E _a (mmHg/ μ L)	veh	-1.3 \pm 0.3	-1.3 \pm 0.3
	dob	-1.5 \pm 0.5	-1.6 \pm 0.1
Δ dP/dt _{max} (mmHg/s)	veh	925 \pm 235	658 \pm 232
	dob	5611 \pm 1256•	4515 \pm 794•

Table 4.8. Effect of a high fat diet on the systolic indices of contractile reserve in C57BL/6 mice. Data are expressed as mean \pm S.E.M; n-numbers are in brackets. • indicates a significant effect (P <0.05) of dobutamine (dob) vs. vehicle (veh) within the same dietary group (paired t -test; two-tailed). An unpaired t -test (two-tailed) was also conducted to assess the impact of HFC on each index in response to dobutamine, however, all indices were unaffected by high fat feeding.

		ApoE ^{-/-}	
		NC (8-9)	HFC (6-7)
Δ HR (bpm)	veh	-4±2	-3±4
	dob	76±13•	52±9•
Δ ESV (μL)	veh	8.8±1.0	6.2±0.8
	dob	-1.1±1.3•	1.8±0.7•
Δ ESP (mmHg)	veh	10.8±2.0	11.8±2.4
	dob	15±3.5	18±3.3•
Δ SV (μL)	veh	6.1±1.0	3.1±0.8
	dob	10±0.8•	4.8±1.0•#
Δ EF (%)	veh	1.1±1.0	0±1.3
	dob	14.1±1.8•	6.5±1.9•#
Δ CO (μL/min)	veh	2053±341	1203±315
	dob	5001±771•	2774±593•#
Δ SW (mmHg*μL)	veh	437±60.8	305.6±76.0
	dob	882.9±112.4•	568.4±120.5•
Δ E _a (mmHg/μL)	veh	-1.7±0.3	-1.80±0.4
	dob	-1.5±0.4	-1.7±0.6
Δ dP/dt _{max} (mmHg/s)	veh	1008±120	908±216
	dob	3851±382•	3813±708•

Table 4.9. Effect of a high fat diet on the systolic indices of contractile reserve in ApoE^{-/-} mice. Data are expressed as mean±S.E.M; n-numbers are in brackets. • indicates a significant effect ($P<0.05$) of dobutamine (dob) vs. vehicle (veh) within the same dietary group (paired t -test; two-tailed) and # indicates a significant effect ($P<0.05$) of diet (unpaired t -test; two-tailed). The red framed boxes highlight the values most relevant.

GPR55 ^{-/-}			
		NC (8-9)	HFC (7-8)
Δ HR (bpm)	veh	-5±8	-3±5
	dob	93±17•	66±9•
Δ ESV (μL)	veh	8.1±1.0	11.1±0.8
	dob	-2.7±1.3•	-0.9±0.8•
Δ ESP (mmHg)	veh	16.3±5.3	18.6±2.3
	dob	11.7±5.6	31.3±5.7•#
Δ SV (μL)	veh	3.6±0.6	5.0±1.1
	dob	8.7±1.2•	8.3±0.7•
Δ EF (%)	veh	-4.1±1.0	-3±1.8
	dob	15.7±2.1•	13.4±0.9•
Δ CO (μL/min)	veh	1165±205	2070±451
	dob	5541±834•	5121±442•
Δ SW (mmHg*μL)	veh	364.3±64.8	646.3±69
	dob	910.8±136.2•	1167.4±117.3•
Δ E _a (mmHg/μL)	veh	-0.8±0.2	-0.7±0.3
	dob	-1.5±0.4•	-1.2±0.2
Δ dP/dt _{max} (mmHg/s)	veh	737±381	1290±63
	dob	4246±511•	7009±873•#

Table 4.10. Effect of a high fat diet on the systolic indices of contractile reserve in GPR55^{-/-} mice. Data are expressed as mean±S.E.M; n-numbers are in brackets. • indicates a significant effect ($P<0.05$) of dobutamine (dob) vs. vehicle (veh) within the same dietary group (paired t -test; two-tailed) and # indicates a significant effect ($P<0.05$) of diet (unpaired t -test; two-tailed). The red framed boxes highlight the values most relevant.

		ApoE ^{-/-} /GPR55 ^{-/-}	
		NC (10-11)	HFC (7)
Δ HR (bpm)	veh	-10±5	-8±6
	dob	55±9•	82±12•
Δ ESV (μL)	veh	9.1±0.8	11.2±1.5
	dob	-1.5±1.6•	-4.7±2.0•
Δ ESP (mmHg)	veh	11.7±1.4	17.5±2.8
	dob	21.6±2.2•	19.9±2.9
Δ SV (μL)	veh	5.8±0.4	5.1±1.3
	dob	9.7±0.7•	11.1±1.0•
Δ EF (%)	veh	-1.2±1.2	-1.6±2.1
	dob	19.7±3.5•	18.4±3.0•
Δ CO (μL/min)	veh	1792±236	1798±437
	dob	4926±459•	6875±866•#
Δ SW (mmHg*μL)	veh	364.0±33.5	473.6±110.7
	dob	1006.6±57.0•	1252.4±116.1•
Δ E _a (mmHg/μL)	veh	-1.8±0.3	-0.7±0.6
	dob	-1.7±0.3	-1.6±0.3
Δ dP/dt _{max} (mmHg/s)	veh	795±152	1244±171
	dob	5181±320•	6457±783•

Table 4.11. Effect of a high fat diet on the systolic indices of contractile reserve in ApoE^{-/-}/GPR55^{-/-} mice. Data are expressed as mean±S.E.M; n-numbers are in brackets. • indicates a significant effect ($P<0.01$) of dobutamine (dob) vs. vehicle (veh) within the same dietary group (paired t -test; two-tailed) and # indicates a significant effect ($P<0.05$) of diet (unpaired t -test; two-tailed). The red framed box highlights the value most relevant.

C57BL/6			
		NC (6-7)	HFC (7)
Δ EDV (μ L)	veh	9.0 \pm 1.1	16.1 \pm 1.6
	dob	6.6 \pm 1.8	8.1 \pm 1.7•
Δ EDP (mmHg)	veh	2.0 \pm 0.2	3.5 \pm 0.4
	dob	1.7 \pm 0.5	0.9 \pm 0.2•
Δ dP/dt _{min} (mmHg/s)	veh	-1122 \pm 366	-746 \pm 338
	dob	-3385 \pm 1229	-3350 \pm 848•

Table 4.12. Effect of a high fat diet on the diastolic indices of contractile reserve in C57BL/6 mice. Data are expressed as mean \pm S.E.M; n-numbers are in brackets. • indicates a significant effect ($P<0.05$) of dobutamine (dob) vs. vehicle (veh) within the same dietary group (paired t -test; two-tailed).

ApoE ^{-/-}			
		NC (9)	HFC (7)
Δ EDV (μ L)	veh	14 \pm 1.7	9.9 \pm 1.5
	dob	8.2 \pm 1.3•	7.4 \pm 1.1•
Δ EDP (mmHg)	veh	2.7 \pm 0.2	2.7 \pm 0.1
	dob	1.2 \pm 0.4•	1.2 \pm 0.3•
Δ dP/dt _{min} (mmHg/s)	veh	-663 \pm 191	-980 \pm 252
	dob	-1486 \pm 474	-3140 \pm 534•#

Table 4.13. Effect of a high fat diet on the diastolic indices of contractile reserve in ApoE^{-/-} mice. Data are expressed as mean \pm S.E.M; n-numbers are in brackets. • indicates a significant effect ($P<0.01$) of dobutamine (dob) vs. vehicle (veh) within the same dietary group (paired t -test; two-tailed) and # indicates a significant effect ($P<0.05$) of diet (unpaired t -test; two-tailed).

GPR55^{-/-}			
		NC (8-9)	HFC (7-8)
Δ EDV (μL)	veh	11.1±1.5	16.2±1.8
	dob	5.2±0.9•	8.4±1.3•
Δ EDP (mmHg)	veh	2.0±0.2	2.3±0.2
	dob	0.4±0.2•	0.6±0.2•
Δ dP/dt_{min} (mmHg/s)	veh	-1063±470	-1602±144
	dob	-2933±926•	-5934±652•#

Table 4.14. Effect of a high fat diet on the diastolic indices of contractile reserve in GPR55^{-/-} mice. Data are expressed as mean±S.E.M; n-numbers are in brackets. • indicates a significant effect ($P<0.05$) of dobutamine (dob) vs. vehicle (veh) within the same dietary group (paired t -test; two-tailed) and # indicates a significant effect ($P<0.05$) of diet (unpaired t -test; two-tailed).

ApoE^{-/-}/GPR55^{-/-}			
		NC (10-11)	HFC (6-7)
Δ EDV (μL)	veh	14.1±0.9	16.9±1.8
	dob	7.5±1.1•	7.8±1.5•
Δ EDP (mmHg)	veh	2.1±0.2	2.2±0.3
	dob	0.5±0.3•	0.3±0.2•
Δ dP/dt_{min} (mmHg/s)	veh	-764±198	-1059±107
	dob	-3334±258•	-3871±615•

Table 4.15. Effect of a high fat diet on the diastolic indices of contractile reserve in ApoE^{-/-}/GPR55^{-/-} mice. Data are expressed as mean±S.E.M; n-numbers are in brackets. • indicates a significant effect ($P<0.05$) of dobutamine (dob) vs. vehicle (veh) within the same dietary group (paired t -test; two-tailed). An unpaired t -test (two-tailed) was also conducted to assess the impact of HFC on each index in response to dobutamine, however, all indices were unaffected by high fat feeding.

4.4. Discussion

4.4.1. The impact of gene deletion on baseline cardiac function

The load-dependent and -independent indices of baseline cardiac function of C57BL/6 mice were relatively low compared to those previously reported for this strain in studies which also adopted the open chest model for PVL analysis (Lips *et al.*, 2004 and Walsh *et al.*, 2014). In the present study, PVL data generated from both male and female mice of each strain were combined in order to perform meaningful statistical analysis, however, female mice had a tendency to exhibit lower values of cardiac function. As Lips and colleagues (2004) conducted PVL analysis in only male C57BL/6 mice and Walsh and colleagues (2014) conducted this type of analysis in C57BL/6 mice where the balance was slightly in favour of males, it is possible that the inclusion of PVL data from female and male C57BL/6 mice in the present study may account for the relatively low indices of baseline cardiac function. Another possibility is that while the study conducted by Walsh and colleagues (2014) was also conducted at RGU, it was done so at a different site on campus where mice could not be held overnight. Consequently, the mice of the Walsh study were transported to RGU and used for experimentation on the same day. In contrast, the mice involved in the present study were housed in the biological services unit (BSU) where mice could be held for a period of up to 5 working days. It is therefore possible that the mice of the Walsh study were more stressed due to the shorter acclimatisation period prior to experimentation, causing their load-dependent and -independent indices of cardiac function to be augmented. Other factors which may have attenuated the cardiac function of the C57BL/6 mice in the present study have also been considered, for example, the anaesthetic mixture administered to mice (ketamine and xylazine), which is reportedly cardiac depressive (reviewed by Pacher *et al.*, 2008). However, the dosing of ketamine and xylazine in the current study was comparable with that of the Walsh study, therefore this possibility seems unlikely. The maintenance of mouse body temperature during each experiment may also have influenced cardiac function, however, great care was taken to minimise the influence of this variable. Furthermore, the relatively low values of baseline cardiac function in the present study are unlikely to have been caused by the early application of the PVL technique as C57BL/6 mice were not the first strain to have their cardiac function assessed using this method.

PVL analysis revealed that baseline systolic and diastolic function of ApoE^{-/-} mice was significantly enhanced compared to WT mice. A different method (Doppler echocardiography) similarly reported that ApoE^{-/-} mice exhibit significantly enhanced systolic function (Vincelette *et al.*, 2006). The HR of

the ApoE^{-/-} mice used in the current study was also significantly elevated, although studies previously reporting this index in the ApoE^{-/-} mouse have been somewhat confounding. According to Vasquez and colleagues (2012), studies which have utilised implanted telemetry devices to wirelessly record HR over short and long-term periods most accurately represent the HR of mice. Telemetric monitoring of the HR of ApoE^{-/-} mice aged 6-8 weeks revealed an increased mean HR (Pelat *et al.*, 2003), which is in line with the findings of the present study. While the present study did not investigate the mechanism(s) via which HR was elevated, the increased basal HR in ApoE^{-/-} mice is thought to be a consequence of augmented sympathetic activity in the presence of normal vagal tone (Hans *et al.*, 2009). However, other studies have reported that ApoE^{-/-} mice are characterised by a defective parasympathetic drive to the heart (Pelat *et al.*, 2003). If the latter is the case, then this would also contribute to an elevated HR in these mice. With regard to the enhanced CO exhibited in the ApoE^{-/-} mice of the present study, it is likely that this index was increased as a direct consequence of the augmented HR (CO=SV x HR). In addition to the enhanced CO, dP/dt_{max} was also greater in the ApoE^{-/-} mice compared to C57BL/6 mice, suggesting an increased inotropic response. Again, this could be due to increased sympathetic drive to the heart rather than any changes in the thickness or collagen deposition within the LV wall (Chapter 3, sections 3.3.7. and 3.3.8., respectively), since these were not altered in ApoE^{-/-} mice.

The present study also demonstrated that the baseline systolic and diastolic function of GPR55^{-/-} mice aged 16-19 weeks was significantly enhanced compared to age-matched WT mice. These findings are in contrast to those reported in the only other study to determine the cardiac function of GPR55^{-/-} mice (Walsh *et al.*, 2014). The Walsh study demonstrated that, while young (10 week old) GPR55^{-/-} mice were characterised by an increased HR, all other load-dependent and -independent indices of cardiac function were unaltered. However, systolic dysfunction was found to develop with age as mature (8 month old) mice were characterised by a significantly attenuated EF and inotropy as evidenced by a reduction in the ESPVR and E_{max} values compared to age-matched WT mice. Considering that compensatory mechanisms (i.e. increased sympathetic activity and circulating catecholamines) are often initiated to maintain systolic function and meet metabolic demands (reviewed by Jackson *et al.*, 2000), it may be that the enhanced systolic function observed in the present study was a compensatory mechanism in response to the early stages of systolic dysfunction. Consequently, the age of the GPR55^{-/-} mice used in the present study (16-19 weeks) may represent a turning point at which compensation occurs. However, as enhanced/compensatory systolic function cannot be maintained indefinitely, systolic dysfunction would ensue with time, which would align with the findings of the Walsh study.

This is the first study to investigate the cardiac function of ApoE^{-/-}/GPR55^{-/-} mice therefore all results reported herein represent innovative findings. Given that the baseline systolic and diastolic function of both ApoE^{-/-} and GPR55^{-/-} mice was enhanced, it may have been expected that the cardiac function of ApoE^{-/-}/GPR55^{-/-} mice would be further enhanced, although this was not the case since ApoE^{-/-}/GPR55^{-/-} mice exhibited similar cardiac function to that of WT mice. The reasons for this are particularly difficult to explain considering that the ApoE^{-/-}/GPR55^{-/-} mouse is so novel. Unfortunately, it was outwith the scope of the thesis to explore the underlying mechanism(s) but it poses an intriguing question that is worthy of further study.

4.4.2. The impact of high fat feeding on baseline cardiac function

The baseline values of cardiac function for the HFC C57BL/6 mice are more in line with those reported in other PVL studies for C57BL/6 mice fed an NC diet (Lips *et al.*, 2004 and Walsh *et al.*, 2014). However, as previously mentioned, the mice were randomised as to when they underwent PVL analysis, therefore the data are regarded as an accurate reflection of events. The present study demonstrated that the systolic function of C57BL/6 mice was improved in response to high fat feeding, which is in contrast to the findings of Louwe and colleagues (2012) who reported a reduction in the systolic function of HFC fed C57BL/6 male, but not female mice. The duration of the dietary period was similar in each study (12 weeks) and while the mice of the Louwe study were slightly older (3-6 weeks), it is not thought that this would account for the contrast in findings. It is suspected that differences in the composition of diet fed to the mice in each study may account for the inconsistencies as the mice of the present study were fed a 21% fat/0.15% cholesterol diet whereas the mice of the Louwe study were fed a diet higher in fat (39.5%/5.5% soy bean oil).

The main change in the HFC fed C57BL/6 mice was an increase in HR, which would account for the increased CO exhibited by these mice. If this had occurred in response to an increase in sympathetic activity, an increase in other variables such as dP/dt_{max} would have been expected. As this was not the case, it seems more likely that a reduced vagal input may have contributed to the increase in chronotropy. In support of this, Hartnett and colleagues (2015) demonstrated that high fat feeding of C57BL/6 mice impairs parasympathetic vagal control of the heart.

High fat feeding of ApoE^{-/-} mice had no impact on cardiac function despite the presence of hyperlipidaemia and fatty streak deposition in the thoracic aortae of these mice (Chapter 3, sections 3.3.5. and 3.3.6., respectively). These findings are in agreement with other studies in which ApoE^{-/-}

mice fed a HFC diet for 4 (Johansson *et al.*, 2005) or 16 weeks (Hans *et al.*, 2011) exhibited cardiac function similar to that of NC fed ApoE^{-/-} mice. While fatty streaks were observed within the thoracic aortae of HFC fed ApoE^{-/-} mice, the degree of and encroachment into the vessel lumen was not investigated. Additionally, coronary atherosclerosis would have likely had a negative impact on the contractile function of these mice, however, as expected in this strain, there was no evidence of coronary atherosclerosis (Chapter 3, section 3.3.9.). While the development of fatty streaks in the aortic root of each mouse group was not assessed, significant narrowing of the aortic root would have been expected to increase the LV contractile force to sustain the flow of blood to organs/tissues. Since the present study did not demonstrate an increase in LV contractility in HFC ApoE^{-/-} mice, it seems unlikely that any fatty streak deposition within the aortic root of these mice would have been of a sufficient size/severity to alter cardiac function.

This is the first study to investigate the effects of high fat feeding on cardiac function in both GPR55^{-/-} and ApoE^{-/-}/GPR55^{-/-} mice. High fat feeding of GPR55^{-/-} and ApoE^{-/-}/GPR55^{-/-} mice, aged 4-7 weeks for a 12 week period resulted in minor reductions in baseline systolic function, however, such reductions indicate a role for GPR55 in maintaining cardiac function in atherosclerosis. One potential explanation for the reduced systolic performance in mice with the gene deletion for GPR55 is that both strains display an obese phenotype. However, obesity is associated more with diastolic (Pascual *et al.*, 2003) rather than systolic dysfunction, yet neither GPR55^{-/-} or ApoE^{-/-}/GPR55^{-/-} mice demonstrated any alterations in baseline diastolic function. However, BP measurements in conscious GPR55^{-/-} mice have shown that these mice are hypertensive (Walsh *et al.*, 2015), and since hypertension has been linked to systolic dysfunction (Verdecchia *et al.*, 2005 and Ogah *et al.*, 2011), this could represent the underlying mechanism for the observed changes in some of the indices of systolic function in both strains with a deletion of GPR55. However, the apical approach for PVL analysis used in the present study precludes the measurement of arterial blood pressure and therefore it is not possible to say whether or not the presence of hypertension may have contributed to the observed changes. Additionally, plasma lipid profiling demonstrated that HFC fed GPR55^{-/-} mice exhibited normal profiles whereas those of the ApoE^{-/-}/GPR55^{-/-} mice fed HFC were extremely dyslipidaemic. As a result, changes in the cardiac function of HFC fed mice with the genetic deletion of GPR55 are not linked to the degree of hyperlipidaemia.

4.4.3. The impact of gene deletion on contractile reserve

Stress tests are commonly used to detect cardiac dysfunction in humans and in animals. In humans, this is typically carried out by means of exercise testing. However, in animals, stress tests are more commonly induced by pharmacological agents, as controlled exercise in animals can prove challenging. Dobutamine, an α_1/β_1 -adrenoceptor agonist is the pharmacological agent often used in studies (Wiesmann *et al.*, 2001, Kreissl *et al.*, 2006 and Tyrankiewicz *et al.*, 2013) as it stimulates cardiac function but has minimum peripheral haemodynamic effects.

In the present study, dobutamine induced positive chronotropic and inotropic responses of a similar magnitude in all groups therefore gene deletion had no significant impact on contractile reserve. In terms of the ApoE^{-/-} mice, this finding is in contrast to that of Vincelette and colleagues (2006) who reported that 16 month old ApoE^{-/-} mice are characterised by a reduced contractile reserve (determined by Doppler echocardiography). Although the ApoE^{-/-} mice in the present study exhibited modest hyperlipidaemia and a marked deposition of fatty streaks within the thoracic aorta (Chapter 3, sections 3.3.5. and 3.3.6. respectively), these mice were much younger (16-19 weeks of age) at the time of analysis and therefore it is likely that the extent of atherosclerotic lesion development in these mice had not yet reached a severity capable of impairing their contractile reserve. While Vincelette and colleagues (2006) did not investigate the mechanisms which led to a reduced contractile reserve in the ApoE^{-/-} mice, they did however speculate that the impairment may have been the result of endothelial dysfunction and coronary atherosclerosis, reducing the supply of blood to the heart. However, as ApoE^{-/-} mice do not develop coronary artery plaques (Coleman *et al.*, 2006), the latter seems highly unlikely.

The finding that the contractile reserve of GPR55^{-/-} mice aged 16-19 weeks was unaltered in the present study is again inconsistent with the findings of Walsh and colleagues (2014) who conducted a dobutamine (10 μ g/kg) stress test on young (10 week old) and mature (8 month old) GPR55^{-/-} mice and reported that GPR55^{-/-} mice at either age were characterised by an impaired contractile reserve. While compensatory mechanisms i.e. increased sympathetic activity and circulating catecholamines are initiated to maintain systolic function and meet metabolic demands, chronic β_1 -adrenoceptor stimulation during the compensatory period leads to the downregulation (Bristow *et al.*, 1986) and uncoupling of β_1 -adrenoceptors, the latter commonly referred to as 'desensitisation' (Takahashi *et al.*, 1992). Unfortunately, the downregulation and desensitisation of β_1 -adrenoceptors leads to systolic dysfunction and with its progression, an impaired contractile reserve (reviewed by

Lymperopoulos *et al.*, 2013). As previously mentioned in section 4.4.1., the age of the mice used in the present study may represent a mid-point between 'compensation' and the progression to systolic dysfunction. It is therefore possible that this applies to the contractile reserve data and if so, would explain the differences between the contractile reserve data of the present study and that of the Walsh study. Moreover, as both the ApoE^{-/-} and GPR55^{-/-} mice of the present study exhibited a normal contractile reserve, it is not surprising that the contractile reserve of ApoE^{-/-}/GPR55^{-/-} mice was unaltered.

4.4.4. The impact of high fat feeding on contractile reserve

While high fat feeding did not alter the contractile reserve of WT mice, it impaired the contractile reserve of ApoE^{-/-} mice. In contrast, high fat feeding of both GPR55^{-/-} and ApoE^{-/-}/GPR55^{-/-} mice enhanced their contractile reserve.

The finding of an unaltered contractile reserve in response to high fat feeding in WT mice is in contrast to the findings of Fu and colleagues (2017) who reported that 12 weeks of high fat feeding impaired the contractile reserve of C57BL/6 mice. It is suspected that the disparity in findings may be due to the mice of the Fu study consuming a diet containing a higher percentage of fat (34.9% vs. 21% fat). Calligaris and colleagues (2013) also reported a reduced contractile reserve in C57BL/6 mice in response to high fat feeding, however, the duration of the dietary period had been considerably longer (8 or 16 months) which is likely to account for the contrast in findings.

In terms of HFC fed ApoE^{-/-} mice, Vincelette and colleagues (2006) also demonstrated an impaired contractile reserve in their ApoE^{-/-} mice, however, the mice involved in the Vincelette study were aged (16 months) and had been fed an NC diet. Interestingly, Heinonen and colleagues (2011) reported a preserved but reduced contractile reserve in a different HFC fed model of atherosclerosis (LDLR^{-/-}ApoB^{100/100} mice). As this model is characterised by a plasma total cholesterol concentration lower than that of ApoE^{-/-} mice (Véniant *et al.*, 2000), this may explain why the contractile reserve of these mice was 'preserved', although reduced. As the HFC fed ApoE^{-/-} mice of the present study were highly dyslipidaemic, it may be that dyslipidaemia leads to a downregulation in β_1 -adrenoceptor expression or sensitivity in the heart thus impairing the contractile reserve of these mice. Despite conducting a thorough literature search, it would appear that the potential relationship between dyslipidaemia and cardiac β_1 -adrenoceptor function has not yet been investigated. Consequently, this poses an exciting new line of enquiry and is worthy of future investigation.

GPR55^{-/-} and ApoE^{-/-}/GPR55^{-/-} mice exhibiting an enhanced contractile reserve indicates that in the latter stages of atherosclerosis, GPR55 is involved in maladaptive adrenergic signalling of the heart. Despite the initial suggestion that the impaired contractile reserve of ApoE^{-/-} mice may have occurred as a consequence of their dyslipidaemic plasma profile negatively impacting cardiac β_1 -adrenoceptor function, it would appear that the impaired contractile reserve of these mice occurred via a lipid-independent mechanism as both ApoE^{-/-} and ApoE^{-/-}/GPR55^{-/-} mice exhibited similar dyslipidaemic plasma profiles.

It was initially thought that obesity *per se* may increase β -adrenoceptor sensitivity and increase the contractile reserve of HFC fed mice with a gene deletion for GPR55 as these mice exhibited an obese phenotype. However, a study conducted in rats reported that the expression of β_1 -adrenoceptors and the G-protein (G_s) to which it binds are unaffected by obesity in the isolated papillary muscle, as is the overall sensitivity of β -adrenoceptors in this tissue (Ferron *et al.*, 2015). Moreover, Carroll and colleagues (2002) reported in the isolated rabbit heart that obesity-induced reductions in responsiveness to the non-selective β -adrenoceptor agonist, isoproterenol, are not linked to changes in the sensitivity or expression of β -adrenoceptors in this tissue. Together, these reports suggest that obesity *per se* is unlikely to be responsible for the enhanced contractile reserve exhibited by the mice deficient in the gene for GPR55. Further investigation is now required to elucidate in what way(s) the genetic deletion of GPR55 leads to an enhanced contractile reserve.

4.4.5. Conclusion

In summary, the current study set out to determine the role of GPR55 in the cardiac function of atherosclerosis prone mice. While the present study utilised PVL analysis, an invasive method to determine the cardiac function of mice, non-invasive imaging such as cardiac MRI and echocardiography are more routinely used in the clinical setting. As a reduced EF ($\leq 35\%$ or $\leq 40\%$ depending on the trial) has been the most common index of cardiac function used for entry criteria to recruit patients into clinical trials investigating systolic heart failure (SOLVD investigators *et al.*, 1991, Cohn *et al.*, 2001, Pitt *et al.*, 1999 and McMurray *et al.*, 2014), a reduced EF was used as the main indicator of systolic dysfunction within the present study. HFC fed ApoE^{-/-}/GPR55^{-/-} mice exhibited systolic dysfunction (a reduced EF as a consequence of an increased ESV; $EF = ((EDV - ESV)/EDV) \times 100$), while HFC fed ApoE^{-/-} mice exhibited a normal EF. From these findings, it can therefore be determined that GPR55 exhibits a protective role in terms of maintaining baseline systolic function in atherosclerosis prone mice. In contrast, GPR55 contributed to the impaired

contractile reserve of these mice. The latter therefore indicates that in the later stages of atherosclerosis, GPR55 is involved in maladaptive adrenergic signalling of the heart.

Chapter 5:

The impact of GPR55 activation in myocardial ischaemia/reperfusion injury

5.1. Introduction

Ex vivo observations have determined that GPR55 promotes the development of fatty streaks in the thoracic aortae of mice suffering from atherosclerosis (Chapter 3). In contrast, an important role for GPR55 in the maintenance of cardiac function of these mice, *in vivo*, has been demonstrated (Chapter 4). Together, these findings suggest a complex role for GPR55 in atherosclerosis.

A recent study by Kurano and colleagues (2015) measured the plasma concentration of a range of lysophospholipids, including LPI, in patients undergoing coronary angiography at the time of an acute coronary event. Circulating levels of total plasma LPI were increased at this time, the source of which was suggested to be activated platelets at the site of plaque rupture. Considering that GPR55 is the only reported LPI receptor in mammalian tissue (Oka *et al.*, 2007), that GPR55 is expressed on ventricular cardiomyocytes and GPR55 activation increases $[Ca^{2+}]_i$ in these cells (Yu *et al.*, 2013), the presence of an increased concentration of LPI in the vicinity of cardiomyocytes may have important implications for the pathogenesis of myocardial I/R injury. In support of this, it has been demonstrated that the administration of a GPR55 antagonist, cannabidiol (CBD), to rats *in vivo*, reduces infarct size (Durst *et al.*, 2007 and Walsh *et al.*, 2010) and suppresses ischaemia-induced cardiac arrhythmias (Walsh *et al.*, 2010). Additionally, it has recently been demonstrated that CBD is protective in a rat model of cerebral ischaemia, through a mechanism thought to involve the upregulated expression of the Na^+-Ca^{2+} exchanger (NCX) proteins 2 and 3 (NCX2 and NCX3, respectively) (Khaksar and Bigdeli, 2017).

5.1.1. GPR55 signalling in the cardiomyocyte

Several studies have attempted to define the signalling mechanisms of GPR55. However, due to its complex pharmacology and lack of selective ligands, characterising just how this GPCR elicits its effects has proved challenging. It would appear that the pathway via which GPR55 signals varies based upon the cell/tissue type and also by the ligand with which it is activated. Interestingly, the application of LPI to HEK293 cells stably expressing GPR55 has been reported to induce an oscillatory and prolonged Ca^{2+} release from the SR as a result of PLC activation (Henstridge *et al.*, 2009). Further investigation concluded that such Ca^{2+} release was dependent on $G\alpha_{13}$ and that signalling downstream of this G-protein subunit was via RhoA/ROCK - a pathway recognised for its important role in various fundamental cellular processes that lead to cardiovascular disease (reviewed by Satoh *et al.*, 2011). More recently and for the first time, the signalling of the LPI/GPR55 system on and

within cardiomyocytes was investigated (Yu *et al.*, 2013), where it was reported that LPI can initiate separate signalling pathways via GPR55 which are dependent on the location of this GPCR. The first pathway demonstrated that LPI-induced GPR55 activation at the sarcolemma mediates an increase in $[Ca^{2+}]_i$ via Ca^{2+} influx through LTCCs and IP_3 -dependent Ca^{2+} release. Secondly, it was demonstrated that GPR55 activation by LPI at the membrane of intracellular organelles promotes Ca^{2+} release via endolysosomal NAADP-sensitive two-pore channels. $[Ca^{2+}]_i$ was further enhanced in each pathway by CICR via RYRs. On the basis that LPI induces $[Ca^{2+}]_i$ release via a GPR55-dependent mechanism in cardiomyocytes and that $[Ca^{2+}]_i$ overload of cardiomyocytes is a key event in myocardial I/R injury (Hausenloy and Yellon, 2013), it is possible that LPI-mediated activation of GPR55 may contribute to this type of injury. Thus, the present study was conducted to investigate this. Moreover, as activation of ROCK (Henstridge *et al.*, 2009 and Oka *et al.*, 2010) and IP_3 receptors (IP_3R) (Lauckner *et al.*, 2008, Henstridge *et al.*, 2009 and Yu *et al.*, 2013) have commonly been reported in the signalling of the LPI/GPR55 system, the present study investigated the involvement of the ROCK/ IP_3R pathway in any observed changes to myocardial tissue injury mediated by LPI-induced activation of GPR55.

5.1.2. Aims

Taken together, the evidence suggests that activation of GPR55 during an acute coronary event may contribute to myocardial tissue injury. To test this hypothesis, this study investigated 1) if the ROCK/ IP_3R signalling pathway was involved following GPR55 activation in mouse and human cardiomyocytes, 2) the impact of GPR55 activation on infarct size by administering exogenous LPI to the coronary circulation of isolated C57BL/6 (wildtype; WT) and $GPR55^{-/-}$ mouse hearts during an I/R protocol, and 3) if the ROCK/ IP_3R signalling pathway was involved in any observed changes to infarct size, using the same I/R protocol and challenging WT mouse hearts with LPI in the absence and presence of various protein inhibitors.

5.2. Methods

5.2.1. Effect of GPR55 activation on the DMR activity of cultured cardiomyocytes and investigation of the signalling pathway following GPR55 activation

miPSC and hiPSC-derived cardiomyocytes were cultured as outlined in Chapter 2, section 2.1.1.1. Following cell culture, the wells of each microplate were gently washed with buffer 1 (HBSS, HEPES (20mM), 0.01% BSA and <0.1% DMSO; pH7.4) using an ELx Microplate Washer (Bio-Tek, Sweden).

Separate plates containing each cell line, along with the corresponding compound source plates were then incubated in the Corning® Epic® system and the high throughput screening of compounds conducted as described in Chapter 2, section 2.1.2. Such screening of compounds involved the application of L- α -Lysophosphatidylinositol (LPI; 1nM-30 μ M) to the cells. To confirm that cellular responses to LPI were as a consequence of GPR55 activation, the effect of LPI (10 μ M; approximate EC₅₀) in the presence of CBD (1 μ M) was determined. Finally, the ROCK inhibitor, Y-27632 dihydrochloride (Y-27632; 10 μ M & 50 μ M) and the IP₃R inhibitor, xestospongin C (xest C; 3 μ M, 5 μ M & 10 μ M) were used to investigate the signalling mechanisms involved in the cellular response to GPR55 activation. Moreover, vehicle controls (<0.1% DMSO) were included in each set of experiments.

5.2.2. Isolated heart studies

The Langendorff isolated heart model has been widely utilised over the years to investigate the mechanisms via which myocardial I/R injury mediates its deleterious effects on the myocardium (Chocron *et al.*, 1996, Temsah *et al.*, 1999, Bopassa *et al.*, 2005 and Griecsová *et al.*, 2015). This particular model was chosen for use in the present study as it allows for a wide range of physiological, biochemical, morphological and pharmacological parameters to be assessed in the absence of effects mediated by other organs. For an extensive review of this technique see Liao and colleagues (2012).

Male/female WT (24.4 \pm 0.5g) and GPR55^{-/-} mice (23.0 \pm 0.5g) were age matched (9-12 weeks) and randomised into appropriate experimental groups using random number generator software (Stat Trek, 2013) prior to commencing experimental protocols. Mice were anaesthetised and isolated heart experiments performed according to the protocol detailed in Chapter 2, section 2.3.5. Hearts from WT (n=14) and GPR55^{-/-} (n=5) mice were utilised in the initial I/R studies (30 minutes no-flow global ischaemia (GI) followed by 30 minutes reperfusion) to determine the effect of an absence of GPR55 on myocardial infarct size. Subsequently, to determine the effect of GPR55 activation on infarct size, WT (n=15) and GPR55^{-/-} (n=7) hearts were challenged with LPI (10 μ M) either 10 minutes prior to the onset of ischaemia or during the early reperfusion period. A further series of experiments were then conducted using hearts from WT mice to determine if pharmacological blockade of GPR55 (with CBD; 1 μ M (n=5)) or ROCK inhibition (with Y-27632 dihydrochloride; 10 μ M and 50 μ M (n=6 for each concentration)), 5 minutes prior to myocardial GPR55 activation could attenuate any GPR55 mediated effects on infarct size. Contemporaneous vehicle controls (0.1% DMSO; n=14) were

included throughout. Infarct size was then measured according to the protocol described in Chapter 2, section 2.3.6.

5.2.3. Statistics

To ensure that the studies planned within this chapter had sufficient statistical power, power calculations were conducted prior to experiments taking place and were based on data from previous experiments performed in the lab. Power calculations recommended an $n=8$ for isolated heart studies. See below for the power calculation conducted for the assessment of drug intervention on myocardial infarct size:

To assess the effect of two compounds (X and Y), there would be three randomly assigned experimental groups: vehicle control, compound X and compound Y. For myocardial infarct size, power calculations for a one-way ANOVA to detect a 30% reduction in infarct size compared to control values (e.g. 42% of left ventricular volume in treated animals vs. 60% in controls, equating to a reduction in 18 percentage points of left ventricular volume), with a standard deviation of 10% indicates that a group size of 8 would have 85% power to detect this difference.

Within this chapter, data was excluded if a heart suffered any arrhythmic activity or if data was outwith the $\text{mean} \pm 2x$ (standard deviations). Data are expressed as $\text{mean} \pm \text{S.E.M}$ throughout (unless otherwise stated). Comparisons were performed using an unpaired *t*-test (two-tailed) and multiple comparisons performed using a one-way ANOVA followed by a 'Bonferroni' post-hoc test. All statistical tests were carried out using GraphPad Prism[®] 4 software (GraphPad Software, Inc., USA) and differences between data deemed significant where $P < 0.05$.

5.3. Results

5.3.1. Effect of GPR55 activation on the DMR activity of cultured miPSC-derived cardiomyocytes and investigation of the signalling pathway following GPR55 activation

LPI induced a concentration-dependent increase in DMR activity (indicative of changes in cell activity) in miPSC-derived cardiomyocytes (Figure 5.1.). The response to LPI (10 μ M; approximate EC_{50}) was rapid, with an immediate onset, and reached peak activity after 10 minutes (Figure 5.2. A). When

compared to the DMR activity induced by vehicle, LPI (10 μ M) significantly increased the DMR activity of the miPSC-derived cardiomyocytes (185.9 \pm 16.3 vs. 29.4 \pm 2.6; P <0.001; Figure 5.2. A and B). Co-application of CBD (1 μ M) completely blocked the LPI response (36.9 \pm 8.9 vs. 185.9 \pm 16.3; P <0.001; Figure 5.2. A & B), confirming an action of LPI through GPR55. Y-27632 dihydrochloride (10 μ M and 50 μ M) also inhibited the cellular response to LPI (26.4 \pm 2.1 and 34.1 \pm 3.3 vs. 185.9 \pm 16.3, respectively; P <0.001; Figure 5.2. C & D), whereas xest C (5 μ M) did not (147.1 \pm 5.4 vs. 140 \pm 1.0; Figure 5.2. E). Unfortunately, due to an error in the compound plate, LPI (10 μ M) was only present in two of the three plates run through the Corning[®] Epic[®] system (Figure 5.2. E), however, it is clear from the responses in Figure 5.2. B and D that LPI (10 μ M) mediates a statistically significant increase in the DMR activity of miPSC-derived cardiomyocytes. Moreover, cellular application of all individual agents alone (excluding LPI) induced changes in DMR activity similar to that observed with the vehicle.

5.3.2. Effect of GPR55 activation on the DMR activity of cultured hiPSC-derived cardiomyocytes and investigation of the signalling pathway following GPR55 activation

The DMR response of hiPSC-derived cardiomyocytes was concentration dependent when challenged with LPI (Figure 5.3.). Moreover, LPI (10 μ M; approximate EC₅₀) significantly increased the DMR activity of the hiPSC-derived cardiomyocytes when compared to that induced by vehicle (128.5 \pm 5.3 vs. 32.2 \pm 2.9; P <0.001; Figure 5.4. A). Co-application of CBD (1 μ M) fully inhibited the response to 10 μ M LPI (33.3 \pm 2.1 vs. 128.5 \pm 5.3; P <0.001; Figure 5.4. A), demonstrating GPR55 activation via LPI. Y-27632 dihydrochloride (10 μ M and 50 μ M) also inhibited the cellular response to LPI (35.0 \pm 2.1 and 30.8 \pm 1.2 vs. 128.5 \pm 5.3, respectively; P <0.001; Figure 5.4. B), however, the IP₃R antagonist, xest C (5 μ M & 10 μ M) failed to do so (127.3 \pm 3.9 and 129.8 \pm 3.3 vs. 128.5 \pm 5.3, respectively; Figure 5.4. C). Moreover, cellular application of all individual agents alone (excluding LPI) induced changes in DMR activity similar to that observed with the vehicle.

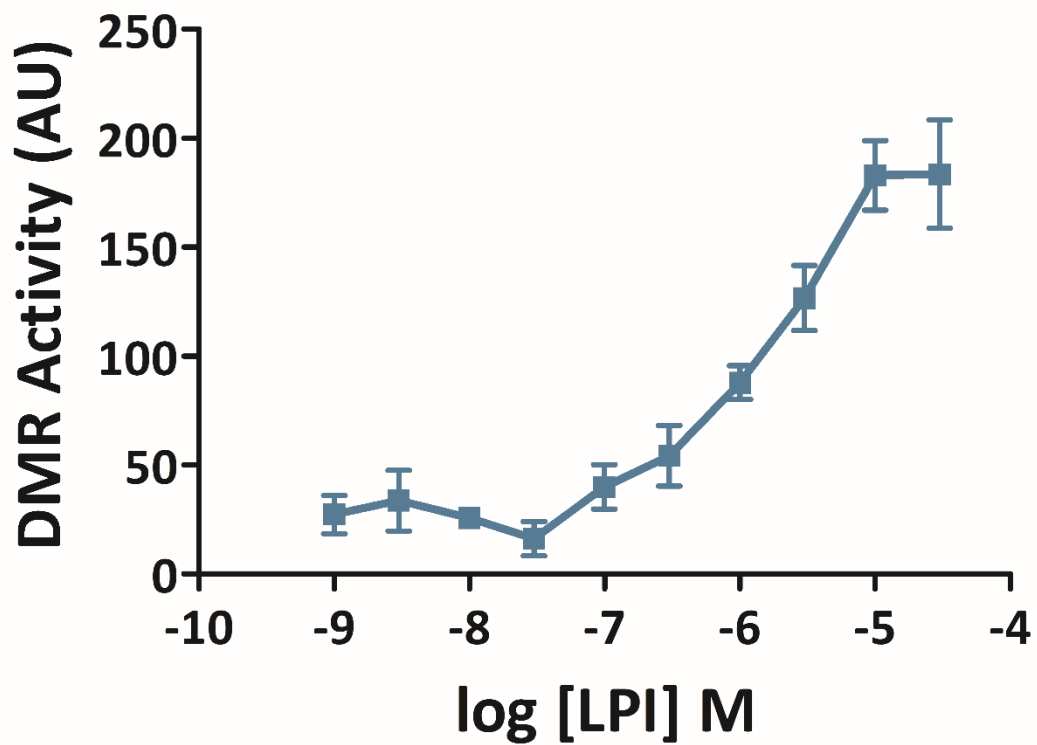


Figure 5.1. DMR activity of miPSC-derived cardiomyocytes in response to LPI (1nM-30 μ M). Each concentration of LPI was examined in duplicate samples in each plate and four independent experiments (i.e. four individual plates) assessed by the Corning® Epic® system. Data are expressed as the mean \pm S.E.M. of all four plates combined. The mean peak cellular response to LPI (10 μ M) occurred at 10 minutes (see Figure 5.2. A) therefore data was extracted at this time point. AU; arbitrary units.

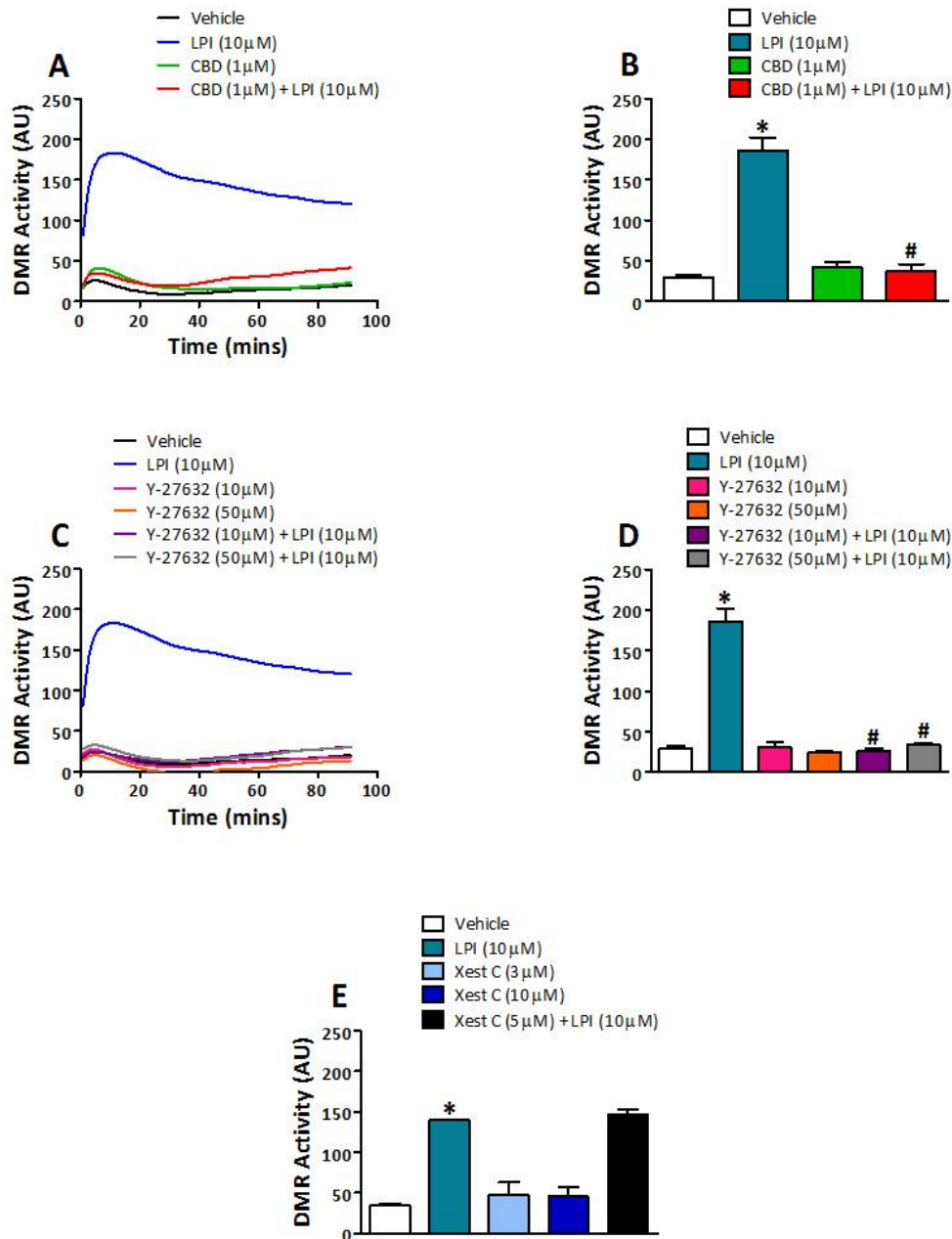


Figure 5.2. Investigation of the signalling pathway following receptor activation with LPI (10µM) in miPSC-derived cardiomyocytes. miPSC-derived cardiomyocytes were challenged with LPI (10µM) in the absence and presence of protein inhibitors and the consequent DMR activity plotted against time (mins); A and C. The peak DMR response to LPI (10µM) in the absence and presence of protein inhibitors; B, D and E. Each compound was examined in duplicate samples in each plate. Data are expressed as the mean DMR responses of plates; A and C or mean±S.E.M of plates; B, D and E. n=4; A & B, n=4-5; C & D and n=2-3; E. * $P < 0.001$ vs. Vehicle and # $P < 0.001$ vs. LPI (10µM); one-way ANOVA followed by a 'Bonferroni' post-hoc test.

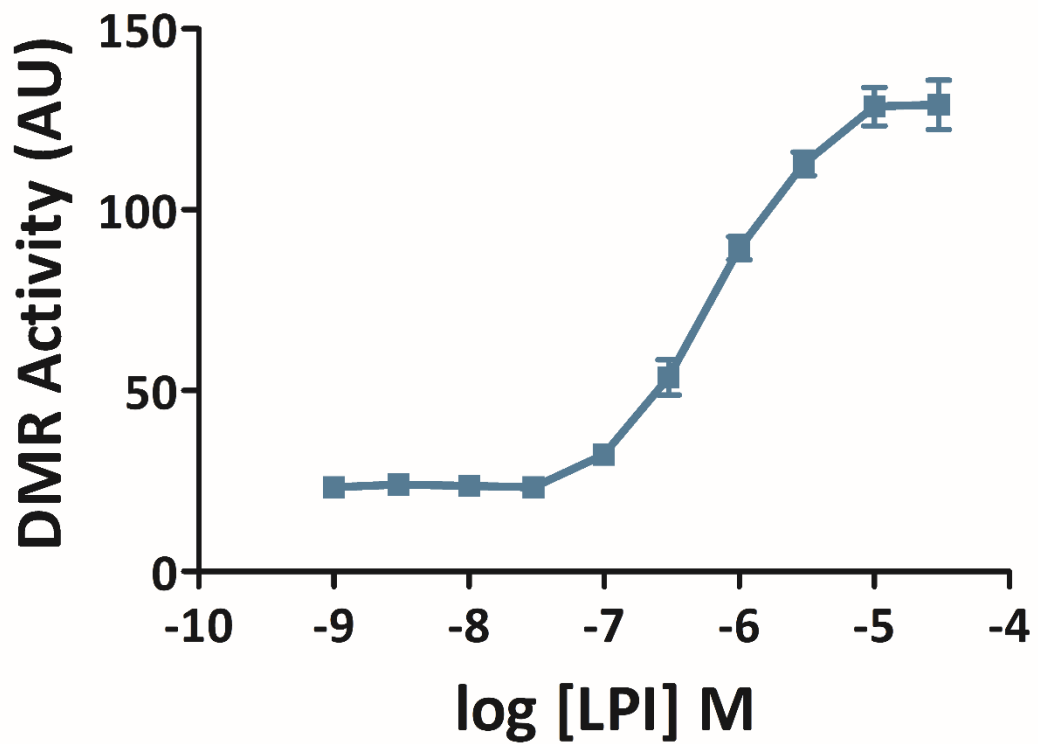


Figure 5.3. DMR activity of hiPSC-derived cardiomyocytes in response to LPI (1nM-30 μ M). Data are expressed as the mean \pm S.E.M. of plates; n=3. The mean peak cellular response to LPI (10 μ M) occurred at 20 minutes therefore data was extracted at this time point.

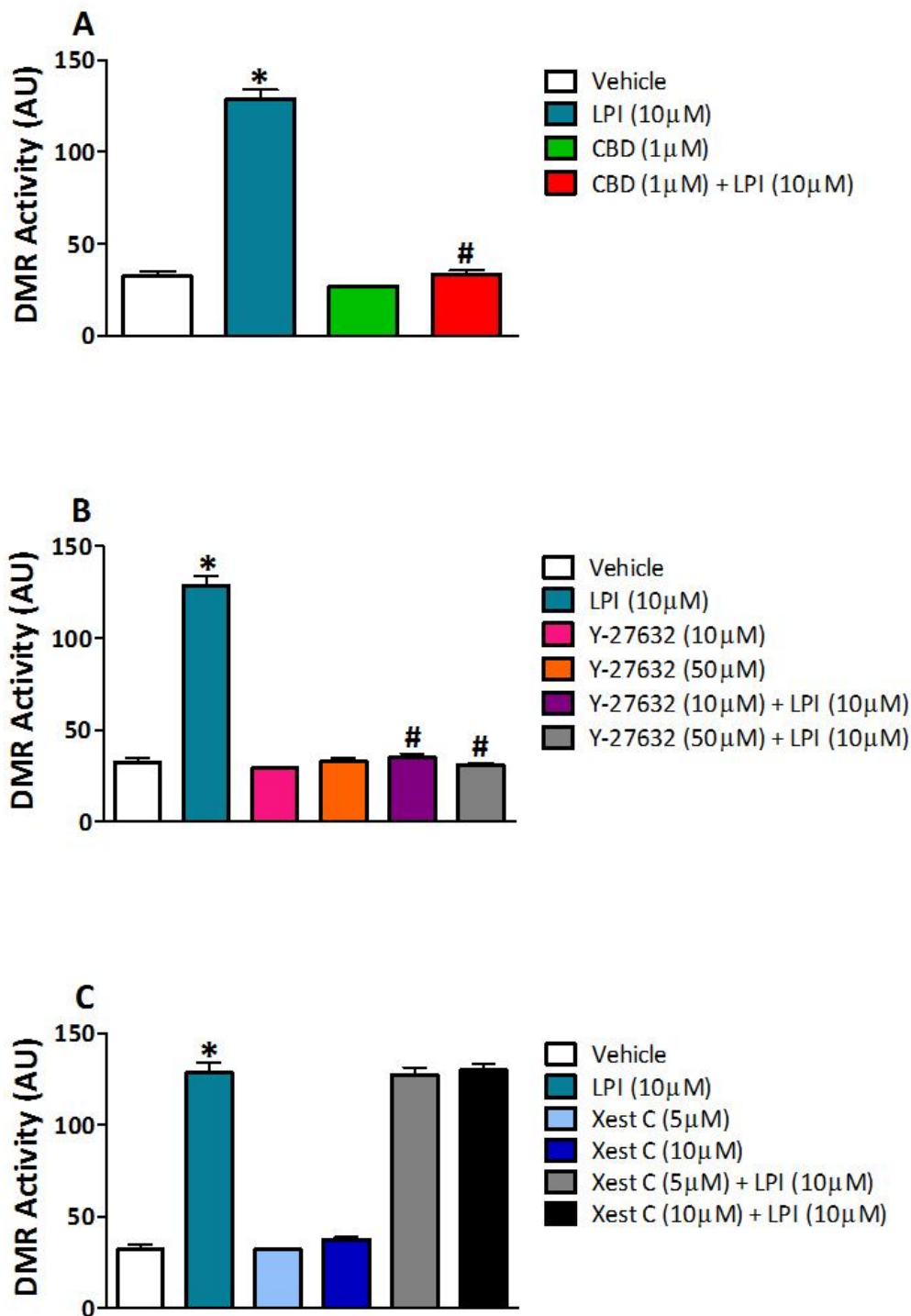


Figure 5.4. Investigation of the signalling pathway following receptor activation with LPI (10µM) in hiPSC-derived cardiomyocytes. The peak DMR response to LPI (10µM) in the absence and presence of protein inhibitors; A, B and C. Data are expressed as mean±S.E.M. of plates; n=3. * $P < 0.001$ vs. Vehicle and # $P < 0.001$ vs. LPI (10µM); one-way ANOVA followed by a 'Bonferroni' post-hoc test.

5.3.3. Effect of GPR55 activation on myocardial I/R injury and investigation of the signalling pathway following GPR55 activation

Infarct size did not significantly differ between the hearts of WT and GPR55^{-/-} mice when subjected to 30 minutes of no-flow GI followed by 30 minutes reperfusion (37.6±3.5 vs. 37.0±3.2%; Figure 5.5 A). However, WT hearts challenged with LPI (10µM) prior to GI had significantly larger infarcts (51.4±4.1 vs. 37.6±3.5%; *P*<0.05; Figure 5.5. B), a finding which was not seen when LPI was administered post-GI (38.1±3.3 vs. 37.6±3.5%; Figure 5.5. B). Representative images of vehicle (0.1% DMSO) and LPI (10µM administered prior to GI) treated hearts are shown in Figures 5.5. C and D, respectively. LPI (10µM) administration to GPR55^{-/-} hearts, prior to GI, did not significantly alter infarct size (48.0±5.4 vs. 37.0±3.1%; Figure 5.5. E), confirming that LPI increases infarct size via a GPR55-dependent mechanism. CBD (1µM) failed to inhibit the injury induced by LPI (47.0±2.7 vs. 51.4±4.1%) although hearts challenged with CBD (1µM) alone, had significantly larger infarcts when compared to those treated with vehicle (54.5±5.9 vs. 37.6±3.5%; *P*<0.05; Figure 5.6. A). Conversely, Y-27632 dihydrochloride (10µM & 50µM) prevented LPI from mediating an increase in infarct size (42.4±7.4 and 35.5±7.8% vs. 37.6±3.5%, respectively; Figure 5.6. B) compared to vehicle treated hearts.

5.4. Discussion

The findings of Chapters 3 and 4 indicate a complex role for GPR55 in atherosclerosis. On the basis that atherosclerotic plaque rupture within the coronary vasculature often precedes myocardial I/R injury (Virmani *et al.*, 2005), the principal aims of this study were to determine the impact of GPR55 activation on the outcome of myocardial I/R injury and to establish the signalling pathway(s) through which any observed changes occurred. These aims were addressed by investigating the signalling mechanisms following GPR55 activation at the level of the cardiomyocyte and subsequently by conducting an I/R protocol in hearts isolated from WT and GPR55^{-/-} mice and challenging them with LPI in the absence and presence of protein inhibitors.

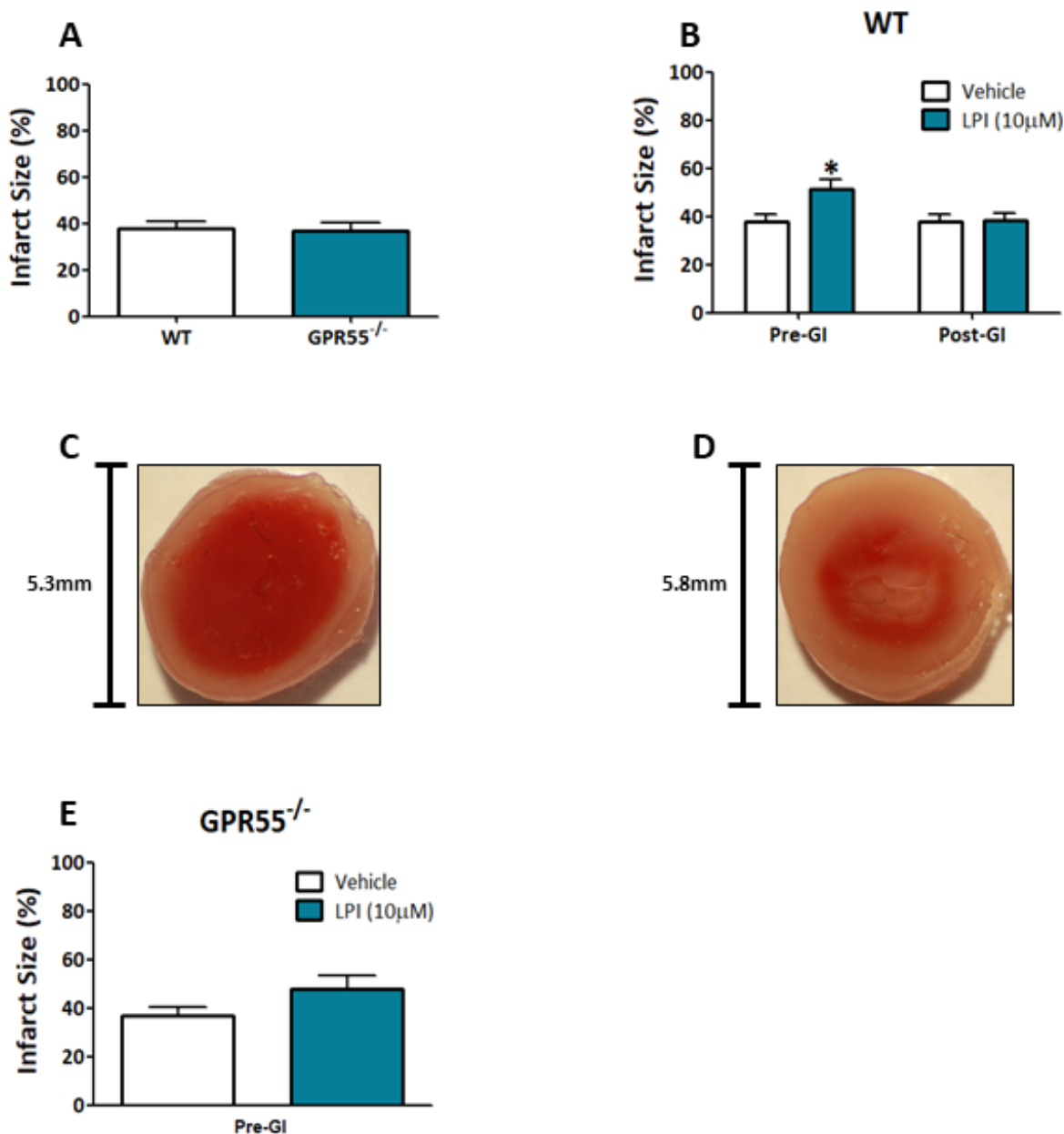


Figure 5.5. Effect of GPR55 gene deletion and GPR55 activation on myocardial I/R injury. Infarct size was measured as a % of the total ventricular area. The effect of GPR55 gene deletion on myocardial I/R injury; A. I/R injury sustained in WT hearts administered LPI (10µM) pre- or post-GI; B. Pre-GI, vehicle and LPI (10µM) treated heart sections; C and D, respectively. The red and peach areas denote viable and infarcted tissue, respectively. I/R injury sustained in GPR55^{-/-} hearts, administered LPI (10µM) pre-GI; E. Data are expressed as mean±S.E.M. A; n=14 & 5 for WT and GPR55^{-/-} hearts, respectively. B (pre-GI); n=14 & 15 for vehicle and LPI (10µM) treated hearts, respectively. B (post-GI); n= 14 & 9 for vehicle and LPI (10µM) treated hearts, respectively. E; n=5 & 7 for vehicle and LPI (10µM) treated hearts, respectively. **P*<0.05 vs. vehicle; unpaired *t*-test (two-tailed).

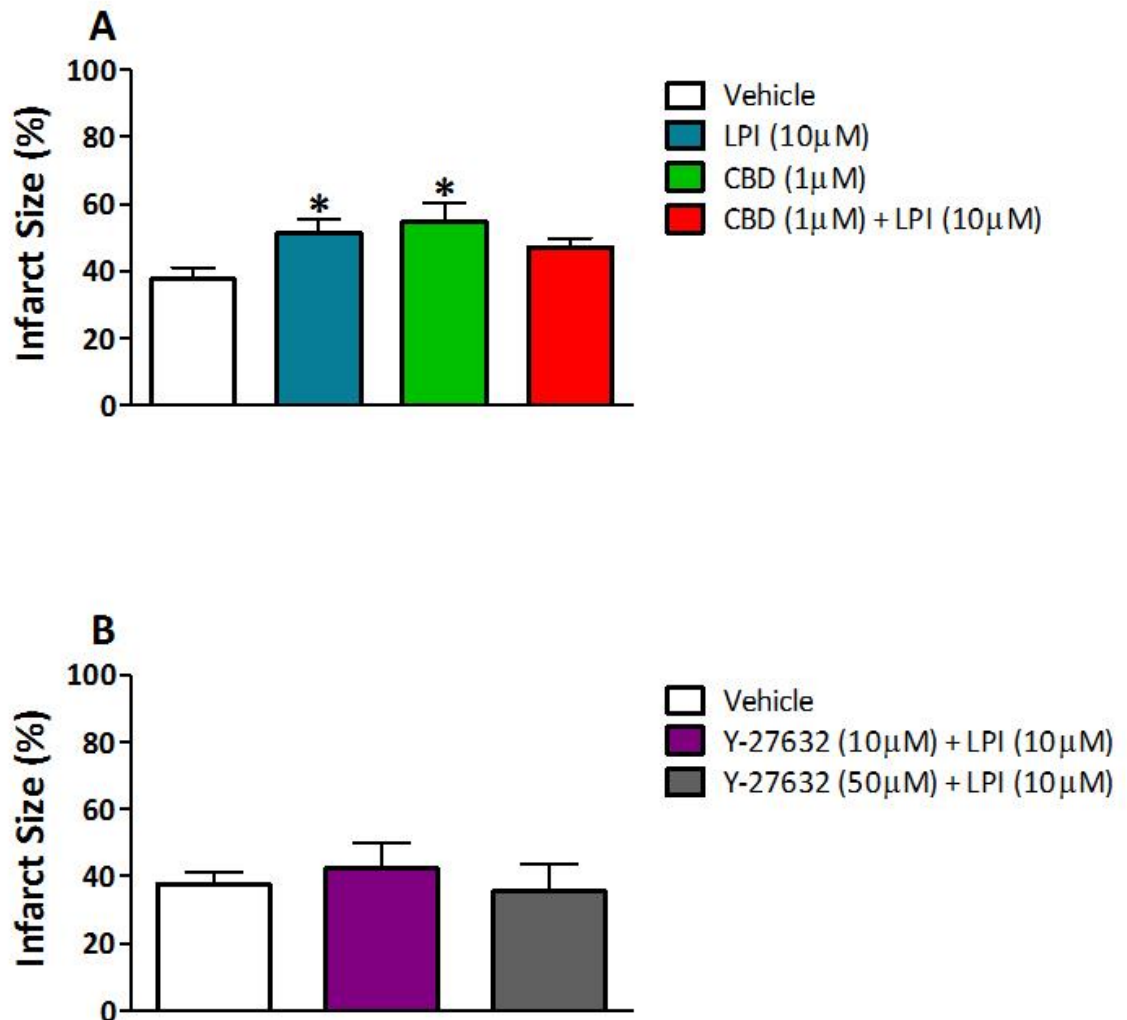


Figure 5.6. Investigation of the signalling pathway following GPR55 activation in myocardial I/R injury. I/R injury sustained in WT hearts administered LPI (10µM) pre-GI in the absence and presence of protein inhibitors; A and B. Data are expressed as mean±S.E.M. A; n=14, 15, 7 & 5 for vehicle, LPI (10µM), CBD (1µM) and LPI (10µM) + CBD (1µM), respectively and B; n=14, 6 & 6 for vehicle, LPI (10µM) + Y-27632 (10µM) and LPI (10µM) + Y-27632 (50µM), respectively. **P*<0.05 vs. vehicle; one-way ANOVA followed by a ‘Bonferroni’ post-hoc test.

5.4.1. Investigation of the signalling pathway following GPR55 activation in miPSC and hiPSC-derived cardiomyocytes

The activation of GPCRs within a cell membrane triggers the cytoskeletal reorganisation of cellular proteins which can be detected optically, in real-time, by changes in cellular density (measured as DMR activity). In the present study, Corning® Epic® technology, a label-free and non-invasive method designed to monitor the DMR activity of biologically relevant cells was employed to explore the signalling pathway of GPR55 in cardiomyocytes following its activation. The time course of cellular DMR in miPSC-derived cardiomyocytes in response to LPI was rapid with immediate onset. Analysis of the time course not only indicated GPCR activation but ascertained that the DMR activity in response to LPI peaked at 10 minutes. The information regarding peak activity was consequently used as an indicator of the time point at which LPI should be administered to the isolated hearts of WT mice prior to the induction of GI in the studies investigating the impact of GPR55 activation on myocardial I/R injury (results discussed in section 5.4.2).

Confirmation that LPI was acting via GPR55 in miPSC-derived cardiomyocytes to mediate the increase in DMR activity was obtained by blocking the cellular response to LPI with the GPR55 antagonist, CBD. Previously, Yu and colleagues (2013) reported that the intra- or extracellular application of LPI to cardiomyocytes increased $[Ca^{2+}]_i$ by initiating separate signalling pathways via GPR55 which were dependent on the cellular location of this receptor. One of the signalling pathways mediated an increase in $[Ca^{2+}]_i$ via LTCCs and IP_3 -dependent Ca^{2+} release in response to LPI-induced GPR55 activation at the sarcolemma. Moreover, Ali and colleagues (2015) reported in cardiomyocytes that CBD depressed contractility by suppressing LTCCs and inhibiting excitation-contraction coupling (E-C coupling). Taking these findings together, it may be possible that under physiological conditions, the LPI/GPR55 system has a role in Ca^{2+} homeostasis within the cardiomyocyte and consequently, in the E-C coupling of such cells.

With regard to the signalling of the LPI/GPR55 system in miPSC-derived cardiomyocytes, the ROCK inhibitor, Y-27632 dihydrochloride confirmed the downstream involvement of this kinase by inhibiting the DMR response to LPI. While the involvement of ROCK, downstream of LPI-induced GPR55 activation has been documented in GPR55-HEK293 cells (Henstridge *et al.*, 2009) and the rat mesenteric artery via an endothelial site of action (Al Suleimani and Hiley, 2015), this is the first time its involvement has been reported in the signalling of this system in cardiomyocytes. Downstream from ROCK, GPR55 has been shown to signal through numerous second messengers including PLC

and IP₃ (reviewed by Ross, 2009). As both GPR55 (Yu *et al.*, 2013) and IP₃R signalling (Signore *et al.*, 2013) have been shown to be important in the E-C coupling of ventricular cardiomyocytes, the role of IP₃R in LPI-mediated changes in DMR activity was then investigated. Co-application of the IP₃R antagonist, xestospongin C with LPI to miPSC-derived cardiomyocytes failed to attenuate the GPR55 mediated increase in DMR activity suggesting that LPI-induced GPR55 activation of these cells does not involve IP₃Rs. This is in contrast to the findings of Yu and colleagues (2013) who demonstrated IP₃-dependent Ca²⁺ release upon GPR55 activation with LPI in rat neonatal ventricular cardiomyocytes. However, it is noteworthy that confirmation of the involvement of IP₃Rs in the LPI-mediated increase in [Ca²⁺]_i of this study was done so via the dual blockade of IP₃Rs with xestospongin C and heparin, the latter a competitive antagonist of all IP₃R subtypes (Saleem *et al.*, 2014). Moreover, it has been reported in DT40 cells stably expressing single subtypes of the mammalian IP₃R that xestospongin C is not an effective inhibitor of IP₃-induced Ca²⁺ release (Saleem *et al.*, 2014). Therefore, the sole application of xestospongin C with LPI to the miPSC-derived cardiomyocytes in the present study may represent a limitation of this research and consequently, IP₃R participation, downstream of LPI-induced GPR55/ROCK activation in this cell type cannot be definitively ruled out. In another study, Al Suleimani and Hiley (2015) reported that activation of GPR55 by LPI in rat endothelial cells mediated a biphasic increase in [Ca²⁺]_i where ROCK was involved in each phase, although more so in the latter. IP₃Rs were also reportedly involved in both phases as inhibiting this receptor with 2-aminoethoxydiphenyl borate (2-APB) caused a reduction in [Ca²⁺]_i. However, 2-APB has targets other than IP₃Rs, for example, store operated Ca²⁺ channels (Bootman *et al.*, 2002) therefore this study does not conclusively determine the extent to which IP₃Rs are involved in the LPI/GPR55 mediated increase in [Ca²⁺]_i. Together, these findings suggest that the involvement of IP₃Rs downstream of LPI-induced GPR55 activation in the cardiovascular system requires further investigation.

Importantly, the finding that the LPI-induced increase in DMR activity of miPSC-derived cardiomyocytes, mediated via a GPR55/ROCK dependent mechanism, was replicable in hiPSC-derived cardiomyocytes, suggests the possibility of a translational role for the LPI/GPR55 system in the human heart.

5.4.2. The impact of GPR55 activation on myocardial I/R injury

To determine whether endogenously produced LPI activated GPR55 and altered cardiac tissue injury, control hearts from WT and GPR55^{-/-} mice were subjected to GI followed by reperfusion. In the

present study, infarct size did not differ between control hearts from WT and GPR55^{-/-} mice, which may suggest that sufficient endogenous LPI was not produced by the heart to alter tissue injury. A recent study conducted in rats demonstrated a six-fold increase in the cardiac LPI (18:0) concentration following asphyxia-induced cardiac arrest (Kim *et al.*, 2015a), however, this study was conducted *in vivo* and did not measure myocardial infarct size. It is therefore unclear whether there is a correlation between the cardiac LPI concentration alone and any myocardial tissue injury in this model. Moreover, a recent clinical study by Kurano and colleagues (2015) which measured the plasma concentration of a range of lysophospholipids in patients undergoing coronary angiography, demonstrated a positive correlation between plasma LPI and patients with acute coronary syndrome (ACS). In this study, the authors recorded plasma concentrations of 3 μ M LPI in ACS patients and suggested that the primary source of LPI was activated platelets at the site of plaque rupture. As the data from the present study demonstrated a tissue damaging effect of exogenous LPI in the micromolar range, it is possible that in the absence of other organs and tissues (perhaps contributing to the plasma LPI concentration) that the isolated WT hearts alone do not have the capacity to generate micromolar concentrations of LPI in response to ischaemia and may explain the comparable infarcts between control and GPR55^{-/-} hearts.

The administration of LPI to WT hearts, prior to GI, mediated an increase in myocardial tissue damage which was subsequently attributed to LPI-induced activation of GPR55 as no significant increase in infarct size was observed in response to this lysophospholipid in the hearts from GPR55^{-/-} mice. Pre-treatment with the GPR55 antagonist, CBD, at the concentration previously used in the studies involving the miPSC-derived cardiomyocytes and Corning[®] Epic[®] technology, failed to attenuate the myocardial tissue injury induced by LPI. Moreover, the administration of CBD alone to WT hearts mediated an increase in infarct size, however, this was not entirely unexpected as Durst and colleagues (2007) reported that the cardioprotective effect of CBD in myocardial I/R injury *in vivo* is not replicated in the isolated heart. The authors suggested that the cardioprotective effect of CBD, *in vivo*, may be due to a systemic immunomodulatory effect such as a reduction in IL-6 levels. However, due to only residual inflammatory cells being present in the isolated heart, the inability of CBD to attenuate injury is not surprising and would suggest that the myocardial tissue injury is due to a detrimental effect on the cardiomyocytes themselves. Additionally, it has been demonstrated that CBD acts on receptors other than GPR55, however, this appears to be dependent on the situation (Walsh *et al.*, 2015) therefore it may be possible that CBD acts as an antagonist of GPR55 under physiological conditions and an antagonist of another or other receptor(s) such as CB₂ in the pathological setting of myocardial I/R tissue injury. The activation of CB₂ receptors during such injury

is reportedly protective both *in vivo* (Wang *et al.*, 2012b) and *in vitro* (Lépicier *et al.*, 2003 and Lépicier *et al.*, 2007). As CBD reportedly exhibits high potency as an antagonist of the CB₂ receptor agonists in membranes from Chinese hamster ovary (CHO) cells transfected with human CB₂ receptors (Thomas *et al.*, 2007), it may be that such antagonism extends to the cardiomyocyte, however, this remains to be investigated. If CB₂ receptors are activated in the isolated heart during I/R injury, this notion supports why the administration of CBD alone to the isolated, WT hearts of the present study mediated an increase in myocardial tissue damage and poses a reason as to why CBD did not reduce infarct size when administered with LPI.

The time at which LPI was administered to the hearts of WT mice proved critical in the development of the myocardial tissue damage as injury was only exacerbated when LPI was administered pre-GI. Such a finding is indicative that GPR55 activation during the ischaemic period is pivotal in mediating such damage. As [Ca²⁺]_i overload is one of the main mediators of ischaemic damage and LPI-induced activation of GPR55 has previously been reported to mediate an increase in [Ca²⁺]_i in ventricular cardiomyocytes, it is a possibility that the LPI/GPR55 system mediated the increase in myocardial tissue damage pre-GI by contributing to [Ca²⁺]_i overload. Moreover, a key instigator of damage during reperfusion is the generation of ROS from both the myocardium and inflammatory cells (Braunersreuther and Jaquet, 2012). As GPR55 activation has previously been reported to exert antioxidant effects in human neutrophils by inhibiting CB₂ receptor-mediated respiratory burst (Balenga *et al.*, 2011), the lack of a post-GI effect on infarct size in response to LPI-induced GPR55 activation, may be due to the LPI/GPR55 system mediating antioxidant activity within the myocardium as only residual inflammatory cells are present in the isolated heart. However, as neither [Ca²⁺]_i nor oxidative stress have been investigated in the present study, the possible involvement of these mechanisms requires confirmation.

With regard to the myocardial tissue injury observed in the current study, it seems improbable that such damage would have been mediated as a consequence of LPI-induced coronary artery constriction as perfusion pressure from a similar study conducted in our lab was unchanged by the exogenous administration of LPI (data not shown). Furthermore, Marichal-Cancino and colleagues (2013) demonstrated that LPI inhibited vasopressor responses induced by both electrical nerve stimulation and noradrenaline in pithed rats via a GPR55-dependent mechanism, indicating that LPI itself is vasodepressive. This therefore suggests that the administration of LPI would lead to an increased rather than decreased coronary flow. Conversely, a study observed that the administration of LPI to cultured rat coronary artery smooth muscle cells (SMCs) mediated an increase in Ca²⁺ influx

(Smani *et al.*, 2007) which suggests that LPI may induce vasoconstriction of the coronary artery in an *in vivo* model. This however, is yet to be demonstrated and it remains to be established whether the LPI-induced increase in Ca^{2+} influx of the SMCs involved in this study was via a GPR55-dependent or independent mechanism. Furthermore, endothelial cells also play an important role in vascular tone therefore the effect of the LPI/GPR55 system on both SMCs and endothelial cells must be considered. With regard to the latter cell type, LPI exerted both GPR55-dependent and independent effects on EA.hy296 endothelial cells (Bondarenko *et al.*, 2010). The GPR55-dependent effects of LPI in this study mediated temporary membrane hyperpolarisation suggesting that the LPI/GPR55 system may induce arterial vasodilation. On this basis, it again seems unlikely that vasoconstriction of the coronary artery would be linked to the LPI-induced GPR55 activation which exacerbated myocardial tissue injury in the present study. In support of this, Al Suleimani and Hiley (2015) reported that LPI relaxed the rat mesenteric artery in a GPR55 and endothelium-dependent manner.

Through the use of the ROCK inhibitor, Y-27632 dihydrochloride, it was deduced that following LPI-induced GPR55 activation, a ROCK-dependent mechanism was responsible for the exacerbation of the myocardial I/R injury mediated in the present study. It is assumed that while Y-27632 dihydrochloride is capable of inhibiting both isoforms of ROCK, its protective effect on the myocardium most likely occurred as a result of inhibition of ROCK II, as this is the predominant isoform in the heart (Nakagawa *et al.*, 1996). The involvement of a ROCK-dependent mechanism in this setting seems plausible as its association with myocardial I/R injury has been well documented (Bao *et al.*, 2004, Hamid *et al.*, 2007 and Zhang *et al.*, 2014). In particular, the pharmacological inhibition of ROCK has proven pivotal in determining the role of this kinase in the setting of myocardial I/R injury and has established that amongst many other cardioprotective effects, ROCK inhibition can reduce infarct size by activating the PI3K/protein kinase B (Akt)/endothelial nitric oxide synthase (eNOS) pathway (Wolfrum *et al.*, 2004). Moreover, such inhibition can preserve post-infarction cardiac systolic function through various mechanisms including increased collateral blood flow to the myocardium resulting from eNOS preservation (Yada *et al.*, 2005). In contrast to the frequently observed cardioprotective effects of ROCK inhibition using hydroxyfasudil and fasudil, the administration of Y-27632 dihydrochloride alone to WT hearts did not affect infarct size in the present study (data not shown). However, this finding is not entirely unexpected as the protective effects associated with ROCK inhibition are more commonly associated with events that occur after several hours of myocardial reperfusion (Wolfrum *et al.*, 2004 and Zhang *et al.*, 2014), whereas the reperfusion period in the present study was relatively short (30 minutes).

Overall, the present study established that LPI-induced GPR55 activation, pre-GI, exacerbates myocardial tissue injury via a ROCK-dependent mechanism. As it has previously been reported that activation of the LPI/GPR55 system increases the $[Ca^{2+}]_i$ of ventricular cardiomyocytes (Yu *et al.*, 2013) and that the inhibition of ROCK prevents LPI-mediated Ca^{2+} signalling in GPR55-HEK293 cells (Henstridge *et al.*, 2009), it is possible that changes in $[Ca^{2+}]_i$ may be responsible for the exacerbated tissue injury in LPI treated, WT hearts. $[Ca^{2+}]_i$ overload of cardiomyocytes is widely recognised as one of the key events in myocardial I/R injury (Mozaffari *et al.*, 2013) with such overload following a series of biochemical and metabolic changes within the myocardium in response to ischaemia (discussed in Chapter 1, section 1.3.2.). Upon reperfusion of ischaemic myocardium, cardiomyocytes become re-energised, however, the re-energisation of cardiomyocytes suffering from $[Ca^{2+}]_i$ overload often results in cardiomyocyte hypercontracture due to the uncontrolled contraction of myofibrils within these cells. Consequently, deformation of the cytoskeleton occurs and cell shape is altered, leading to irreversible cell shortening and cardiomyocyte death (Ladilov *et al.*, 1997). Interestingly, Yu and colleagues (2013) demonstrated that the LPI/GPR55 system increased $[Ca^{2+}]_i$ partially via LTCCs in rat neonatal ventricular cardiomyocytes, therefore, it may be that Ca^{2+} entry via these channels represents a possible mechanism via which the myocardial I/R injury observed in the present study was exacerbated. Mocanu and colleagues (1999) investigated the effects of mibefradil, an L-Type and T-Type Ca^{2+} channel blocker on myocardial I/R injury and reported that it attenuated infarct size, however, the LTCC blocker, amlodipine, failed to mediate such cardioprotection suggesting that the activation of T-Type Ca^{2+} channels in myocardial I/R injury is more likely to mediate damage. On this basis, it may be that the LPI/GPR55 system contributes to $[Ca^{2+}]_i$ overload via the activation of T-Type Ca^{2+} channels. This, however, remains to be investigated.

Finally, myocardial I/R injury is reduced when antagonists of the NHX are administered either prior to ischaemia or pre-reperfusion (Rohmann *et al.*, 1995 and Linz *et al.*, 1998). It has been suggested that LPI does not directly affect the NHX (Goel *et al.*, 2003), therefore it seems unlikely that the LPI-induced exacerbation of myocardial tissue injury in the present study is due to increased activity of this antiporter. However, lysophosphatidycholine (LPC), a closely related lysophospholipid has been found to increase cardiac injury by activating the NHX (Hoque *et al.*, 1997) via an indirect mechanism involving a second messenger pathway (Goel *et al.*, 2003). As Wallert and colleagues (2015) have shown that the activation of the NHX in fibroblasts is dependent on RhoA/ROCK activation, it is possible that LPI may exacerbate myocardial I/R injury via an indirect action on the NHX, subsequent to its activation of ROCK, however, this requires further investigation. Moreover, the effects of LPI on the expression and activation of the NCX in cardiomyocytes has not been investigated, therefore it is

possible that LPI, via either a direct or indirect action on this antiporter, may increase its reverse mode activity, consequently contributing to $[Ca^{2+}]_i$ overload and the exacerbation of myocardial tissue injury. However, doubt has been cast upon this theory as Bondarenko and colleagues (2017) recently reported that LPI inhibits endothelial cell hyperpolarization to histamine and ACh by suppressing Ca^{2+} entry driven by the reverse mode of the NCX and that such inhibition occurs independent of GPCRs and superoxide anions. While this has not been demonstrated in cardiomyocytes, should it be the case, then the LPI/GPR55 system causing the NCX to work in reverse mode to contribute to $[Ca^{2+}]_i$ overload and the exacerbation of myocardial tissue injury seems improbable, however, further investigation is required to confirm or deny this.

5.4.3. Conclusion

In summary, the current study set out to investigate the role of GPR55 in myocardial I/R injury in the isolated mouse heart. LPI-induced GPR55 activation, pre-GI, mediated an increase in myocardial infarct size through a ROCK-dependent mechanism. Most importantly, the finding that GPR55 signals through this mechanism in hiPSC as well as miPSC-derived cardiomyocytes illustrates that both species adopt the same signalling pathway and suggests the possibility of a translational role for the LPI/GPR55 system in the human heart.

Chapter 6:

General Discussion

6.1. Key findings

Very little information on the role of GPR55 in cardiovascular physiology and pathophysiology exists and the two studies which have investigated the function of GPR55 in atherosclerosis have reported conflicting findings. The present study therefore sought to investigate 1) the role of GPR55 in the development of atherosclerosis, 2) if GPR55 has a role in the cardiac function of mice suffering from atherosclerosis, 3) the signalling pathway by which LPI activates cardiomyocytes, 4) the impact of GPR55 on the outcome of myocardial I/R injury, and 5) the signalling mechanisms by which GPR55 elicits any observed effects on the myocardium in response to such injury.

6.1.1. GPR55 regulates fat deposition in atherosclerosis

The present study has determined that HFC fed ApoE^{-/-}/GPR55^{-/-} mice were characterised by an obese phenotype that occurred as a consequence of the genetic deletion of GPR55. Furthermore, tissue weight analysis indicated that the increased adiposity in these mice was predominantly due to an augmented deposition of abdominal fat. Despite this being the first report linking GPR55 to the regulation of fat deposition in atherosclerosis, Meadows and colleagues (2016) have reported that GPR55 regulates the fat mass of healthy mice, a finding which was also observed in the present study. While the current study did not investigate the root cause of the increased fat mass, evidence from literature and an unpublished study conducted in the Wainwright laboratory provide a basis for speculation. These studies reported that NC or HFC fed GPR55^{-/-} mice had a food intake comparable to that of C57BL/6 mice fed NC (Meadows *et al.*, 2016) or HFC (Hair, 2016; unpublished data), respectively. Additionally, evidence of GPR55^{-/-} mice exhibiting decreased spontaneous and voluntary physical activity has also been reported (Meadows *et al.*, 2016). Taken together, it seems likely that the HFC fed ApoE^{-/-}/GPR55^{-/-} mice of the present study did not consume a greater quantity of food than HFC fed ApoE^{-/-} mice but were less physically active which consequently resulted in their increased adiposity. However, in order to confirm or deny this, further experimental investigation is required.

6.1.2. The hyperlipidaemic plasma profile associated with atherosclerosis occurs via a GPR55-independent mechanism

This study has been the first to investigate if a relationship exists between GPR55 and the hyperlipidaemic plasma profile of the ApoE^{-/-} mouse. An augmented TC and LDL concentration in the

plasma of NC and HFC fed ApoE^{-/-} mice was observed in the present study, which is in agreement with several other studies where ApoE^{-/-} mice have been fed an NC (Stapleton *et al.*, 2007) or HFC diet (Fukao *et al.*, 2010, Han *et al.*, 2015 and Kim *et al.*, 2015b). With the aid of the novel ApoE^{-/-}/GPR55^{-/-} mouse, this study has established that regardless of diet, the hyperlipidaemic plasma profile of the ApoE^{-/-} mouse is as a consequence of the deletion of the gene for ApoE and is not associated with GPR55. This study is therefore the first to report that GPR55 does not regulate or contribute to the hyperlipidaemic plasma profile evident in the setting of atherosclerosis.

6.1.3. GPR55 promotes the development of fatty streaks within the vasculature

It was also established that GPR55 promotes the development of fatty streaks within the thoracic aorta of the HFC fed ApoE^{-/-} mouse. On the basis of the previously discussed plasma lipid data, it was determined that the increased deposition of fatty streaks occurred via a lipid-independent mechanism. Unfortunately, it was outwith the scope of the present study to investigate the mechanism(s) by which GPR55 mediated such fatty streak deposition, however, other literature which has suggested a pro-atherogenic role for GPR55 can provide a basis for conjecture. It is well established that during the early stages of plaque development, macrophages of the vessel wall phagocytose ox-LDL via endocytosis and consequently, become lipid laden foam cells. The study conducted by Lanuti and colleagues (2015) demonstrated that GPR55 activation with O-1602, aggravated oxidised LDL-induced lipid accumulation and inflammatory responses, while reducing cholesterol efflux from human foam cells. The endogenous activation of GPR55 in the ApoE^{-/-} mouse may therefore mediate the same processes, in turn promoting the development of fatty streaks within the thoracic aortae of these mice. However, further investigation is required to prove or disprove this.

6.1.4. GPR55 maintains systolic function but impairs contractile reserve in atherosclerosis

Investigating the role of GPR55 in the cardiac function of the ApoE^{-/-} mouse model of atherosclerosis has revealed that when atherosclerosis has been exacerbated by high fat feeding, GPR55 exhibits a protective role in terms of maintaining baseline systolic function. Furthermore, the administration of the α_1/β_1 -adrenoceptor agonist, dobutamine, revealed that GPR55 contributes to the impaired contractile reserve of these mice. Together, these findings indicate that there may be a role for GPR55 in the control of adrenergic signalling in the atherosclerotic heart and possibly a role for this

receptor in the development of heart failure. Further experiments are now required to establish the interaction between GPR55 and cardiac α_1/β_1 -adrenoceptors in atherosclerosis.

6.1.5. LPI signals via a GPR55/ROCK-dependent mechanism in cardiomyocytes

Perhaps most importantly, this study has determined that upon activation with LPI, GPR55 signals through ROCK in hiPSC, as well as miPSC-derived cardiomyocytes, illustrating that both mice and humans adopt the same signalling pathway. Consequently, this suggests the possibility of a translational role for the LPI/GPR55 system in the human heart. Furthermore, while Yu and colleagues (2013) demonstrated that the LPI/GPR55 system signalled via L-type Ca^{2+} channels and IP_3Rs in cardiomyocytes, this is the first study to report the signalling of this system through ROCK in this cell type.

6.1.6. LPI exacerbates myocardial I/R injury via a GPR55/ROCK-dependent mechanism

In the isolated heart, LPI exacerbated myocardial tissue injury via a GPR55/ROCK dependent mechanism. Cardiomyocyte ROCK activation in response to LPI represents a plausible mechanism as there is strong evidence that ROCK activation is an important event in the damage mediated by myocardial I/R injury (Bao *et al.*, 2004 and Hamid *et al.*, 2007). As $[\text{Ca}^{2+}]_i$ overload is one of the key mechanisms via which this type of injury occurs (Hausenloy and Yellon, 2013) and LPI-induced GPR55 activation reportedly increases $[\text{Ca}^{2+}]_i$ in GPR55-HEK293 cells (Oka *et al.*, 2007, Henstridge *et al.*, 2009 and Oka *et al.*, 2009) and rat neonatal ventricular cardiomyocytes (Yu *et al.*, 2013), it seemed logical to investigate first in cardiomyocytes, if the antagonism of IP_3R -induced $[\text{Ca}^{2+}]_i$ release, downstream of ROCK activation, would prevent LPI signalling. Despite the present study having demonstrated that xestospongin C (an IP_3R antagonist) blocked LPI signalling in miPSC- and hiPSC-derived cardiomyocytes, it was subsequently reported by Saleem and colleagues (2014) that xestospongin C is an ineffective inhibitor of IP_3 -induced Ca^{2+} release. Consequently, the present study cannot confirm nor rule out the involvement of IP_3Rs in LPI/GPR55 signalling in these cells. Further studies utilising a more selective IP_3R antagonist are now required to investigate the involvement of IP_3Rs in the signalling of the LPI/GPR55 system in cardiomyocytes.

The present study also observed that the GPR55 antagonist, CBD, failed to prevent the exacerbation of myocardial tissue injury mediated by the LPI/GPR55 system in the isolated mouse heart. However, this finding is in agreement with Durst and colleagues (2007) who reported that CBD only reduced

myocardial I/R injury in their *in vivo* rat model and not in the isolated rat heart. On this basis, CBD cannot be ruled out as a potential inhibitor of the myocardial I/R injury exacerbated by the LPI/GPR55 system. Further studies are consequently required to establish if 1) LPI exacerbates myocardial I/R injury *in vivo* and, 2) if CBD can mitigate such injury *in vivo*.

6.2. Clinical relevance

Since the findings of the present study indicate that GPR55 is a double-edged sword, it may be that targeting GPR55 to improve one condition may exacerbate another. This should be an important consideration in terms of the clinical relevance of this study's findings, discussed below.

6.2.1. Obesity

GPR55 is involved in the regulation of fat mass (predominantly abdominal fat), therefore this receptor may represent a new drug target in obesity. Furthermore, as an increased abdominal circumference is deemed a risk factor for the development of type 2 diabetes (Wang *et al.*, 2005), targeting GPR55 with the aim of reducing obesity, may also reduce the prevalence of type 2 diabetes.

6.2.2. Atherosclerosis development

The observation that GPR55 promotes the development of fatty streaks within the thoracic aorta, via a lipid independent mechanism suggests that lipid lowering drugs alone i.e. statins, would not be sufficient in terms of preventing the deposition of such streaks. However, clinically, an antagonist of GPR55 may reduce the incidence of fatty streaks and/or halt their development.

6.2.3. Myocardial I/R injury

Myocardial tissue injury was exacerbated upon GPR55 activation by LPI, pre-GI. On this basis, the administration of a GPR55 antagonist pre-myocardial infarction may reduce myocardial I/R injury. However, this treatment would not be practical from a clinical perspective as it is not possible to predict the exact time point at which a myocardial infarction will occur. Nevertheless, GPR55 antagonism may be useful in instances where it is necessary to cease circulatory function, for example, heart transplantation during which I/R injury routinely occurs.

6.3. Future studies

6.3.1. Examination of the mechanism(s) via which the LPI/GPR55 system contributed to fatty streak development within the vasculature

The present study demonstrated that GPR55 is involved in the development of fatty streaks within the thoracic aortae of HFC fed ApoE^{-/-} mice, however, the mechanism(s) via which GPR55 contributed to such development were not investigated. Recently, Stančić and colleagues (2015) demonstrated that the GPR55 antagonist, CID16020046, protected against intestinal inflammation by reducing the migration of macrophages. As atherosclerosis is also an inflammatory condition, GPR55 may be involved in the monocyte/macrophage migration associated with the early development of fatty streaks within the vasculature. It would therefore be of interest to examine monocyte/macrophage migration in HFC fed ApoE^{-/-} and ApoE^{-/-}/GPR55^{-/-} mice to determine if this is the case.

6.3.2. Studies to confirm or deny the involvement of [Ca²⁺]_i overload in the myocardial I/R injury exacerbated by the LPI/GPR55 system

While the current study demonstrated that the pre-GI activation of GPR55 by LPI exacerbates myocardial tissue injury, the underlying mechanisms via which this occurred were not investigated. Considering that [Ca²⁺]_i overload of cardiomyocytes is one of the key events in mediating myocardial I/R injury (Mozaffari *et al.*, 2013) and that the LPI/GPR55 system increases [Ca²⁺]_i in a variety of cell types such as EA.hy926 endothelial cells (Waldeck-Weiermair *et al.*, 2008), GPR55-HEK293 cells (Henstridge *et al.*, 2009, Oka *et al.*, 2007 and Oka *et al.*, 2009) and rat neonatal ventricular cardiomyocytes (Yu *et al.*, 2013), it would be interesting to investigate if a link exists between the two. I/R injury could be simulated in isolated cardiomyocytes via hypoxia/reoxygenation injury. Using the ratiometric dye, Fura-2, the [Ca²⁺]_i of the cardiomyocytes could be monitored in response to the activation of GPR55 by LPI during the hypoxic period.

6.4. Limitations

The use of a conditional knockout mouse, where GPR55 deletion was limited to the heart would have proven extremely useful in this study, however, GPR55 floxed mice are not yet available. Consequently, the present study utilised the global GPR55 knockout mouse model as it currently

represents the most accurate means of gaining insight into the role of GPR55 in cardiovascular physiology and pathophysiology.

6.5. Conclusions

This study has determined that in terms of atherosclerosis, GPR55 is double-edged sword. In the presence of high fat feeding, GPR55 regulates risk factors associated with atherosclerosis (i.e. body weight and fat mass) while promoting the development of fatty streaks within the vasculature, via a lipid independent mechanism. In terms of cardiac function, *in vivo* experiments demonstrated that GPR55 exerts a protective role in atherosclerosis by maintaining systolic function, yet negatively affects contractile reserve. Moreover, isolated heart experiments revealed that LPI-induced GPR55 activation augments myocardial infarct size through a ROCK-dependent mechanism. Excitingly, this study also demonstrated that the LPI/GPR55 system signals through ROCK in hiPSC, as well as miPSC-derived cardiomyocytes, therefore suggesting the possibility of a translational role for the LPI/GPR55 system in the human heart. On the basis of such findings, GPR55 may represent a promising new target in the prevention or treatment of atherosclerosis and myocardial I/R injury.

Chapter 7:

References

Abbas, A.K., Lichtman, A.H. and Pillai, Shiv. (2007) *Cellular and molecular immunology*. Sixth Edition. Philadelphia: Saunders Elsevier

Alexander, S.P., Davenport, A.P., Kelly, E., Marrion, N., Peters, J.A., Benson, H.E., Faccenda, E., Pawson, A.J., Sharman, J.L., Southan, C., Davies, J.A. and CGTP Collaborators. (2015) The Concise Guide to PHARMACOLOGY 2015/16: G protein-coupled receptors. *Br J Pharmacol.* **172**, 5744-869

Ali, R.M., Al Kury, L.T., Yang, K.H., Qureshi, A., Rajesh, M., Galadari, S., Shuba, Y.M., Howarth, F.C. and Oz, M. (2015) Effects of cannabidiol on contractions and calcium signaling in rat ventricular myocytes. *Cell Calcium.* **57**, 290-9

Allen, S.P., Darley-Usmar, V.M., McCormack, J.G. and Stone, D. (1993) Changes in mitochondrial matrix free calcium in perfused rat hearts subjected to hypoxia-reoxygenation. *J Mol Cell Cardiol.* **25**, 949-58

Al Suleimani, Y.M. and Hiley, C.R. (2015) The GPR55 agonist lysophosphatidylinositol relaxes rat mesenteric resistance artery and induces Ca(2+) release in rat mesenteric artery endothelial cells. *Br J Pharmacol.* **172**, 3043-57

Al Suleimani, Y.M. and Hiley, C.R. (2016) Characterization of calcium signals provoked by lysophosphatidylinositol in human microvascular endothelial cells. *Physiol Res.* **65**, 53-62

Andradas, C., Blasco-Benito, S., Castillo-Lluva, S., Dillenburg-Pilla, P., Diez-Alarcia, R., Juanes-García, A., García-Taboada, E., Hernando-Llorente, R., Soriano, J., Hamann, S., Wenners, A., Alkatout, I., Klapper, W., Rocken, C., Bauer, M., Arnold, N., Quintanilla, M., Megías, D., Vicente-Manzanares, M., Urigüen, L., Gutkind, J.S., Guzmán, M., Pérez-Gómez, E. and Sánchez, C. (2016) Activation of the orphan receptor GPR55 by lysophosphatidylinositol promotes metastasis in triple-negative breast cancer. *Oncotarget.* **7**, 47565-47575

Anselmi, A., Abbate, A., Girola, F., Nasso, G., Biondi-Zoccai, G.G., Possati, G. and Gaudino, M. (2004) Myocardial ischemia, stunning, inflammation, and apoptosis during cardiac surgery: a review of evidence. *Eur J Cardiothorac Surg.* **25**, 304-11

Armstrong, M.L., Heistad, D.D., Marcus, M.L., Megan, M.B. and Piegors, D.J. (1985) Structural and hemodynamic response of peripheral arteries of macaque monkeys to atherogenic diet. *Arteriosclerosis*. **5**, 336-46

Balenga, N.A., Aflaki, E., Kargl, J., Platzer, W., Schröder, R., Blättermann, S., Kostenis, E., Brown, A.J., Heinemann, A. and Waldhoer, M. (2011) GPR55 regulates cannabinoid 2 receptor-mediated responses in human neutrophils. *Cell Res*. **21**, 1452-69

Bao, W., Hu, E., Tao, L., Boyce, R., Mirabile, R., Thudium, D.T., Ma, X.L., Willette, R.N. and Yue, T.L. (2004) Inhibition of Rho-kinase protects the heart against ischemia/reperfusion injury. *Cardiovasc Res*. **61**, 548-58

Basu, R., Oudit, G.Y., Wang, X., Zhang, L., Ussher, J.R., Lopaschuk, G.D. and Kassiri, Z. (2009) Type 1 diabetic cardiomyopathy in the Akita (Ins2WT/C96Y) mouse model is characterized by lipotoxicity and diastolic dysfunction with preserved systolic function. *Am J Physiol Heart Circ Physiol*. **297**, H2096-108

Beattie, J.H., Duthie, S.J., Kwun, I.S., Ha, T.Y. and Gordon, M.J. (2009) Rapid quantification of aortic lesions in apoE(-/-) mice. *J Vasc Res*. **46**, 347-52

Beaussier, H., Masson, I., Collin, C., Bozec, E., Laloux, B., Calvet, D., Zidi, M., Boutouyrie, P. and Laurent, S. (2008) Carotid plaque, arterial stiffness gradient, and remodeling in hypertension. *Hypertension*. **52**, 729-36

Bentzon, J.F., Otsuka, F., Virmani, R. and Falk, E. (2014) Mechanisms of plaque formation and rupture. *Circ Res*. **114**, 1852-66

Bers, D.M. (2002) Cardiac excitation-contraction coupling. *Nature*. **415**, 198-205

BHF. High Cholesterol. [online]. Available from: <https://www.bhf.org.uk/heart-health/risk-factors/high-cholesterol> [accessed 17th February 2017]

Bjursell, M., Ryberg, E., Wu, T., Greasley, P.J., Bohlooly-Y, M. and Hjorth, S. (2016) Deletion of Gpr55 Results in Subtle Effects on Energy Metabolism, Motor Activity and Thermal Pain Sensation. *PLoS One*. **11**, e0167965

Bond, J.M., Herman, B. and Lemasters, J.J. (1991) Protection by acidotic pH against anoxia/reoxygenation injury to rat neonatal cardiac myocytes. *Biochem Biophys Res Commun*. **179**, 798-803

Bondarenko, A., Waldeck-Weiermair, M., Naghdi, S., Poteser, M., Malli, R. and Graier, W.F. (2010) GPR55-dependent and -independent ion signalling in response to lysophosphatidylinositol in endothelial cells. *Br J Pharmacol*. **161**, 308-20

Bondarenko, A.I., Montecucco, F., Panasiuk, O., Sagach, V., Sidoryak, N., Brandt, K.J. and Mach, F. (2017) GPR55 agonist lysophosphatidylinositol and lysophosphatidylcholine inhibit endothelial cell hyperpolarization via GPR-independent suppression of Na⁺-Ca²⁺ exchanger and endoplasmic reticulum Ca²⁺ refilling. *Vascul Pharmacol*. **89**, 39-48

Bonetti, P.O., Lerman, L.O. and Lerman, A. (2003) Endothelial dysfunction: a marker of atherosclerotic risk. *Arterioscler Thromb Vasc Biol*. **23**, 168-75

Bootman, M.D., Collins, T.J., Mackenzie, L., Roderick, H.L., Berridge, M.J. and Peppiatt, C.M. (2002) 2-aminoethoxydiphenyl borate (2-APB) is a reliable blocker of store-operated Ca²⁺ entry but an inconsistent inhibitor of InsP₃-induced Ca²⁺ release. *FASEB J*. **16**, 1145-50

Bopassa, J.C., Michel, P., Gateau-Roesch, O., Ovize, M. and Ferrera, R. (2005) Low-pressure reperfusion alters mitochondrial permeability transition. *Am J Physiol Heart Circ Physiol*. **288**, H2750-5

Borradaile, N.M., Buhman, K.K., Listenberger, L.L., Magee, C.J., Morimoto, E.T., Ory, D.S. and Schaffer, J.E. (2006) A critical role for eukaryotic elongation factor 1A-1 in lipotoxic cell death. *Mol Biol Cell*. **17**, 770-8

Braunersreuther, V. and Jaquet, V. (2012) Reactive oxygen species in myocardial reperfusion injury: from physiopathology to therapeutic approaches. *Curr Pharm Biotechnol*. **13**, 97-114

Bristow, M.R., Ginsburg, R., Umans, V., Fowler, M., Minobe, W., Rasmussen, R., Zera, P., Menlove, R., Shah, P. and Jamieson, S. (1986) Beta 1- and beta 2-adrenergic-receptor subpopulations in nonfailing and failing human ventricular myocardium: coupling of both receptor subtypes to muscle contraction and selective beta 1-receptor down-regulation in heart failure. *Circ Res.* **59**, 297-309

Bucholz, E.M., Rathore, S.S., Reid, K.J., Jones, P.G., Chan, P.S., Rich, M.W., Spertus, J.A. and Krumholz, H.M. (2012) Body mass index and mortality in acute myocardial infarction patients. *Am J Med.* **125**, 796-803

Bucholz, E.M., Beckman, A.L., Krumholz, H.A., Krumholz, H.M. (2016) Excess weight and life expectancy after acute myocardial infarction: The obesity paradox reexamined. *Am Heart J.* **172**, 173-81

Busche, M.N. and Stahl, G.L. (2010) Role of the complement components C5 and C3a in a mouse model of myocardial ischemia and reperfusion injury. *Ger Med Sci.* **8**, pii: Doc20

Calligaris, S.D., Lecanda, M., Solis, F., Ezquer, M., Gutiérrez, J., Brandan, E., Leiva, A., Sobrevia, L. and Conget, P. (2013) Mice long-term high-fat diet feeding recapitulates human cardiovascular alterations: an animal model to study the early phases of diabetic cardiomyopathy. *PLoS One.* **8**, e60931

Caligiuri, G., Levy, B., Pernow, J., Thorén, P. and Hansson, G.K. (1999) Myocardial infarction mediated by endothelin receptor signaling in hypercholesterolemic mice. *Proc Natl Acad Sci U S A.* **96**, 6920-4

Carey, L.M., Gutierrez, T., Deng, L., Lee, W.H., Mackie, K. and Hohmann, A.G. (2017) Inflammatory and Neuropathic Nociception is Preserved in GPR55 Knockout Mice. *Sci Rep.* **7**, 944

Carroll, J.F., Kyser, C.K. and Martin, M.M. (2002) beta-Adrenoceptor density and adenylyl cyclase activity in obese rabbit hearts. *Int J Obes Relat Metab Disord.* **26**, 627-32

Castelli, W.P., Anderson, K., Wilson, P.W. and Levy, D. (1992) Lipids and risk of coronary heart disease. The Framingham Study. *Ann Epidemiol.* **2**, 23-8

- Chancey, A.L., Brower, G.L., Peterson, J.T. and Janicki, J.S. (2002) Effects of matrix metalloproteinase inhibition on ventricular remodeling due to volume overload. *Circulation*. **105**, 1983-8
- Chiu, H.C., Kovacs, A., Ford, D.A., Hsu, F.F., Garcia, R., Herrero, P., Saffitz, J.E. and Schaffer, J.E. (2001) A novel mouse model of lipotoxic cardiomyopathy. *J Clin Invest*. **107**, 813-22
- Chiu, J.J. and Chien, S. (2011) Effects of disturbed flow on vascular endothelium: pathophysiological basis and clinical perspectives. *Physiol Rev*. **91**, 327-87
- Chiurchiù, V., Lanuti, M., De Bardi, M., Battistini, L. and Maccarrone, M. (2015) The differential characterization of GPR55 receptor in human peripheral blood reveals a distinctive expression in monocytes and NK cells and a proinflammatory role in these innate cells. *Int Immunol*. **27**, 153-60
- Chocron, S., Alwan, K., Toubin, G., Kantelip, B., Clement, F., Kantelip, J.P. and Etievent, J.P. (1996) Effects of myocardial ischemia on the release of cardiac troponin I in isolated rat hearts. *J Thorac Cardiovasc Surg*. **112**, 508-13
- Cohn, J.N., Tognoni, G. and Valsartan Heart Failure Trial Investigators. (2001) A randomized trial of the angiotensin-receptor blocker valsartan in chronic heart failure. *N Engl J Med*. **345**, 1667-75
- Cola, M.S., Gava, A.L., Meyrelles, S.S. and Vasquez, E.C. (2010) Endothelial dysfunction of resistance vessels in female apolipoprotein E-deficient mice. *Lipids Health Dis*. **9**, 51
- Coleman, R., Hayek, T., Keidar, S. and Aviram, M. (2006) A mouse model for human atherosclerosis: long-term histopathological study of lesion development in the aortic arch of apolipoprotein E-deficient (E0) mice. *Acta Histochem*. **108**, 415-24
- Console-Bram, L., Brailoiu, E., Brailoiu, G.C., Sharir, H. and Abood, M.E. (2014) Activation of GPR18 by cannabinoid compounds: a tale of biased agonism. *Br J Pharmacol*. **171**, 3908-17
- Crauwels, H.M., Van Hove, C.E., Holvoet, P., Herman, A.G. and Bult, H. (2003) Plaque-associated endothelial dysfunction in apolipoprotein E-deficient mice on a regular diet. Effect of human apolipoprotein AI. *Cardiovasc Res*. **59**, 189-99

Csont, T., Bereczki, E., Bencsik, P., Fodor, G., Görbe, A., Zvara, A., Csonka, C., Puskás, L.G., Sántha, M. and Ferdinandy, P. (2007) Hypercholesterolemia increases myocardial oxidative and nitrosative stress thereby leading to cardiac dysfunction in apoB-100 transgenic mice. *Cardiovasc Res.* **76**, 100-9

Dalen, H., Thorstensen, A., Romundstad, P.R., Aase, S.A., Stoylen, A. and Vatten, L.J. (2011) Cardiovascular risk factors and systolic and diastolic cardiac function: a tissue Doppler and speckle tracking echocardiographic study. *J Am Soc Echocardiogr.* **24**, 322-32

Díaz-Arteaga, A., Vázquez, M.J., Vazquez-Martínez, R., Pulido, M.R., Suarez, J., Velásquez, D.A., López, M., Ross, R.A., de Fonseca, F.R., Bermudez-Silva, F.J., Malagón, M.M., Diéguez, C. and Nogueiras, R. (2012) The atypical cannabinoid O-1602 stimulates food intake and adiposity in rats. *Diabetes Obes Metab.* **14**, 234-43

Donnan, P.T., Boyle, D.I., Broomhall, J., Hunter, K., MacDonald, T.M., Newton, R.W. and Morris, A.D. (2002) Prognosis following first acute myocardial infarction in Type 2 diabetes: a comparative population study. *Diabet Med.* **19**, 448-55

Dorn, G.W. (2007) The fuzzy logic of physiological cardiac hypertrophy. *Hypertension.* **49**, 962-70

Drazner, M.H. (2011) The progression of hypertensive heart disease. *Circulation.* **123**, 327-34

Drosatos, K. and Schulze, P.C. (2013) Cardiac lipotoxicity: molecular pathways and therapeutic implications. *Curr Heart Fail Rep.* **10**, 109-21

Durst, R., Danenberg, H., Gallily, R., Mechoulam, R., Meir, K., Grad, E., Beerli, R., Pugatsch, T., Tarsish, E. and Lotan, C. (2007) Cannabidiol, a nonpsychoactive Cannabis constituent, protects against myocardial ischemic reperfusion injury. *Am J Physiol Heart Circ Physiol.* **293**, H3602-7

d'Uscio, L.V., Smith, L.A. and Katusic, Z.S. (2001) Hypercholesterolemia impairs endothelium-dependent relaxations in common carotid arteries of apolipoprotein e-deficient mice. *Stroke.* **32**, 2658-64

Fan, D., Takawale, A., Lee, J. and Kassiri, Z. (2012) Cardiac fibroblasts, fibrosis and extracellular matrix remodeling in heart disease. *Fibrogenesis Tissue Repair.* **5**, 15

Ferrari, R., Balla, C., Malagù, M., Guardigli, G., Morciano, G., Bertini, M., Biscaglia, S. and Campo, G. (2017) Reperfusion Damage - A Story of Success, Failure, and Hope. *Circ J.* **81**, 131-141

Ferron, A.J., Jacobsen, B.B., Sant'Ana, P.G., de Campos, D.H., de Tomasi, L.C., Luvizotto Rde, A., Cicogna, A.C., Leopoldo, A.S. and Lima-Leopoldo, A.P. (2015) Cardiac Dysfunction Induced by Obesity Is Not Related to β -Adrenergic System Impairment at the Receptor-Signalling Pathway. *PLoS One.* **10**, e0138605

Freiman, P.C., Mitchell, G.G., Heistad, D.D., Armstrong, M.L. and Harrison, D.G. (1986) Atherosclerosis impairs endothelium-dependent vascular relaxation to acetylcholine and thrombin in primates. *Circ Res.* **58**, 783-9

Fu, Q., Hu, Y., Wang, Q., Liu, Y., Li, N., Xu, B., Kim, S., Chiamvimonvat, N. and Xiang, Y.K. (2017) High-fat diet induces protein kinase A and G-protein receptor kinase phosphorylation of β_2 -adrenergic receptor and impairs cardiac adrenergic reserve in animal hearts. *J Physiol.* **595**, 1973-1986

Fukao, K., Shimada, K., Naito, H., Sumiyoshi, K., Inoue, N., Iesaki, T., Kume, A., Kiyonagi, T., Hiki, M., Hirose, K., Matsumori, R., Ohsaka, H., Takahashi, Y., Toyoda, S., Itoh, S., Miyazaki, T., Tada, N. and Daida, H. (2010) Voluntary exercise ameliorates the progression of atherosclerotic lesion formation via anti-inflammatory effects in apolipoprotein E-deficient mice. *J Atheroscler Thromb.* **17**, 1226-36

Gao, J., Katagiri, H., Ishigaki, Y., Yamada, T., Ogihara, T., Imai, J., Uno, K., Hasegawa, Y., Kanzaki, M., Yamamoto, T.T., Ishibashi, S. and Oka, Y. (2007) Involvement of apolipoprotein E in excess fat accumulation and insulin resistance. *Diabetes.* **56**, 24-33

Garcia-Dorado, D. and Oliveras, J. (1993) Myocardial oedema: a preventable cause of reperfusion injury? *Cardiovasc Res.* **27**, 1555-63

Ge, F., Hu, C., Hyodo, E., Arai, K., Zhou, S., Lobdell, H., Walewski, J.L., Homma, S. and Berk, P.D. (2012) Cardiomyocyte triglyceride accumulation and reduced ventricular function in mice with obesity reflect increased long chain Fatty Acid uptake and de novo Fatty Acid synthesis. *J Obes.* **2012**, 205648

GEN. [online]. Available from:

https://www.genengnews.com/media/images/article//Fig1_EpicCellularAssay2321842101.jpg

[accessed 11th January 2017]

Getz, G.S. and Reardon, C.A. (2012) Animal models of atherosclerosis. *Arterioscler Thromb Vasc Biol.* **32**, 1104-15

Glagov, S., Weisenberg, E., Zarins, C.K., Stankunavicius, R. and Kolettis, G.J. (1987) Compensatory enlargement of human atherosclerotic coronary arteries. *N Engl J Med.* **316**, 1371-5

Goel, D.P., Ford, L.D. and Pierce, G.N. (2003) Lysophospholipids do not directly modulate Na⁽⁺⁾-H⁺ exchange. *Mol Cell Biochem.* **251**, 3-7

Griecsová, L., Farkašová, V., Gáblóvský, I., Khandelwal, V.K., Bernátová, I., Tatarková, Z., Kaplan, P. and Ravingerová, T. (2015) Effect of maturation on the resistance of rat hearts against ischemia. Study of potential molecular mechanisms. *Physiol Res.* **64**, S685-96

Griffiths, E.J. and Halestrap, A.P. (1995) Mitochondrial non-specific pores remain closed during cardiac ischaemia, but open upon reperfusion. *Biochem J.* **307**, 93-8

Grinstein, S., Woodside, M., Sardet, C., Pouyssegur, J. and Rotin, D. (1992) Activation of the Na⁺/H⁺ antiporter during cell volume regulation. Evidence for a phosphorylation-independent mechanism. *J Biol Chem.* **267**, 23823-8

Gyöngyösi, M., Winkler, J., Ramos, I., Do, Q.T., Firat, H., McDonald, K., González, A., Thum, T., Díez, J., Jaisser, F., Pizard, A. and Zannad, F. (2017) Myocardial fibrosis: biomedical research from bench to bedside. *Eur J Heart Fail.* **19**, 177-191

Halestrap, A.P. (1991) Calcium-dependent opening of a non-specific pore in the mitochondrial inner membrane is inhibited at pH values below 7. Implications for the protective effect of low pH against chemical and hypoxic cell damage. *Biochem J.* **278**, 715-9

Halestrap, A.P., Clarke, S.J. and Javadov, S.A. (2004) Mitochondrial permeability transition pore opening during myocardial reperfusion--a target for cardioprotection. *Cardiovasc Res.* **61**, 372-85

Hamid, S.A., Bower, H.S. and Baxter, G.F. (2007) Rho kinase activation plays a major role as a mediator of irreversible injury in reperfused myocardium. *Am J Physiol Heart Circ Physiol.* **292**, H2598-606

Han, H., Cui, W., Wang, L., Xiong, Y., Liu, L., Sun, X. and Hao, L. (2015) Lutein prevents high fat diet-induced atherosclerosis in ApoE-deficient mice by inhibiting NADPH oxidase and increasing PPAR expression. *Lipids.* **50**, 261-73

Hans, C.P., Feng, Y., Naura, A.S., Zerfaoui, M., Rezk, B.M., Xia, H., Kaye, A.D., Matrougui, K., Lazartigues, E. and Boulares, A.H. (2009) Protective effects of PARP-1 knockout on dyslipidemia-induced autonomic and vascular dysfunction in ApoE mice: effects on eNOS and oxidative stress. *PLoS One.* **4**, e7430

Hans, C.P., Feng, Y., Naura, A.S., Troxclair, D., Zerfaoui, M., Siddiqui, D., Jihang, J., Kim, H., Kaye, A.D., Matrougui, K., Lazartigues, E. and Boulares, A.H. (2011) Opposing roles of PARP-1 in MMP-9 and TIMP-2 expression and mast cell degranulation in dyslipidemic dilated cardiomyopathy. *Cardiovasc Pathol.* **20**, e57-68

Hansen, P.R. (1995) Role of neutrophils in myocardial ischemia and reperfusion. *Circulation.* **91**, 1872-85

Hansmann, G., Wagner, R.A., Schellong, S., Perez, V.A., Urashima, T., Wang, L., Sheikh, A.Y., Suen, R.S., Stewart, D.J. and Rabinovitch, M. (2007) Pulmonary arterial hypertension is linked to insulin resistance and reversed by peroxisome proliferator-activated receptor-gamma activation. *Circulation.* **115**, 1275-84

Hartnett, S., Gao, H., Schnack, S. and Li, Y. (2015) Reduced vagal control of the heart in high-fat diet mice: a potential role of increased butyrylcholinesterase. *Physiol Rep.* **3**, pii: e12609

Hasty, A.H., Shimano, H., Osuga, J., Namatame, I., Takahashi, A., Yahagi, N., Perrey, S., Iizuka, Y., Tamura, Y., Amemiya-Kudo, M., Yoshikawa, T., Okazaki, H., Ohashi, K., Harada, K., Matsuzaka, T., Sone, H., Gotoda, T., Nagai, R., Ishibashi, S. and Yamada, N. (2001) Severe hypercholesterolemia, hypertriglyceridemia, and atherosclerosis in mice lacking both leptin and the low density lipoprotein receptor. *J Biol Chem.* **276**, 37402-8

Hausenloy, D.J. and Yellon, D.M. (2013) Myocardial ischemia-reperfusion injury: a neglected therapeutic target. *J Clin Invest.* **123**, 92-100

Heart Diseases. [online]. Available from: <http://whatcardiologyis.com/coronary-artery-disease-2/> [accessed 27th November 2017]

Heinonen, S.E., Merentie, M., Hedman, M., Mäkinen, P.I., Loponen, E., Kholová, I., Bosch, F., Laakso, M. and Ylä-Herttuala, S. (2011) Left ventricular dysfunction with reduced functional cardiac reserve in diabetic and non-diabetic LDL-receptor deficient apolipoprotein B100-only mice. *Cardiovasc Diabetol.* **10**:59

Henstridge, C.M., Balenga, N.A., Ford, L.A., Ross, R.A., Waldhoer, M. and Irving, A.J. (2009) The GPR55 ligand L-alpha-lysophosphatidylinositol promotes RhoA-dependent Ca²⁺ signaling and NFAT activation. *FASEB J.* **23**, 183-93

Henstridge, C.M., Balenga, N.A., Kargl, J., Andradas, C., Brown, A.J., Irving, A., Sanchez, C. and Waldhoer, M. (2011) Minireview: recent developments in the physiology and pathology of the lysophosphatidylinositol-sensitive receptor GPR55. *Mol Endocrinol.* **25**, 1835-48

Heusch, G., Boengler, K. and Schulz, R. (2010) Inhibition of mitochondrial permeability transition pore opening: the Holy Grail of cardioprotection. *Basic Res Cardiol.* **105**, 151-4

Hoey, E.T., Pakala, V., Teoh, J.K. and Simpson, H. (2014) The role of imaging in hypertensive heart disease. *Int J Angiol.* **23**, 85-92

Hoffman, J.I. and Buckberg, G.D. (1978) The myocardial supply:demand ratio--a critical review. *Am J Cardiol.* **41**, 327-32

Hofmann, S.M., Perez-Tilve, D., Greer, T.M., Coburn, B.A., Grant, E., Basford, J.E., Tschöp, M.H. and Hui, D.Y. (2008) Defective lipid delivery modulates glucose tolerance and metabolic response to diet in apolipoprotein E-deficient mice. *Diabetes.* **57**, 5-12

Hoque, A.N., Haist, J.V. and Karmazyn, M. (1997) Na(+)-H+ exchange inhibition protects against mechanical, ultrastructural, and biochemical impairment induced by low concentrations of lysophosphatidylcholine in isolated rat hearts. *Circ Res.* **80**, 95-102

Huang, Y., Walker, K.E., Hanley, F., Narula, J., Houser, S.R. and Tulenko, T.N. (2004) Cardiac systolic and diastolic dysfunction after a cholesterol-rich diet. *Circulation.* **109**, 97-102

Huang, Z.H., Reardon, C.A. and Mazzone, T. (2006) Endogenous ApoE expression modulates adipocyte triglyceride content and turnover. *Diabetes.* **55**, 3394-402

Hunt, B.J. and Jurd, K.M. (1998) Endothelial cell activation. A central pathophysiological process. *BMJ.* **316**, 1328-9

Iantorno, M., Campia, U., Di Daniele, N., Nistico, S., Forleo, G.B., Cardillo, C. and Tesouro, M. (2014) Obesity, inflammation and endothelial dysfunction. *J Biol Regul Homeost Agents.* **28**, 169-76

Imbernon, M., Whyte, L., Diaz-Arteaga, A., Russell, W.R., Moreno, N.R., Vazquez, M.J., Gonzalez, C.R., Díaz-Ruiz, A., Lopez, M., Malagón, M.M., Ross, R.A., Dieguez, C. and Nogueiras, R. (2014) Regulation of GPR55 in rat white adipose tissue and serum LPI by nutritional status, gestation, gender and pituitary factors. *Mol Cell Endocrinol.* **383**, 159-69

Ishibashi, S., Brown, M.S., Goldstein, J.L., Gerard, R.D., Hammer, R.E. and Herz, J. (1993) Hypercholesterolemia in low density lipoprotein receptor knockout mice and its reversal by adenovirus-mediated gene delivery. *J Clin Invest.* **92**, 883-93

Jackson, G., Gibbs, C.R., Davies, M.K. and Lip, G. Y. H. (2000) ABC of heart failure. *Pathophysiology.* *BMJ.* **320**, 167-170

Jawień, J., Nastalek, P. and Korbut, R. (2004) Mouse models of experimental atherosclerosis. *J Physiol Pharmacol.* **55**, 503-17

Jennings, R.B. and Reimer, K.A. (1981) Lethal myocardial ischemic injury. *Am J Pathol.* **102**, 241-55

Jennings, R.B. and Reimer, K.A. (1991) The cell biology of acute myocardial ischemia. *Annu Rev Med.* **42**, 225-46

Johansson, M.E., Hägg, U., Wikström, J., Wickman, A., Bergström, G. and Gan, L.M. (2005) Haemodynamically significant plaque formation and regional endothelial dysfunction in cholesterol-fed ApoE^{-/-} mice. *Clin Sci (Lond)*. **108**, 531-8

Johns, D.G., Behm, D.J., Walker, D.J., Ao, Z., Shapland, E.M., Daniels, D.A., Riddick, M., Dowell, S., Staton, P.C., Green, P., Shabon, U., Bao, W., Aiyar, N., Yue, T.L., Brown, A.J., Morrison, A.D. and Douglas, S.A. (2007) The novel endocannabinoid receptor GPR55 is activated by atypical cannabinoids but does not mediate their vasodilator effects. *Br J Pharmacol*. **152**, 825-31

Kalogeris, T., Baines, C.P., Krenz, M. and Korthuis, R.J. (2012) Cell biology of ischemia/reperfusion injury. *Int Rev Cell Mol Biol*. **298**, 229-317

Kangavari, S., Matetzky, S., Shah, P.K., Yano, J., Chyu, K.Y., Fishbein, M.C. and Cercek, B. (2004) Smoking increases inflammation and metalloproteinase expression in human carotid atherosclerotic plaques. *J Cardiovasc Pharmacol Ther*. **9**, 291-8

Kargl, J., Balenga, N., Parzmair, G.P., Brown, A.J., Heinemann, A. and Waldhoer, M. (2012) The cannabinoid receptor CB1 modulates the signaling properties of the lysophosphatidylinositol receptor GPR55. *J Biol Chem*. **287**, 44234-48

Kargl, J., Brown, A.J., Andersen, L., Dorn, G., Schicho, R., Waldhoer, M. and Heinemann, A. (2013) A selective antagonist reveals a potential role of G protein-coupled receptor 55 in platelet and endothelial cell function. *J Pharmacol Exp Ther*. **346**, 54-66

Kawara, T., Derksen, R., de Groot, J.R., Coronel, R., Tasseront, S., Linnenbank, A.C., Hauer, R.N., Kirkels, H., Janse, M.J. and de Bakker, J.M. (2001) Activation delay after premature stimulation in chronically diseased human myocardium relates to the architecture of interstitial fibrosis. *Circulation*. **104**, 3069-75

Kehat, I. and Molkenkin, J.D. (2010) Molecular pathways underlying cardiac remodeling during pathophysiological stimulation. *Circulation*. **122**, 2727-35

Ketonen, J., Shi, J., Martonen, E. and Mervaala, E. (2010) Periadventitial adipose tissue promotes endothelial dysfunction via oxidative stress in diet-induced obese C57Bl/6 mice. *Circ J*. **74**, 1479-87

Khaksar, S. and Bigdeli, M.R. (2017) Anti-excitotoxic effects of cannabidiol are partly mediated by enhancement of NCX2 and NCX3 expression in animal model of cerebral ischemia. *Eur J Pharmacol.* **794**, 270-279

Khandoudi, N., Bernard, M., Cozzone, P. and Feuvray, D. (1990) Intracellular pH and role of Na⁺/H⁺ exchange during ischaemia and reperfusion of normal and diabetic rat hearts. *Cardiovasc Res.* **24**, 873-8

Kilkenny, C., Browne, W., Cuthill, I.C., Emerson, M. and Altman, D.G. (2010) Animal research: Reporting in vivo experiments: The ARRIVE guidelines. *Br J Pharmacol.* **160**, 1577-1579

Kim, J.A., Montagnani, M., Chandrasekran, S. and Quon, M.J. (2012) Role of lipotoxicity in endothelial dysfunction. *Heart Fail Clin.* **8**, 589-607

Kim, J., Lampe, J.W., Yin, T., Shinozaki, K. and Becker, L.B. (2015a) Phospholipid alterations in the brain and heart in a rat model of asphyxia-induced cardiac arrest and cardiopulmonary bypass resuscitation. *Mol Cell Biochem.* **408**, 273-81

Kim, C.H., Mitchell, J.B., Bursill, C.A., Sowers, A.L., Thetford, A., Cook, J.A., van Reyk, D.M. and Davies, M.J. (2015b) The nitroxide radical TEMPOL prevents obesity, hyperlipidaemia, elevation of inflammatory cytokines, and modulates atherosclerotic plaque composition in apoE^{-/-} mice. *Atherosclerosis.* **240**, 234-41

Kim, J., Yin, T., Shinozaki, K., Lampe, J.W. and Becker, L.B. (2016) Potential of lysophosphatidylinositol as a prognostic indicator of cardiac arrest using a rat model. *Biomarkers.* 2016 Dec 8:1-9. [Epub ahead of print]

Kloner, R.A. and Jennings, R.B. (2001) Consequences of brief ischemia: stunning, preconditioning, and their clinical implications: part 1. *Circulation.* **104**, 2981-9

Kloner, R.A. (2013) Current state of clinical translation of cardioprotective agents for acute myocardial infarction. *Circ Res.* **113**, 451-63

Kreissl, M.C., Wu, H.M., Stout, D.B., Ladno, W., Schindler, T.H., Zhang, X., Prior, J.O., Prins, M.L., Chatziioannou, A.F., Huang, S.C. and Schelbert, H.R. (2006) Noninvasive measurement of cardiovascular function in mice with high-temporal-resolution small-animal PET. *J Nucl Med.* **47**, 974-80

Kremshofer, J., Siwetz, M., Berghold, V.M., Lang, I., Huppertz, B. and Gauster, M. (2015) A role for GPR55 in human placental venous endothelial cells. *Histochem Cell Biol.* **144**, 49-58

Krijnen, P.A., Nijmeijer, R., Meijer, C.J., Visser, C.A., Hack, C.E. and Niessen, H.W. (2002) Apoptosis in myocardial ischaemia and infarction. *J Clin Pathol.* **55**, 801-11

Kubes, P., Suzuki, M. and Granger, D.N. (1991) Nitric oxide: an endogenous modulator of leukocyte adhesion. *Proc Natl Acad Sci U S A.* **88**, 4651-5

Kumar, S., Chen, M., Li, Y., Wong, F.H., Thiam, C.W., Hossain, M.Z., Poh, K.K., Hirohata, S., Ogawa, H., Angeli, V. and Ge, R. (2016) Loss of ADAMTS4 reduces high fat diet-induced atherosclerosis and enhances plaque stability in ApoE(-/-) mice. *Sci Rep.* **6**, 31130

Kume, N., Cybulsky, M.I. and Gimbrone, M.A. Jr. (1992) Lysophosphatidylcholine, a component of atherogenic lipoproteins, induces mononuclear leukocyte adhesion molecules in cultured human and rabbit arterial endothelial cells. *J Clin Invest.* **90**, 1138-44

Kurano, M., Suzuki, A., Inoue, A., Tokuhara, Y., Kano, K., Matsumoto, H., Igarashi, K., Ohkawa, R., Nakamura, K., Dohi, T., Miyauchi, K., Daida, H., Tsukamoto, K., Ikeda, H., Aoki, J. and Yatomi, Y. (2015) Possible involvement of minor lysophospholipids in the increase in plasma lysophosphatidic acid in acute coronary syndrome. *Arterioscler Thromb Vasc Biol.* **35**, 463-70

Kurian, G.A., Rajagopal, R., Vedantham, S. and Rajesh, M. (2016) The Role of Oxidative Stress in Myocardial Ischemia and Reperfusion Injury and Remodeling: Revisited. *Oxid Med Cell Longev.* **2016**, 1656450

Kwon, Y.S., Jang, J.S., Lee, C.W., Kim, D.K., Kim, U., Seol, S.H., Kim, D.I., Jo, Y.W., Jin, H.Y., Seo, J.S., Yang, T.H., Kim, D.K. and Kim, D.S. (2010) Comparison of Plaque Composition in Diabetic and Non-

Diabetic Patients With Coronary Artery Disease Using Multislice CT Angiography. *Korean Circ J.* **40**, 581-6

Ladilov, Y.V., Siegmund, B., Balser, C. and Piper, H.M. (1997) Simulated ischemia increases the susceptibility of rat cardiomyocytes to hypercontracture. *Circ Res.* **80**, 69-75

Lansky, A.J., Ng, V.G., Maehara, A., Weisz, G., Lerman, A., Mintz, G.S., De Bruyne, B., Farhat, N., Niess, G., Jankovic, I., Lazar, D., Xu, K., Fahy, M., Serruys, P.W. and Stone, G.W. (2012) Gender and the extent of coronary atherosclerosis, plaque composition, and clinical outcomes in acute coronary syndromes. *JACC Cardiovasc Imaging.* **5**, S62-72

Lanuti, M., Talamonti, E., Maccarrone, M. and Chiurchiù, V. (2015) Activation of GPR55 Receptors Exacerbates oxLDL-Induced Lipid Accumulation and Inflammatory Responses, while Reducing Cholesterol Efflux from Human Macrophages. *PLoS One.* **10**, e0126839

Lauckner, J.E., Jensen, J.B., Chen, H.Y., Lu, H.C., Hille, B. and Mackie K. (2008) GPR55 is a cannabinoid receptor that increases intracellular calcium and inhibits M current. *Proc Natl Acad Sci U S A.* **105**, 2699-704

Laufs, U., Wassmann, S., Czech, T., Münzel, T., Eisenhauer, M., Böhm, M. and Nickenig, G. (2005) Physical inactivity increases oxidative stress, endothelial dysfunction, and atherosclerosis. *Arterioscler Thromb Vasc Biol.* **25**, 809-14

Leist, M., Single, B., Castoldi, A.F., Kühnle, S. and Nicotera, P. (1997) Intracellular Adenosine Triphosphate (ATP) Concentration: A Switch in the Decision Between Apoptosis and Necrosis *J Exp Med.* **185**, 1481–1486

Lépicier, P., Bouchard, J.F., Lagneux, C. and Lamontagne, D. (2003) Endocannabinoids protect the rat isolated heart against ischaemia. *Br J Pharmacol.* **139**, 805-15

Lépicier, P., Lagneux, C., Sirois, M.G. and Lamontagne, D. (2007) Endothelial CB1-receptors limit infarct size through NO formation in rat isolated hearts. *Life Sci.* **81**, 1373-80

Levick, J.R. (2010) *An introduction to cardiovascular physiology*. Fifth edition. Chapters 4, 6, 14 and 15. UK: Hodder Arnold

Li, K., Fichna, J., Schicho, R., Saur, D., Bashashati, M., Mackie, K., Li, Y., Zimmer, A., Göke, B., Sharkey, K.A. and Storr, M. (2013) A role for O-1602 and G protein-coupled receptor GPR55 in the control of colonic motility in mice. *Neuropharmacology*. **71**, 255-63

Liao, R., Podesser, B.K. and Lim, C.C. (2012) The continuing evolution of the Langendorff and ejecting murine heart: new advances in cardiac phenotyping. *Am J Physiol Heart Circ Physiol*. **303**, H156-67

Lin, Y., Bai, L., Chen, Y., Zhu, N., Bai, Y., Li, Q., Zhao, S., Fan, J. and Liu, E. (2015) Practical assessment of the quantification of atherosclerotic lesions in apoE^{-/-} mice. *Mol Med Rep*. **12**, 5298-306

Linz, W., Albus, U., Crause, P., Jung, W., Weichert, A., Schölkens, B.A. and Scholz, W. (1998) Dose-dependent reduction of myocardial infarct mass in rabbits by the NHE-1 inhibitor cariporide (HOE 642). *Clin Exp Hypertens*. **20**, 733-49

Lips, D.J., van der Nagel, T., Steendijk, P., Palmen, M., Janssen, B.J., van Dantzig, J.M., de Windt, L.J. and Doevendans, P.A. (2004) Left ventricular pressure-volume measurements in mice: comparison of closed-chest versus open-chest approach. *Basic Res Cardiol*. **99**, 351-9

Liu, L., Mu, Y., Han, W. and Wang, C. (2014) Association of hypercholesterolemia and cardiac function evaluated by speckle tracking echocardiography in a rabbit model. *Lipids Health Dis*. **13**:128

Liu, B., Song, S., Ruz-Maldonado, I., Pingitore, A., Huang, G.C., Baker, D., Jones, P.M. and Persaud, S.J. (2016) GPR55-dependent stimulation of insulin secretion from isolated mouse and human islets of Langerhans. *Diabetes Obes Metab*. **18**, 1263-1273

López, B., Querejeta, R., González, A., Larman, M. and Díez, J. (2012) Collagen cross-linking but not collagen amount associates with elevated filling pressures in hypertensive patients with stage C heart failure: potential role of lysyl oxidase. *Hypertension*. **60**, 677-83

Louwe, M.C., van der Hoorn, J.W., van den Berg, S.A., Jukema, J.W., Romijn, J.A., van Dijk, K.W., Rensen, P.C., Smit, J.W. and Steendijk, P. (2012) Gender-dependent effects of high-fat lard diet on cardiac function in C57Bl/6J mice. *Appl Physiol Nutr Metab*. **37**, 214-24

Lymperopoulos, A., Rengo, G. and Koch, W.J. (2013) Adrenergic nervous system in heart failure: pathophysiology and therapy. *Circ Res.* **113**, 739-53

Ma, Y., Wang, W., Zhang, J., Lu, Y., Wu, W., Yan, H. and Wang, Y. (2012) Hyperlipidemia and atherosclerotic lesion development in Ldlr-deficient mice on a long-term high-fat diet. *PLoS One.* **7**, e35835

Mackie, K and Stella, N. (2006) Cannabinoid receptors and endocannabinoids: evidence for new players. *AAPS J.* **8**, 298-306

Mak, K.H., Moliterno, D.J., Granger, C.B., Miller, D.P., White, H.D., Wilcox, R.G., Califf, R.M. and Topol, E.J. (1997) Influence of diabetes mellitus on clinical outcome in the thrombolytic era of acute myocardial infarction. GUSTO-I Investigators. Global Utilization of Streptokinase and Tissue Plasminogen Activator for Occluded Coronary Arteries. *J Am Coll Cardiol.* **30**, 171-9

Marichal-Cancino, B.A., Manrique-Maldonado, G., Altamirano-Espinoza, A.H., Ruiz-Salinas, I., González-Hernández, A., MaassenVanDenBrink, A. and Villalón, C.M. (2013) Analysis of anandamide- and lysophosphatidylinositol-induced inhibition of the vasopressor responses produced by sympathetic stimulation or noradrenaline in pithed rats. *Eur J Pharmacol.* **721**, 168-77

McCully, J.D., Wakiyama, H., Hsieh, Y.J., Jones, M. and Levitsky, S. (2004) Differential contribution of necrosis and apoptosis in myocardial ischemia-reperfusion injury. *Am J Physiol Heart Circ Physiol.* **286**, H1923-35

McElmurray, J.H., Mukherjee, R., New, R.B., Sampson, A.C., King, M.K., Hendrick, J.W., Goldberg, A., Peterson, T.J., Hallak, H., Zile, M.R. and Spinale, F.G. (1999) Angiotensin-converting enzyme and matrix metalloproteinase inhibition with developing heart failure: comparative effects on left ventricular function and geometry. *J Pharmacol Exp Ther.* **291**, 799-811

McHugh, D., Wager-Miller, J., Page, J. and Bradshaw, H.B. (2012) siRNA knockdown of GPR18 receptors in BV-2 microglia attenuates N-arachidonoyl glycine-induced cell migration. *J Mol Signal.* **7**, 10

McKillop, A.M., Moran, B.M., Abdel-Wahab, Y.H. and Flatt, P.R. (2013) Evaluation of the insulin releasing and antihyperglycaemic activities of GPR55 lipid agonists using clonal beta-cells, isolated pancreatic islets and mice. *Br J Pharmacol.* **170**, 978-90

McKillop, A.M., Moran, B.M., Abdel-Wahab, Y.H., Gormley, N.M. and Flatt, P.R. (2016) Metabolic effects of orally administered small-molecule agonists of GPR55 and GPR119 in multiple low-dose streptozotocin-induced diabetic and incretin-receptor-knockout mice. *Diabetologia.* **59**, 2674-2685

McLenachan, J.M. and Dargie, H.J. (1990) Ventricular arrhythmias in hypertensive left ventricular hypertrophy. Relationship to coronary artery disease, left ventricular dysfunction, and myocardial fibrosis. *Am J Hypertens.* **3**, 735-40

McMurray, J.J., Packer, M., Desai, A.S., Gong, J., Lefkowitz, M.P., Rizkala, A.R., Rouleau, J.L., Shi, V.C., Solomon, S.D., Swedberg, K., Zile, M.R. and PARADIGM-HF Investigators and Committees. (2014) Angiotensin-neprilysin inhibition versus enalapril in heart failure. *N Engl J Med.* **371**, 993-1004

Meadows, A., Lee, J.H., Wu, C.S., Wei, Q., Pradhan, G., Yafi, M., Lu, H.C. and Sun, Y. (2016) Deletion of G-protein-coupled receptor 55 promotes obesity by reducing physical activity. *Int J Obes (Lond).* **40**, 417-24

Messner, B and Bernhard, D. (2014) Smoking and cardiovascular disease: mechanisms of endothelial dysfunction and early atherogenesis. *Arterioscler Thromb Vasc Biol.* **34**, 509-15

Mewton, N., Liu, C.Y., Croisille, P., Bluemke, D. and Lima, J.A. (2011) Assessment of myocardial fibrosis with cardiovascular magnetic resonance. *J Am Coll Cardiol.* **57**, 891-903

Meyrelles, S.S., Peotta, V.A., Pereira, T.M. and Vasquez, E.C. (2011) Endothelial dysfunction in the apolipoprotein E-deficient mouse: insights into the influence of diet, gender and aging. *Lipids Health Dis.* **10**, 211

Minicucci, M.F., Azevedo, P.S., Polegato, B.F., Paiva, S.A. and Zornoff, L.A. (2011) Heart failure after myocardial infarction: clinical implications and treatment. *Clin Cardiol.* **34**, 410-4

Mocanu, M.M., Gadgil, S., Yellon, D.M. and Baxter, G.F. (1999) Mibefradil, a T-type and L-type calcium channel blocker, limits infarct size through a glibenclamide-sensitive mechanism. *Cardiovasc Drugs Ther.* **13**, 115-22

Montecucco, F., Bondarenko, A.I., Lenglet, S., Burger, F., Piscitelli, F., Carbone, F., Roth, A., Liberale, L., Dallegri, F., Brandt, K.J., Fraga-Silva, R.A., Stergiopoulos, N., Di Marzo, V. and Mach, F. (2016) Treatment with the GPR55 antagonist CID16020046 increases neutrophil activation in mouse atherogenesis. *Thromb Haemost.* **116**, 987-997

Moreno-Navarrete, J.M., Catalán, V., Whyte, L., Díaz-Arteaga, A., Vázquez-Martínez, R., Rotellar, F., Guzmán, R., Gómez-Ambrosi, J., Pulido, M.R., Russell, W.R., Imbernón, M., Ross, R.A., Malagón, M.M., Dieguez, C., Fernández-Real, J.M., Frühbeck, G. and Nogueiras R. (2012) The L- α -lysophosphatidylinositol/GPR55 system and its potential role in human obesity. *Diabetes.* **61**, 281-91

Mozaffari, M.S., Liu, J.Y., Abebe, W. and Baban, B. (2013) Mechanisms of load dependency of myocardial ischemia reperfusion injury. *Am J Cardiovasc Dis.* **3**, 180-96

Murphy, E. and Steenbergen, C. (2008) Ion transport and energetics during cell death and protection. *Physiology (Bethesda).* **23**, 115-23

Nakagawa, O., Fujisawa, K., Ishizaki, T., Saito, Y., Nakao, K. and Narumiya, S. (1996) ROCK-I and ROCK-II, two isoforms of Rho-associated coiled-coil forming protein serine/threonine kinase in mice. *FEBS Lett.* **392**, 189-93

Nakashima, Y., Plump, A.S., Raines, E.W., Breslow, J.L. and Ross, R. (1994) ApoE-deficient mice develop lesions of all phases of atherosclerosis throughout the arterial tree. *Arterioscler Thromb.* **14**, 133-40

Napoli, C., D'Armiento, F.P., Mancini, F.P., Postiglione, A., Witztum, J.L., Palumbo, G. and Palinski, W. (1997) Fatty streak formation occurs in human fetal aortas and is greatly enhanced by maternal hypercholesterolemia. Intimal accumulation of low density lipoprotein and its oxidation precede monocyte recruitment into early atherosclerotic lesions. *J Clin Invest.* **100**, 2680-90

Naresh, N.K., Butcher, J.T., Lye, R.J., Chen, X., Isakson, B.E., Gan, L.M., Kramer, C.M., Annex, B.H. and Epstein, F.H. (2016) Cardiovascular magnetic resonance detects the progression of impaired myocardial perfusion reserve and increased left-ventricular mass in mice fed a high-fat diet. *J Cardiovasc Magn Reson.* **18**, 53

Neely, J.R., Liedtke, A.J., Whitmer, J.T. and Rovetto, M.J. (1975) Relationship between coronary flow and adenosine triphosphate production from glycolysis and oxidative metabolism. *Recent Adv Stud Cardiac Struct Metab.* **8**, 301-21

Newman, W.P., Freedman, D.S., Voors, A.W., Gard, P.D., Srinivasan, S.R., Cresanta, J.L., Williamson, G.D., Webber, L.S. and Berenson, G.S. (1986) Relation of serum lipoprotein levels and systolic blood pressure to early atherosclerosis. The Bogalusa Heart Study. *N Engl J Med.* **314**, 138-44

Oberst, A. (2016) Death in the fast lane: what's next for necroptosis? *FEBS J.* **283**, 2616-25

Ogah, O.S., Akinyemi, R.O., Adegbite, G.D., Udofia, O.I., Udoh, S.B., Adesina, J.O., Ojo, O.S., Alabi, A.A., Majekodunmi, T., Osinfade, J.K., Ogundipe, R.F. and Falase, A.O. (2011) Prevalence of asymptomatic left ventricular systolic dysfunction in hypertensive Nigerians: echocardiographic study of 832 subjects. *Cardiovasc J Afr.* **22**, 297-302

Oka, S., Nakajima, K., Yamashita, A., Kishimoto, S. and Sugiura, T. (2007) Identification of GPR55 as a lysophosphatidylinositol receptor. *Biochem Biophys Res Commun.* **362**, 928-34

Oka, S., Toshida, T., Maruyama, K., Nakajima, K., Yamashita, A. and Sugiura, T. (2009) 2-Arachidonoyl-sn-glycero-3-phosphoinositol: a possible natural ligand for GPR55. *J Biochem.* **145**, 13-20

Oka, S., Kimura, S., Toshida, T., Ota, R., Yamashita, A. and Sugiura, T. (2010) Lysophosphatidylinositol induces rapid phosphorylation of p38 mitogen-activated protein kinase and activating transcription factor 2 in HEK293 cells expressing GPR55 and IM-9 lymphoblastoid cells. *J Biochem.* **147**, 671-8

Pacher, P., Nagayama, T., Mukhopadhyay, P., Bátkai, S. and Kass, D.A. (2008) Measurement of cardiac function using pressure-volume conductance catheter technique in mice and rats. *Nat Protoc.* **3**, 1422-34

- Paigen, B., Holmes, P.A., Mitchell, D. and Albee, D. (1987a) Comparison of atherosclerotic lesions and HDL-lipid levels in male, female, and testosterone-treated female mice from strains C57BL/6, BALB/c, and C3H. *Atherosclerosis*. **64**, 215-21
- Paigen, B., Morrow, A., Holmes, P.A., Mitchell, D. and Williams, R.A. (1987b) Quantitative assessment of atherosclerotic lesions in mice. *Atherosclerosis*. **68**, 231-40
- Park, T.S., Hu, Y., Noh, H.L., Drosatos, K., Okajima, K., Buchanan, J., Tuinei, J., Homma, S., Jiang, X.C., Abel, E.D. and Goldberg, I.J. (2008) Ceramide is a cardiotoxin in lipotoxic cardiomyopathy. *J Lipid Res*. **49**, 2101-12
- Pascual, M., Pascual, D.A., Soria, F., Vicente, T., Hernández, A.M., Tébar, F.J. and Valdés, M. (2003) Effects of isolated obesity on systolic and diastolic left ventricular function *Heart*. **89**, 1152–1156
- Pelat, M., Dessy, C., Massion, P., Desager, J.P., Feron, O. and Balligand, J.L. (2003) Rosuvastatin decreases caveolin-1 and improves nitric oxide-dependent heart rate and blood pressure variability in apolipoprotein E^{-/-} mice in vivo. *Circulation*. **107**, 2480-6
- Pendse, A.A., Arbones-Mainar, J.M., Johnson, L.A., Altenburg, M.K. and Maeda, N. (2009) Apolipoprotein E knock-out and knock-in mice: atherosclerosis, metabolic syndrome, and beyond. *J Lipid Res*. **50**, S178-82
- Piñeiro, R. and Falasca, M. (2012) Lysophosphatidylinositol signalling: new wine from an old bottle. *Biochim Biophys Acta*. **1821**, 694-705
- Piper, H.M., García-Dorado, D. and Ovize, M. (1998) A fresh look at reperfusion injury. *Cardiovasc Res*. **38**, 291-300
- Piper, H.M., Abdallah, Y. and Schäfer, C. (2004) The first minutes of reperfusion: a window of opportunity for cardioprotection. *Cardiovasc Res*. **61**, 365-71
- Pitt, B., Zannad, F., Remme, W.J., Cody, R., Castaigne, A., Perez, A., Palensky, J. and Wittes, J. (1999) The effect of spironolactone on morbidity and mortality in patients with severe heart failure. Randomized Aldactone Evaluation Study Investigators. *N Engl J Med*. **341**, 709-17

Rafieian-Kopaei, M., Setorki, M., Doudi, M., Baradaran, A. and Nasri, H. (2014) Atherosclerosis: process, indicators, risk factors and new hopes. *Int J Prev Med.* **5**, 927-46

Raman, K.G., Gandley, R.E., Rohland, J., Zenati, M.S. and Tzeng, E. (2011) Early hypercholesterolemia contributes to vasomotor dysfunction and injury associated atherogenesis that can be inhibited by nitric oxide. *J Vasc Surg.* **53**, 754-63

Rang, H.P., Dale, M.M., Ritter, J.M. and Flower, R.J. (2007) *Rang and Dale's Pharmacology*. Sixth Edition. Chapters: 3 and 9. China: Churchill Livingstone Elsevier

Reimer, K.A., Lowe, J.E., Rasmussen, M.M. and Jennings, R.B. (1977) The wavefront phenomenon of ischemic cell death. 1. Myocardial infarct size vs duration of coronary occlusion in dogs. *Circulation.* **56**, 786-94

Rohmann, S., Weygandt, H. and Minck, K.O. (1995) Preischemic as well as postischemic application of a Na⁺/H⁺ exchange inhibitor reduces infarct size in pigs. *Cardiovasc Res.* **30**, 945-51

Romero-Zerbo, S.Y., Rafacho, A., Díaz-Arteaga, A., Suárez, J., Quesada, I., Imbernon, M., Ross, R.A., Dieguez, C., Rodríguez de Fonseca, F., Nogueiras, R., Nadal, A. and Bermúdez-Silva, F.J. (2011) A role for the putative cannabinoid receptor GPR55 in the islets of Langerhans. *J Endocrinol.* **211**, 177-85

Ross, R.A. (2009) The enigmatic pharmacology of GPR55. *Trends Pharmacol Sci.* **30**, 156-63

Ruiz-Meana, M., Garcia-Dorado, D., Hofstaetter, B., Piper, H.M. and Soler-Soler, J. (1999) Propagation of cardiomyocyte hypercontracture by passage of Na⁽⁺⁾ through gap junctions. *Circ Res.* **85**, 280-7

Ryberg, E., Larsson, N., Sjögren, S., Hjorth, S., Hermansson, N.O., Leonova, J., Elebring, T., Nilsson, K., Drmota, T. and Greasley PJ (2007) The orphan receptor GPR55 is a novel cannabinoid receptor. *Br J Pharmacol.* **152**, 1092-101

Sabaté, M., Kay, I.P., de Feyter, P.J., van Domburg, R.T., Deshpande, N.V., Ligthart, J.M., Gijzel, A.L., Wardeh, A.J., Boersma, E. and Serruys, P.W. (1999) Remodeling of atherosclerotic coronary arteries varies in relation to location and composition of plaque. *Am J Cardiol.* **84**, 135-40

- Saleem, H., Tovey, S.C., Molinski, T.F. and Taylor, C.W. (2014) Interactions of antagonists with subtypes of inositol 1,4,5-trisphosphate (IP3) receptor. *Br J Pharmacol.* **171**, 3298-312
- Sambandam, N. and Lopaschuk, G.D. (2003) AMP-activated protein kinase (AMPK) control of fatty acid and glucose metabolism in the ischemic heart. *Prog Lipid Res.* **42**, 238-56
- Saraste, A. and Pulkki, K. (2000) Morphologic and biochemical hallmarks of apoptosis. *Cardiovasc Res.* **45**, 528-37
- Satoh, K., Fukumoto, Y. and Shimokawa, H. (2011) Rho-kinase: important new therapeutic target in cardiovascular diseases. *Am J Physiol Heart Circ Physiol.* **301**, H287-96
- Sawzdargo, M., Nguyen, T., Lee, D.K., Lynch, K.R., Cheng, R., Heng, H.H., George, S.R. and O'Dowd, B.F. (1999) Identification and cloning of three novel human G protein-coupled receptor genes GPR52, PsiGPR53 and GPR55: GPR55 is extensively expressed in human brain. *Brain Res Mol Brain Res.* **64**, 193-8
- Schäfer, A., Wiesmann, F., Neubauer, S., Eigenthaler, M., Bauersachs, J. and Channon, K.M. (2004) Rapid regulation of platelet activation in vivo by nitric oxide. *Circulation.* **109**, 1819-22
- Schicho, R., Bashashati, M., Bawa, M., McHugh, D., Saur, D., Hu, H.M., Zimmer, A., Lutz, B., Mackie, K., Bradshaw, H.B., McCafferty, D.M., Sharkey, K.A. and Storr, M. (2011) The atypical cannabinoid O-1602 protects against experimental colitis and inhibits neutrophil recruitment. *Inflamm Bowel Dis.* **17**, 1651-64
- Schierwagen, R., Maybüchen, L., Zimmer, S., Hittatiya, K., Bäck, C., Klein, S., Uschner, F.E., Reul, W., Boor, P., Nickenig, G., Strassburg, C.P., Trautwein, C., Plat, J., Lütjohann, D., Sauerbruch, T., Tacke, F. and Trebicka, J. (2015) Seven weeks of Western diet in apolipoprotein-E-deficient mice induce metabolic syndrome and non-alcoholic steatohepatitis with liver fibrosis. *Sci Rep.* **5**, 12931
- Schwartzkopff, B., Brehm, M., Mundhenke, M. and Strauer, B.E. (2000) Repair of coronary arterioles after treatment with perindopril in hypertensive heart disease. *Hypertension.* **36**, 220-5

Sheu, W.H., Shieh, S.M., Fuh, M.M., Shen, D.D., Jeng, C.Y., Chen, Y.D. and Reaven, G.M. (1993) Insulin resistance, glucose intolerance, and hyperinsulinemia. Hypertriglyceridemia versus hypercholesterolemia. *Arterioscler Thromb.* **13**, 367-70

Shimada, K., Kishimoto, C., Okabe, T.A., Hattori, M., Murayama, T., Yokode, M. and Kita, T. (2007) Exercise training reduces severity of atherosclerosis in apolipoprotein E knockout mice via nitric oxide. *Circ J.* **71**, 1147-51

Signore, S., Sorrentino, A., Ferreira-Martins, J., Kannappan, R., Shafaie, M., Del Ben, F., Isobe, K., Arranto, C., Wybieralska, E., Webster, A., Sanada, F., Ogórek, B., Zheng, H., Liu, X., del Monte, F., D'Alessandro, D.A., Wunimenghe, O., Michler, R.E., Hosoda, T., Goichberg, P., Leri, A., Kajstura, J., Anversa, P. and Rota, M. (2013) Inositol 1, 4, 5-Triphosphate Receptors and Human Left Ventricular Myocytes. *Circulation.* **128**, 10.1161

Sinha-Hikim, I., Sinha-Hikim, A.P., Shen, R., Kim, H.J., French, S.W., Vaziri, N.D., Crum, A.C., Rajavashisth, T.B. and Norris, K.C. (2011) A novel cystine based antioxidant attenuates oxidative stress and hepatic steatosis in diet-induced obese mice. *Exp Mol Pathol.* **91**, 419-28

Smani, T., Domínguez-Rodríguez, A., Hmadcha, A., Calderón-Sánchez, E., Horrillo-Ledesma, A. and Ordóñez, A. (2007) Role of Ca²⁺-independent phospholipase A2 and store-operated pathway in urocortin-induced vasodilatation of rat coronary artery. *Circ Res.* **101**, 1194-203

Smith, C.W., Entman, M.L., Lane, C.L., Beaudet, A.L., Ty, T.I., Youker, K., Hawkins, H.K. and Anderson, D.C. (1991) Adherence of neutrophils to canine cardiac myocytes in vitro is dependent on intercellular adhesion molecule-1. *J Clin Invest.* **88**, 1216-23

SOLVD Investigators, Yusuf, S., Pitt, B., Davis, C.E., Hood, W.B. and Cohn, J.N. (1991) Effect of enalapril on survival in patients with reduced left ventricular ejection fractions and congestive heart failure. *N Engl J Med.* **325**, 293-302

Spinale, F.G., Coker, M.L., Thomas, C.V., Walker, J.D., Mukherjee, R. and Hebbar, L. (1998) Time-dependent changes in matrix metalloproteinase activity and expression during the progression of congestive heart failure: relation to ventricular and myocyte function. *Circ Res.* **82**, 482-95

Stančić, A., Jandl, K., Hasenöhr, C., Reichmann, F., Marsche, G., Schuligoi, R., Heinemann, A., Storr, M. and Schicho, R. (2015) The GPR55 antagonist CID16020046 protects against intestinal inflammation. *Neurogastroenterol Motil.* **27**, 1432-45

Stapleton, P.A., Goodwill, A.G., James, M.E. and Frisbee, J.C. (2007) Altered mechanisms of endothelium-dependent dilation in skeletal muscle arterioles with genetic hypercholesterolemia. *Am J Physiol Regul Integr Comp Physiol.* **293**, R1110-9

Strydom, H.C., Chandler, A.B., Glagov, S., Guyton, J.R., Insull, W. Jr., Rosenfeld, M.E., Schaffer, S.A., Schwartz, C.J., Wagner, W.D. and Wissler, R.W. (1994) A definition of initial, fatty streak, and intermediate lesions of atherosclerosis. A report from the Committee on Vascular Lesions of the Council on Arteriosclerosis, American Heart Association. *Circulation.* **89**, 2462-78

Strydom, H.C., Chandler, A.B., Dinsmore, R.E., Fuster, V., Glagov, S., Insull, W. Jr., Rosenfeld, M.E., Schwartz, C.J., Wagner, W.D. and Wissler, R.W. (1995) A definition of advanced types of atherosclerotic lesions and a histological classification of atherosclerosis. A report from the Committee on Vascular Lesions of the Council on Arteriosclerosis, American Heart Association. *Circulation.* **92**, 1355-74

Stat Trek. [online]. Available from: <http://stattrek.com/> [accessed 18th February 2013]

Stokes, K.Y., Cooper, D., Taylor, A. and Granger, D.N. (2002) Hypercholesterolemia promotes inflammation and microvascular dysfunction: role of nitric oxide and superoxide. *Free Radic Biol Med.* **33**, 1026-36

Stubbins, R.E., Holcomb, V.B., Hong, J. and Núñez, N.P. (2012) Estrogen modulates abdominal adiposity and protects female mice from obesity and impaired glucose tolerance. *Eur J Nutr.* **51**, 861-70

Sun, L. and Wang, X. (2014) A new kind of cell suicide: mechanisms and functions of programmed necrosis. *Trends Biochem Sci.* **39**, 587-93

Takahashi, M., Shichiri, G., Amano, M., Kanamori, T. and Kinoshita, M. (1992) Increased uncoupling of beta-, beta 1- and beta 2-adrenoceptor to myocardial contraction in failing human myocardium. *Jpn Circ J.* **56**, 701-9

Talini, E., Di Bello, V., Bianchi, C., Palagi, C., Delle Donne, M.G., Penno, G., Nardi, C., Canale, M.L., Del Prato, S., Mariani, M. and Miccoli, R. (2008) Early impairment of left ventricular function in hypercholesterolemia and its reversibility after short term treatment with rosuvastatin A preliminary echocardiographic study. *Atherosclerosis.* **197**, 346-54

Temsah, R.M., Netticadan, T., Chapman, D., Takeda, S., Mochizuki, S. and Dhalla, N.S. (1999) Alterations in sarcoplasmic reticulum function and gene expression in ischemic-reperfused rat heart. *Am J Physiol.* **277**, H584-94

Thomas, A., Baillie, G.L., Phillips, A.M., Razdan, R.K., Ross, R.A. and Pertwee, R.G. (2007) Cannabidiol displays unexpectedly high potency as an antagonist of CB1 and CB2 receptor agonists in vitro. *Br J Pharmacol.* **150**, 613-23

Toth, P.P. (2008) Subclinical atherosclerosis: what it is, what it means and what we can do about it. *Int J Clin Pract.* **62**, 1246-54

Townsend, N., Bhatnagar, P., Wilkins, E., Wickramasinghe, K. and Rayner, M. (2015) *Cardiovascular Disease Statistics 2015*. Book 146. Chapter 1. England: British Heart Foundation

Tranum-Jensen, J., Janse, M.J., Fiolet, W.T., Krieger, W.J., D'Alnoncourt, C.N. and Durrer, D. (1981) Tissue osmolality, cell swelling, and reperfusion in acute regional myocardial ischemia in the isolated porcine heart. *Circ Res.* **49**, 364-81

Tyrankiewicz, U., Skorka, T., Jablonska, M., Petkow-Dimitrow, P. and Chlopicki, S. (2013) Characterization of the cardiac response to a low and high dose of dobutamine in the mouse model of dilated cardiomyopathy by MRI in vivo. *J Magn Reson Imaging.* **37**, 669-77

Vakeva, A.P., Agah, A., Rollins, S.A., Matis, L.A., Li, L. and Stahl, G.L. (1998) Myocardial infarction and apoptosis after myocardial ischemia and reperfusion: role of the terminal complement components and inhibition by anti-C5 therapy. *Circulation.* **97**, 2259-67

Van Oostrom, O., Velema, E., Schoneveld, A.H., de Vries, J.P., de Bruin, P., Seldenrijk, C.A., de Kleijn, D.P., Busser, E., Moll, F.L., Verheijen, J.H., Virmani, R. and Pasterkamp, G. (2005) Age-related changes in plaque composition: a study in patients suffering from carotid artery stenosis. *Cardiovasc Pathol.* **14**, 126-34

Varadarajan, S.G., An, J., Novalija, E., Smart, S.C. and Stowe, D.F. (2001) Changes in $[Na^{+}]_{(i)}$, compartmental $[Ca^{2+}]$, and NADH with dysfunction after global ischemia in intact hearts. *Am J Physiol Heart Circ Physiol.* **280**, H280-93

Varga, Z.V., Kupai, K., Szűcs, G., Gáspár, R., Pálóczi, J., Faragó, N., Zvara, A., Puskás, L.G., Rázga, Z., Tiszlavicz, L., Bencsik, P., Görbe, A., Csonka, C., Ferdinandy, P. and Csont, T. (2013) MicroRNA-25-dependent up-regulation of NADPH oxidase 4 (NOX4) mediates hypercholesterolemia-induced oxidative/nitrative stress and subsequent dysfunction in the heart. *J Mol Cell Cardiol.* **62**, 111-21

Vasquez, E.C., Peotta, V.A. and Meyrelles, S.S. (2012) Cardiovascular autonomic imbalance and baroreflex dysfunction in the apolipoprotein E-deficient mouse. *Cell Physiol Biochem.* **29**, 635-46

Véniant, M.M., Sullivan, M.A., Kim, S.K., Ambroziak, P., Chu, A., Wilson, M.D., Hellerstein, M.K., Rudel, L.L., Walzem, R.L. and Young, S.G. (2000) Defining the atherogenicity of large and small lipoproteins containing apolipoprotein B100. *J Clin Invest.* **106**, 1501-10

Verbeuren, T.J., Jordaens, F.H., Van Hove, C.E., Van Hoydonck, A.E. and Herman, A.G. (1990) Release and vascular activity of endothelium-derived relaxing factor in atherosclerotic rabbit aorta. *Eur J Pharmacol.* **191**, 173-84

Verdecchia, P., Angeli, F., Gattobigio, R., Sardone, M. and Porcellati, C. (2005) Asymptomatic left ventricular systolic dysfunction in essential hypertension: prevalence, determinants, and prognostic value. *Hypertension.* **45**, 412-8

Vincelette, J., Martin-McNulty, B., Vergona, R., Sullivan, M.E. and Wang, Y.X. (2006) Reduced cardiac functional reserve in apolipoprotein E knockout mice. *Transl Res.* **148**, 30-6

Virmani, R., Kolodgie, F.D., Burke, A.P., Finn, A.V., Gold, H.K., Tulenko, T.N., Wrenn, S.P. and Narula, J. (2005) Atherosclerotic plaque progression and vulnerability to rupture: angiogenesis as a source of intraplaque hemorrhage. *Arterioscler Thromb Vasc Biol.* **25**, 2054-61

Waldeck-Weiermair, M., Zoratti, C., Osibow, K., Balenga, N., Goessnitzer, E., Waldhoer, M., Malli, R. and Graier, W.F. (2008) Integrin clustering enables anandamide-induced Ca²⁺ signaling in endothelial cells via GPR55 by protection against CB1-receptor-triggered repression. *J Cell Sci.* **121**, 1704-17

Wallert, MA., Hammes, D., Nguyen, T., Kiefer, L., Berthelsen, N., Kern, A., Anderson-Tiege, K., Shabb, J.B., Muhonen, W.W., Grove, B.D. and Provost, J.J. (2015) RhoA Kinase (Rock) and p90 Ribosomal S6 Kinase (p90Rsk) phosphorylation of the sodium hydrogen exchanger (NHE1) is required for lysophosphatidic acid-induced transport, cytoskeletal organization and migration. *Cell Signal.* **27**, 498-509

Walsh, M.C., Bourcier, T., Takahashi, K., Shi, L., Busche, M.N., Rother, R.P., Solomon, S.D., Ezekowitz, R.A. and Stahl, G.L. (2005) Mannose-binding lectin is a regulator of inflammation that accompanies myocardial ischemia and reperfusion injury. *J Immunol.* **175**, 541-6

Walsh, S.K., Hepburn, C.Y., Kane, K.A. and Wainwright, C.L. (2010) Acute administration of cannabidiol in vivo suppresses ischaemia-induced cardiac arrhythmias and reduces infarct size when given at reperfusion. *Br J Pharmacol.* **160**, 1234-42

Walsh, S.K., Hector, E.E., Andréasson, A.C., Jönsson-Rylander, A.C. and Wainwright, C.L. (2014) GPR55 deletion in mice leads to age-related ventricular dysfunction and impaired adrenoceptor-mediated inotropic responses. *PLoS One.* **9**, e108999

Walsh, S.K., Hepburn, C.Y., Keown, O., Åstrand, A., Lindblom, A., Ryberg, E., Hjorth, S., Leslie, S.J., Greasley, P.J. and Wainwright, C.L. (2015) Pharmacological profiling of the hemodynamic effects of cannabinoid ligands: a combined in vitro and in vivo approach. *Pharmacol Res Perspect.* **3**, e00143

Wang, Y., Rimm, E.B., Stampfer, M.J., Willett, W.C. and Hu, F.B. (2005) Comparison of abdominal adiposity and overall obesity in predicting risk of type 2 diabetes among men. *Am J Clin Nutr.* **81**, 555-63

Wang, H.T., Liu, C.F., Tsai, T.H., Chen, Y.L., Chang, H.W., Tsai, C.Y., Leu, S., Zhen, Y.Y., Chai, H.T., Chung, S.Y., Chua, S., Yen, C.H. and Yip, H.K. (2012a) Effect of obesity reduction on preservation of heart function and attenuation of left ventricular remodeling, oxidative stress and inflammation in obese mice. *J Transl Med.* **10**, 145

Wang, P.F., Jiang, L.S., Bu, J., Huang, X.J., Song, W., Du, Y.P. and He, B. (2012b) Cannabinoid-2 receptor activation protects against infarct and ischemia-reperfusion heart injury. *J Cardiovasc Pharmacol.* **59**, 301-7

Wang, Y., Qiu, J., Luo, S., Xie, X., Zheng, Y., Zhang, K., Ye, Z., Liu, W., Gregersen, H. and Wang, G. (2016) High shear stress induces atherosclerotic vulnerable plaque formation through angiogenesis. *Regen Biomater.* **3**, 257-67

WebMD®. [online]. Available from: <https://www.webmd.com/heart/picture-of-the-heart#1> [accessed 27th November 2017]

Whitman, S.C. (2004) A practical approach to using mice in atherosclerosis research. *Clin Biochem Rev.* **25**, 81-93

Whyte, L.S., Ryberg, E., Sims, N.A., Ridge, S.A., Mackie, K., Greasley, P.J., Ross, R.A., Rogers, M.J. (2009) The putative cannabinoid receptor GPR55 affects osteoclast function in vitro and bone mass in vivo. *Proc Natl Acad Sci U S A.* **106**, 16511-6

Widmaier, E.P., Raff, H. and Strang, K.T. (2006) *Vander's Human Physiology : The Mechanisms of Body Function*. Tenth Edition. Chapters: 3, 5, 12 and 16. New York: McGraw-Hill

Wiesmann, F., Ruff, J., Engelhardt, S., Hein, L., Dienesch, C., Leupold, A., Illinger, R., Frydrychowicz, A., Hiller, K.H., Rommel, E., Haase, A., Lohse, M.J. and Neubauer, S. (2001) Dobutamine-stress magnetic resonance microimaging in mice : acute changes of cardiac geometry and function in normal and failing murine hearts. *Circ Res.* **88**, 563-9

Wilhelmsen, K., Khakpour, S., Tran, A., Sheehan, K., Schumacher, M., Xu, F. and Hellman, J. (2014) The endocannabinoid/endovanilloid N-arachidonoyl dopamine (NADA) and synthetic cannabinoid

WIN55,212-2 abate the inflammatory activation of human endothelial cells. *J Biol Chem.* **289**, 13079-100

Wolfrum, S., Dendorfer, A., Rikitake, Y., Stalker, T.J., Gong, Y., Scalia, R., Dominiak, P. and Liao, J.K. (2004) Inhibition of Rho-kinase leads to rapid activation of phosphatidylinositol 3-kinase/protein kinase Akt and cardiovascular protection. *Arterioscler Thromb Vasc Biol.* **24**, 1842-7

Wu, C.S., Chen, H., Sun, H., Zhu, J., Jew, C.P., Wager-Miller, J., Straiker, A., Spencer, C., Bradshaw, H., Mackie, K. and Lu, H.C. (2013) GPR55, a G-protein coupled receptor for lysophosphatidylinositol, plays a role in motor coordination. *PLoS One.* **8**, e60314

Xia, N., Horke, S., Habermeier, A., Closs, El., Reifenberg, G., Gericke, A., Mikhed, Y., Münzel, T., Daiber, A., Förstermann, U. and Li, H. (2016a) Uncoupling of Endothelial Nitric Oxide Synthase in Perivascular Adipose Tissue of Diet-Induced Obese Mice. *Arterioscler Thromb Vasc Biol.* **36**, 78-85

Xia, N. and Li, H. (2016b) The role of perivascular adipose tissue in obesity-induced vascular dysfunction. *Br J Pharmacol.* 2016 Oct 20. doi: 10.1111/bph.13650. [Epub ahead of print]

Yabluchanskiy, A., Ma, Y., Iyer, R.P., Hall, M.E. and Lindsey, M.L. (2013) Matrix metalloproteinase-9: Many shades of function in cardiovascular disease. *Physiology (Bethesda).* **28**, 391-403

Yada, T., Shimokawa, H., Hiramatsu, O., Kajita, T., Shigeto, F., Tanaka, E., Shinozaki, Y., Mori, H., Kiyooka, T., Katsura, M., Ohkuma, S., Goto, M., Ogasawara, Y. and Kajiya, F. (2005) Beneficial effect of hydroxyfasudil, a specific Rho-kinase inhibitor, on ischemia/reperfusion injury in canine coronary microcirculation in vivo. *J Am Coll Cardiol.* **45**, 599-607

Yaghoubi, M., Oliver-Krasinski, J., Cayatte, A.J. and Cohen, R.A. (2000) Decreased sensitivity to nitric oxide in the aorta of severely hypercholesterolemic apolipoprotein E-deficient mice. *J Cardiovasc Pharmacol.* **36**, 751-7

Yamamoto, K., Masuyama, T., Sakata, Y., Nishikawa, N., Mano, T., Yoshida, J., Miwa, T., Sugawara, M., Yamaguchi, Y., Ookawara, T., Suzuki, K. and Hori, M. (2002) Myocardial stiffness is determined by ventricular fibrosis, but not by compensatory or excessive hypertrophy in hypertensive heart. *Cardiovasc Res.* **55**, 76-82

Yamashita, A., Oka, S., Tanikawa, T., Hayashi, Y., Nemoto-Sasaki, Y. and Sugiura, T. (2013) The actions and metabolism of lysophosphatidylinositol, an endogenous agonist for GPR55. *Prostaglandins Other Lipid Mediat. Prostaglandins Other Lipid Mediat.* **107**, 103-16

Yu, J., Deliu, E., Zhang, X.Q., Hoffman, N.E., Carter, R.L., Grisanti, L.A., Brailoiu, G.C., Madesh, M., Cheung, J.Y., Force, T., Abood, M.E., Koch, W.J., Tilley, D.G. and Brailoiu, E. (2013) Differential Activation of Cultured Neonatal Cardiomyocytes by Plasmalemmal Versus Intracellular G Protein-coupled Receptor 55. *J Biol Chem.* **288**, 22481-92

Zeihner, A.M., Drexler, H., Wollschläger, H. and Just, H. (1991) Modulation of coronary vasomotor tone in humans. Progressive endothelial dysfunction with different early stages of coronary atherosclerosis. *Circulation.* **83**, 391-401

Zhang, J., Liu, X.B., Cheng, C., Xu, D.L., Lu, Q.H. and Ji, X.P. (2014) Rho-kinase inhibition is involved in the activation of PI3-kinase/Akt during ischemic-preconditioning-induced cardiomyocyte apoptosis. *Int J Clin Exp Med.* **7**, 4107-14

Zhao, L.Y., Li, J., Yuan, F., Li, M., Zhang, Q., Huang, Y.Y., Pang, J.Y., Zhang, B., Sun, F.Y., Sun, H.S., Li, Q., Cao, L., Xie, Y., Lin, Y.C., Liu, J., Tan, H.M. and Wang, G.L. (2015) Xylometazoline B attenuates atherosclerotic plaque formation and endothelial dysfunction in apolipoprotein e deficient mice. *Mar Drugs.* **13**, 2306-26

Zhou, Y.T., Grayburn, P., Karim, A., Shimabukuro, M., Higa, M., Baetens, D., Orci, L. and Unger, R.H. (2000) Lipotoxic heart disease in obese rats: implications for human obesity. *Proc Natl Acad Sci U S A.* **97**, 1784-9

Zhou, T., Chuang, C.C. and Zuo, L. (2015) Molecular Characterization of Reactive Oxygen Species in Myocardial Ischemia-Reperfusion Injury. *Biomed Res Int.* **2015**, 864946

Zhu, X.Y., Daghini, E., Rodriguez-Porcel, M., Chade, A.R., Napoli, C., Lerman, A. and Lerman, L.O. (2007) Redox-sensitive myocardial remodeling and dysfunction in swine diet-induced experimental hypercholesterolemia. *Atherosclerosis.* **193**, 62-9

Zorov, D.B., Juhaszova, M. and Sollott, S.J. (2006) Mitochondrial ROS-induced ROS release: an update and review. *Biochim Biophys Acta*. **1757**, 509-17

Zweier, J.L., Flaherty, J.T. and Weisfeldt, M.L. (1987) Direct measurement of free radical generation following reperfusion of ischemic myocardium. *Proc Natl Acad Sci U S A*. **84**, 1404-7